



# COMSAT Technical Review

## Volume 2 Number 2, Fall 1972

*Advisory Board* Joseph V. Charyk  
William W. Hagerty  
Sidney Metzger  
Wilbur L. Pritchard

*Editorial Board* Pier L. Bargellini, Chairman  
Robert C. Barthle  
N. K. M. Chitre  
S. H. Durrani  
Leonard Golding  
Gary D. Gordon  
Geoffrey Hyde  
Joachim Kaiser  
Edward J. Martin  
Emeric Podraczky  
Helmo Raag  
Edmund S. Rittner

*Managing Editor* Lawrence Weekley, Jr.

*Technical Editor* Leonard F. Smith

iv DEDICATION

v EDITORIAL NOTE

vii FOREWORD **Sidney Metzger**

271 THE INTELSAT IV SPACECRAFT **E. T. Jilg**, EDITOR

391 LAUNCH AND ORBITAL INJECTION OF INTELSAT IV SATELLITES  
**A. M. McCaskill, D. V. Neill, A. A. Satterlee**

437 THE INTELSAT IV COMMUNICATIONS SYSTEM  
**P. L. Bargellini**, EDITOR

573 TRANSLATIONS OF ABSTRACTS IN THIS ISSUE  
FRENCH 573  
SPANISH 575

The COMSAT TECHNICAL REVIEW is published twice a year by the Communications Satellite Corporation (COMSAT). Subscriptions including postage, \$5.00 U. S. per year; single copies, \$3.00 U. S. Bulk rates are available upon request. Remittances for subscriptions should be made payable to The Treasurer, COMSAT, and addressed to COMSAT TECHNICAL REVIEW, Room 5273, 950 L'Enfant Plaza, S. W., Washington, D. C. 20024, U. S. A.

*The papers in this issue are based upon work performed under the sponsorship of the International Telecommunications Satellite Consortium (INTELSAT). The views expressed are not necessarily those of INTELSAT.*

## **Dedication**

This INTELSAT IV issue of COMSAT TECHNICAL REVIEW is dedicated to the memory of the late Siegfried H. Reiger. As Vice President, Technical, of the Communications Satellite Corporation (COMSAT), and as Chairman of the Technical Subcommittee of the International Communications Satellite Consortium (INTELSAT), his vision and driving initiative led in large measure to the decision to go ahead with the INTELSAT IV program at a time when many were hesitant to do so. As the program proceeded, his technical leadership and profound understanding of spacecraft physics, space flight and communications contributed invaluable to the ultimate success of INTELSAT IV.



**Siegfried H. Reiger**

## **Editorial Note**

*The purpose of this issue of the COMSAT TECHNICAL REVIEW is to collect in a single volume information about the various aspects of the INTELSAT IV satellites.*

*The first INTELSAT IV satellite was launched on January 25, 1971, and positioned over the Atlantic Ocean. Following three other launches (in December 1971, January 1972, and June 1972), four INTELSAT IV satellites are now operational. These satellites have succeeded the INTELSAT III series through which global commercial satellite communications were first established in 1968-69, and are now the backbone of the INTELSAT system.*

*It is appropriate to recall that these accomplishments occurred within the decade after President Kennedy's statement that a worldwide commercial communications satellite system would be a U. S. goal. The Communications Satellite Act of 1962, the establishment of the Communications Satellite Corporation (COMSAT) in 1963, the formation of the International Telecommunications Satellite Consortium (INTELSAT) in 1964, and the launch of INTELSAT I (Early Bird) in 1965 were early important steps toward the achievement of the present global system.*

*The INTELSAT IV program is recognized as a significant milestone in the history of electrical communications. It marks a further coming of age of satellite communications by providing capacity and coverage beyond anything previously available.*

*Any discussion of INTELSAT IV would be incomplete without a fundamental tribute to the international consortium. The INTELSAT IV is the most important program undertaken by INTELSAT, and the success of this program confirms the effectiveness of the unique international partnership through which the global commercial communications satellite system has been achieved.*

*A program of this magnitude is clearly the result of the efforts of many individuals, organizations and entities. Their contributions are gratefully acknowledged here.*

**The Editorial Board**  
COMSAT TECHNICAL REVIEW

# **Foreword**

SIDNEY METZGER

This special INTELSAT IV issue describes at some length various technical aspects of the satellite itself, its effect on the earth station requirements, and its operational use. Some of the planning phases, historical events, and critical decisions encountered in the development of the INTELSAT IV communications satellite system are presented in this foreword.

INTELSAT IV is actually only the second series of satellites specifically designed for INTELSAT global commercial communications satellite service, even though it is the fourth generation of INTELSAT commercial communications satellites. INTELSAT I (Early Bird) was an experimental satellite with some operational capability. Its principal purpose was to provide answers to questions concerning the application of geostationary satellites to commercial telephone traffic. If successful (as it was), it could then be used for commercial operation. INTELSAT II was an improved version of INTELSAT I, and was designed and put into orbit as a result of a specific request by the National Aeronautics and Space Administration (NASA) to provide communications in connection with the Apollo manned space flight program, and also to provide additional capacity for commercial traffic. INTELSAT III was the first satellite specifically designed for global commercial communications satellite service, and INTELSAT IV was the second such satellite.

In designing a new series of communications satellites, one must keep in mind a number of goals and requirements that constitute real improvements over the older models. The following briefly shows the improve-

---

*Sidney Metzger is Assistant Vice President and Chief Scientist of COMSAT.*

ments made with each new generation of satellites and outlines some of the driving forces that necessitated or permitted such improvements.

INTELSAT I used two 25-MHz bandwidth repeaters which covered 10 percent of the allocated 500 MHz. It provided service only to the northern hemisphere of the earth, using a squinted toroidal antenna beam. It had no multiple-access capability when used with existing commercially available FDM/FM multiplex systems and lacked storage battery power for operation during eclipses.

Despite these shortcomings, INTELSAT I proved that a geostationary satellite was indeed suitable for global communications service. The following points were demonstrated: (a) successful interconnection with terrestrial networks; (b) acceptability of the transmission delay inherent in synchronous satellites; and (c) practicability of position and attitude control over long periods of time. Thus, after the successful launch of INTELSAT I in April 1965, specifications were prepared for a global satellite that would overcome the existing shortcomings and embody the following features: (a) operation over the full 500-MHz bandwidth; (b) coverage of the entire visible earth with an efficient directional antenna; (c) provision for multiple access to the satellite with dozens of separate radio frequency carriers; and (d) operation during eclipses.

At about the same time in 1965, the need arose to provide satellite communications between the U.S. mainland and NASA tracking stations situated in Australia, Ascension Island, and on ships in various oceans in connection with the Apollo manned space flights. INTELSAT I could not meet these requirements, and in view of the first Apollo launch date (the second half of 1966), neither could the new satellite (later to become INTELSAT III, but then on the drawing board) be built in time. Thus, it was deferred and an interim satellite, INTELSAT II, was then specified. A contract for it was let in the last quarter of 1965. The short development cycle for INTELSAT II did not permit the incorporation of all of the desirable features listed previously, but sufficient technical progress had been made since the design of INTELSAT I to incorporate some of these features. In particular, INTELSAT II had a single repeater of 130-MHz bandwidth, useful for multiple access; it employed tunnel diode amplifiers and a low-level TWT amplifier which reduced the number of components previously required; it had sufficient battery power for eclipse operation; and its toroidal antenna pattern illuminated the entire visible earth.

The weight capability of the Thor-Delta launch vehicle used for INTELSAT I had kept pace with the development of satellite technology, thereby permitting the inclusion of these advanced features in the satellite.

Thus, after INTELSAT I had shown the feasibility of a concept, INTELSAT III was in the planning stage while INTELSAT II was satisfying a specific requirement. Requests for proposals for INTELSAT III were placed with industry in 1965.

By that time, new horizons were already opening. It was deemed desirable to look into applications for communications satellites for other than point-to-point communications: specifically, aeronautical and maritime communications.

Study contracts were then let to two companies for a multipurpose satellite. The results of these studies showed that an advanced 5,000-voice-circuit satellite (later to be INTELSAT IV) could be established in orbit as early as mid-1970. The operational need for such a satellite had been confirmed by estimates of anticipated international traffic requirements in the 1970-1971 time period.

Pressure for additional capacity earlier than 1970 stirred some interest in building an augmented INTELSAT III, to be designated INTELSAT III½. However, by the time responses for INTELSAT III½ and INTELSAT IV were received and evaluated, new traffic forecasts showed that 1971 would be the critical year in which it would be necessary to introduce satellites of larger capacity than INTELSAT III. Thus, in July 1968 the International Telecommunications Satellite Consortium (INTELSAT) decided, upon the recommendation of COMSAT as Manager for INTELSAT, that the procurement of the full-fledged INTELSAT IV should proceed without the INTELSAT III½ intermediate step.

The multipurpose satellite approach, though technically feasible, was not viable for nontechnical reasons. The flexibility of such a satellite to handle traffic and the possibility of obtaining greater e.i.r.p. by using narrow spot-beam (4.5°) antennas in addition to the wider global-beam (18°) antennas were retained from the multipurpose approach and incorporated into the design of the INTELSAT IV series. It was clear that the Thor-Delta launch vehicle series used for INTELSATS I, II, and III would not be adequate for the larger INTELSAT IV. The Titan-Agena vehicle was considered first, but was later replaced by the Atlas-Centaur.

Two proposals for an INTELSAT IV were finally evaluated. They differed principally in the method of stabilization, one being spin-stabilized with a despun antenna section, and the other being body-stabilized. In view of the previous experience with spin stabilization in INTELSATS I, II and III, this technique was again chosen for INTELSAT IV.

The approach chosen by INTELSAT called for a satellite with 12 repeaters, each with a 36-MHz bandwidth. Four of these were permanently

connected to a global-beam antenna for TV, SPADE\* and other uses requiring wide geographic coverage; four others were switchable by ground command to either a global- or a spot-beam antenna; the remaining four were switchable to either a global- or the second spot-beam antenna. Traffic capacities of each satellite ranged from 3,000 to 9,000 two-way telephone circuits, or up to 12 TV channels, or mixtures thereof, depending on the arrangement of the repeaters and antennas and the makeup of the traffic.

A contract was awarded to the Hughes Aircraft Co. in 1968 to build four INTELSAT IV satellites. A number of technical problems remained to be solved. One of the important features of INTELSAT IV is its "Gyrostat" stabilization, an approach employed when it is desirable to build a spacecraft which is to be spun around its minimum moment-of-inertia axis. This technique, which is a particular version of the "dual-spin" method of stabilization, was first used in the TACSAT spacecraft.† Both TACSAT and INTELSAT IV consist of a nonspinning platform coupled, through a bearing interface, to a rotor which spins about the minimum moment-of-inertia of the satellite.

Generally, energy dissipation within the rotor tends to destabilize the spacecraft unless it is spinning about its axis of maximum moment-of-inertia. To counteract this destabilizing source in dual-spin spacecraft, it is necessary to place on the nonspinning platform a nutation damper which acts as an energy dissipation device by providing forces opposing those which tend to destabilize the spacecraft. Principal causes of destabilizing forces are fuel slosh and structural vibrations.

One of several interesting problems encountered and successfully solved during the INTELSAT IV program is summarized in the following. Prelaunch computations on TACSAT indicated that the destabilizing forces were orders of magnitude smaller than the stabilizing force of the damper placed on the nonspinning platform. Nevertheless, immediately following launch and the initiation of TACSAT operation, the nutation angle did not decay as expected, but maintained a fairly constant level of about 1 degree. This nutation disappeared within a few weeks, only to reappear occasionally

for short-term intervals. Fortunately, for the beamwidths involved on the TACSAT vehicle, the observed 1-degree nutation had no significant effect on the mission.

Shortly after TACSAT was launched, studies were initiated to predict the stability of INTELSAT IV. It was found that the major uncertainty was the magnitude of the energy dissipated by the hydrazine liquid propellant in the four sphere-cone tanks housed in the rotor. This result indicated the need to investigate the energy dissipation rate due to fuel slosh.

Experimental programs were run in parallel with analytical studies. As a back-up measure, an active nutation damper which consisted of two accelerometers working in conjunction with the axial thrusters, was added to INTELSAT IV, in addition to the existing passive dampers.

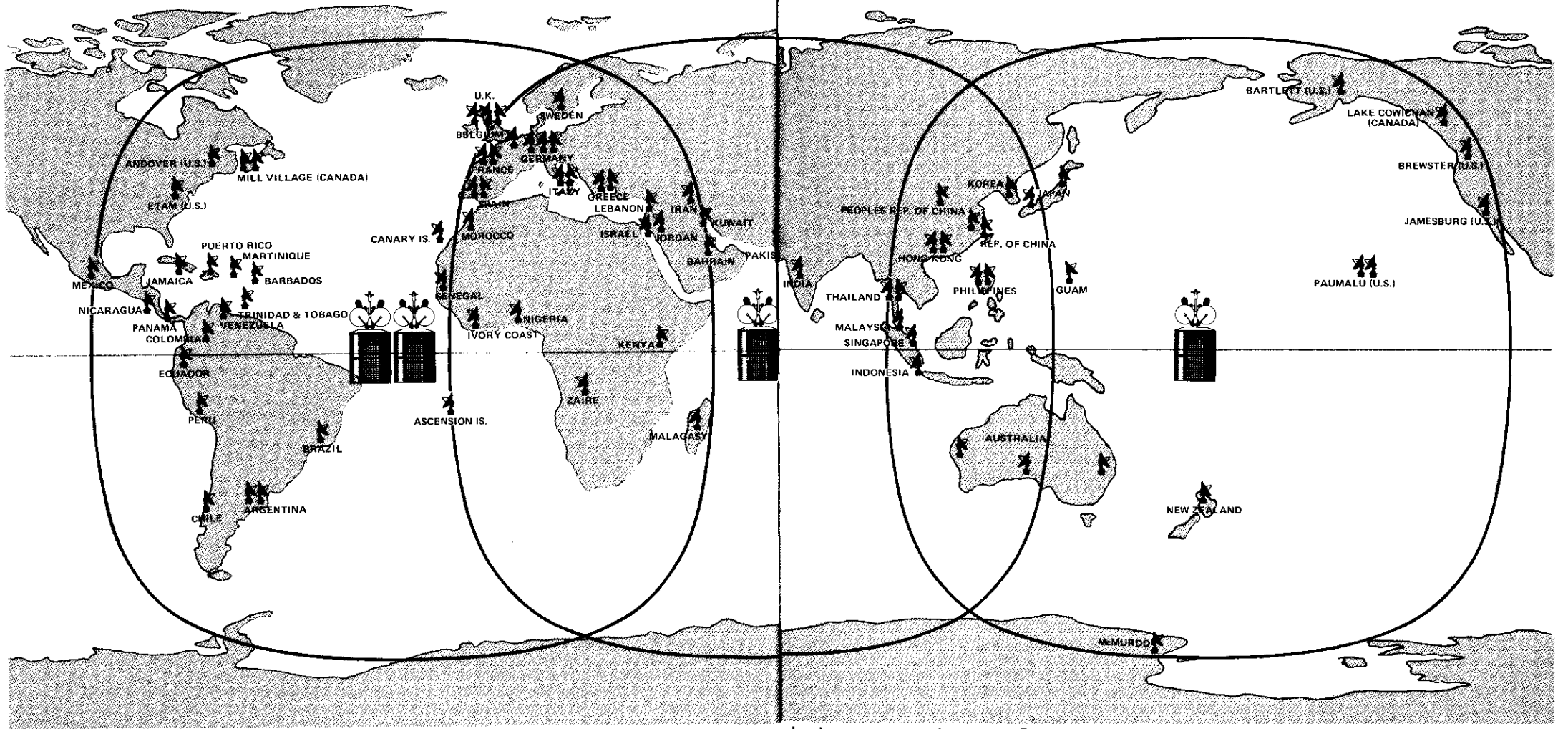
The destabilizing effects of fuel slosh in orbit have been in accord with predictions, and the active nutation damper has been used during launch as planned. Since the satellite performance has been normal, the use of the active damper in orbit has not been required.

All four INTELSAT IV satellite launches have been successful. The Atlas-Centaur performance has been outstanding, with a maximum error of 30 miles at apogee. The electrical performance of the repeaters has met all specifications, and the mechanically despun sections operate smoothly.

The excellent results obtained reflect a substantial cooperative effort, not only within INTELSAT, but also between COMSAT as Manager and the suppliers, including Hughes Aircraft Company as the prime contractor, the various subcontractors, NASA, and General Dynamics.

\* SPADE is a system designed for countries with relatively light traffic to a number of other countries. It is based on demand assignment of a single RF carrier for each voice channel. This system is to be placed in operation by the end of 1972.

† TACSAT I, a U.S. satellite for tactical communications, was successfully injected into synchronous orbit in 1969.



The global system of INTELSAT IV satellites and operational earth stations  
(as of December 1972)

**Index: INTELSAT IV, communications satellites, telecommunication, spacecraft control, spacecraft guidance, spacecraft propulsion, telemetry**

## ***The Intelsat IV Spacecraft***

E. T. JILG, EDITOR

### ***Abstract***

In describing the INTELSAT IV communications satellite, each subsystem is treated separately. The satellite, which is designed for a 7-year lifetime, weighs 1,410 kg at launch and 730 kg after apogee motor firing. The entire communications subsystem is on the despun portion of the satellite. Each of two global coverage 6-GHz antennas feeds a pair of redundant 500-MHz-bandwidth receivers. Each of twelve 36-MHz-wide channels is amplified by one of a pair of redundant output TWTs. There are two global transmit antennas and two steerable spot-beam antennas with 4.5-degree beamwidths.

The major part of the satellite (450 kg) spins at a nominal 51 rpm and includes the electric power, despun control, and positioning and orientation subsystems. Useful DC power of 365 watts is provided by two cylindrical solar panels; two 25-cell Ni-Cd batteries maintain power during eclipse. The satellite spins about a minimum moment-of-inertia axis, and stability is maintained by two pendulous eddy current dampers.

### ***Introduction***

The INTELSAT IV satellite is a 1,400-kg (3,100-lb) active communications repeater intended for commercial service in the INTELSAT system. It is launched by the Atlas-Centaur and is designed to have an operating life of seven years. It employs 2-body spin stabilization. Figure 1 is a photograph of the F-3 spacecraft immediately prior to encapsulation for launch. Figure 2 shows the major elements of the satellite.

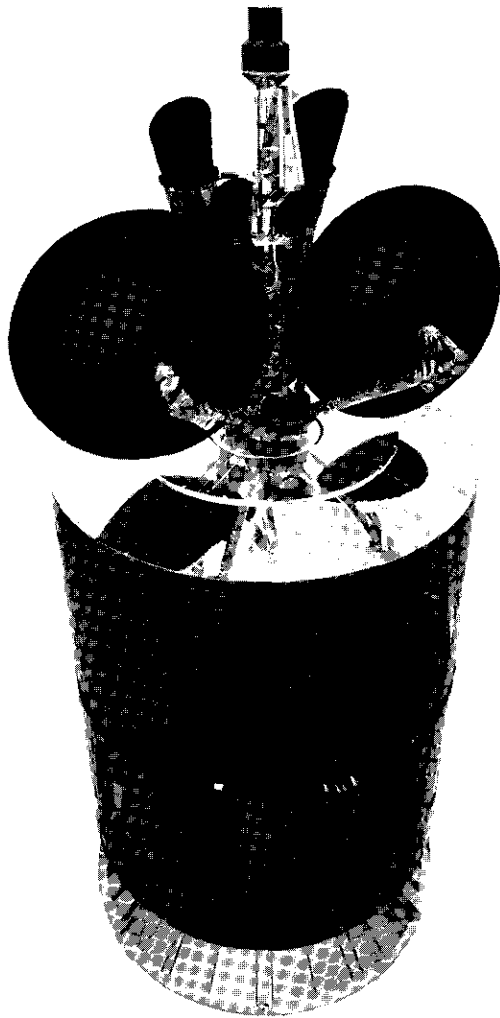


Figure 1. Photograph of the F-3 Spacecraft Immediately Prior to Encapsulation for Launch

The communications subsystem is the payload of the satellite. It consists of the receive antennas, receiver, input multiplexer, output traveling wave tube amplifiers (TWTAs), output multiplexers, and transmit antennas. Each of two global-coverage, 6-GHz horn antennas feeds a pair of

redundant 500-MHz-bandwidth receivers. (Any one of the four receivers provides full communications receive capability.)

Each receiver is comprised of a 6-GHz tunnel diode amplifier (TDA), a notch filter, a 6-/4-GHz mixer, a 4-GHz tunnel diode amplifier, and a low-level TWTA. The input multiplexer separates the communications band into twelve 36-MHz channels; each channel is amplified by one of a pair of redundant output TWTAs. Output multiplexers recombine the channels and feed them to the transmit antennas. There are two global transmit antennas and two spot-beam antennas with beamwidths of 4.5°. The entire communications subsystem is mounted on the despun portion of the spacecraft so that power transfer across the rotary interface is at DC rather than RF.

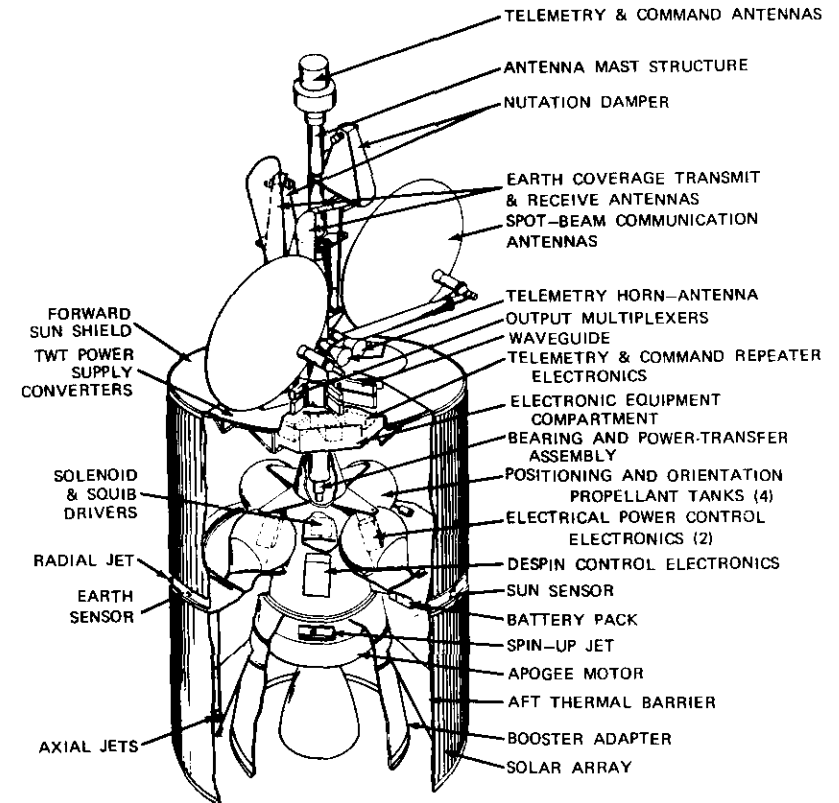


Figure 2. Major Elements of the Satellite

The despun control subsystem (DCS) provides a drive signal to the motor between the spinning and despun portions of the spacecraft. In normal operation this drive signal orients the despun platform to point the antennas toward the earth. Reference data for earth orientation are obtained from one of three earth infrared horizon sensors, from one of two sun sensors (using an offset clock inside the despun control electronics), or from ground command. Ground command is used to produce desired non-zero inertial rates for transfer orbit operations. As they sweep by a pair of despun side magnets, pickup coils on the spinning side produce output pulses which supply relative position feedback data to the DCS.

Because the despun platform station must be nearly stationary to maintain the nutational stability of the satellite, the DCS includes a "rate hold" feature. If the despun reference is lost, this logic function uses the most recent rate information to preserve the relative rotor-to-stator motion. In-orbit tests have confirmed the stability of this operating mode over periods of several hours.

The processing electronics subsystem of the DCS consists of redundant digital torque command generators cross-coupled to redundant analog motor drivers. The entire subsystem is located on the spinning section. In addition to motor drive signals, the DCS provides sensor data to the telemetry system to permit ground determination of spacecraft attitude.

The bearing and power transfer assembly (BAPTA) comprises the rotary interface between the spinning and despun portions of the satellite. Contained within the titanium housing of the BAPTA are the electric power slip ring assembly and a 4-channel rotary transformer for telemetry and command signal transfer. Angular contact ball bearings are the rotating interface.

The BAPTA contains the permanent magnet armature and the field coil; these elements compose the motor that produces the torque to counterbalance friction effects in the bearings and slip rings. The resolver, which is adjacent to the motor windings, provides properly phased sine and cosine modulation to permit the motor to operate without brushes. The coils and magnets for relative position feedback to the DCS are also in the BAPTA. A "loose" labyrinth seal and nylasint reservoirs, as well as an impregnated bearing retainer, help to ensure a lubricant lifetime calculated to be an order of magnitude greater than mission life. Finally, the BAPTA provides for an ordnance-released double-vee clamp to minimize the launch loads on the bearings.

The electric power subsystem provides 365 watts of useful DC power to the spacecraft loads in sunlight and during 90 annual eclipses of up to

70-minutes duration each. Power is provided by the two cylindrical solar panels which form the spinning "skin" of the satellite and by two 25-cell nickel-cadmium batteries distributed in multicell packs on the spinning platform ribs. Distribution is through two separate unregulated buses, which may be paralleled by ground command. Battery charge and discharge have in practice been controlled by ground command, although an automatic discharge capability is provided. Battery reconditioning under ground control is also available.

Telemetry data from the satellite are provided at 4 GHz through either an omnidirectional antenna, used during transfer orbit with increased output power provided by a communications TWT, or from an earth-coverage conical horn driven by a 100-mW solid-state transmitter, used during communications service.

A pair of encoders, one spinning and one despun, can operate in one of three modes to provide spacecraft data. In pulse-code modulation (PCM), the most common mode, words from spinning and despun encoders are interleaved to form a 64-word frame at 1 kbps. Command register status, spacecraft operating status, and engineering data are contained in the frame. In the frequency modulation (FM) real-time mode, an analog representation of sensor output and timing pulses is provided. The FM accelerometer mode gives a direct indication of spacecraft nutation. In addition to these primary modes, one of the two redundant encoder chains may be used as a broadband acoustic monitor of the BAPTA. All other parts of the subsystem are fully redundant.

Commanding is performed at microwave frequency in a slot between two communications channels. The signal is received by an omnidirectional bicone antenna atop the mast and demodulated by redundant command receivers, which extract a binary pulse train and pass it to two redundant spinning encoders and two redundant despun encoders. The subsystem provides 95 commands on the spinning side and 160 commands on the despun side. In addition to performing the ground command function, it provides a series of commands to configure the spacecraft and spin it up after separation. An automatic nutation control unit may be used to operate the axial hydrazine jets so that nutation can be reduced below a preset  $0.5^\circ$  threshold.

The antenna positioner mechanisms are used to steer spot-beam reflectors so that the beams are pointed at desired locations on earth within satellite visibility. The positioner consists of a 2-axis gimbal, a drive motor and gear train, and a potentiometer position indicator.

The positioning and orientation (P&O) subsystem uses hydrazine as a

monopropellant to provide velocity, attitude, and spin-speed control over the mission life of the satellite. Upon spacecraft separation from the Centaur, the P&O subsystem automatically produces free-body satellite spin-up to about 51 rpm. On ground command, this subsystem is used to reorient the satellite from the orbit normal attitudes at injection to the attitude for apogee motor fire. After motor firing, it may be used to damp nutation. The satellite is then reoriented to operating attitude and drifted to its desired location.

For the remainder of the mission, hydrazine is used to overcome perturbing forces acting on the satellite. These include solar and lunar forces which precess the orbit plane and affect its inclination, earth gravitational irregularities which drift the satellite in-plane, and solar pressure forces which disturb the attitude. The total mission velocity increment required for these functions is about 430 m/s (1,400 ft/s). The subsystem consists of two separate but cross-connected halves, each containing two conospheric tanks, three catalytic thrusters and their associated valves and filters, a spin-up reservoir, a fill valve, a pressure transducer, and piping.

The apogee motor is a polybutadiene propellant, solid-fuel rocket with a filament-wound case. Its total weight is about 710 kg (1,560 lb). Its purpose is to provide a velocity increment of 1,800 m/s (5,900 ft/s) to the spacecraft to change its orbit inclination, eccentricity, and altitude to equatorial, circular, and synchronous, respectively.

Two pendulous eddy current nutation dampers are located on the despun side, high on the antenna mast. These dampers perform the vital function of providing a nutation-induced energy dissipation on the despun body that is greater than the corresponding dissipation on the spinning side. This is a condition necessary to maintain the stability of 2-body spinning satellites with inertia ratios similar to those of INTELSAT IV. One damper is narrowly tuned for high damping over a narrow nutation frequency range and the other is broadly tuned.

The despun structure is fundamentally a cylindrical tubular mast from which various loads are cantilevered. The major load is the despun compartment, consisting of two annular shelves and interconnecting axial ribs. All of the despun communications units are mounted on this compartment. Additional despun loads are the antennas and feeds and the nutation dampers. The spinning structure is conical with a cantilevered, ribbed shelf supporting the solar panels, batteries, and P&O subsystem. Spinning electronic units are mounted on the cone's outer surface and the apogee motor is supported by the cone's inner surface. An additional structural element, the adapter, remains attached to the Centaur after spacecraft separation.

Thermal control of the INTELSAT IV satellite is primarily passive; the only active elements are the local resistance heaters on the BAPTA, apogee motor, receivers, and hydrazine lines. Passive control of the internal components exploits the approximately 20°C (70°F) in-sun environment provided by a black cylinder spinning normal to the sun line. Compensation for the local power dissipation by the TWTAs at the antenna end of the cylinder is provided by the high emittance-to-absorptance ratio of the second-surface-mirrored sunshield. Antenna farm components have been selected to tolerate wide temperature excursion because they are subject to multiple sun intensities caused by sunshield specular reflection and to the lack of spinning "integration." High-emittance, outer-surfaced, multiple-layer insulation has partially alleviated this effect.

### **Communications subsystem**

IRVING DOSTIS

The communications subsystem of the INTELSAT IV satellite is used as an in-orbit microwave repeater to receive, amplify, frequency translate, and retransmit various types of communications signals. The information carried by the signals is varied and includes voice (telephone), data (high and low bit rates), and color television. This information is generally modulated onto carriers using either frequency modulation (FM) or multiphase modulation (PM). These carriers may be present at all times and carry various numbers of telephone channels (24 to 1,800) as in standard radio-relay transmission; they may be voice actuated as in SPADE; or they may occur only in short time bursts as in TDMA.

The simplified transponder design shown in Figure 3 was developed to provide the performance required for the various communications techniques and to allow flexibility in frequency utilization. The basic elements of this transponder are the broadband "front end," consisting of the 6-GHz antenna and receiver sections to provide frequency translation from 6 GHz to 4 GHz; the channelizing or receive multiplexer assemblies, which include amplitude and group-delay equalizers to separate the communications band into twelve 36-MHz channels; and the output section, which

---

*Irving Dostis is Manager of the Radio Frequency Department, Space Segment Implementation Division, COMSAT.*

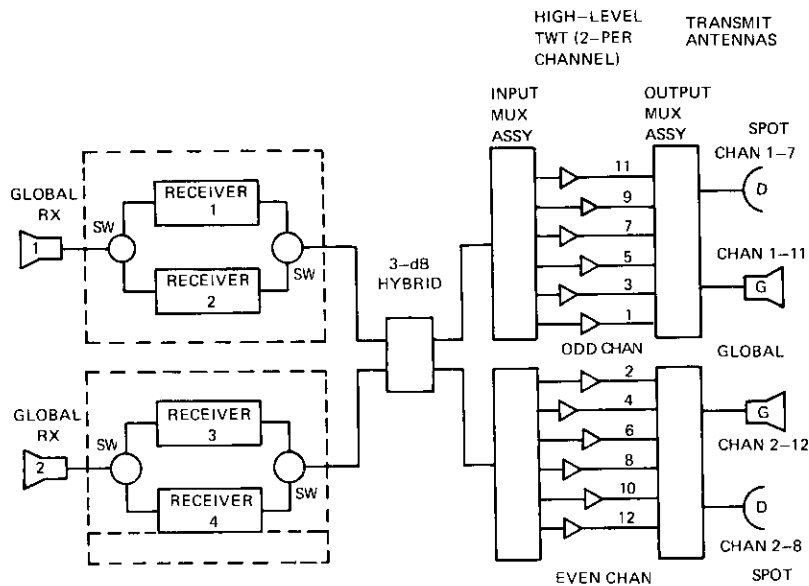


Figure 3. Transponder Block Diagram

includes the high-level traveling wave tubes, the output multiplexer assemblies, and the transmit antennas. To optimize the communications capacity relative to projected traffic requirements, two sets of transmit antennas are provided, one for global and one for spot-beam (with a 3-dB beamwidth of 4.5°) coverage.

In this design, the front end is intended to operate linearly: i.e., with minimum distortion and interchannel interference. The channelizing multiplexers separate the signals so that the output end may amplify them to an adequate power level with minimum interaction between channels. The principal performance parameters for the front end are the gain-to-noise temperature ratio (G/T), the gain and gain slope as functions of frequency, and the intelligible crosstalk ratio (IXTR). For the channelizing filters and output section, the principal parameters are in-band amplitude and group-delay response, out-of-band attenuation, saturated e.i.r.p.,\* and IXTR. These performance parameters are discussed in the following sections and the basic system requirements are given in Table 1.

Present results indicate that all communications performance requirements are met.

TABLE 1. PERFORMANCE REQUIREMENTS

a. General System Requirements			
Parameter	Requirement		
G/T Measured at Antenna to Receiver Interface (dB/°K)	-18.6		
Differential Phase, Δφ, at All Illuminations ≤ P <sub>in</sub> = -55 dBW/m <sup>2</sup> (deg)	≤ 1.5		
IXTR* for Total P <sub>in</sub> ≤ -55 dBW/m <sup>2</sup> and Ratio of Modulated to Unmodulated Carrier Power ≤ 20 dB	≤ 193 - 20 log f <sub>m</sub>		
e.i.r.p. (dBW)			
Global Channels	22.0 min. over ±8.5°		
Spot-Beam Channels	33.7 min. over ±2.25°		
Flux Density for Saturation (dBW/m <sup>2</sup> )	-73.7 to -55.7		
b. System Requirements for Various Frequency Bands			
Frequency Band (MHz)	Gain Slope (dB/MHz)	Gain Delay (ns)	IXTR (dB)
f <sub>c</sub> ± 12.6	0.03	+1.5 to -2.1	174 - 20 log f <sub>m</sub>
f <sub>c</sub> ± 14.4	0.05	+4.5 to -2.4	174 - 20 log f <sub>m</sub>
f <sub>c</sub> ± 16.2	0.20	+16.4 to -3.5	155 - 20 log f <sub>m</sub>
f <sub>c</sub> ± 18.0	0.70	+50.0 to -5.0	155 - 20 log f <sub>m</sub>

\* Input section requirement.

The elements comprising the communications system are all mounted on the despun portion of the INTELSAT IV spacecraft, thus eliminating the requirement for microwave rotating joints. The input and output multiplexer assemblies are mounted on separate shelves of the despun compartment, which are called the forward and aft shelves. These shelves are connected by brackets which are used as mounting supports for the high-level TWTs. The communications receivers are mounted in the intershelf space. Waveguide runs are used to connect the antennas to the appropriate receiver or output multiplexer.

\* Effective radiated power relative to isotropic.

### Receive antennas

Each of the global receive antennas is connected by a waveguide run and a bandpass filter to one pair of the redundant repeaters, as shown in Figure 3. All of the global antennas use a vertically mounted horn and a 45° flat plate reflector for redirecting the beam. All transmit and receive antennas are optically aligned to the mast assembly to provide proper pointing.

The receive antennas, which are left-hand circularly polarized, have a nominal peak gain of 20.5 dB at the band center frequency, and a nominal 3.5-dB peak-to-beam-edge gain variation for the required 17° coverage. Axial ratios are nominally less than 3 dB over the required region. Figure 4 is a typical contour diagram of a receive antenna. The distortion noted in this diagram appears on all global antenna patterns as a result of interaction among adjacent antennas, the mast, nutation dampers, and other elements mounted in the vicinity of the antenna. Figure 5 shows the

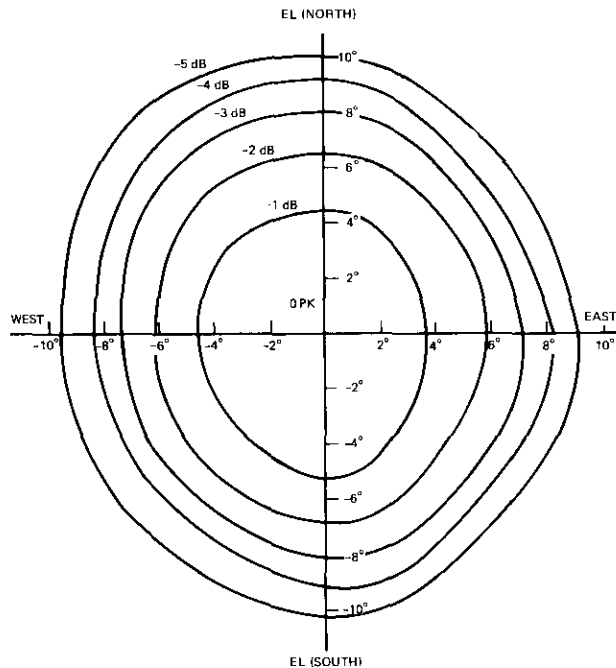


Figure 4. Typical Global Receive Antenna Gain Contour Diagram

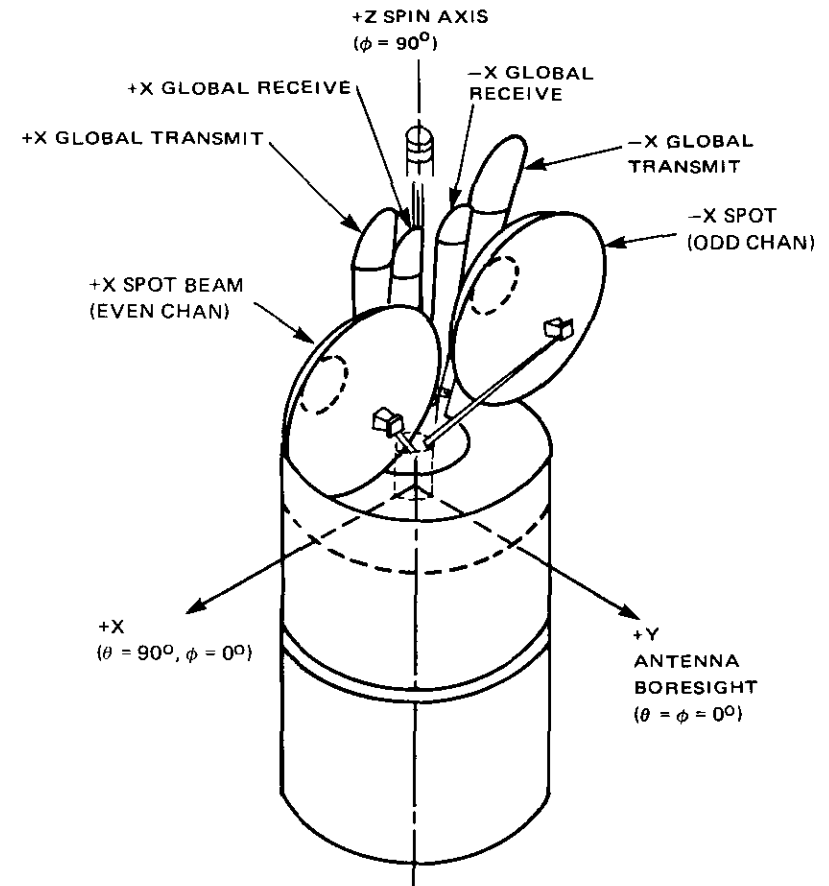


Figure 5. Antenna Subsystem on Spacecraft

arrangement of the antennas on a completed spacecraft and despun compartment.

### Transmit antennas

The global coverage transmit antennas, which are right-hand circularly polarized, have a peak gain of approximately 20.5 dB at beam center, a nominal beamwidth of 17°, and an axial ratio less than 3 dB over the required coverage area. Figure 6 is a typical contour diagram for a global transmit antenna.

The spot-beam transmit antennas, which are also right-hand circularly polarized, have a nominal peak gain at beam center of approximately

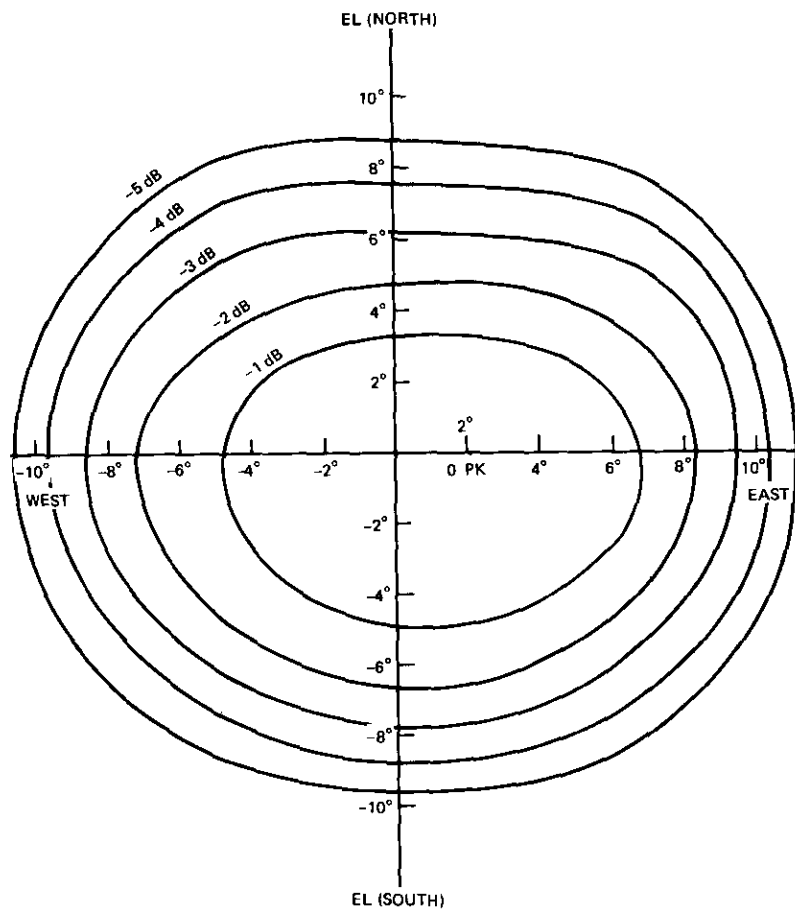


Figure 6. Typical Contour Diagram of Global Transmit Antenna

31.7 dB, and a 3-dB beamwidth of 4.5°. The odd and even output channels are connected to the  $-x$  and  $+x$  spot-beam antennas, respectively.

The spot beams may be steered to any position on the earth by mechanical movement of the parabolic reflectors. The feed horn is fixed in position and does not move during positioning. The spot beams are normally positioned to provide coverage for high-capacity routes. Typically, the east and west beams are positioned to cover Western Europe and the northeast section of the United States, respectively, in the Atlantic region. The position of the parabolic reflector is monitored by using carefully calibrated telemetry signals. Figure 7 is a typical pattern for a spot beam.

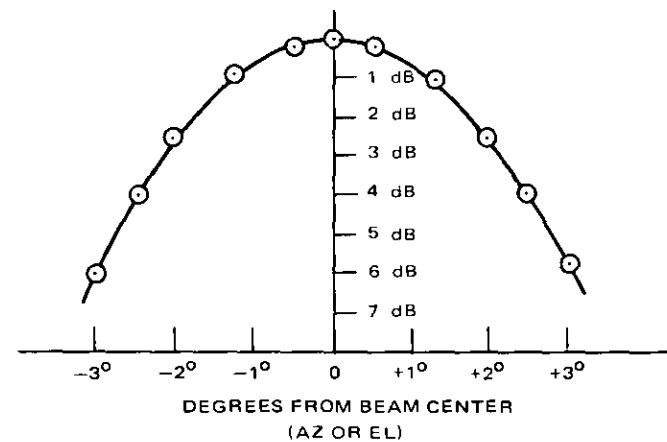


Figure 7. Typical Spot-Beam Antenna Pattern

Each receiver chain contains the following major units (see Figure 8): 6-GHz TDA, a notch filter, a 2-/4-/6-GHz mixer, a local oscillator, a 4-GHz TDA, and a low-level TWT. Because of the severe linearity requirements on the complete chain, each unit of the receiver has stringent design specifications. To meet the applicable input section design specifications given in Table 1, the receiver chains were constrained to meet the requirements listed in Table 2. The input section includes all units between the receive antennas and the input to the high-level TWTs. Active thermal control is used in each receiver to minimize performance variations caused by temperature changes.

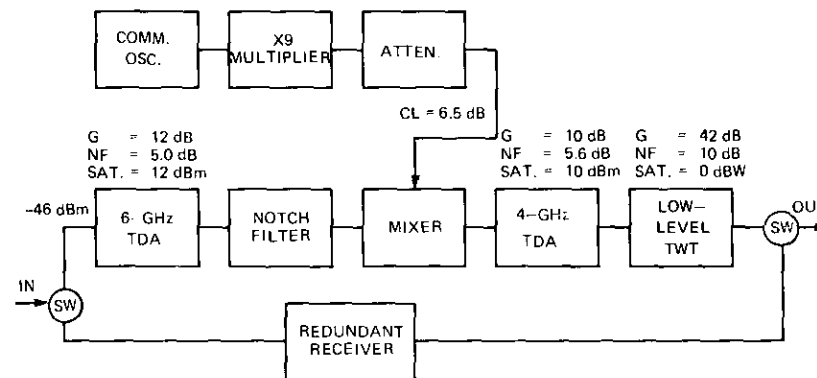


Figure 8. Receiver Block Diagram

TABLE 2. RECEIVER REQUIREMENTS

Parameter	Requirement
Noise Figure (dB)	$\leq 9.0$
$\Delta\phi$ from No Input to $P_{in} \leq -49$ dBm (deg)	$\leq 1.5$
Gain Slope (dB/MHz)	$\leq 0.015$
IXTR for $P_{in} \leq 49$ dBm and Other Conditions Given in Table 1	$\leq 198 - 20 \log f_m$
Allowable C/3IM/(dB)	
-49-dBm Input Power to Rx	36
-55-dBm Input Power to Rx	48
-60-dBm Input Power to Rx	58

Typical frequency and NF responses for a complete receiver are presented in Figure 9, which indicates favorable agreement between the budgeted and measured performances for these parameters. For example, the measured gain slope of the overall receiver does not exceed 0.01 dB/MHz at any point in the passband. This provides a sufficient margin for temperature effects. The gain slopes obtained from the frequency response by graphical techniques and direct measurement are well correlated. The differential phase measured for the receiver is lower than the specified value, however. This nonlinearity affects both the intelligible crosstalk and the level of the intermodulation noise generated within the receiver.

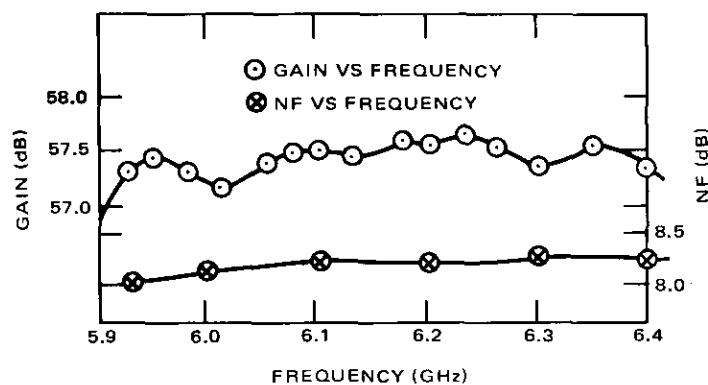


Figure 9. Receiver Characteristics

The amplitude linearity was controlled by ensuring that the actual input power level was sufficiently backed off from the saturation point of each unit. The approximate saturated output power of each unit of the receiver is given in Figure 8.

Intermodulation products generated by the amplitude and phase nonlinearities of the receiver not only contribute noise, but can also generate intelligible crosstalk problems. In FDM/FM transmission, this contribution to crosstalk is generated when the receiver's intermodulation products interact with the large gain slopes on the skirts of the channelizing filters to produce amplitude modulation (AM). This AM is then converted to PM and crosstalk by AM-PM conversion of the final or output TWT. Similarly, interaction between the intermodulation products and the phase characteristics of the channelizing filters can produce AM and thus intelligible crosstalk.

The performance of the receivers and units comprising the receiver meets the subsystem and unit requirements with reasonable margins. This has ensured that the overall system specifications affected by the receiver can be satisfied.

### Input multiplexer assembly

The input multiplexers divide the assigned frequency band into 12 communications channels, each having a usable bandwidth of 36 MHz. The 12 channels are arranged into lower and upper bands, each containing six channels. These two bands are separated by 20 MHz, which is used for telemetry and command functions. The band centers of adjacent channels in the upper and lower bands are separated by 40 MHz. Frequency channelization, accomplished by grouping the filters and equalizers into odd and even channels and placing each group on a separate subassembly, called the odd or even channel multiplexer assembly, is shown in Figure 10. The odd channel assembly is shown in Figure 11. Multiplexing in this

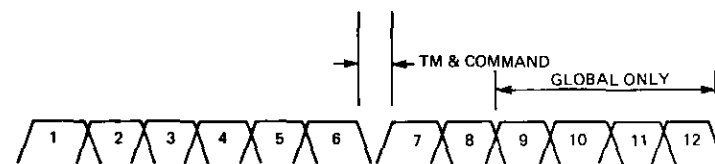


Figure 10. Channel Allocations

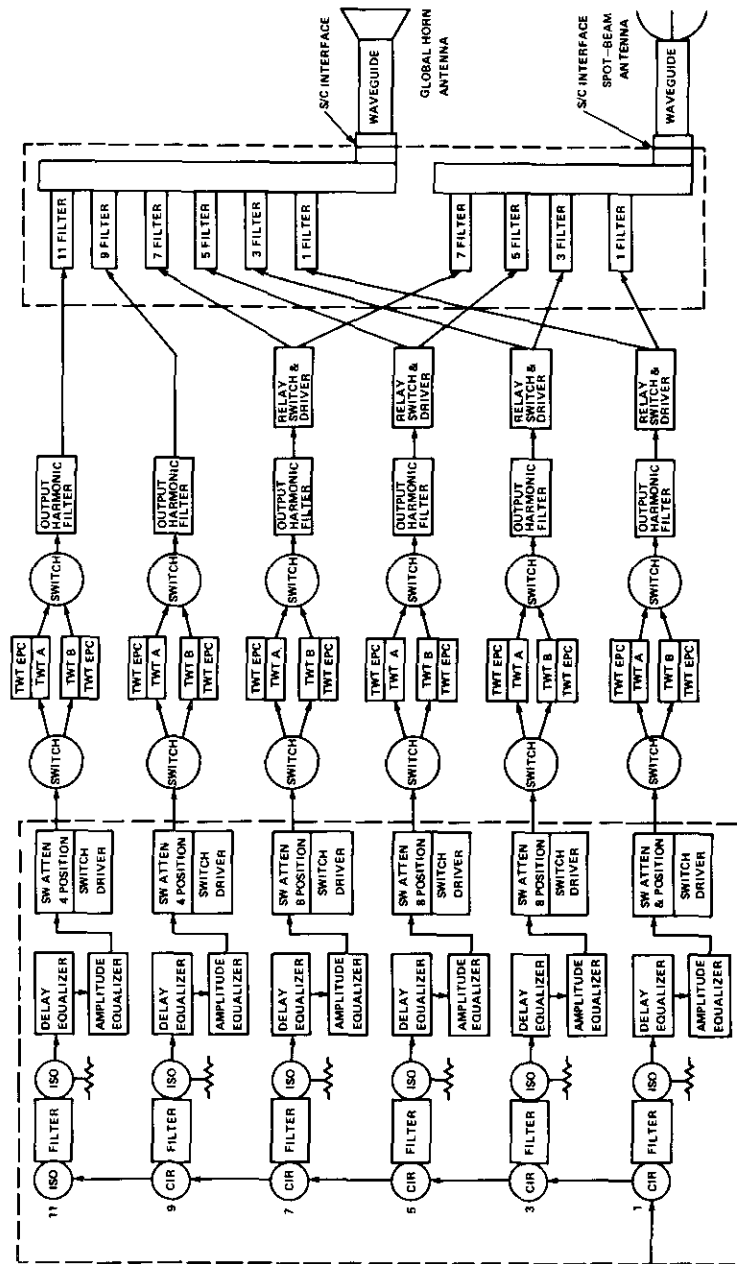


Figure 11. Block Diagram of Channelized Section

manner reduces the interaction between adjacent channels on the same multiplexer.

Each channel of the odd or even input multiplexer assembly consists of a 10-section Tchebycheff filter, a 5-cavity group-delay equalizer, an amplitude equalizer, and a 4- or 8-position switch attenuator. Each filter input on a specified multiplexer is connected to the next by using a circulator, which provides proper routing and matching. Increasing insertion loss is encountered as the signal is routed to the higher frequency channels of the input multiplexer because of multiple passes through routing circulators. Radio frequency energy not transmitted through any of the filters is terminated in a load at the end of the circulator chain.

The principal performance parameters affected by the input multiplexer assemblies are in-band amplitude, group-delay response, and out-of-band response for each channel. In-band amplitude and group-delay response affect IXTR and delay noise; out-of-band rejection affects the multipath distortion contributed by amplitude and phase variations as well as the IXTR caused by receiver intermodulation products. Intelligent crosstalk can be minimized in the in-band region by using amplitude and delay equalizers to reduce the gain and group-delay slopes encountered by any signal before reaching the output TWT. Multipath contributions are minimized by providing sufficient out-of-band rejection.

The required gain slope and delay for the signal path preceding the output TWT were given in Table 1. The out-of-band rejection must exceed 30 dB for any signal greater than 25 MHz from the band center of each channel under all environmental conditions (temperature and vacuum) encountered in orbit. This requirement has dictated the use of Invar for the filters and equalizers and the use of tuning corrections to account for frequency shifts caused by removal of the air dielectric in orbit. Amplitude and delay variations caused by temperature variations have also been reduced to negligible levels by using Invar.

The measured performance of the input multiplexer assemblies for every communications subsystem has exceeded the design specifications. Typical results for one channel of an input multiplexer are presented in Figure 12.

**Output TWT**

The final amplification stage of each communications channel is provided by either of the redundant pair of high-level TWTs. The "A" or "B" TWT is selected by commanding the proper power converter and circulator switches.

The AM-PM conversion was not measured for all flight TWTs, since this parameter is directly related to phase shift versus drive.  
 The output of each high-level TWT is carefully matched by using a

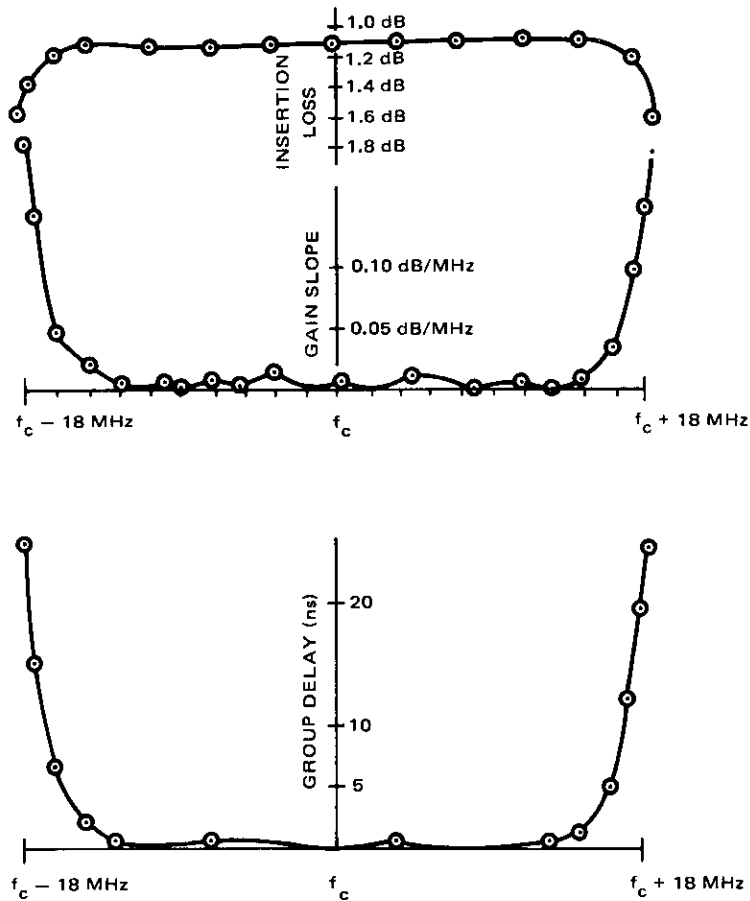


Figure 12. *Input Multiplexer Performance*

The high-level TWT is a permanent magnet-focused, high-reliability, space-qualified TWT. It has a nominal saturated output power of 6 watts and a saturated gain of 58 dB. Additionally, it has been required to meet stringent differential phase shift vs drive, C/3IM, frequency response, efficiency, and weight requirements. Typical performance of a high-level TWT is compared with its nominal specifications in Figure 13. The specifications for saturated output power and gain varied slightly from channel to channel because of the particular implementation losses.

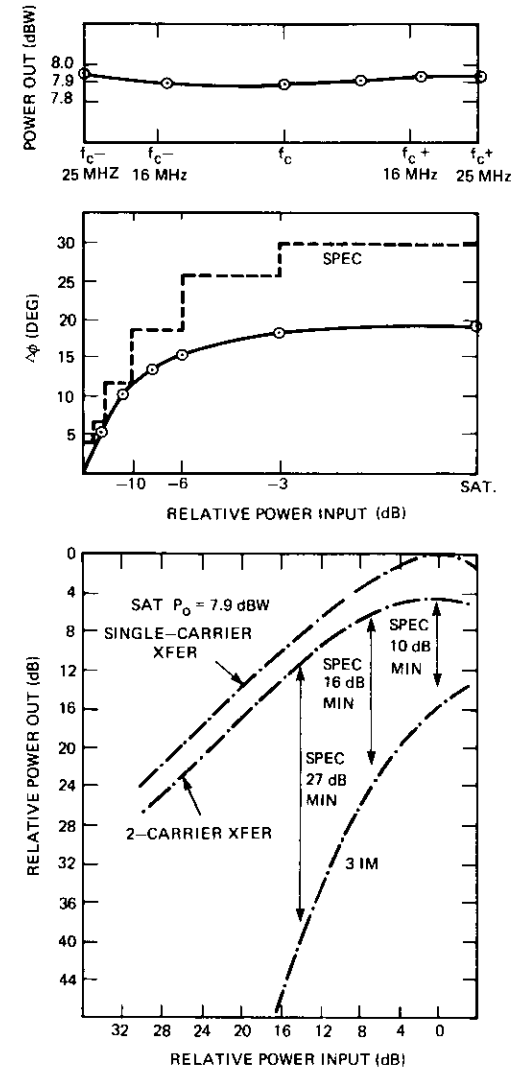


Figure 13. *High-Level TWT Performance*

stub tuner to provide a proper termination for reflected signals from the harmonic filters placed in each channel's output section.

### Output multiplexers

The output of each high-level TWT is fed to one of four output multiplexer assemblies through a harmonic filter and a network of switches, as shown in Figure 11. Four output multiplexers are included on each spacecraft to accomplish the routing to the two global and two spot-beam transmit antennas. Odd channels can be connected to one of the global horns or to the  $-x$  spot-beam transmit antenna, whereas even channels go to the second global antenna or the  $+x$  spot-beam antenna. Channels 1 through 8 can be switched on command to either a global or a spot-beam antenna, whereas channels 9 through 12 can be used only for global transmission. Each global output multiplexer assembly contains six filters, which are interconnected by a waveguide manifold to reduce losses. The spot-beam multiplexers require only four filters each. Channelizing into odd and even sections simplifies the filtering in the output section by providing 40-MHz spacing between adjacent channels on each manifold.

Each filter and the interconnecting manifold is constructed of Invar and then silver plated. The filters are 6-section Tchebycheff filters which are tuned for an equiripple bandwidth of approximately 40 MHz. This tuning is wider than for the 38-MHz equiripple bandwidth used on the input filtering so that all in-band contributions to amplitude and delay variations are small. The response of a typical channel in the output section is shown in Figure 14.

### System performance

The communications subsystem of the INTELSAT IV satellite undergoes extensive performance and environmental tests. All units used in the communications system are tested for electrical and mechanical performance. After successful unit tests are completed, each unit is integrated into its subsystem and the subsystem is carefully evaluated.

Receiver testing, for example, includes all input parameters previously described for ambient temperature and pressure, as well as high vacuum, temperature extremes, and vibration. These tests are performed after each unit of the receiver, e.g., TDAs, mixer, and low-level TWTs, has been successfully tested for comparable parameters under similar conditions. The various subsystems are integrated into the communications

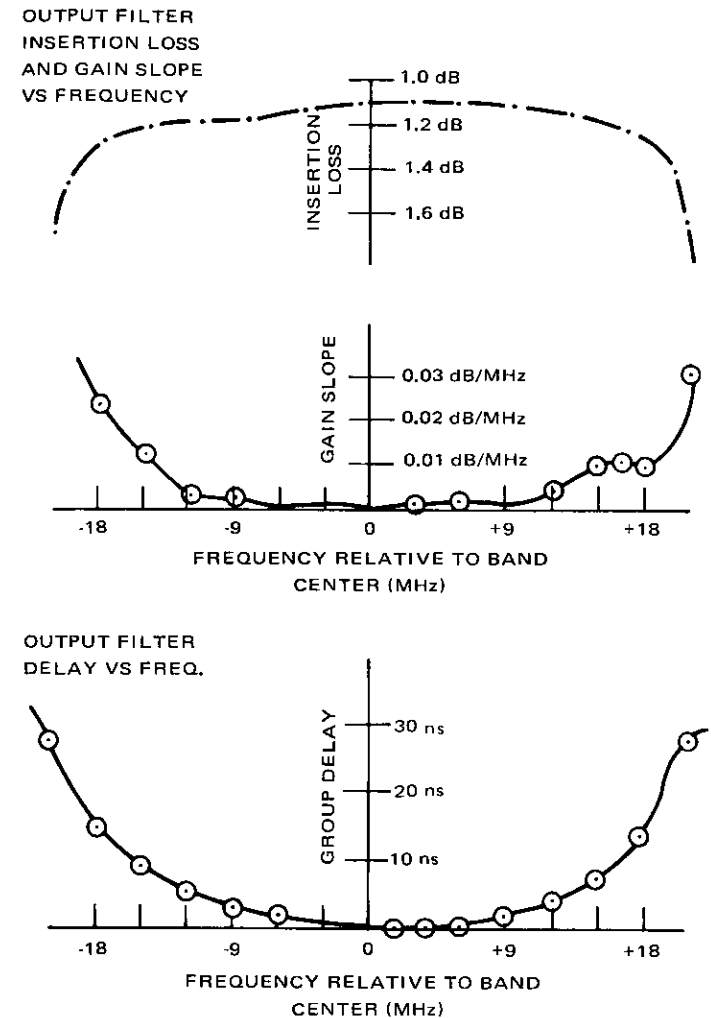


Figure 14. Output Multiplexer Performance

compartment after their tests are complete, and the compartment is then tested for performance. Inconsistencies between final performance data and predictions based on unit data previously obtained are investigated prior to proceeding.

The tested compartment is integrated into the antenna subsystem,

which has undergone similar testing, and assembled into the complete spacecraft, which is then subjected to acceptance (qualification) testing. During acceptance testing, the overall communications performance is evaluated in an anechoic chamber (see Figure 15). Performance parameters include e.i.r.p., receive G/T, IXTR, frequency response, system gain, total group delay, and spurious response. Performance is verified at the start and end of all environmental tests to ensure that no major degradation has occurred as a result of environmental testing.

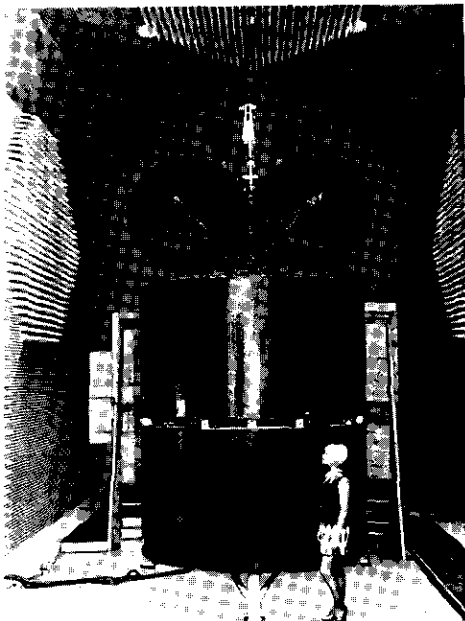


Figure 15. INTELSAT IV Communications Satellite in Anechoic Chamber

Typical measured values of performance parameters are compared with the applicable specifications in Figures 16 through 20. The results indicate that adequate margins exist for all specified parameters. The measured values of global e.i.r.p., receiver G/T, system gain, and IXTR were obtained in an anechoic chamber. The spot-beam e.i.r.p. was derived from a combination of unit power and far-field antenna measurements. The frequency response data were measured during the integration of the

communications subsystem and show the frequency response for a large range of input drives. A comparison of measured in-orbit values and prelaunch values for global and spot-beam e.i.r.p., receive G/T, system gain, and frequency response shows favorable agreement.

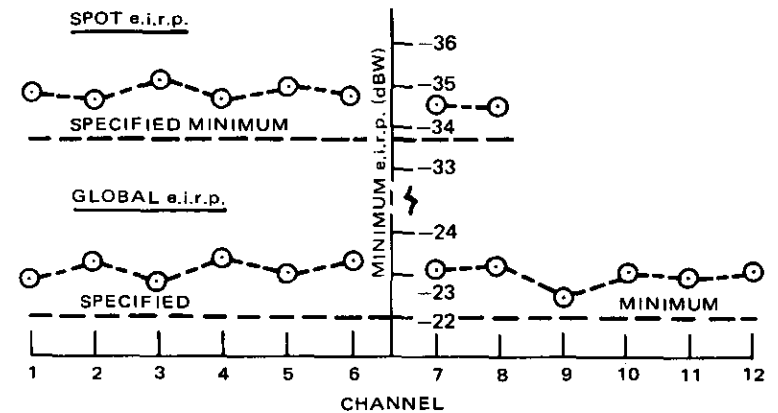


Figure 16. Spot- and Global-Beam e.i.r.p.

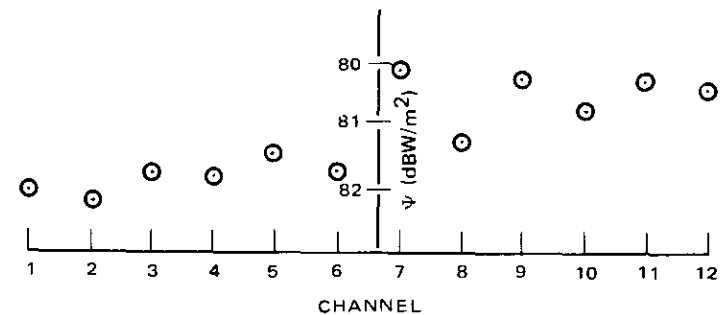


Figure 17. Typical Illumination for Saturation (0-dB attenuation)

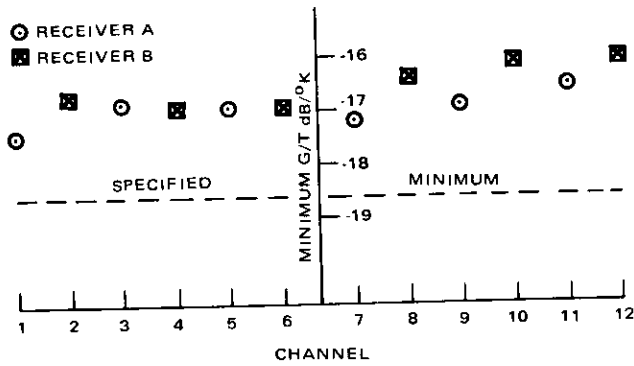


Figure 18. Repeater G/T

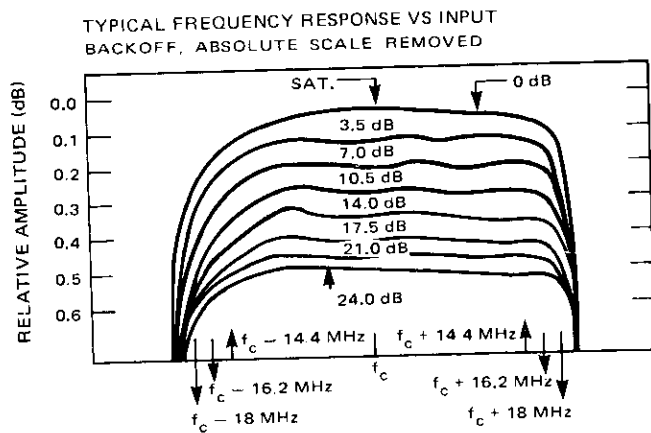


Figure 19. Complete Transponder Frequency Response

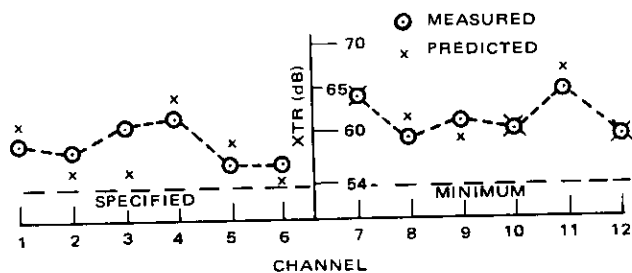


Figure 20. Intelligible Crosstalk Performance

### Despin control subsystem

L. B. RICKS

The despin control subsystem (DCS) is a sampled-data feedback control system which orients the communications payload platform toward the earth while the rotor spins about an axis normal to the orbit plane (in final synchronous orbit). Input data are derived from rotor-mounted sensors and compared with feedback data derived from a master index pulse generator (MIPG). This generator consists of a rotor-mounted coil and two platform shaft-mounted magnets which are separated by 180°. The pulse output rate is therefore twice the platform-to-rotor relative rate ( $2f_z$ ).

Input data are counted up to form a pulse train which is twice the rotor rate ( $2f_s$ ) for comparison with  $2f_z$  signals and generation of error signals. The control system is mechanized so that a null or zero error condition occurs when  $2f_s$  and  $2f_z$  signals are 90° out of phase (see Figure 21).

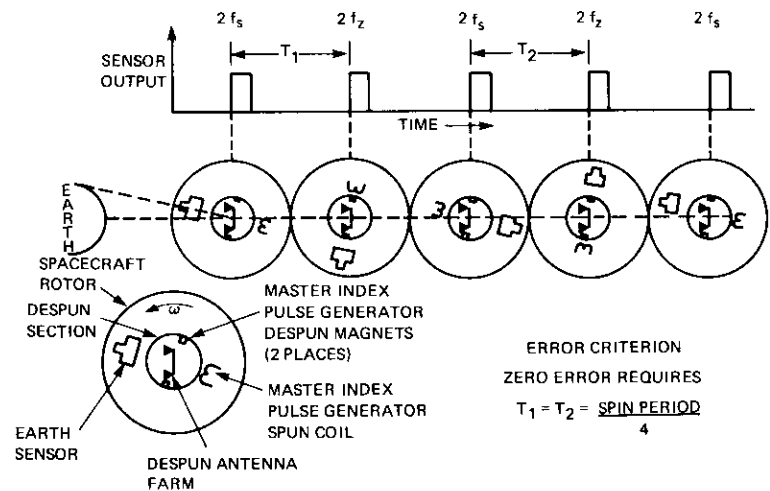


Figure 21. Formation of DCS Error Signal

L. B. Ricks is Manager of the Electronics Department, Space Segment Implementation Division, COMSAT.

Operation of the DCS as a closed-loop system is shown in Figure 22. Four control loops are used: position, rate, friction, and command.

Two complete sets of despinn control electronics (DCE), shown in Figure 23, are provided for redundancy. The various sensor inputs are processed by the sensor electronics to generate uniform digital pulses. Operational mode selection logic permits command selection of the sensor to be used (earth or sun). A time-of-day delay must be used in conjunction with the sun mode as described later. The phase-lock loop (PLL) generates clock signals and  $2f_s$  pulse trains in phase lock with input sensor pulses. Error signals are computed for the four control loops in the torque command generator. These signals are weighted, summed, and modulated to form a suitable input to the motor drive resolver. The resolver output is then demodulated and amplified to drive the motor windings.

**Operational mode**

The DCE is capable of operating in four different modes: earth sensor, sun sensor, pseudo-earth, and rate memory hold. In the earth sensor mode the earth's leading horizon is detected as an input reference. A mechanical bias in MIPG alignment is used to phase  $2f_s$  signals so that the payload compartment is pointing toward the center of the earth when control system null is reached (see Figure 21).

In the sun sensor mode the sun sensor is used as an input reference to generate  $2f_s$  pulses in the phase-lock loop. These pulses are delayed in a sun clock register to coincide with the earth's leading edge. Ground commands are used to establish the sun clock delay according to time of day. Once initially established, this delay is automatically updated every five seconds, and the register operates as a 24-hour clock. Periodic updating by ground command is required because of accumulating differences between a 24-hour day and an actual solar day.

In the pseudo-earth mode, reference input pulses are generated by ground equipment and synchronized to any available rotor-mounted sensor. This mode may be used as an emergency ground control for despinn. In transfer orbit, pseudo-earth pulses are used to establish a suitable inertial platform rate during apogee motor fire. Pseudo-earth pulses are also used to establish a constant  $2f_s$  frequency in rate memory hold mode.

In the rate memory hold mode, external input pulses are removed and the phase-lock loop maintains the last computed output frequency ( $2f_s$ ). The platform is therefore driven at a fixed relative rate determined by the last input frequency. During transfer orbit, rate memory hold is used to

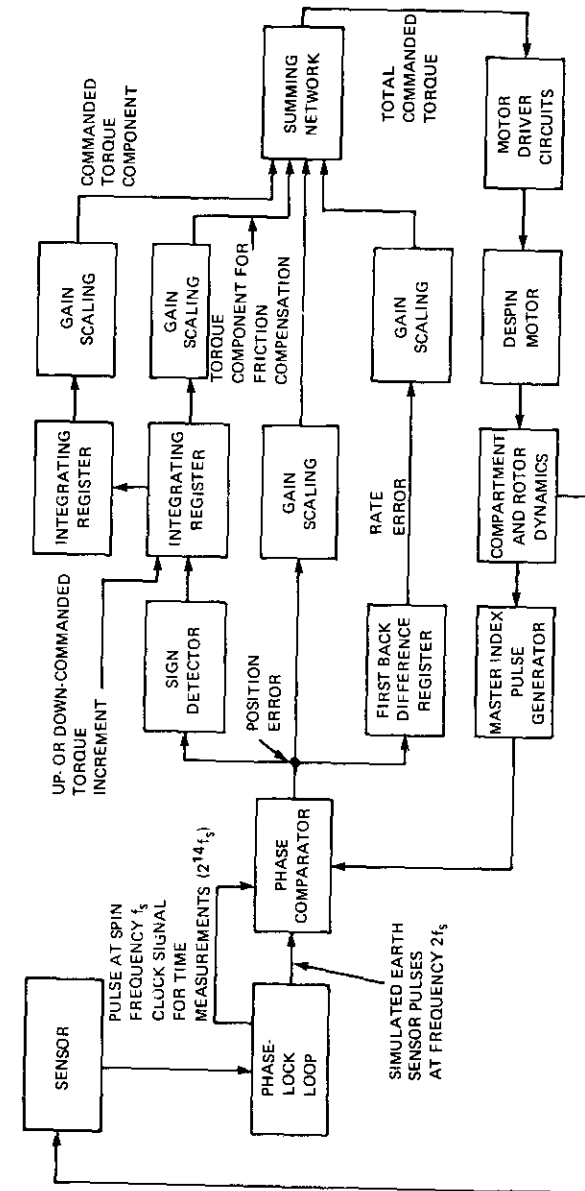


Figure 22. Despin Control Functional Block Diagram

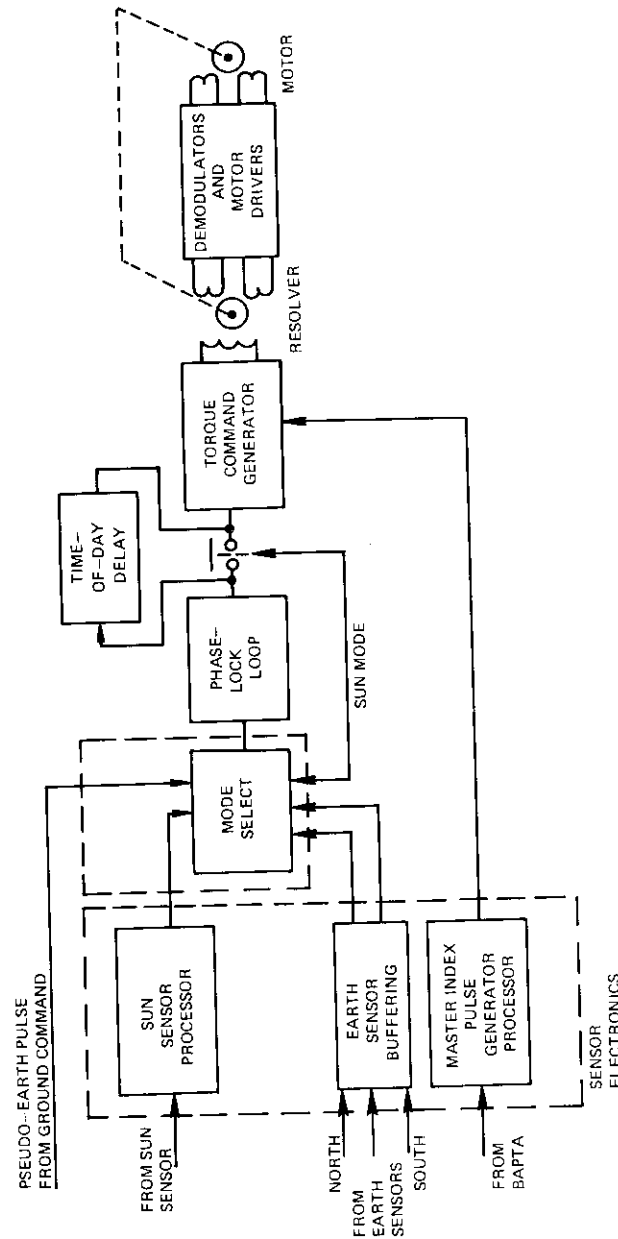


Figure 23. Despin Control Electronics Simplified Block Diagram

maintain an optimum platform inertial rate so that stability can be provided when the satellite is not under ground station surveillance.

### Input sensors

**Earth Sensors.** The earth sensor is a narrow-beam, horizon-crossing indicator which senses radiance in the 14.5- to 15.5-micron region ( $\text{CO}_2$  band). The leading edge pulses are used as a reference for despin control. Leading and trailing edge information is telemetered for attitude determination.

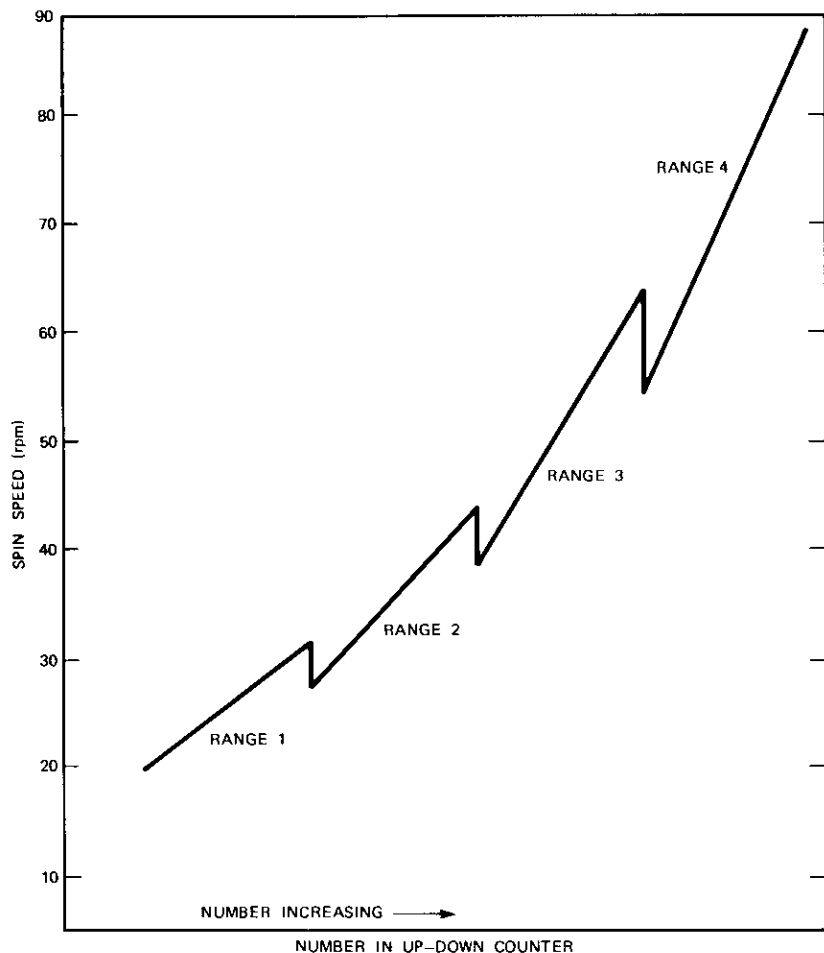
The sensor consists of an optical barrel assembly and a housing containing the electronics. The barrel assembly contains all of the optical elements and the earth detector. Two spectral filters limit the band from 14.5–15.5 microns. The detecting thermistor-bolometer, mounted behind a hemispherical immersion lens, is masked to provide a  $1.5^\circ$  by  $1.5^\circ$  field of view. Temperature compensation of the detector is accomplished by using a matching thermistor which is shielded from incoming infrared energy in a bridge circuit.

The active thermistor changes resistance when energy is absorbed, creating an imbalance in a bridge whose output is capacitively coupled to a preamplifier chain. Subsequent processing circuitry differentiates the detector output and generates positive pulses as the sensor scans from cold space across the earth's leading edge, and negative pulses at the trailing edge. Positive and negative pulses are segregated and threshold detected at 50 percent of their peak values. Hence, variations in the earth radiance level or detector sensitivity are compensated.

Moon discrimination is accomplished by blanking all pulse outputs unless the input persists for longer than 5 milliseconds. Sun interference is eliminated by switching, on ground command, to one of three earth sensors. These sensors are aligned at  $83.8^\circ$ ,  $90^\circ$ , and  $96.2^\circ$  to the spin axis. Since the apparent sun disc has a diameter of  $4^\circ$ , there are at least two sensors available as despin references for all values of sun declination.

**Sun Sensor.** The sun sensor consists of an N/P silicon solar cell, a load resistor, and two housing assemblies which form fan-shaped fields of view. One fan beam describes a plane which contains the spacecraft spin axis. The pulse generated when this beam encounters the sun is used for despin reference and for spin rate determination. The second fan beam is canted at  $35^\circ$  to the first. The rotation angle between the output of the two fan beams as they scan the sun is proportional to the spacecraft sun angle and



Figure 25. Spin Speed vs  $N$ 

proportional to the position error and is transferred into a position register. After it is converted to voltage, the position error is modulated to form a suitable input to the motor driver.

**Rate Error.** Rate error is derived in the torque command generator by determining the change in position error between the current value and the most recent past value. This measurement is accomplished in a ripple

TABLE 3. DESPIN SUBSYSTEM DESIGN PARAMETERS

Performance Characteristics	
Acquisition Time	<15 min
Pointing Accuracy	$\leq 0.16^\circ$ , $3\sigma$
Operational Transients	$\leq 1^\circ$ for 15 s
Spin-Speed Range	40-60 rpm, normal 20-80 rpm, maximum (degraded pointing performance)
Control Loop Parameters	
Position Loop	
Gain*	5.48 N·m (4 ft-lb)/radian
Resolution	0.022°
Data Rate	two samples/revolution
Dynamic Range*	$\pm 0.274$ N·m ( $\pm 0.2$ ft-lb)
Rate Loop	
Gain*	34.3 N·m (25 ft-lb)/ $\Delta$ rad/sample
Resolution	0.022°/sample
Data Rate	two samples/revolution
Dynamic Range*	$\pm 0.84$ N·m ( $\pm 0.615$ ft-lb)/sample
Steady-State Error Corrector (friction torque compensation loop)	
Resolution*	0.00127 N·m (0.00094 ft-lb)/step
Data Rate	one sample/16 revolutions
Dynamic Range*	$\pm 2.27$ N·m ( $\pm 1.66$ ft-lb)
Modes of Operation	sun and earth modes only; inhibited to hold last value in pseudo-earth mode
Command Torque Bias	
Resolution*	0.00127 N·m (0.00094 ft-lb)/step
Dynamic Range*	$\pm 2.27$ N·m ( $\pm 1.66$ ft-lb)

\* Values double for 2-motor-driver operation.

down-counter, which is reset by the previous sample enable received by the up-counter. The value of the previous position error is then entered into the down-counter. During the new sample time, both the down-counter and the up-counter receive and count pulses. If the previous count is the same as the current count, the down-counter reaches a nominal value which corresponds to no rate error, i.e., no change in the phase comparison value of the up-counter. This measurement is then shifted to a rate register,

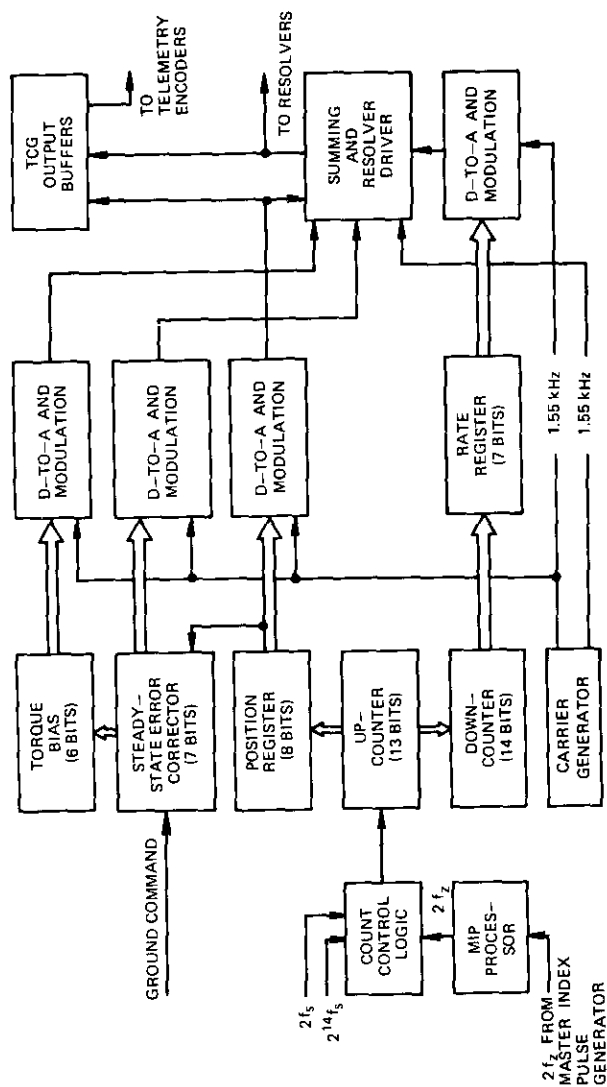


Figure 26. Torque Command Generator

digital-to-analog (D/A) converted, modulated, and summed with the position error.

**Steady-State Error Corrector Counter.** The steady-state error corrector is an up-/down-counter which samples the sign of the position error every 16 spacecraft revolutions. If the sign of the position error remains the same over a period of time, the up-/down-counter is moved backward or forward one count (0.00106 N·m, or 0.00078 ft-lb), depending on the polarity. The accumulated effect of this sampling is to create a torque which nulls pointing error. During steady-state operation, the error corrector will limit cycle plus and minus one count. Updating is disabled in the pseudo-earth mode to provide full control by ground equipment.

**Torque Bias Counter.** The torque bias counter is an up-/down-counter which is shifted forward or backward by ground control through the steady-state error corrector counter. These two counters are actually in series so that the error corrector can automatically control the full dynamic range of torque. (The torque bias counter contains the most significant bits). Torque bias commands are used to initiate the DCE at a nominal friction bias in lieu of slow, automatic update by the error corrector.

Initial loop acquisition causes the despun compartment to point either toward the earth or  $180^\circ$  away from the earth because  $2f_s$  feedback information can satisfy null conditions in two directions. If the system acquires while pointing away from the earth, torque bias commands are used to overpower all loops for a "sector switch."

The contents of the steady-state error corrector counter and the torque bias counter are separately converted from digital to analog, modulated, and summed with position and rate error signals to form a total despun error signal.

#### Motor drive system

The output of the torque command generator is a 1.55-kHz square wave which has a peak value proportional to the magnitude of the total commanded torque (see Figure 27). Relative to a reference generator of the same frequency, the output signal is either in phase or  $180^\circ$  out of phase, depending on the sign of the commanded torque. This modulated 1.55-kHz signal is used to excite the primary winding of the motor resolver.

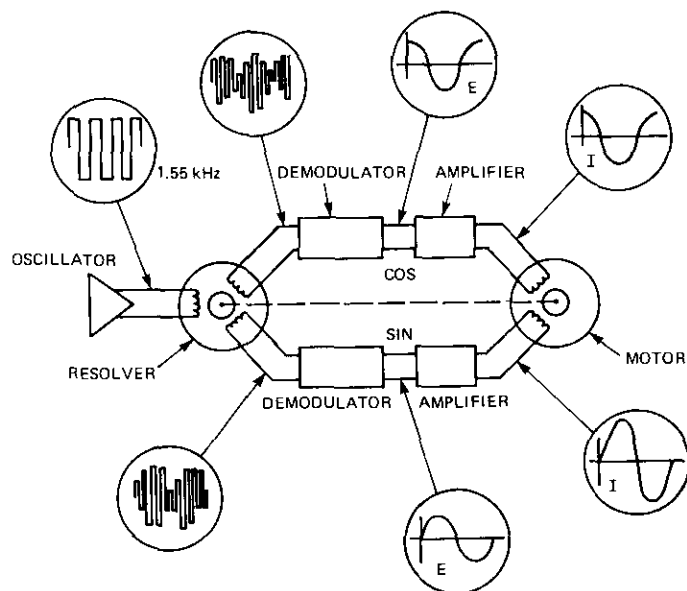


Figure 27. Motor Drive System

The secondary windings of the motor resolver produce a 1.55-kHz output modulated by the sine and cosine of the relative station angle of stator to rotor. Subsequent demodulation of the secondary winding output signal yields a voltage which is proportional to the torque command and varies with the sine or cosine of the rotation angle. The resulting sine and cosine waveforms are the inputs to the motor drivers. Each motor driver consists of two out-of-phase class A amplifiers, each driving one end of a motor coil. One pair (cosine and sine) is driven by the motor drive circuits in a given set of despin control electronics; however, either set of despin control electronics can control either or both motor drive circuits.

The motor is essentially a 2-phase, 16-pole, AC motor which requires in-phase sine and cosine driving voltages to generate the required rotating magnetic field. For the motor to operate as a "brushless DC motor," these voltages must be artificially generated by the resolver as previously described. Figure 28 illustrates the basic despin motor speed and torque characteristics.

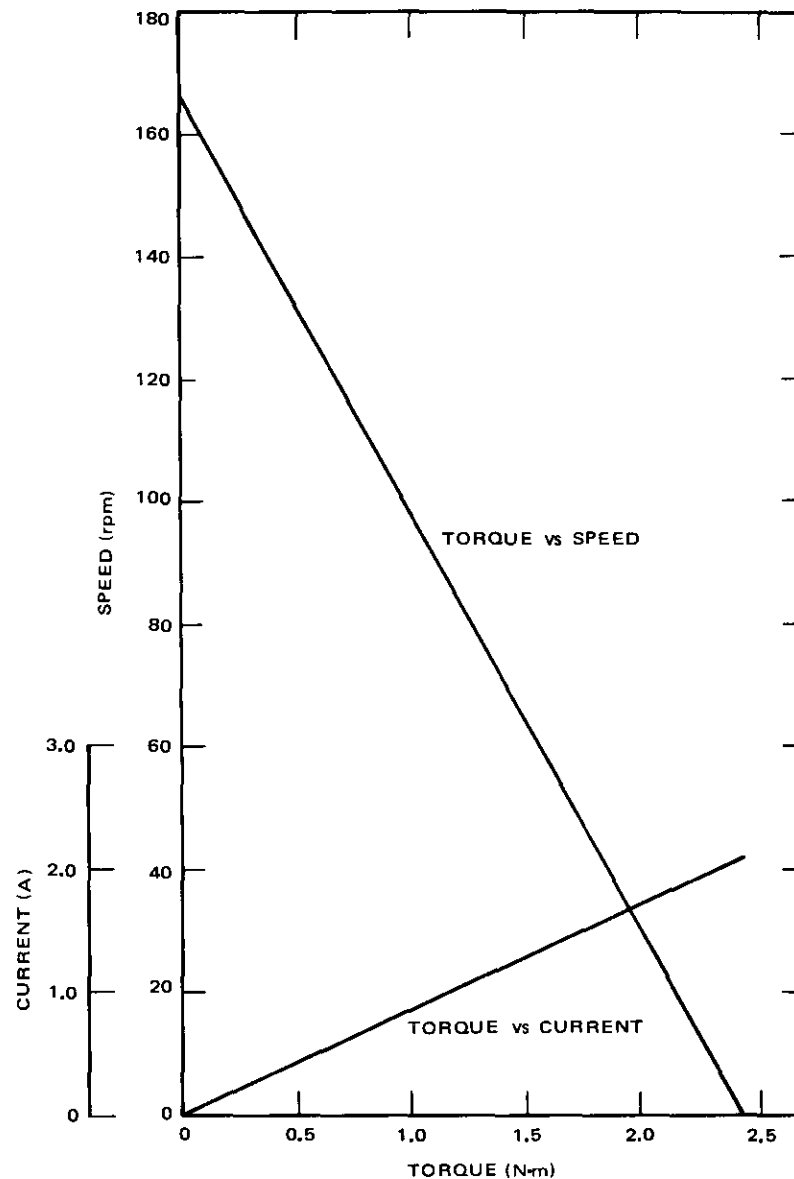


Figure 28. HS 312 Despin Motor Characteristics

### System response

The control parameters of Table 3 resulted from an extensive performance tradeoff under various conditions of input and output (friction) disturbances. Such factors as system response to input noise, friction variations, natural limit-cycle behavior of the control loops, stability, spin changes, and missed and erroneous input pulses were investigated in detail by computer simulation and actual spacecraft test.

Because of the limit-cycle behavior of the control system and because the phase-lock loop is a nonfiltering-type loop, the upper bound on gain is limited by input sensor noise. Figure 29 indicates typical performance in the earth sensor mode with a 3-sigma zero-to-peak jitter of  $0.15^\circ$  in 1- and 2-motor-driver configurations. The corresponding input jitter for the sun sensor is about  $0.03^\circ$  zero-to-peak. The sun mode is used continuously except during eclipse seasons.

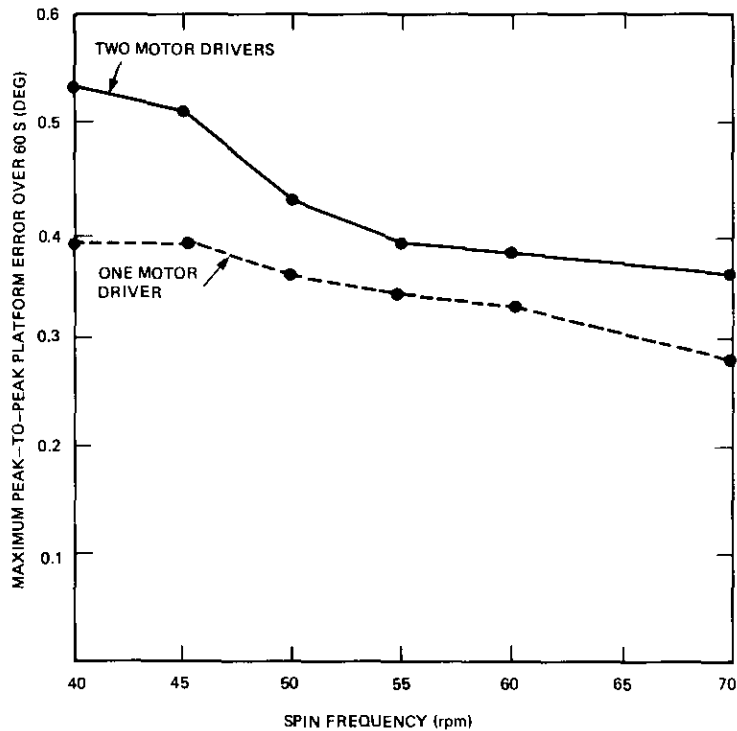


Figure 29. INTELSAT IV DCS Response ( $3\sigma$  noise =  $0.15^\circ$ , zero to peak)

The lower bound on gain is determined by the system response to low-frequency friction variations. The curve of Figure 30 illustrates the control system response to friction changes occurring at various frequencies for 1- and 2-motor-driver operation. Comparison of Figures 29 and 30 reveals the nature of the tradeoff between conflicting performance parameters.

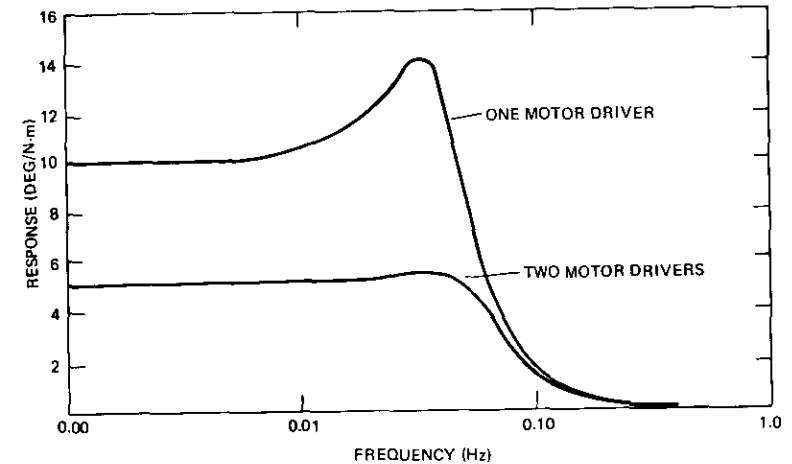


Figure 30. INTELSAT IV DCS Bearing Friction Variation Frequency Response (45 rpm)

### Test verification of performance

The object of the INTELSAT IV test program is to continuously monitor and record DCS parameters to demonstrate long-term performance. Extensive instrumentation is necessary to differentiate between actual DCS behavior and externally caused disturbances. In general, the test program consists of 48 hours of mixed simulation, 96 hours of initial integrated system tests, 16 hours of computer open-loop checks, 120 hours of thermal/vacuum tests, various functional checks, 96 hours of final integrated system tests, 24 hours of prelaunch integrated system tests at Cape Kennedy, and 4 hours of prelaunch computer open-loop checks. These tests will be described briefly in the following paragraphs.

**Mixed Simulation.** In mixed simulation, each flight despin control electronics unit is placed in a thermal chamber and operated as a closed-loop

system with an analog computer and digital interface unit. The analog computer simulates 3-axis dynamics, and the interface unit generates sensor input and master index pulse generator signals. The purpose of this simulation is to compile a complete mission profile including anomalies. Steady-state performance is analyzed for all DCS operational modes over the entire rpm range and under various conditions of friction torque noise and input sensor noise.

Mission profile studies during mixed simulation include the following items:

- a. satellite separation and spin-up;
- b. sector switching;
- c. apogee motor fire;
- d. transient response to various input perturbations such as nutation, missing or erroneous input pulses, and step changes in torque;
- e. flat spin recovery techniques;
- f. jet firing maneuvers; and
- g. various failure mode tests.

The mixed simulation output is a continuous, real-time plot of 8 to 16 variables, depending on the specific test being conducted. A most important feature of these tests is that they make it possible to relate available spacecraft telemetry to dynamic variables, such as platform rate and platform position off-axis rates. This test technique has proven to be an extremely flexible and useful method of evaluating system performance under both normal and abnormal conditions. Agreement with in-orbit performance signatures has been excellent.

**Computer Open-Loop Checks.** The DCE is functionally checked by the system test equipment computer at intervals during the test program when spin table operation is not practicable (for example, before and after vibration tests). The computer forms signals (simulated earth and MIPG pulses) which are used as inputs to DCE test points. The DCE is then commanded to all operational modes to see if the control loops are properly nulled in each case. Operation of the phase-lock loop over its entire rpm range is checked by sweeping with a slow  $2f_s$  frequency ramp while monitoring the position error.

**Integrated Systems Test (IST).** During integrated system tests, a completely assembled spacecraft is mounted on a spin table. To avoid wind effects on the platform, the spinning rotor is enclosed by a wooden structure and separated from the platform by a partial baffle. The platform is

also enclosed by an upper wooden structure to avoid air currents in the test area. The spacecraft is carefully aligned with respect to a heated-plate earth target and a sun target. A scaled target is mounted on the outer rim of the platform so that pointing deviation may be viewed through a theodolite. In addition, a black-to-white vertical transition target is mounted above this scale. This target is aligned to a Physitek optical tracker, which yields a continuous, high-resolution recording of the pointing direction.

The purpose of the DCS integrated systems test is to construct a test matrix of all operational modes at the nominal in-orbit spin speed (51 rpm) while monitoring all available system parameters. The test output consists of the following recorded data:

- a. optical tracker indication of pointing direction and "jitter";
- b. digital-to-analog (D/A) converted waveform of the despin control electronics computed position error (spacecraft telemetry);
- c. D/A converted waveform of the despin control electronics computed total despin torque (spacecraft telemetry);
- d. D/A converted rotor-mounted sensor output pulses;
- e. D/A converted phase-lock loop input flip-flop, which is driven by input sensors (hardline test point);
- f. D/A converted phase-lock loop internal frequency (hardline test point of  $2f_s$ );
- g. analog waveform of each earth sensor's postamplifier output (hardline test point);
- h. voltage waveform of the sine and cosine motor drive signals (hardline test point);
- i. magnetic recording of both PCM streams (spacecraft telemetry);
- j. D/A converted magnetic pickup on the spin table (hardline test point); and
- k. spacecraft bearing accelerometer signal (telemetry).

These data enable test engineers to evaluate system performance in real time and to isolate problems in specific areas of the DCE or test equipment setup. For each mode of operation, the test equipment computer is used to form statistical distributions (histograms) of DCE computed positions to be compared with optical tracker position indications. The total commanded torque is also periodically summed and averaged over a 15-minute sample. The dynamic torque capability of the motor drive system is measured by commanding the torque bias over the full range of the torque bias register while restraining the platform with a calibrated spring.

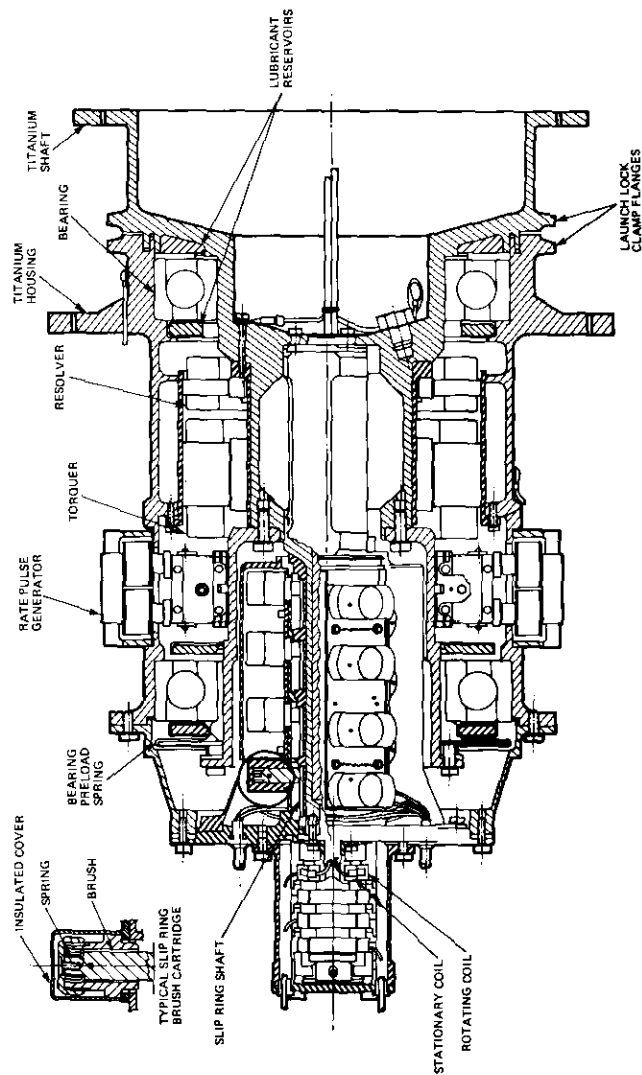


Figure 31. Bearing and Power Transfer Assembly

After the formal matrix of tests has been completed, the DCS is subjected to a "hands off" single mode of despun operation for 24 hours. The purpose of this operation is to establish a quiet environment for demonstration of steady-state "glitch-free" performance.

**Thermal Vacuum Test.** The thermal vacuum instrumentation and test techniques are essentially the same as those used during the integrated system test. A test matrix is established to sample various operational modes for each thermal condition. In addition, the sun clock is checked to determine whether an equivalent  $180^\circ$  rotation occurs in 12 hours, and the input pulses are removed so that the rate memory hold frequency stability can be checked for one hour.

### **Bearing and power transfer assembly**

J. W. OUELLETTE

The bearing and power transfer assembly (BAPTA), shown in Figure 31, forms the rotating interface between the despun, earth-oriented communications platform and the spinning stabilization rotor, which mounts the spinning platform and the solar panels. The 2-piece titanium BAPTA shaft is mounted on the despun platform and the titanium BAPTA housing is supported by an extension of the spinning rotor's thrust cone. Two separable angular contact bearings mounted back to back form the mechanical rotating interface.

Electrical power transfer is achieved through a slip ring assembly with cartridge-type brushes. A 4-channel rotary transformer is employed for telemetry and command signal transfer. Two permanent magnets and two coils are utilized to derive rotational rate information for the DCS. Located between the two bearings is a brushless DC motor whose torquer is driven by the DCS to compensate for mechanical friction losses in the bearings and the slip ring assembly. The motor's resolver furnishes the information required for the electrical commutation performed by the DCS motor drivers. Thermal control is achieved through passive thermal

*J. W. Ouellette is a member of the Technical Staff in the Mechanics Department, Space Segment Implementation Division, COMSAT.*

finishes and active heaters, with thermistors indicating the actual in-flight thermal conditions.

Bearing sizing for this type of application involves numerous considerations, many of which are interactive. The spun and despun sections of the satellite have different thermal configurations, each subject to variations in bulk temperature. Angular contact bearings, with their relatively large diametral internal clearance, were selected to minimize sensitivity to the potential radial gradients.

The effects of the major design constraints on bearing and preload selection are outlined in Table 4. Clearance for the electrical power and signal transfer system, in conjunction with the shaft wall thickness required for structural stability, established the minimum bearing bore.

TABLE 4. BEARING SELECTION FACTORS

Major Design Constraints	Bearing			
	Bore	Outer Diameter	Ball Size and Number	Preload
Geometrical	Established Minimum	—	—	—
Maximized Structural Stability (in-orbit)	Large	Large	—	High
Minimized Cyclic Fatigue	Small	Small	Optimum Ratio	Low*
Minimized Power Consumption	Small	Small	—	Low*

\* Minimum level established by ball grade and "ball skidding" considerations.

Dunkerley's equation indicates the relative dependence of the satellite's first resonant frequency,  $\omega_s$ , upon the fundamental resonant frequencies of the despun platform,  $\omega_\Delta$ , the rotor,  $\omega_p$ , and the BAPTA,  $\omega_\beta$ :

$$\frac{1}{\omega_s^2} \doteq \frac{1}{\omega_\Delta^2} + \frac{1}{\omega_p^2} + \frac{1}{\omega_\beta^2}$$

The nonlinear preload characteristics of the bearings were employed to determine the optimum preload for maintaining the satellite fundamental resonant frequency commensurate with a reasonable in-orbit operating friction torque level. Mounting the bearings in the double-back con-

figuration yielded an effective spacing of 23 cm (9 in.) to further enhance the BAPTA stiffness. Table 5 lists the bearing features.

Bearing noise is minimized by ensuring that raceway brinnelling is minimized during launch. During launch, the bearings are off-loaded by a W clamp, which transfers up to 90 percent of the load directly from the shaft to the housing. Bearing preload is achieved by using a double Belleville spring in a clamped-clamped configuration at the aft bearing. Because of its relatively high radial stiffness without clearance, this configuration prevents viscous damping in the rotor. As a result of the axially sliding surfaces common to coil spring preload systems, this viscous damping effect could have functioned as a satellite dedamper.

TABLE 5. BEARING FEATURES

Type	angular contact ball bearing with a separable outer race
Material	440C CRES, CEVM
Bore	90 mm
Outer Diameter	140 mm
Width	24 mm
Dimensional Tolerances	ABEC* 7
Number of Balls	16
Ball Diameter	15 mm (19/32 inch)
Ball Grade	10
Nominal Curvature	
Inner Race	52.0 percent
Outer Race	52.5 percent
Diametral Internal Clearance	0.13 ± 0.01 mm
Nominal Contact Angle	24° - 26°
Retainer Design	single piece, ball riding
Retainer Material	cotton base, phenolic laminate with a 2- to 4-percent oil absorptivity

\* ABEC is the Annular Bearing Engineering Committee of the Anti-Friction Bearing Manufacturing Association, Inc.

Instead of a positive seal, a labyrinth seal was selected for the dynamic interface between the BAPTA shaft and housing. The amount of bearing

lubricant was determined by multiplying the lubricant loss rate resulting from evaporation by a liberal design factor.

At the steady-state in-orbit operational environment, lubricant depletion occurs in the molecular flow regime. The fundamental relationship may be expressed as

$$Q = \frac{4E(P_2 - P_1)}{3f_s(q_1, q_2, q_3)}$$

where  $E = (8kT/\pi m)^{1/2}$

$Q \triangleq$  molecular flow rate

$P_j \triangleq$  pressure at boundary  $j$

$f_s(q_1, q_2, q_3) \triangleq$  molecular flow impedance factor dependent upon orifice geometry

$k \triangleq$  Boltzmann's constant

$T \triangleq$  absolute temperature

$m \triangleq$  mass of molecule.

The overall molecular flow system can be modeled as shown in Figure 32 to include the lubricant impregnated reservoirs and bearing retainers at the molecular lubricant sources. The impedances,  $z_i$ , represent the BAP-TA's internal geometrical configuration with the labyrinth seal as the load

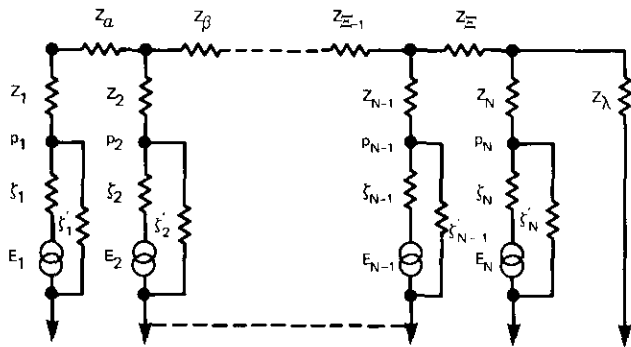


Figure 32. Molecular Flow Equivalent Circuit Method

impedance,  $z_\lambda$ . The lubricant sources and their internal impedances are represented by  $E_i$  and  $\zeta_i$ , respectively, in Figure 32. Conservative calculations, which disregarded the lubricant reservoir's contributions, predicted the Ball Brothers Research Corporation's Vac-Kote lubricant depletion period profile shown in Figure 33.

The slip-ring assembly consists of four coin-silver rings, each having an outside diameter of 2.54 cm (1 in.), mounted in tandem. Three wires are connected to each ring, and three individual brush assemblies, located

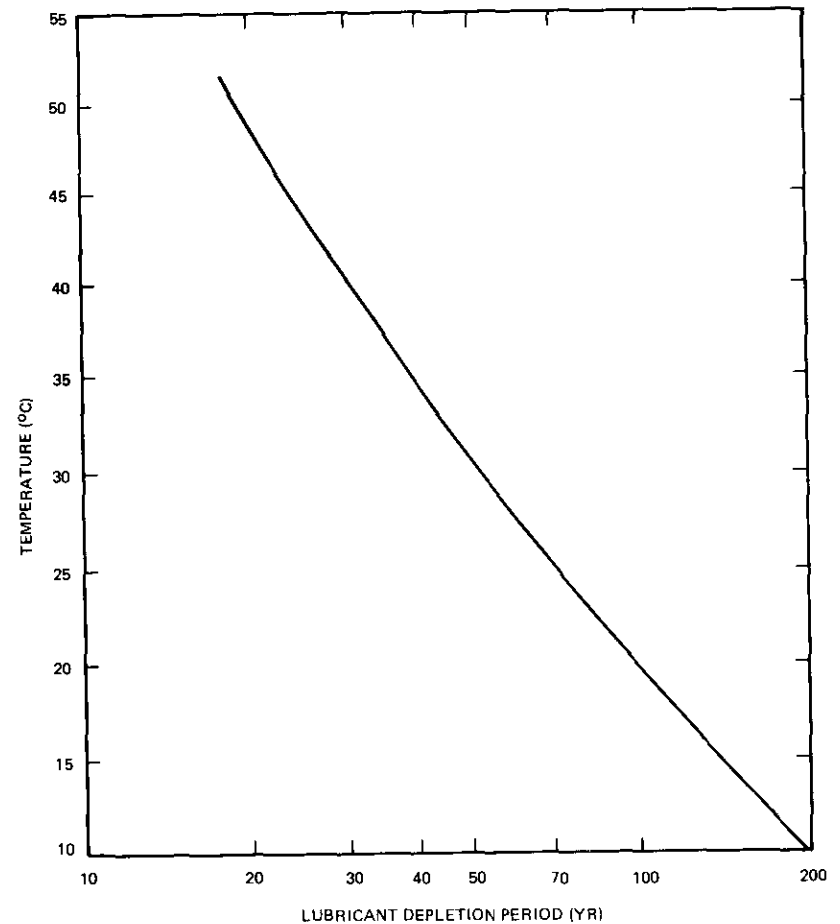


Figure 33. Lubricant Depletion Period Profile

120° apart, are in contact with each ring. Figure 34 is an electrical schematic of this configuration, and the design parameters are outlined in Table 6.

TABLE 6. SLIP RING DESIGN PARAMETERS

Rated Current Capacity	7.5 A/ring
Electrical Noise	<20 mV
Number of Brushes	12 (3 per ring)
Number of Rings	4
Number of Brush Tracks	12 (3 per ring)
Brush Size (contact surface)	0.508 cm × 0.635 cm = 0.323 cm <sup>2</sup>
Brush Force	0.588 N
Brush Current Density	7.75 A/cm <sup>2</sup>
Rated Brush Current Capacity	2.5 A
Useful Brush Length	3.81 mm including 3.3 safety factor
Brush Material	Stackpole SM-476 (85-percent Ag, 3-percent C, 12-percent MoS <sub>2</sub> )
Ring Material	coin silver (90-percent Ag, 10-percent Cu) MIL-S-13282, grade C, temp 6 full hard
Insulation Material	plastic laminate (epoxy-glass fiber) L-P-509, type IV, grade G-10

The brush holders, constructed of yellow brass, are cartridge-type holders. Brush pressure is maintained by compression springs, which are held in place with a threaded brass cap acting as the spring backup plate. The upper half of the brush holder is then covered with a plastic cover for insulation and debris management. The brush holders are mounted on three insulated plates, each containing four brushes. The plates are attached to a machined hexagonal aluminum rotating housing.

A labyrinth seal and barrier system between the ring and housing is incorporated for physical brush debris control. All metal surfaces of the slip ring housing are covered with a conformal coating to enhance electrical isolation.

The rotary transformer consists of four channels: two to transmit multiplexed signals from the spinning to the despun encoders, and two to transmit commands from the command receivers to the spinning decoders.

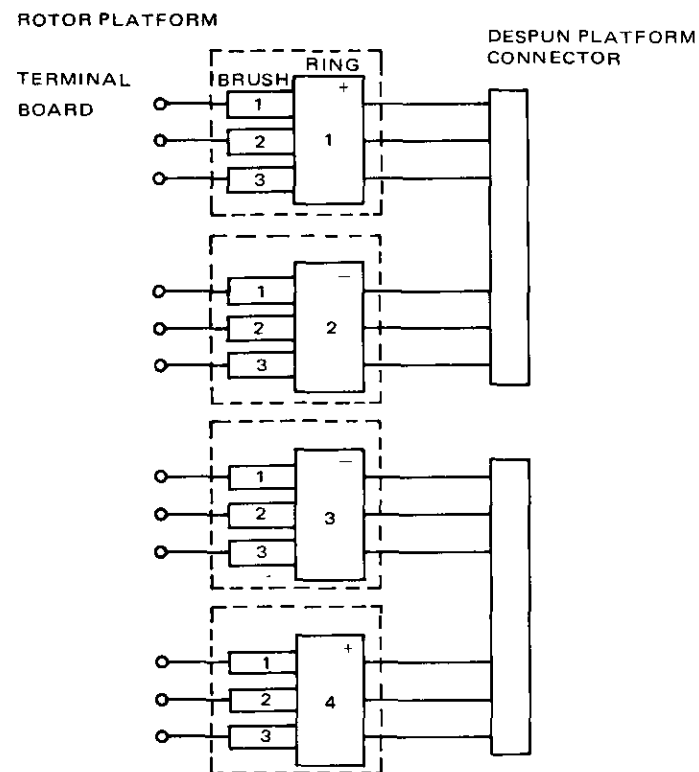


Figure 34. Slip Ring Electrical Schematic

Both rotor and stator portions of the transformer utilize ferrite cores with wound coils. Each channel has a closely matched pair of ferrite cores for the rotor and stator windings. Signal transfer is independent of shaft position, speed, and direction. Figure 35 is a sectional view of the transformer and Figure 36 is an electrical schematic.

To meet efficiency and low-noise requirements, the gap between stator and rotor must be small. Hence, it is necessary to maintain close dimensional control of the ferrite cores. An air gap of 0.254 mm (0.010 in.) allows a radial misalignment and eccentricity of 0.127 mm (0.005 in.) without degrading the signal. An axial overlap of pole faces allows  $\pm 0.38$ -mm ( $\pm 0.015$ -in.) axial movement without changing the magnetic characteristics. As indicated in Figure 35, teflon bumpers are provided at aft and

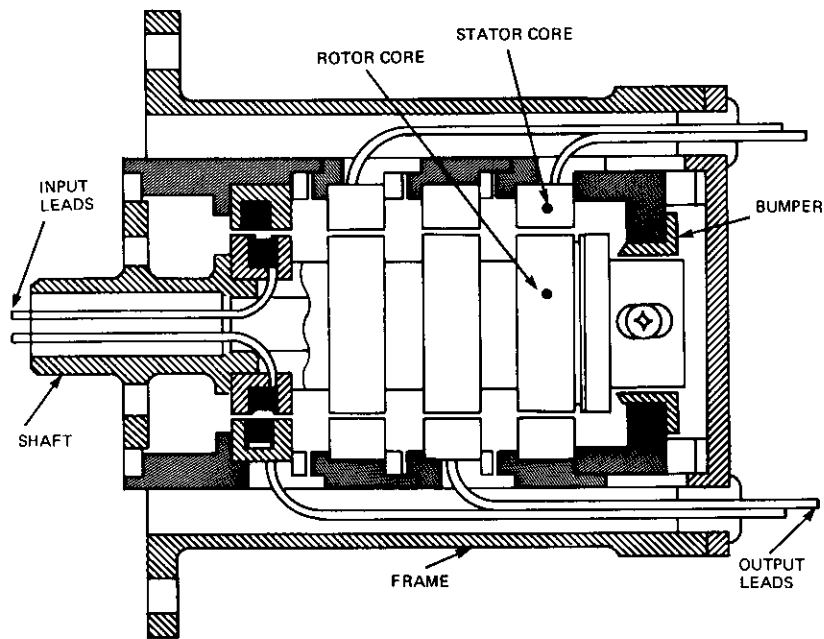


Figure 35. Rotary Transformer Sectional View

forward ends of the rotary transformer to prevent contact between cores during spacecraft vibration.

The transformer characteristics are summarized in Table 7. A typical frequency versus gain transmission profile is shown in Figure 37.

TABLE 7. ROTARY TRANSFORMER CHARACTERISTICS

Peak Signal Level	15 V peak-to-peak
Signal Source Impedance	300 $\Omega$
Load Impedance	4,000-6,000 $\Omega$
Harmonic Distortion	0.1 percent above 10 kHz
Signal Isolation	-45 dB, 5-50 kHz
Number of Turns	400
Winding	no. 40 AWG
Core Material	Ferrite

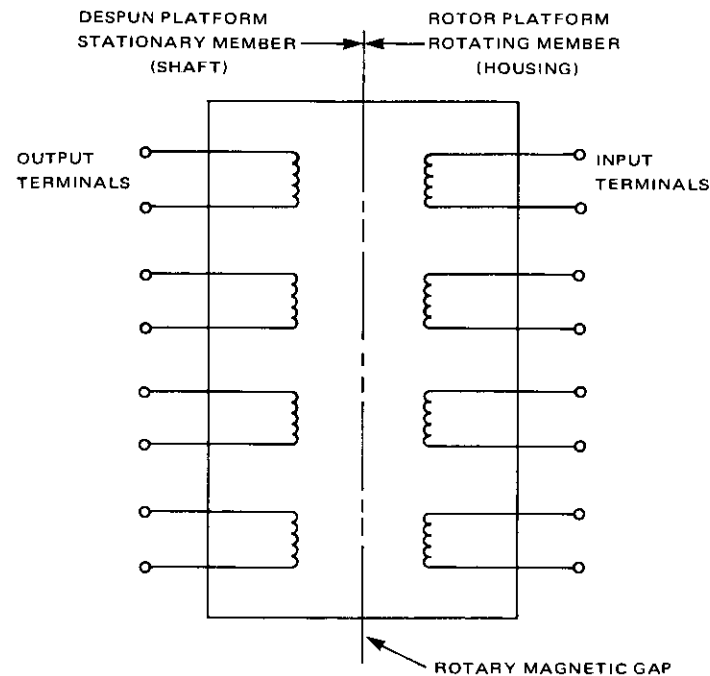


Figure 36. Rotary Transformer Electrical Schematic

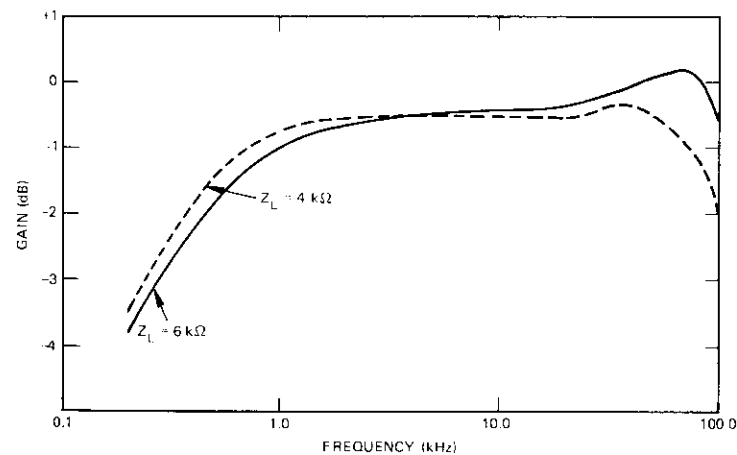


Figure 37. Typical Rotary Transformer Gain/Frequency Response

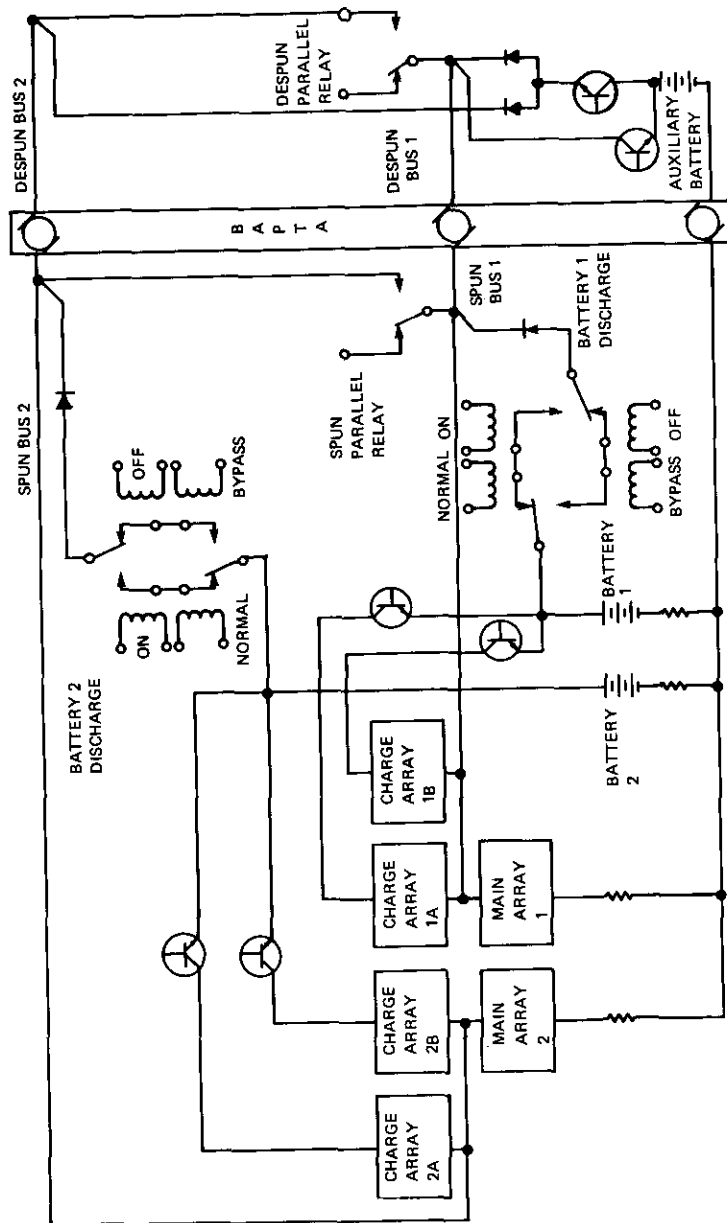


Figure 38. Electrical Power Subsystem Block Diagram

## Electrical power subsystem

F. S. OSUGI

The INTELSAT IV power subsystem consists of two cylindrical solar panels, two 25-cell nickel-cadmium batteries, a battery controller, two commandable relays for bus paralleling, an auxiliary battery, and miscellaneous commandable switches for heater and valve control. Its performance requirements are shown in Table 8. It is a positive-polarity, 2-bus system, in which each bus powers approximately one-half of the spacecraft load. Although buses are designed to operate independently over the total spacecraft operating life, bus paralleling relays are provided for unexpected operating modes.

Each main panel is conservatively designed to provide approximately 200 watts to the load and 25 additional watts for battery charging after seven years in orbit. An additional 14 watts of power is provided on each panel's charge array to boost the main bus voltage sufficiently to charge the 25-cell battery.

Battery operation is designed to be semiautomatic. Low bus voltage causes the battery to be automatically connected to the bus. A command is required to disconnect the battery from the bus. Each battery has two charge arrays and each array is commandable individually.

### System configuration

Figure 38 shows the power subsystem configuration. The subsystem consists of two spinning solar panels termed main array 1 and main array 2. Each main array forms a spacecraft bus, the negative panel terminal connected through a shunt. There are two separate temperature monitors on each panel. Power is supplied from each panel directly to the loads on the spinning section and through slip rings to the loads on the despun section.

*F. S. Osugi is Manager of the Electric Power Branch, Space Segment Implementation Division, COMSAT.*

TABLE 8. INTELSAT IV POWER SUBSYSTEM REQUIREMENTS

Parameter	Performance Requirement
<b>Solar Panel Bus</b>	
Number of Buses	2
Polarity	positive
Output Voltage at Combined Output ≥ 397.1 W	23.8 V
Maximum Voltage When Emerging from Eclipse	48.0 V
Paralleling of Buses	paralleled or unparalleled by com- mand on either side of slip rings
<b>Battery Discharge to Each Solar Panel Bus</b>	
Set Point for Automatic Discharge Turn-On	24.1 ± 0.15 V
Voltage Transient on Battery Turn-On	+10-V maximum step change
Discharge Turn-Off	by ground command
<b>Total Output Current (both batteries)</b>	
Minimum Bus Voltage During 1.2-hr Bat- tery Discharge	15.2 A
Discharge Command	24.1 V
	battery discharge ON/OFF
<b>Battery Charge</b>	
Battery Charge Current at End of 7 Years	1.0 A per battery (1.45 A max)
Battery Charge Command	
2/3 Charge Array	one ON command per battery
1/3 Charge Array	one ON command per battery
All Charge Arrays	one OFF command per battery
<b>Battery Reconditioning</b>	
Nominal Discharge Current	0.25 A
Command	ON/OFF for each battery
<b>Auxiliary Battery</b>	
Voltage	maintain voltage above 21.3 V into a continuous load of 1.4 A for 0.7 hr or 5.0 A for 30 s
<b>Telemetry Shunts</b>	
Rating	20 A (200-mV output)
Number Provided	6

Charge arrays designated 1a, 1b, 2a, and 2b are connected as shown through commandable switches to the batteries. The charge arrays for each battery have current ratings in a one-to-two ratio so that one-third, two-thirds, or three-thirds of the available charge current may be selected.

The outputs of the charge arrays, main arrays, and battery are all connected to the battery controller. Controls for both batteries are located in a single electronics assembly. This assembly includes commandable switches for selecting the desired charge current and power relays for connecting the battery to the bus. These power relays can be opened or closed on command and closed automatically when the bus voltage drops below the set point. Commandable reconditioning switches are also located inside the battery controllers; the power resistors in series with them are mounted to the spacecraft on the outside of the controller assembly. Two commandable relay assemblies, which are used to parallel the buses, are provided, one on each side of the slip ring assembly. This arrangement permits cross-connection of loads and buses in the event of slip ring failure.

An auxiliary battery assembly on the despun section ensures that continuous power will be provided to critical loads located on the despun section during launch. Momentary loss of power caused by slip ring vibration or relay chatter cannot be tolerated. The auxiliary battery charges from one bus and discharges to both buses. After final orbit is achieved, the auxiliary battery is no longer needed.

Spacecraft power is distributed through redundant wiring via two separate buses. The spinning and despun grounds are structurally isolated at the BAPTA to prevent current flow through its bearings. Spacecraft power users (e.g., communications and telemetry and command subsystems) provide their own regulators and converters. All spacecraft units provide overload protection (in case of component failure) in the form of active current limiting, current limiting resistors, fusing resistors, or filament fuses.

#### Bus voltage performance

The bus voltage varies between the upper voltage limit (48 volts), determined by the cold solar panel emerging from eclipse, and the lower limit (23.8 volts) of the battery discharge control set point. When the discharge control set point is reached, the fully charged battery is switched directly to the bus. This places a step voltage increase of up to 10 volts on the bus. All spacecraft power-using systems have been designed to accept this bus transient. However, for conservative operation (e.g., to minimize the transient effect), it has been elected to manually control battery turn-on

during the eclipse season. This is done by commanding the battery on just before eclipse is entered and before the panel voltage decreases to the automatic set point.

### Power requirements

A summary of power requirements is presented in Table 9. With the exception of the P&O heaters, the continuous loads (excluding battery charging) require an essentially constant current over the operating range of 24.2 to 48 volts. The normal bus voltage range is 24.2 to 33 volts (except for post-eclipse transients). Each TWT in the communications repeater has a redundant unit on the same bus.

TABLE 9. SPACECRAFT LOAD SUMMARY <sup>a</sup>

a. Continuous Load			
Load	Bus 1 (mA)	Bus 2 (mA)	Both Buses (mA)
<b>Communications</b>			
TWT Group 1 (six odd channels) <sup>b</sup>	5,900		5,900
TWT Group 2 (six even channels) <sup>b</sup>		5,900	5,900
Receiver 1 <sup>b</sup>	— <sup>c</sup>		
Receiver 2 <sup>b</sup>	— <sup>c</sup>		
Receiver 3 <sup>b</sup>		660	660
Receiver 4 <sup>b</sup>		— <sup>c</sup>	
			<i>Subtotal</i>
			12,460
<b>Telemetry and Command</b>			
Spinning Encoder 1 <sup>b</sup>	— <sup>c</sup>		
Spinning Encoder 2 <sup>b</sup>		140	140
Spinning Decoder 1	40		40
Spinning Decoder 2		40	40
Despun Encoder 1 <sup>b</sup>	— <sup>c</sup>		
Despun Encoder 2 <sup>b</sup>		95	95
Despun Decoder 1	36		36
Despun Decoder 2		36	36
Command Receiver 1	50		50
Command Receiver 2		50	50
Beacon Transmitter 1	90		90
Beacon Transmitter 2		90	90
			<i>Subtotal</i>
			667

TABLE 9. SPACECRAFT LOAD SUMMARY <sup>a</sup> (continued)

a. Continuous Load (Continued)			
Load	Bus 1 (mA)	Bus 2 (mA)	Both Buses (mA)
<b>Attitude Control</b>			
Earth Sensors 1, 2, 3	38	76	114
Despin Electronics 1 <sup>b</sup>	240		240
Despin Electronics 2 <sup>b</sup>		— <sup>c</sup>	
Despin Motor Drive 1 <sup>b,d</sup>	250		250
Despin Motor Drive 2 <sup>b</sup>		— <sup>c</sup>	
BAPTA Heater 1	215		215
BAPTA Heater 2 <sup>b,e</sup>			
BAPTA Heater 3 <sup>b,e</sup>			
			<i>Subtotal</i>
			819
<b>Miscellaneous</b>			
P&O Heaters <sup>b</sup>	210	245	455
Power Control Electronics	10	10	20
Pressure Transducers 1, 2	5	5	10
			<i>Subtotal</i>
			485
<b>TOTAL (excluding battery charge)</b>			
	7,084	7,347	14,431
<b>Battery Charge</b>			
7-Year Equinox <sup>b</sup>	1,000	1,000	2,000
7-Year Solstice <sup>b</sup>	333	333	666
<b>b. Intermittent Load <sup>b</sup></b>			
Load	Bus 1 (mA)	Bus 2 (mA)	
Antenna Position Motor	2,500		
Spin-Up Latch Valve	1,700	1,700	
Axial Jet	600	600	
Radial Jet	600	600	
Spin-Up Jet	600	600	
Accelerometer	40	40	

TABLE 9. SPACECRAFT LOAD SUMMARY <sup>a</sup> (continued)

b. Intermittent Load <sup>b</sup> (continued)		
Load	Bus 1 (mA)	Bus 2 (mA)
Despin Motor (max. torque)	1,000	1,000
Auxiliary Battery Charge	150	
Cross-Connect Valve		4,500
Apogee Motor Heater 1 <sup>c</sup>	480	
Apogee Motor Heater 2		480
Apogee Motor Heater 3	620	
Apogee Motor Heater 4		620
Squibs <sup>e</sup>		
BAPTA	16,000	16,000
Apogee Motor <sup>b</sup>	8,000	8,000

<sup>a</sup> All values are at 24.2-volt bus except as noted.  
<sup>b</sup> Command controlled.  
<sup>c</sup> Redundant unit.  
<sup>d</sup> Nominal torque = 9.41 cm/kg (0.14 ft/lb); with both motor drivers on, an additional 1.8 A can be delivered to the motor.  
<sup>e</sup> Heaters can be used when required.  
<sup>f</sup> 31 VDC.  
<sup>g</sup> 28 VDC.

Spacecraft power requirements during the launch phase are typically 2.8 amperes on bus 1 and 2.5 amperes on bus 2. These loads will be supplied by the batteries during the period between 20 minutes prior to lift-off and emergence into sunlight, i.e., typically a total of 40 minutes. Each of the two batteries will be fully charged with a usable capacity of 18 ampere-hours, which will easily satisfy the 1.9- and 1.7-ampere-hour requirements for buses 1 and 2. If brush/slip ring chatter should occur, the auxiliary battery will supply current to the despin loads during the interrupt period.

Table 10 is a summary of the solar panel and battery power and ampere-hour margins, showing the impact of utilizing all BAPTA heaters and accommodating increased despin motor torque.

TABLE 10. POWER MARGIN ANALYSIS

a. Comparison of Load Currents with and without BAPTA Heaters and Increased Despin Motor Torque			
	Load Current (mA)		
	Equinox, Both Buses	Battery	Summer Solstice, Both Buses
	Solar Panel	Battery	Solar Panel
Normal Operation			
Total Continuous Load	14,431	14,431	14,431
Battery Charge	2,000		666
<b>TOTAL</b>	<b>16,431</b>	<b>14,431</b>	<b>15,097</b>
Use of All BAPTA Heaters and Increased Despin Motor Torque			
Total Continuous Load	14,431	14,431	14,431
Battery Charge	2,000		666
BAPTA Heater 2	215	215	215
BAPTA Heater 3 <sup>a</sup>	515	515	515
Despin Motor	500	500	500
<b>TOTAL</b>	<b>17,661</b>	<b>15,661</b>	<b>15,812</b>
b. Comparison of Power Margins with and without BAPTA Heaters and Increased Despin Motor Torque			
	Equinox, Both Buses	Summer Solstice, Both Buses	
Solar Panel			
Normal Operation			
Load Current (mA)	16,431	15,097	
Load Power at 24.2 V (W)	398	365	
Available Power at 24.2 V <sup>b</sup>	502	454	
After 7 Years (W)			
Margin (%)	26.1	24.4	

TABLE 10. POWER MARGIN ANALYSIS (continued)

b. Comparison of Power Margins with and without BAPTA Heaters and Increased Despin Motor Torque (continued)		
	Equinox, Both Buses	Summer Solstice, Both Buses
Use of All BAPTA Heaters and Increased Despin Motor Torque <sup>a</sup>		
Load Current (mA)	17,661	15,812
Load Power at 24.2 V (W)	427	383
Available Power at 24.2 V <sup>b</sup> After 7 Years (W)	502	454
Margin (%)	17.6	18.5
Battery		
Normal Operation		
Load Current (mA)	14,431	
Max. Eclipse Capacity (Ahr)	17.3	
Max. Capacity (Ahr)	36	
Depth of Discharge (%)	48	
Use of All BAPTA Heaters and Increased Despin Motor Torque <sup>a</sup>		
Load Current (mA)	15,561	
Max. Eclipse Capacity (Ahr)	18.8	
Max. Capacity (Ahr)	36	
Depth of Discharge (%)	52.2	

<sup>a</sup> BAPTA heater 3 is used only for eclipse season operation.  
<sup>b</sup> Based on predicted and measured values shown in Table 9.

**Solar panel**

**Design Features.** The design features of the solar panel are shown in Table 11. A typical solar panel sector is illustrated in Figure 39.

Cells are mounted on a cylindrical 1.90-cm (3/4-in.), fiberglass-faced aluminum honeycomb substrate. They are presoldered in 3 × 64 cell arrays (main arrays) and in smaller groupings for charge arrays. The presoldered arrays are bonded to the panel, one sector at a time, by using an epoxy adhesive. A vacuum bag is used to apply a small uniform pressure (0.07–0.14 kg/cm<sup>2</sup> or 1–2 psi) during a 3-hour cure at 65.5°C (150°F). Heater blankets are used to maintain the proper temperature.

Cells are of the zero gap configuration, and all silicon surfaces except

TABLE 11. SOLAR PANEL CONFIGURATION DATA

<b>Solar Panels</b>	
Number of Panels	2
Geometric Shape	cylindrical
Diameter	237.5 cm (93.5 in.)
Length	137.2 cm/panel (54 in./panel)
Weight per Panel	
Substrate	17.05 kg (37.6 lb)
Cells, Wire, Diodes, Connector, etc.	18.96 kg (41.8 lb)
	36.01 kg (79.4 lb)
<b>Solar Cells</b>	
Type of Cell	2- × 2-cm (1.27- × 1.27-in.) N/P silicon
Coverglass Thickness	0.030 cm (0.012 in.)
Nominal Cell Thickness	0.033 cm (0.013 in.)
Cell Vendor	Heliotek, TFK, SAT, Ferranti
Nominal Resistivity	10 Ω/cm
<b>Main Arrays</b>	
Number of Sectors per Panel	11
Number of Arrays per Sector	10
Number of Cells in Parallel per Array	3
Total Cells in Parallel per Sector	30
Total Cells in Parallel per Panel	330
Number of Cells in Series per Array	64
Number of Main Array Cells per Panel	21,120
<b>Battery Charge Arrays</b>	
Number of Sectors per Panel	11
Number of Arrays per Sector	3
Number of Cells in Parallel per Array	1
Total Cells in Parallel per Sector	3
Total Cells in Parallel per Panel	33
Number of Cells in Series per Array	42
Number of Charge Array Cells per Panel	1,386
Total Cells per Spacecraft	45,812

the bus bar are protected by the cover slide. Bus bar protection is afforded by the normal solder coating. Variations in the solder thicknesses of cells provided by the four manufacturers result in slightly differing protection from losses caused by low-energy protons. However, all cells are sufficiently protected to meet end-of-life power requirements.

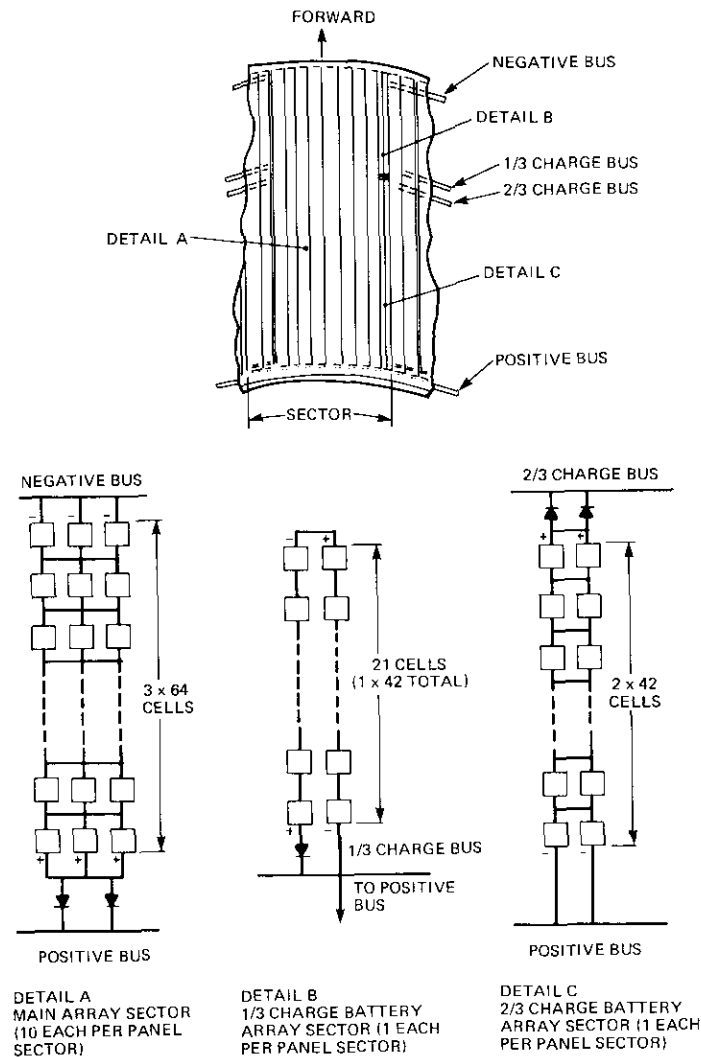


Figure 39. Typical Solar Panel Sector (forward)

The power prediction factors initially used to predict panel performance are shown in Table 12. These prediction factors were used to design the panel. As flight arrays and panels were fabricated, final panel acceptance data were used to upgrade the prediction factors and to demonstrate

adequate panel performance. The use of measured values instead of the initial prediction factors is indicated in the table.

TABLE 12. INTELSAT IV PANEL PERFORMANCE

Performance Parameter	Value
Normal Incidence per Covered Solar Cell Procurement Specification PS 30660-080 <sup>a</sup>	$V_m = 0.445 \text{ V}$ , $I_m = 0.125 \text{ A}$ at $139.6 \text{ mW/cm}^2 \text{ AMO}$ , $25^\circ\text{C}$ ( $I_{sc}/I_m = 1.13$ , $V_{oc}/V_m = 1.258$ )
Temperatures (bulk nominal temperatures plus $5.5^\circ\text{C}$ )	
Summer Solstice	$21.0^\circ\text{C}$
Equinox	$29.5^\circ\text{C}$
Winter Solstice	$25.5^\circ\text{C}$
Temperature Coefficients	$fI_{sc} = +107.25 \mu\text{A}/^\circ\text{C}$ , <sup>a</sup> $fI_m = -184.04 \mu\text{A}/^\circ\text{C}$ , <sup>a</sup> $fV_m = -2.1 \text{ mV}/^\circ\text{C}$ , <sup>a</sup> $fV_{oc} = -2.25 \text{ mV}/^\circ\text{C}$ , <sup>a</sup>
Fabrication Loss Factors	$fI_{sc} = 0.95$ , <sup>a</sup> $fI_m = 0.95$ , <sup>a</sup> $fV_m = 0.979$ , <sup>a</sup> $fV_{oc} = 0.979$ , <sup>a</sup>
Radiation Degradation Factors (7 years)	$fI_{sc} = 0.883$ , $fI_m = 0.883$ , $fV_m = 0.93$ , $fV_{oc} = 0.93$
Transmission Loss Allowance	$fI_{sc} = 0.925$ , <sup>b</sup> $fI_m = 0.925$ , <sup>b</sup>
Instrumentation Error Allowance	$fI_{sc} = 0.99$ , $fI_m = 0.99$ , $fV_m = 0.99$ , $fV_{oc} = 0.99$
Intensity Factors Associated with Each Season	
Summer Solstice	0.8774
Equinox	1.0
Winter Solstice	0.9480
Geometry Factors	
Parallel Main	$fI_{sc}$ and $fI_m = 660 \text{ cells}$
Series Main	$fV_m$ and $fV_{oc} = 64 \text{ cells}$
Parallel Battery Charge	$fI_{sc}$ and $fI_m = 66 \text{ cells}$
Series Battery Charge	$fV_m$ and $fV_{oc} = 42 \text{ cells}$
Curvature Loss Factors and Diode Internal Wiring Drop Factors (worst cases assumed)	$fI_{sc} = 0.94$ , <sup>c</sup> $fI_m = 0.94$ , <sup>c</sup> $fV_m = 1 \text{ V effective}$ , <sup>a</sup> $fV_{oc} = 1 \text{ V effective}$ , <sup>a</sup>
<sup>a</sup> Measured value of $fI_m = 0.98$	
<sup>b</sup> Considered $3\sigma$ values.	
<sup>c</sup> Actual measured values ranged from 0.96 to 0.98.	

The power predictions for the INTELSAT IV panels are based on measurements taken on the Hughes pulsed xenon illuminator. Briefly, the illuminator system measures the output of diode-isolated  $3 \times 64$  cell arrays during a flash of illumination lasting approximately one millisecond. The intensity of the light at the test plane is approximately equal to one sun, and the light spectrum approximates sunlight. No filtering is required to achieve this spectrum.

The features added for this application permit a load sweeping plot of a complete EI curve (16 points) during each 1-millisecond flash and storage and recording of the data. The recorded data can be fed directly into a computer program for complete panel prediction. The original system permitted read out of only one data point per light flash, manual read out and recording of sample-and-hold circuits, and manual card punching for computer input. Figure 40 shows a good correlation between flight data and pulsed xenon predicted data.

#### Battery

The battery configuration data are given in Table 13. During spacecraft

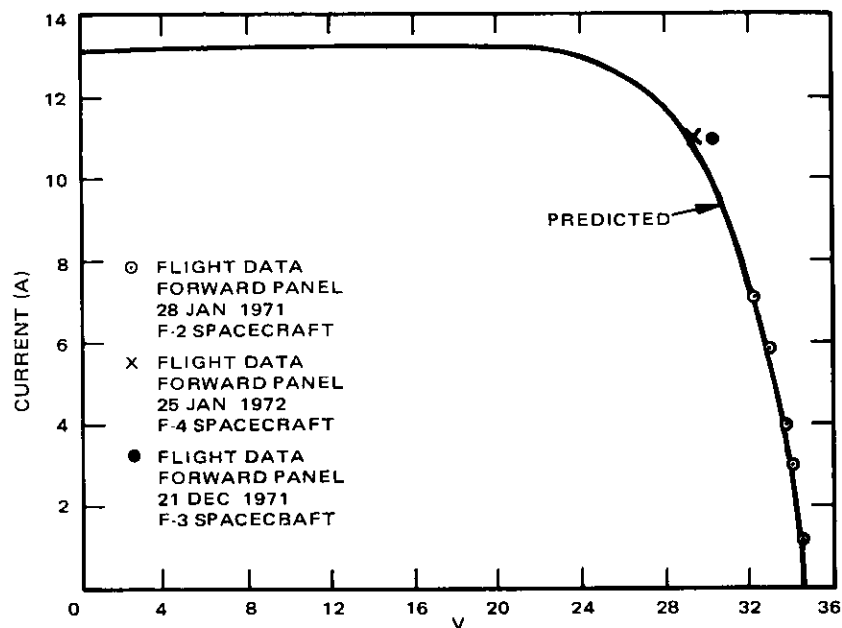


Figure 40. Forward or Aft Main Panel Performance  
(beginning of life, nominal)

development a major effort was directed toward battery thermal design and configuration. The 7-year life requirement for the battery emphasized the importance of maintaining temperatures as low as possible, preferably not higher than 75°F. Examination of available mounting areas and pack configurations resulted in the selection of a multipack arrangement (four 3-cell packs, one 6-cell pack, and one 7-cell pack) for each 25-cell battery. These packs are located on the spacecraft ribs, which are 0.127 cm (50 mils) thick. Rib and pack flatness are controlled to  $\pm 0.025$  cm ( $\pm 10$  mils), and RTV 11 is used as a filler to provide thermal control. Additional thermal control is achieved by commanding charge from full to one-third rate when 110 percent of the discharged energy has been returned.

TABLE 13. BATTERY CONFIGURATION DATA

<b>Batteries</b>	
Number	2
Type	nickel-cadmium
Capacity per Battery, C/2 Discharge to 1.15 V/Cell	18 Ahr
Maximum Depth of Discharge	53 percent
Charge Rate	C/15 minimum
Charge Mode	constant current
<b>Cell Packs</b>	
<b>3-Cell Packs</b>	
Number per Battery	4
Weight per Pack	2.40 kg (5.3 lb)
<b>6-Cell Packs</b>	
Number per Battery	1
Weight per Pack	4.67 kg (10.3 lb)
<b>7-Cell Packs</b>	
Number per Battery	1
Weight per Pack	5.35 kg (11.8 lb)
<b>Cells</b>	
Minimum Cell Voltage on Discharge	1.15 V
Cell Type	hermetically sealed
Cell Vendor	General Electric

The end-of-life charge rate is 1.0 ampere, which is a C/15 nameplate cell rating. The temperature profile of the battery resulting from the passive thermal design is ideal for efficient charging of Ni-Cd cells at a relatively low rate. A typical temperature profile, shown in Figure 41, permits the charge to occur between 4.45°C and 24°C (40°F and 75°F).

A ground test program was performed prior to launch to verify the

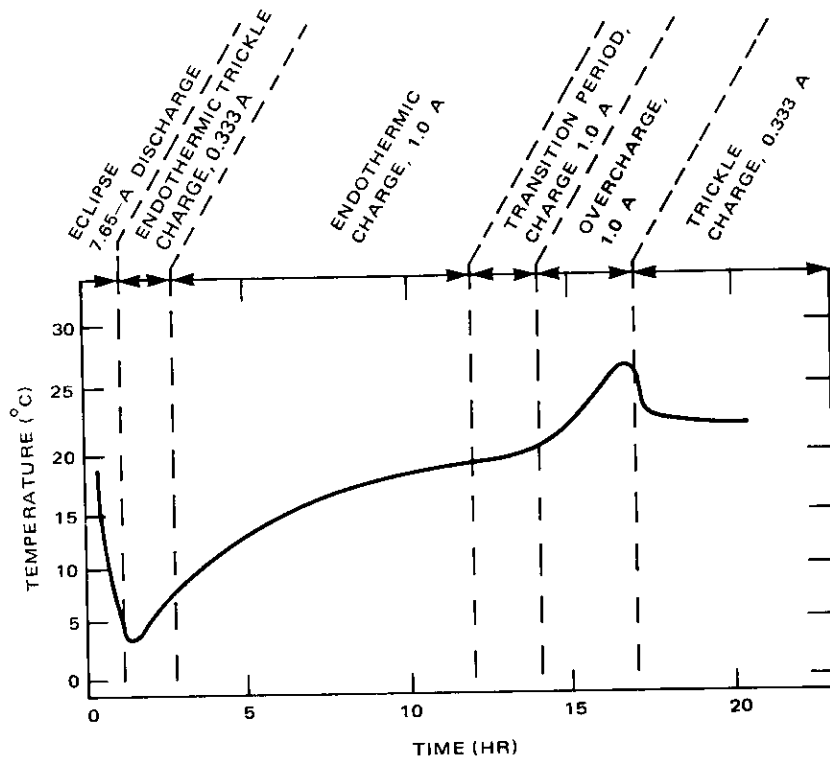


Figure 41. Predicted Nominal Battery Temperature Profile (end of life, 72-minute eclipse)

accuracy of thermal predictions and cell performance with respect to cell voltages, charge rate, storage reconditioning mode, and 7-year operation. A brief discussion of this test program follows.

**Cell voltage performance**

The cell voltage design performance point for this application is 1.10 volts per cell. This point is derived by assuming an open-cell failure and determining the voltage of each cell needed to provide the minimum bus voltage (23.8 volts). All cells are bypassed with diodes to allow the battery to function with an open cell.

The 1.10-volt performance was verified by testing 3-cell packs through four eclipse seasons. The eclipse portion of each eclipse season was in real

time. Each eclipse season was followed by the recommended reconditioning procedure; i.e., each battery was discharged to an average voltage of 1.15 volts per cell at a C/60 rate. (Long-term storage [135 days] between eclipse seasons was not included in this test.) Predicted temperature and time profiles were used during eclipse. For the four seasons tested, the charge current was adjusted for each season to account for the expected degradation. The fourth season simulated the 7-year charge current of C/15. The voltage performance of each season is shown in Table 14, which also includes flight data points for the first three eclipse seasons.

TABLE 14. VOLTAGE PERFORMANCE

Charge Rate	Equivalent Season	$\bar{V}$	Data Source
1.25 A	1st Year	1.20	Test Program
1.20 A	2nd-3rd Years	1.18	Test Program
1.10 A	5th Year	1.17	Test Program
1.00 A	7th Year	1.15	Test Program
1.32 A	1st Eclipse	1.195	F-2 Flight
1.30 A	2nd Eclipse	1.188	F-2 Flight
1.29 A	3rd Eclipse	1.180	F-2 Flight

**Storage reconditioning**

The effects of storage/reconditioning techniques were the subject of a separate test program. In this program, five flight cell test packs were used, each subjected to a different storage mode:

**Pack 1.** Self-discharge, 17.8-kΩ telemetry load, and charge circuit of 12.5-mA "OR" gate current for 135 days; C/36 charging for 48 hours every 30 days to the 120th day; reconditioning procedure initiated on the 125th day.

**Pack 2.** Self-discharge, 17.8-kΩ telemetry load, and charge circuit of 12.5-mA "OR" gate current for 135 days; C/18 charging for 24 hours every 30 days to the 120th day; reconditioning procedure started on the 125th day.

**Pack 3.** 17.8-k $\Omega$  telemetry load, and charge circuit of 12.5-mA "OR" gate current for 135 days; C/36 charging for 135 days; no reconditioning.

**Pack 4.** 17.8-k $\Omega$  telemetry load, and charge circuit of 12.5 mA "OR" gate current for 135 days; C/36 charging for 125 days; reconditioning procedure started on the 125th day.

**Pack 5.** Self-discharge and 17.8-k $\Omega$  telemetry load only for 125 days; discharged to an average of 1.15 volts per cell immediately at the start of 125-day storage period; reconditioning procedure started on the 125th day.

The results of this test are presented in Figure 42. The last of the five modes, in which the cells were stored discharged, demonstrated superior performance, but could not be used unless discharged batteries were acceptable for the other systems. Trickle charge was deemed to result in the worst voltage performance. Other modes provided approximately equivalent performances.

On the F-2 spacecraft, the batteries are stored charged but with both charge and discharge circuits open. Approximately every 30 days the cells are charged at the two-thirds rate for 24 hours. Performance using this storage mode appears satisfactory for the first year's operation.

#### Seven-year performance

Seven-year performance of the battery was verified by running accelerated life tests on two groups of packs, each group consisting of a 3-, 6-, and 7-cell pack. Since 7-year performance could not be verified on a real-time basis prior to launching the first spacecraft, these accelerated tests were performed with seven years of eclipse energy output from the cells at depths of discharge greater than those actually required. The specific charge/discharge regimes were as follows:

- a C/10 rate for 10.4 hours on charge, a C/2 rate for 1.6 hours on discharge, and a total of 363 cycles; and
- a C/5 rate for 6 hours on charge, a C/2 rate for 2 hours on discharge, and a total of 451 cycles.

Both of these tests subjected the cells to a total energy discharge exceeding the expected 7-year flight requirement. Even at the high depth of discharge on the latter test (100 percent of nameplate), the average cell voltage for each cycle exceeded 1.15 volts.

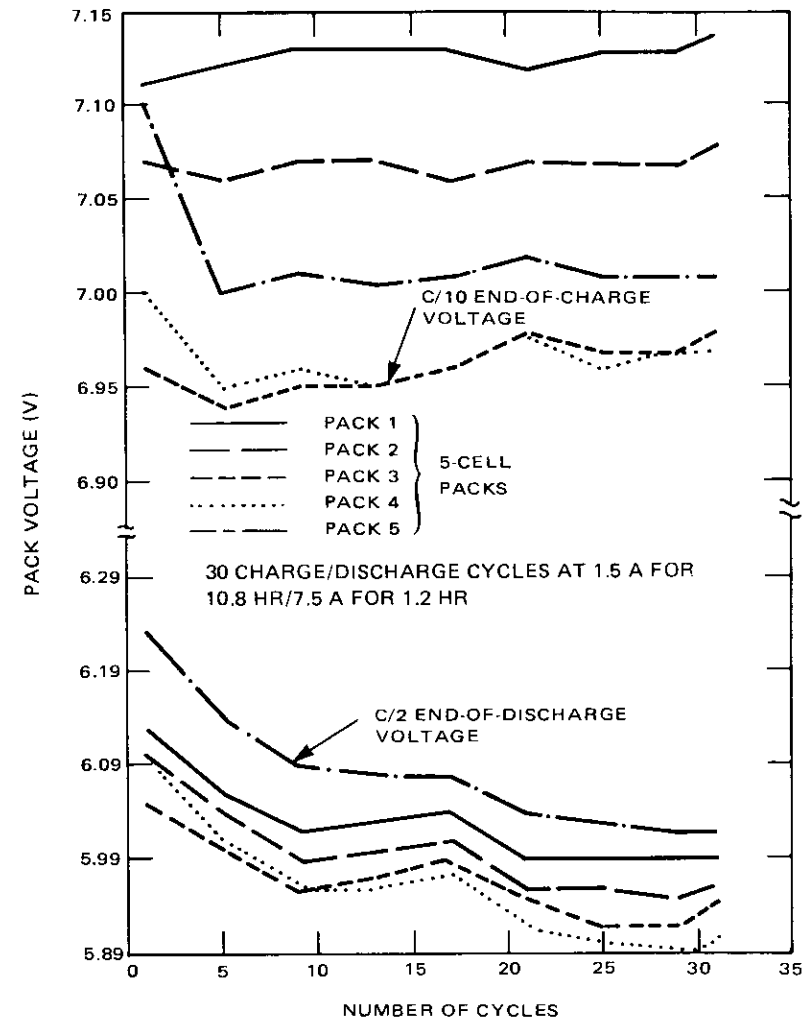


Figure 42. Storage/Reconditioning Test Burn-In After Second 135-Day Storage Period

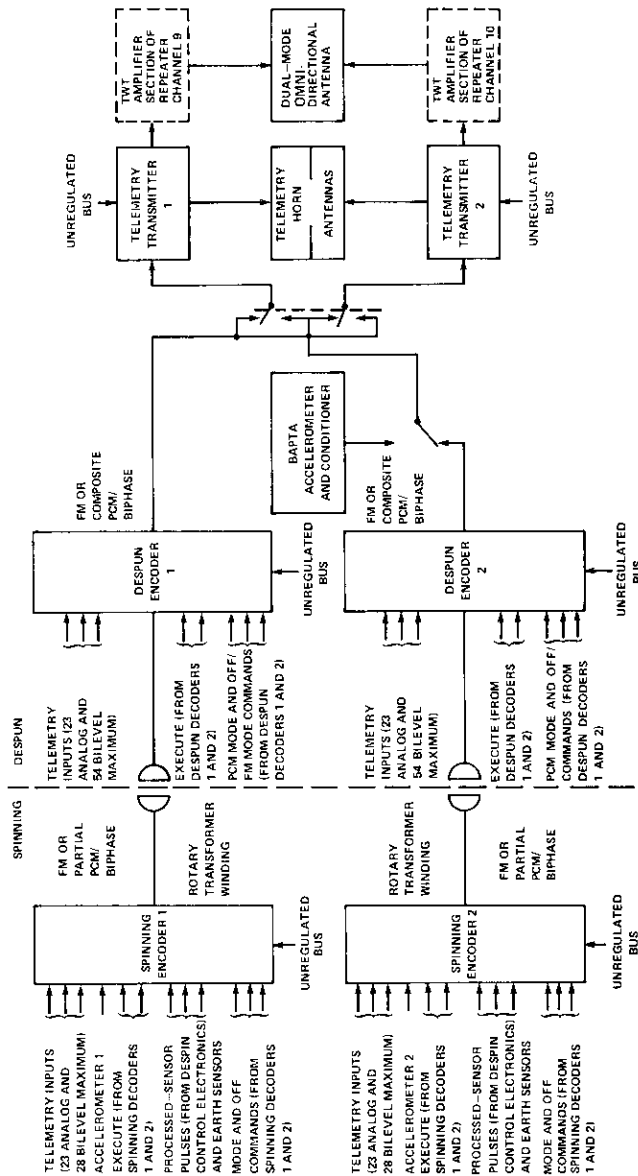


Figure 43. Telemetry Subsystem Block Diagram

## Telemetry and command subsystems

F. W. WEBER

### Telemetry

The INTELSAT IV telemetry subsystem consists of two independent channels providing redundant telemetry information on two separate carrier frequencies (see Figure 43). Telemetry from the spinning and despun sections of the spacecraft is gathered and processed by redundant encoders located on the spinning and despun sides of the rotary interface. Additional redundancy is provided by cross-strapping the inputs to the beacon transmitters so that either data stream can modulate either beacon transmitter.\* Each of the two independent telemetry channels are capable of three primary modes of data processing: PCM, FM real-time, and FM accelerometer modes. In addition, a BAPTA accelerometer mode may be selected in lieu of one of the data streams.

**PCM Mode.** The PCM mode is used for all attitude, thermal control, power, and status information, including command verification. The characteristics of PCM telemetry are listed in Table 15.

TABLE 15. PCM TELEMETRY CHARACTERISTICS

Word Length	8 bits/word
Frame Length	64 words/frame
Bit Rate	1,000 bps
Data Code	IRIG NRZ-M
Frame Synchronization	16 bit (words 0 and 1)
Frame Rate	0.512 s
Modulation	PSK on 32-kHz subcarrier

In the PCM telemetry frame, the even-numbered words represent data gathered on the spinning side, while odd-numbered words represent data

\* This feature is not incorporated in INTELSAT IV F-2, F-3, or F-4.

F. W. Weber is Manager of the Telemetry and Command Branch, Space Segment Implementation Division, COMSAT.

gathered on the despun portion of the satellite. A frame consists of 64 words: 16 digital words, 2 frame synchronization words, and 46 analog words.

In the PCM mode, the spinning encoder receives, processes, and formats data originating on the spinning side of the spacecraft. The output of the spinning encoder, an 8-kHz biphase waveform, drives a rotary transformer which transfers the signal across the spinning/despun interface and provides an input from which a despun encoder recovers the nonreturn-to-zero (NRZ-L) bit stream and derives a coherent clock signal. This bit stream consists of the spinning (even-numbered) words each repeated once (as shown in Figure 44) to yield a spinning frame length of 64 words.

The despun encoder gathers and processes data originating in the despun compartment and interlaces its bit stream word by word with the spinning encoder bit stream, as shown in Figure 44. The despun encoder then converts the composite NRZ-L bit stream into an NRZ-M format and uses it to biphase modulate a coherent 32-kHz subcarrier, which is routed to the beacon transmitter and used to phase modulate the beacon carrier.

**FM Real-Time Mode.** The FM real-time mode provides an analog representation of the occurrence of attitude and timing pulses in a real-time relationship (see Figure 45). The occurrence of a pulse coherently switches the frequency of an IRIG channel 13 subcarrier oscillator (SCO) from its pilot tone to a frequency which corresponds to that kind of pulse. The switching priority, as shown in Table 16, minimizes the loss of pulse data which will occur if two pulses occur simultaneously. The SCO output, which is connected via the rotary transformer through an "OFF" despun encoder to the beacon transmitter, phase modulates the carrier.

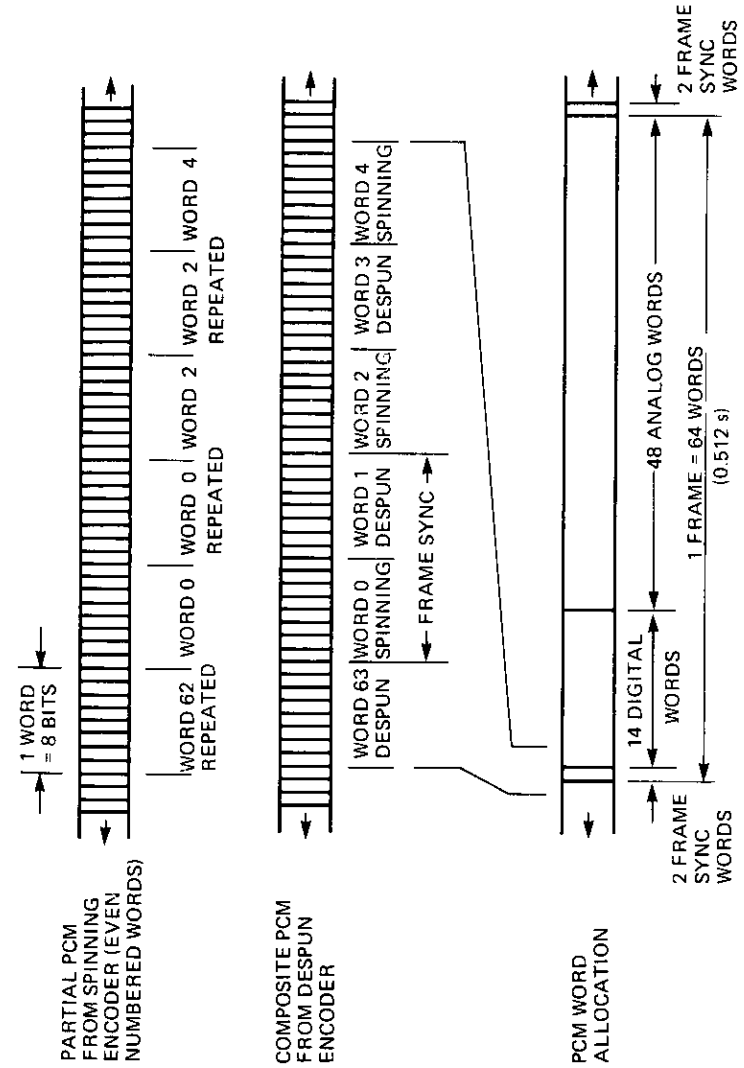


Figure 44. PCM Telemetry Format

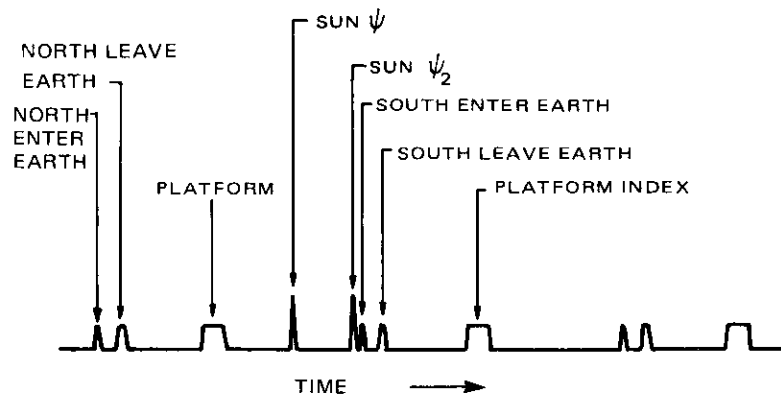


Figure 45. Attitude Real-Time Pulses

TABLE 16. SWITCHING PRIORITY

Real-Time Pulse	Duration	Priority	Frequency
Sun Pulses	5 ms	1	15.059 kHz
Earth Pulses	10 ms*	2	14.222 kHz
Platform Index Pulse	50 ms at 51 rpm	2	14.222 kHz
Command Execute	Variable	3	13.838 kHz
Pilot Tone	Continuous	4	13.454 kHz

\* North leave earth, 20 ms.

**FM Accelerometer Mode.** In the FM accelerometer mode, the output signal of an accelerometer mounted on the outboard edge of the spinning platform provides an analog output proportional to the acceleration. This output frequency modulates an IRIG channel 13 SCO (center frequency = 14.5 kHz) whose output, connected via the rotary transformer through an "OFF" despun encoder to the beacon transmitter, phase modulates the telemetry carrier.

The accelerometer is mounted with its sensitive axis parallel to the spacecraft Z (longitudinal) axis so that it provides an accurate method of measuring spacecraft nutation angle. Two gain levels are available to supply  $\pm 1$  g or  $\pm 0.05$  g full scale. (It should be noted that 12 mg repre-

sents a nutation angle of approximately  $0.5^\circ$ ). The 3-dB frequency response of the accelerometer channel is 0.03 to 35 Hz.

**BAPTA Accelerometer Mode.** The BAPTA accelerometer mode provides a display of the spectrum and amplitudes of acoustical noise excited by the bearing assembly and thus permits in-orbit assessment of the BAPTA's functioning status. This mode also makes it possible to monitor apogee motor performance.

In this mode, a piezoelectric accelerometer mounted on the BAPTA shaft's inner diameter at the forward bearing provides an input to a charge amplifier which drives an IRIG channel F subcarrier oscillator. The output of the SCO, after appropriate filtering, is routed through the output switch to phase modulate the beacon transmitter in the no. 2 telemetry channel. When the BAPTA accelerometer and conditioner (BAC) is "OFF," the output switch connects the output of despun encoder no. 2 to the beacon transmitter (see Figure 43). Characteristics of this mode are listed in Table 17.

TABLE 17. CHARACTERISTICS OF THE BAPTA ACCELEROMETER MODE

IRIG Channel	F
SCO Frequency	93.0 kHz
Modulation	analog FM
Gain Level	
Low Gain	$\pm 0.7$ g full scale
Medium Gain	$\pm 0.07$ g full scale
High Gain	$\pm 0.007$ g full scale
Frequency Response	3 Hz to 10 kHz
Sensitive Axis	perpendicular to spacecraft Z (longitudinal) axis

**RF Telemetry Transmission.** There are two modes of RF telemetry transmission: the earth-coverage mode and the omnidirectional mode. In the earth-coverage mode, the two solid-state telemetry transmitters each drive a separate horn antenna with a microwave carrier phase modulated by the telemetry mode signal from one of the despun encoders. This is the normal on-station mode of telemetry transmission. When omnidirectional telemetry is required (e.g., during transfer orbit), the telemetry transmitter outputs are switched into the TWT amplifiers of repeater

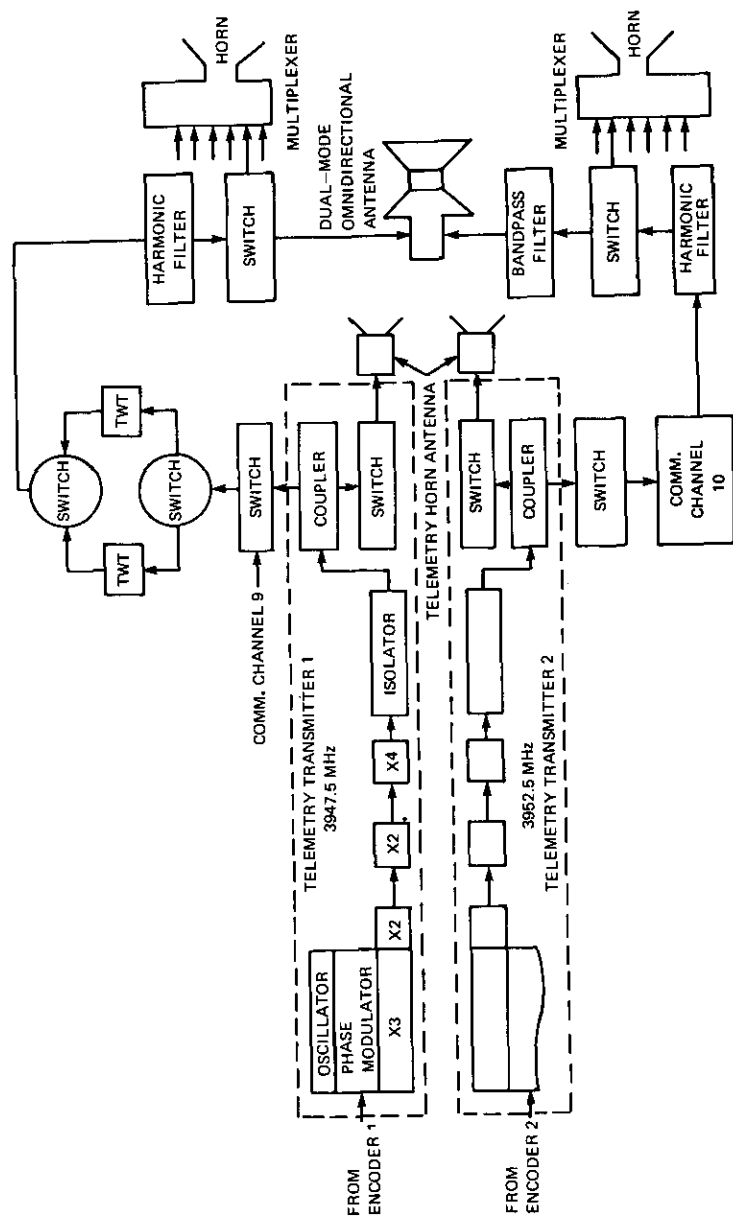


Figure 46. Beacon Transmitter Block Diagram

channels 9 and 10, which are in turn switched to drive a dual-mode omnidirectional bicone antenna.

Table 18 summarizes the RF telemetry performance characteristics. Figure 46 is a block diagram of the beacon transmitter.

TABLE 18. RF TELEMETRY PERFORMANCE CHARACTERISTICS

Parameter	Characteristics
<b>Transmitted Signal</b>	
Carrier Frequencies	3,947.5 and 3,952.5 MHz
Long-Term Frequency Stability	10 <sup>-6</sup> /day
Modulation Index	1.0 ± 0.1 radian
<b>Transfer Orbit</b>	
RF Power Output	+7 dBW e.i.r.p. minimum over 50 percent of transfer orbit centered about apogee
Antenna Type	dual-mode toroidal beam bicone
Polarization	vertical
Gain Over Earth Coverage	3 dB minimum over 40° beamwidth
Transmitter Type	communications subsystem channel 9 and 10 TWTs
Transmitter Power	+7.4 dBW minimum
<b>Synchronous Orbit</b>	
RF Power Output	-1 dBW e.i.r.p. minimum
Antenna Type	horn plus semireflector
Polarization	right-hand circular
Gain Over Earth Coverage	11 dB minimum over 17° beamwidth
Transmitter Type	step recovery diode multiplier
Transmitter Power	-10 dBW minimum
Spin Axis e.i.r.p.	-8 dBW minimum

**Telemetry Subsystem Components.**

*Telemetry Transmitters.* Both solid-state beacon transmitters are identical except that one is at 3,947.5 MHz and the other is at 3,952.5 MHz. An

82-MHz crystal output is multiplied, phase modulated, and gain multiplied to the output frequencies with about 100 mW of power. One radian peak deviation is provided by a 3.8-volt rms sine wave audio input. In the omnidirectional mode, each transmitter output is switched through a 40-dB coupler to the input of repeater channel 9 or 10. The TWAs then provide about 6 watts for transmission by the dual-mode omnidirectional antenna.

*Horn (Earth-Coverage) Antenna.* The earth-coverage telemetry antennas are circularly polarized and provide a minimum gain of 11 dB over a 17° beamwidth. In addition to the main lobe, a 4-dB-gain beam, whose axis is parallel to the spacecraft spin axis, is created by a 45° semireflector located in front of the telemetry horns. This beam provides a ground indication of the satellite rotation phase in case of spacecraft "flat spin" failure.

*Dual-Mode Biconical Antenna.* High-power telemetry is transmitted by a linearly polarized, dual-mode, omnidirectional antenna with a 3-dB minimum gain and a 40° beamwidth. The telemetry bicone and command receive bicone are stacked and housed within a fiberglass thermal shield on the top of the spacecraft antenna farm mast.

*Spinning Encoder.* In the PCM mode, a spinning encoder conditions, multiplexes, and encodes the telemetry data originating on the spinning section of the satellite into a PCM bit stream. In the FM real-time mode, the composite of the real-time pulses coherently switches the frequency of an SCO. In the FM accelerometer mode, the analog output signal of the accelerometer frequency modulates an SCO. Mode commands select the PCM or FM real-time signal or the FM accelerometer signal to drive the rotary transformer.

Timing, which controls all sequence operations within the spinning encoder, including multiplexing, analog-to-digital (A/D) conversion, attitude sensor pulse interval digitizing, and digital formulating, is provided by a 1.024-MHz crystal oscillator and countdown chain.

All input signals are conditioned to ensure that they meet the input range (0-5.12 VDC) and source impedance requirements. A precision transducer supply furnishes an accurate excitation voltage for passive sensors as well as the comparison referenced for the A/D converter. Multiplexers provide analog and digital gating circuits to time multiplex the TM inputs. Analog multiplexer outputs are fed to a successive-approximation-type A/D converter, which encodes each analog signal into a serial 8-bit NRZ-L word to provide an accuracy of better than 0.5 percent

full scale. The outputs of the A/D converter and digital multiplexer are combined at a data node to form the partial PCM bit stream.

The attitude data processor performs a sequence of 10 time interval measurements to facilitate the accurate and rapid determination of satellite attitude. For each measurement, the number of cycles of a 32-kHz reference frequency, derived from the 1.024-MHz crystal oscillator, is counted during the time interval being measured. This count is telemetered along with a 4-bit code identifying the measurement it represents. The inherent measurement resolution is  $\pm 2$  periods of the 32-kHz reference, or approximately 62  $\mu$ s.

The biphasic modulator which converts the NRZ bit stream into a coherent biphasic format also adds an easily recoverable clock for use by the despun decoder. In addition, once each frame, it adds a double-amplitude pulse to which the despun decoder synchronizes its frame timing.

When the encoder is in the FM real-time mode, it accepts and processes various real-time pulses and transmits their occurrences as discrete changes in SCO frequency. The frequency transmitted and the duration of transmission correspond to those of the group including the pulse which has occurred. All of the tone frequencies are within the IRIG channel 13 band. In the FM accelerometer mode, the spinning encoder generates a signal consisting of an IRIG channel 13 subcarrier ( $14.5 \pm 1$  kHz) frequency modulated by the conditioned accelerometer output.

*Despun Encoder.* In its PCM mode, a despun encoder conditions, multiplexes, and encodes the telemetry data originating in the despun compartment into a PCM bit stream, which it synchronizes and merges with the partial PCM from its associated spinning encoder. In the FM mode, a despun encoder switches the spinning encoder FM output to the telemetry transmitter.

In order to merge its PCM words with those of the spinning encoder in the alternating format shown in Figure 44, the despun encoder must derive its bit clock from the spinning encoder bit stream and synchronize the start of its telemetry frame with the spinning encoder double-amplitude frame synchronization pulse. These tasks are performed by the clock and data detector circuit and the synchronization detector circuit, respectively. If the clock detector is unable to derive a bit clock because the spinning encoder has failed or has been commanded off, it will switch the despun encoder to its internal 1.024-MHz crystal oscillator so that despun telemetry may continue to be transmitted.

The formatting logic combines the partial PCM from the spinning en-

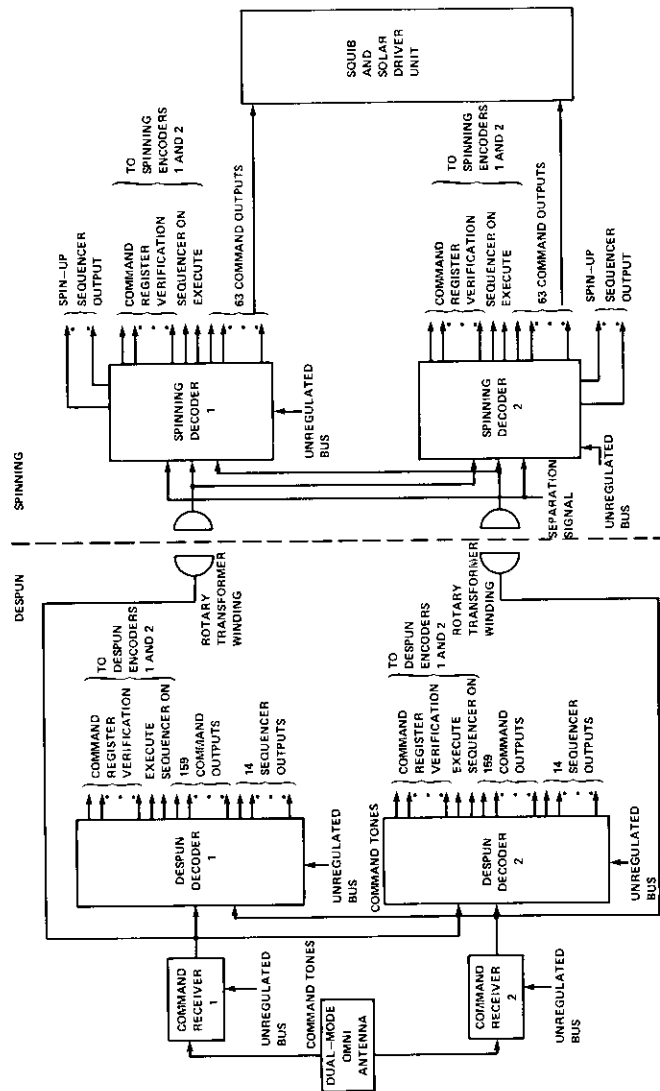


Figure 47. Command Subsystem Block Diagram

coder with the despun encoder PCM. The combined NRZ-L bit stream is then coded into an NRZ-M waveform which biphase modulates the 32-kHz subcarrier output.

The mechanical design of the spinning and despun encoders utilizes two packaging approaches. Integrated circuits (ICs), flat packs, and small associated components are packaged on a "stick" called MICAM (the micro-connection assembly method). The major discrete components are assembled "cordwood style" into welded modules. The MICAMs and welded modules are then mounted in a machined aluminum chassis.

**Command**

The INTELSAT IV command subsystem consists of fully redundant and cross-strapped paired units so that any unit of either pair can fail completely without impairing the spacecraft's ability to receive and execute all commands.

**Command System Operation.** As shown in Figure 47, a microwave command carrier modulated by a binary coded signal is received by the linearly polarized omnidirectional command antenna and demodulated by the redundant command receivers. The output of each receiver drives both despun decoders and one of the redundant rotary transformer windings which transfer the signals across the spinning/despun interface. The secondary of each rotary transformer provides an input for both spinning decoders.

The spinning decoders provide 95 command output lines, and the despun decoders provide 160 command output lines. The types of commands are indicated in Tables 19 and 20, respectively. In addition to its command outputs, each decoder provides a readout of its command register (command verification) and an indication of all execute pulses to two encoders; thus it supplies redundant telemetry for all command occurrences.

TABLE 19. SPINNING COMMANDS

- Hydrazine Thrusters Actuated
- Hydrazine Line Heaters ON and OFF
- Apogee Motor Heaters ON and OFF
- Hydrazine Cross-Connect Valves Open and Closed
- Spin-Up Latching Valves Open and Closed

TABLE 19. SPINNING COMMANDS (continued)

---

BAPTA Spinning Heaters ON and OFF  
 Active Nutation Control ON and OFF  
 TM Encoder ON, OFF, and Mode Select  
 Apogee Motor Fire  
 Despin Control Electronics 1 ON, 2 OFF, and Reverse  
 Pseudo-Earth Pulse  
 Despin Reference Select  
 Despin Sun Mode Clock Correction  
 Despin Torque Bias Positive and Negative Stepping  
 Despin Motor Drive Select  
 Battery Discharge and Charge (2 modes)  
 Spinning Buses Parallel and Separate  
 Battery Discharge Control Normal and Bypass  
 Spin-Up Sequencer Enable and OFF

---

TABLE 20. DESPUN COMMANDS

---

TWT Filament A ON, B OFF, and Reverse  
 TWT HV ON  
 TWT Filament and HV OFF  
 BAPTA Accelerometer ON (3 gain states) and OFF  
 BAPTA Despun Heater ON  
 Auxiliary Battery ON  
 Auxiliary Battery and Despun Heater OFF  
 Global- to Spot-Beam Switches and Reverse  
 Output Channel Attenuator Steps  
 Receiver ON and OFF Commands  
 TM Cross-strapped and Normal  
 Despun Buses, Paralleled and Separate  
 TM Encoders ON (PCM mode)  
 Omnidirectional Beacons ON and OFF  
 Directional Beacons ON and OFF  
 TWT Sequencers Enabled and Disabled  
 TM Encoders OFF (FM mode ON)  
 Antenna Positioner Motors ON and OFF  
 Antenna Positioner Step Direction

---

Upon receipt of a proper command pulse, a squib and solenoid driver unit generates suitable signals for firing the BAPTA clamp, apogee motor squibs, and energizing the latching valves and thruster solenoids in the P&O subsystem.

Table 21 lists the command performance characteristics.

TABLE 21. COMMAND PERFORMANCE CHARACTERISTICS

---

<b>Received Signal</b>	
Carrier Frequency	6-GHz band
Modulation Index	> > 10
RF Field at Satellite	-65 to -85 dBW/m <sup>2</sup>
Power Received at Command Receiver Input	-68.5 to -92.5 dBm over 30° beam
<b>Antenna</b>	
Type	dual-mode, toroidal beam, bicone
Polarization	horizontal
Gain	4 dB min over 34° beam
Cable Losses	2.5 dB max
<b>Receiver</b>	
Noise Figure at Antenna	< 12 dB
Bandwidth	3 MHz
<b>Decoders</b>	
Command Format	multitone
Command Capacity, Spinning Section	95
Command Capacity, Despun Section	160

---

#### Command Subsystem Unit Description.

*Command Receivers and Antenna.* The command microwave units consist of a 6-GHz, toroidal beam, dual-mode antenna, and redundant FM receivers. The dual-mode linearly polarized antenna has two independent outputs with about 5-dB peak gain and a 34° (3-dB) beamwidth.

*Despun and Spinning Decoders.* There are only three major differences between despun and spinning decoders (Figure 48):

- a. the output matrices of despun decoders provide 160 command outputs, while those of spinning decoders provide only 95;
- b. despun decoders each contain a TWT sequencer; and
- c. spinning decoders each contain a spin-up sequencer.

*Description of Logic Circuitry Common to Both Decoders.* Two sets of 1, 0, and EXECUTE tone filters (six different frequencies, as shown in Figure 48) provide a means of identification of the command receiver being used for a given command, since each receiver (or rotary transformer) drives only one set of tone filters. Cross-strapping is achieved by connecting the two corresponding tone filter outputs at the inputs to their respective detector circuits.

When power is turned on, the decoder is initialized by the power turn-on reset circuit. That is, the command register is cleared to all zeros, the count register's count is set at zero, the address check logic is reset, and the full count logic is set at zero. Whenever a 0 or 1 tone pulse is detected, the clock pulse generator provides a clock pulse (CP) to the introduction sequence monitor, which checks the pattern of the incoming data. Upon receipt of the introduction code, the clock pulse generator initializes the decoder in the same manner as for the power turn-on reset discussed previously.

The command register is an 8-bit register. It receives 1s and 0s from the demodulator and register clock pulses (RCPs) from the clock pulse generator. Its output goes to the address check logic, output matrix, and telemetry buffers for parallel entry into redundant telemetry encoders.

When it has counted eight RCPs, the bit count logic provides a pulse to the address check logic; when it has counted 16 RCPs, it provides a pulse to the full count logic. When the address check logic receives its pulse from the bit count logic, it checks the output of the command register (which now contains the address). If the address is correct, an enable signal is sent to the matrix enable; if the address does not check, it inhibits further RCPs and clears the command register. Each decoder has an address plug which permits a change in its address at any time prior to launch. When the bit count logic has counted 16 RCPs, it inhibits further RCPs to prevent false clocking of the command register and also sends an enable signal to the matrix enable circuit.

The use of two series matrix power switches prevents a single component failure in the matrix power switching circuitry from generating a false

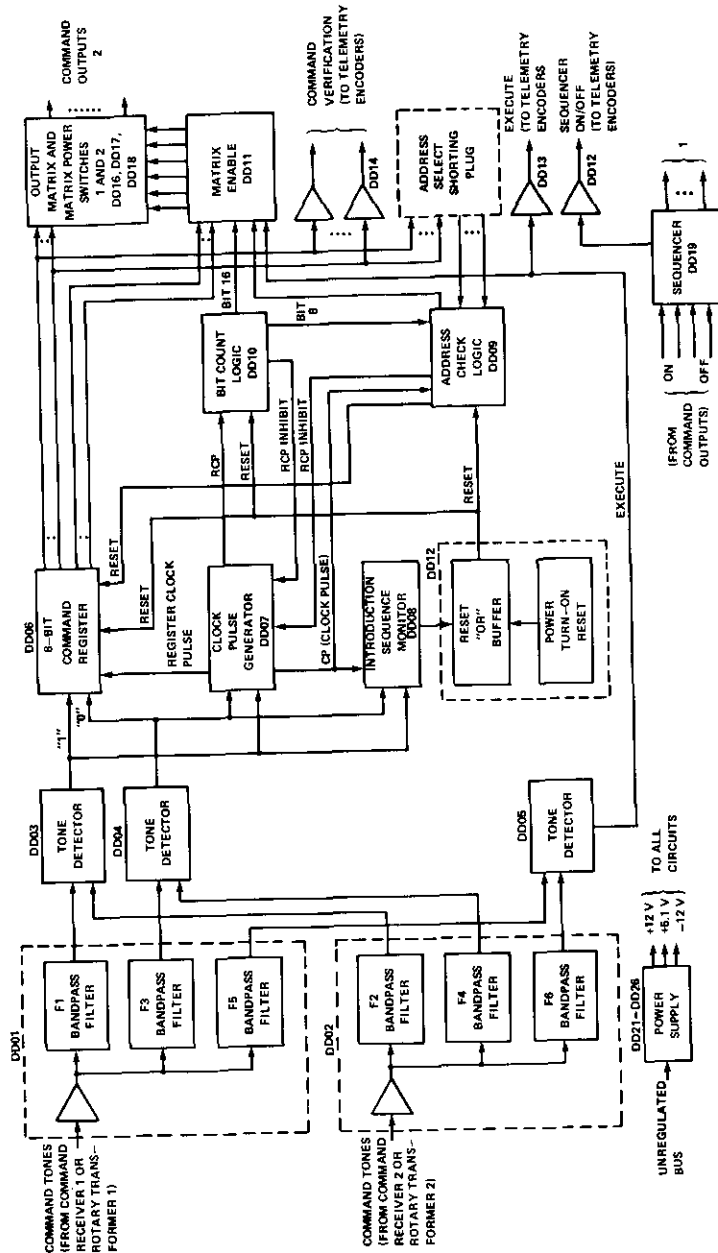


Figure 48. Despun or Spinning Decoder Block Diagram

command. When both matrix power switches are enabled, an execute signal from the EXECUTE tone detector closes both power switches, causing a command pulse to occur on the output selected by the command portion of the command word. The command pulse coincides with and lasts as long as the EXECUTE tone pulse.

*TWT Sequencer (Despun Decoder).* Each despun decoder contains a TWT sequencer which, when turned on by command, times for approximately 45 minutes, generates a sequence of eight command-type output pulses spaced one and three-quarter seconds apart, times for an additional three and three-quarter minutes, generates a second sequence of six pulses, and finally shuts itself off. (It may also be commanded off and reset at any time during its cycle.) The 14 command-type outputs which each TWT sequencer generates appear on separate lines. Each line is wired directly to selected command matrix output lines to execute selected commands.

The TWT sequencers are used to turn on the repeater TWTs after booster separation, during a portion of the transfer orbit when the satellite is not visible to a ground station and is therefore not commandable in the normal manner. The ON command (initializing sequencer timing) is sent approximately five minutes prior to actual launch.

*Spin-Up Sequencer (Spinning Decoder).* Each spinning decoder contains a spin-up sequencer, which is enabled by command prior to launch and initiated by a separation switch signal. The sequencer generates command-type outputs at separate output pins:

- a. two occurring 2.3 seconds after separation and lasting 0.047 second to turn on the despin control electronics and open a latching valve;
- b. one occurring 2.3 seconds after separation and lasting 8.6 seconds to fire spin-up thrusters, recurring 50.2 seconds after separation and lasting 45.8 seconds to fire the spin-up thrusters again; and
- c. five occurring 96.0 seconds after separation and lasting 0.047 second to close the latching valves, turn on the earth sensor mode and the despin motor drives, and enable the active nutation control system.

The spin-up sequencer turns itself off 0.047 second after the last output is generated. Ground command can be used at any time to turn off the sequencer via the ENABLE circuit. When turned off in this manner, the sequencer is protected from inadvertent triggering.

*Squib and Solenoid Driver Unit.* The squib and solenoid drivers actuate pyrotechnic and jet firing functions in the satellite. The squib drivers fire

the apogee motor and the BAPTA release squibs. The solenoid drivers actuate the axial, radial, and spin-up jet valves and the latching valves in the spin-up jet lines.

All of the squib drivers apply power to their respective squibs after specified delay times. The BAPTA clamp release squib drivers are commanded by redundant separation switches. The apogee motor squib drivers are each commanded redundantly by the spinning decoders. From the time when the spacecraft is mated to the adapter until actuation of the separation switches, all squib driver power inputs are directly connected to ground.

Solenoid drivers can be redundantly commanded from either spinning decoder. It is also possible to use either spinning decoder to turn on both axial jets simultaneously.

#### **Active nutation control**

The onboard propulsion and orientation system actively controls and reduces any excessive nutation. Active nutation control is achieved by an axial jet firing appropriately phased and synchronized to the satellite nutation. The two accelerometers mounted on the outboard edge of the spinning platform to provide the signal for the FM accelerometer mode in the telemetry subsystem also provide the necessary amplitude and phase information to ascertain the proper phasing of the axial jet firing commands.

Active nutation control (ANC) can be effected automatically onboard the spacecraft (see Figure 49). In this mode, the accelerometer output is routed to the active nutation damper electronics (ANDE) where, after appropriate processing and filtering, the nutation sinusoid is rectified and fed to a threshold detector. The system is designed to activate at a nutation angle of  $0.5^\circ$ , which corresponds to an acceleration of 12 mg at the location of the transducers. When the nutation amplitude reaches this threshold, the ANDE provides an input pulse to the solenoid driver to fire the axial jet at the proper point in the nutation cycle for a pulse length proportional to the amplitude of nutation. Two independent systems are provided: one consisting of accelerometer no. 1, ANDE no. 1, and axial jet no. 1, and the second consisting of the no. 2 units. In addition to providing a backup to the passive dampers, active nutation control is capable of quickly damping large amplitude nutations. This is an effective means of ensuring stability during transient periods such as transfer orbit and the injection sequence.

It should be noted that ANC can also be achieved manually from the

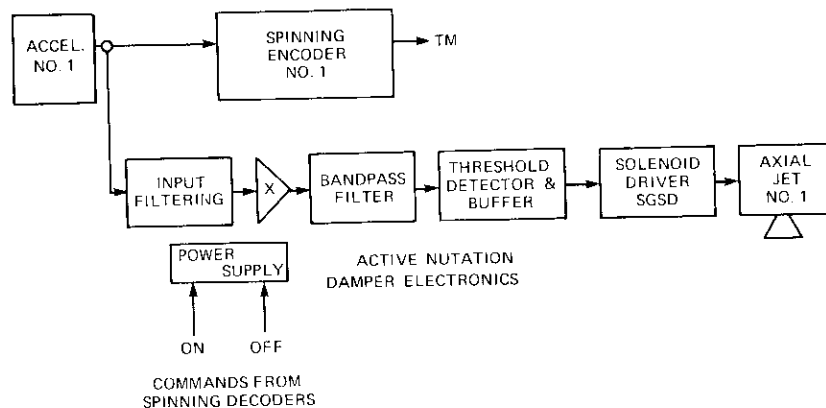


Figure 49. Active Nutation Control

ground by observing the accelerometer signal and commanding the appropriate axial jet at the proper time to allow for the various delays involved.

### Antenna positioner mechanism

W. A. NAKANO

The antenna positioner mechanism (APM) steers the 4.5° spot-beam antenna pattern to selected positions on the earth by moving the parabolic reflector relative to a fixed feed horn. The reflector is mounted on a two-degrees-of-freedom gimbal assembly (north-south and east-west) actuated by a linear jackscrew driven by a stepper motor. The APM consists of three major components: a 2-axis gimbal system, an actuator and drive mechanism, and a potentiometer position indicator.

The two-axis gimbal is coplanar and is located 58.14 cm (22.89 in.) aft of the focal point of the antenna feed, resulting in a 1.93:1 ratio between the antenna beam and the gimbal mechanical angular motion. The east-west gimbal axis of the APM is parallel to the spacecraft spin axis and the

*W. A. Nakano is a member of the Technical Staff in the Mechanics Department, Space Segment Implementation Division, COMSAT.*

north-south gimbal axis is normal to the spin axis. The dish is attached to the N-S gimbal at three points, the N-S gimbal is in turn mounted on the E-W gimbal, and the gimbal system is mounted on a crossarm member attached to the antenna mast.

The aluminum pivot bushings are lubricated by burnished bonded molybdenum disulfide. The friction coefficient of the dry lubricant system is approximately 0.5 in air and 0.01 in vacuum. The APM gimbal and actuator backlash is preloaded by an extension coil spring with a low spring constant (43.75 N/m). This spring is designed to prevent spot-beam dish movement caused by the acceleration field created by despun platform wobble (0.004 g) or spacecraft nutation.

The actuator which drives the gimbal consists of a 15°-per-pulse, phase-switched, 3-phase stepper motor and solenoid operated brake. Phase switching is performed by the antenna positioner electronics (APE), which provide a square wave with a 100-percent duty cycle through the APE sequencer. The last coil which was energized in the pulse train is kept energized as a detent until the APE is turned off. When the APE is turned off, the mechanical brake is engaged, providing a continuous positive lock on the APM system. The mechanical brake is mounted directly on the motor shaft and consists of a set of serrated discs with radial faces. These discs, which are preloaded by a coil spring, are disengaged by energizing a solenoid which pulls them apart against the preload spring. The solenoid is actuated by the same command as the "ON" command of the APE. The stepper motor can be commanded in the clockwise or counter-clockwise direction by the direction control memory of the APE. The motor produces 0.02 N·m (3.0 oz-in.) of torque and weighs 113.4 g (4.5 oz).

The stepper motor output is geared down to a 4:1 ratio by aluminum spur gears, lubricated with molybdenum disulfide, which drive the jackscrew. The total gear ratio from the motor to the angular output of the 25.4-cm (10-in.) gimbal arm is 4,026:1 or 0.00373° per motor step. Both the jackscrew nut and the motor/jackscrew assembly are pivoted to prevent jamming.

The position detector is a continuously variable linear potentiometer providing an electrical analog of the linear motion of the jackscrew. The potentiometer is mounted parallel to the jackscrew with its case clamped to the spur gear/motor housing and its plunger shaft attached to the nut of the jackscrew. Its resistive element is a solid conductive material and is bonded to a stainless steel tubular inner case. The wiper element is made of Paliney wire and is mounted on a plastic wiper block which

slides between parallel rod tracks. The plunger rod is swivel mounted to the wiper block. Because the telemetry signal is the ratio of the voltage input and output of the potentiometer, the position readout is insensitive to extreme temperature variations of the potentiometer element.

### Positioning and orientation subsystem

M. A. VONNEGUT

The positioning and orientation (P&O) subsystem is designed to perform the following in-orbit maneuvers: spacecraft spin-up at spacecraft-Centaur separation, spin-speed control, attitude changes, N-S inclination changes, and E-W maneuvers. These maneuvers are listed in Table 22, which also includes the operational budget for each maneuver. All maneuvers are controlled by ground command. Proper phasing of steady-state firing and pulse firing of the thrusters is achieved by a ground-based synchronous controller which utilizes telemetered sun or earth sensor data.

TABLE 22. POSITIONING AND ORIENTATION MANEUVERS

Maneuver	Thruster	Operation	Budget	
			(m/s)	(ft/s)
Spin-Up	Two Spin-Up	Continuous	0.610	2
Initial Maneuvers	One Axial	Continuous and Pulsing	54.9	180.1
East-West Station-keeping	One Radial	Pulsing	14.6	47.9
North-South Inclination Removal	One or Two Axial	Continuous	358.4	1,175.9
Attitude Change	One Axial	Pulsing	0.305	1
Spin-Speed Control	One Spin-Up	Pulsing	4.17	13.7

M. A. Vonnegut was formerly Manager of the Spacecraft Engineering Branch, Space Segment Implementation Division, COMSAT.

The propulsion and orientation subsystem has been designed so that equal quantities of monopropellant hydrazine ( $N_2H_4$ ) are contained in two independent subsystems. As shown in Figure 50, the P&O system contains four tanks, two axial thrusters, two radial thrusters, two spin-up thrusters, two fill and drain valves, two pressure transducers, two plenum reservoirs, two latching valves, and six in-line filters.

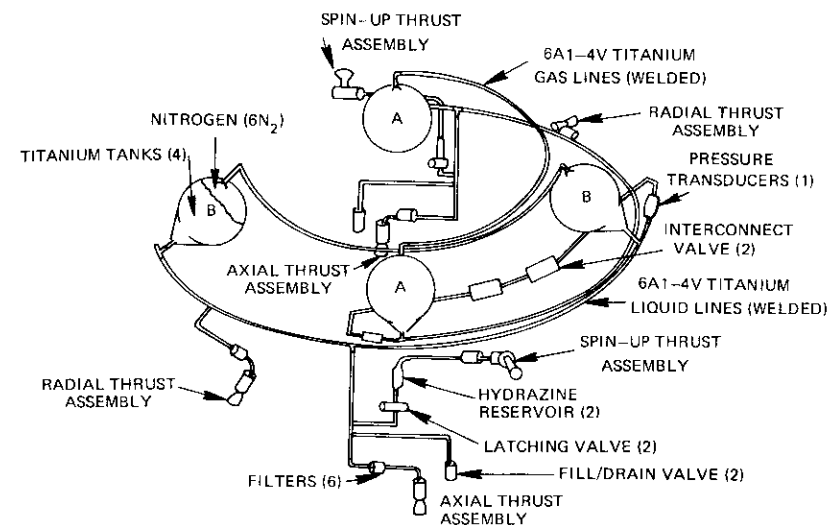


Figure 50. INTELSAT IV Positioning and Orientation System

The primary external forces acting on the spacecraft at synchronous altitude are sun and moon gravity forces, which tend to change the orbit inclination; perturbation caused by the triaxiality of the earth; and solar torques. To meet the spacecraft requirements each of these disturbances must be corrected periodically.

The large quantity of propellant expelled through the axial jets results in a large amount of uncertainty in the axial thrust direction; hence, significant spin-speed changes may occur. To provide a positive means of spin-speed control, the axial jets are biased  $0.5^\circ$  in the spin-down direction. At the end of a year or sooner, spin-speed trim can readily be achieved by the spin-up thrusters.

After the spacecraft has separated from the Centaur, the spin-up thrusters provide a means of spinning up the spacecraft to obtain stabilization for the duration of the mission. A propellant reservoir or a plenum between the spin-up thrusters and the latching valve contains the propellant for the

spin-up maneuver. The thrusters fire for eight seconds, followed by a waiting period of approximately 40 seconds for propellant tank settling and the remainder of the spin-up.

Over the 7-year life of the spacecraft, the tank pressure will vary from the initial pressure of 1.72 mN/m<sup>2</sup> (250 psi) to a final pressure of 0.690 mN/m<sup>2</sup> (100 psi). The thrusters are capable of firing in either the pulsing or the continuous firing mode. The standard firing duration is a pulse of 117 ms; however, the thrusters are operable from a pulse of 25 ms to the continuous mode.

The interconnect lines are 6.35-mm (0.25-in.) welded titanium tubing to minimize both gas and liquid leakage. The only mechanical joints in the design are the fill and drain valve and the propellant valve seats. With titanium-to-steel joints, diffusion bonded transition sections are used. The propellant tanks are conospherical in design, and have two ports, one at the apex of the cone section and the other 180° away. Because of the gravitational field, this design facilitates off-loading during spacecraft testing. Four of these tanks, which are each designed for a working pressure of 2.07 mN/m<sup>2</sup> (300 psia) absolute, carry 136 kg (300 lb) of hydrazine; the hydrazine is forced to the tank outlet on the apex of the cone section by the centrifugal field created by the spinning spacecraft.

The dual seat propellant valve for flow control into the catalytic thruster consists basically of electromagnetic and permanent magnets, a flapper and flexure tube spring assembly, and dual tungsten carbide seats. The valve operates as follows:

- a. The valve is closed and the armature is touching the closed position permanent magnet poles.
- b. The electromagnet is energized and the downstream poppet is moved from its seat.
- c. After the downstream poppet travels about 0.102 mm (0.004 in.) a striker pin contacts the upstream poppet and forces it off its seat allowing fluid to flow.
- d. When both poppets reach maximum opening, the armature is captured by the open position permanent magnet poles.
- e. When the electrical signal is removed, the electromagnetic field collapses. The permanent magnet forces are no longer sufficient to overcome the spring forces of the flexure tube and the valve returns to the closed position.

The thruster assembly is shown in Figure 51. The major components are the propellant manifold and the thrust chamber and nozzle assembly. The

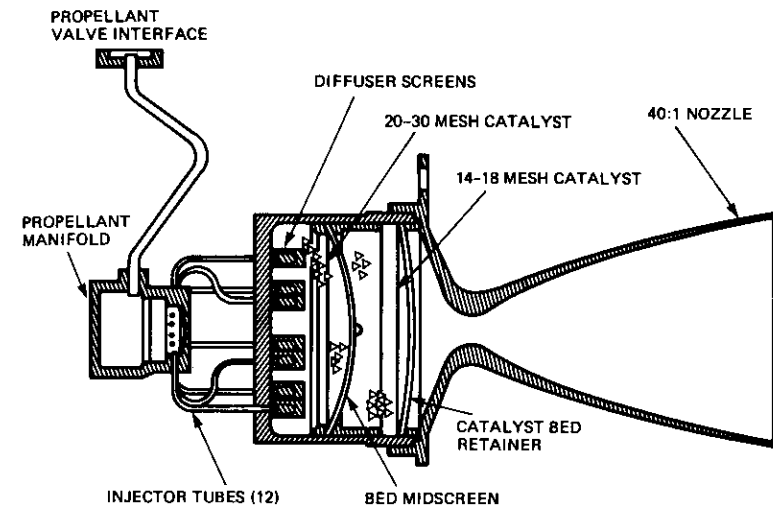
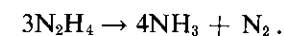
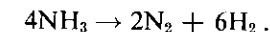


Figure 51. Thrust Assembly

manifold distributes hydrazine into the thrust assembly through 12 injector tubes. On entering the chamber, the propellant is again distributed into the catalyst bed by diffuser screens. The thrust chamber contains Shell 405 catalyst, which decomposes the hydrazine according to the following chemical reaction:



A portion of the ammonia is then further decomposed:



This portion of the ammonia that is decomposed is called the ammonia decomposition factor and is approximately equal to 0.4. The ammonia, nitrogen, and hydrogen are then exhausted through a converging-diverging nozzle to produce thrust. The nozzle expansion ratio is 40:1.

The thrust assembly performance changes over the mission life of the spacecraft because the pressure in the system decreases as the propellant is expelled. The initial thrust is nominally 25.4 N (5.7 lb) at 1.72 mN/m<sup>2</sup> (250 psia) absolute, and decreases to 12.0 N (2.7 lb) at 0.690-mN/m<sup>2</sup> (100-psia) absolute tank pressure, as shown in Figure 52, which is a plot of thrust vs tank pressure. The 3-sigma limits, which represent the statis-

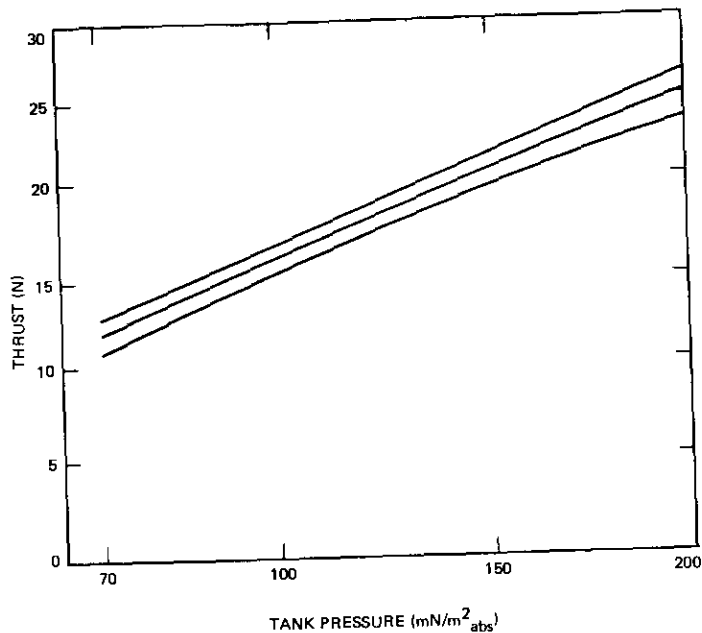


Figure 52. Thrust vs Tank Pressure

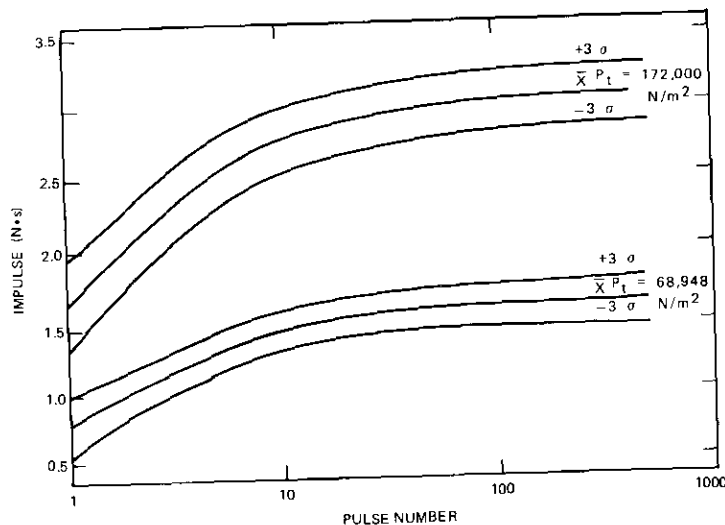


Figure 53. INTELSAT IV Thrust, Impulse vs Pulse Number

tical data of all flight thrusters, are also shown. Continuous thrusting is used for both spacecraft spin-up maneuvers and north-south station-keeping.

The pulsing performance shown in Figure 53 is the relationship between the total impulse and pulse number for two different tank pressures corresponding to the initial and final pressures of the P&O subsystem. The range between these two values is usually referred to as the blowdown range. The nominal value is shown with the 3-sigma range for flight thrusters. A 0.117-second valve operation has been utilized to standardize all thrusters. It can be seen that the thruster becomes more efficient as the pulse number becomes larger.

### Apogee motor

N. R. LARDY

The apogee motor is a high-performance, high-reliability space vehicle rocket motor which uses solid propellant. It is similar in design, materials, and fabrication techniques to the INTELSAT II and III apogee motors. Figure 54 is a cross-section of the overall configuration. The motor has a total loaded weight of 706.69 kg (1,558 lb) and provides a  $\delta v$  of 1,800 m/s (5,900 ft/s) to a spacecraft having an initial mass of 13.55 kN (3,050 lb). The nominal propellant weight is 1,383.45 kg (1,416 lb). It has been designed and developed to deliver this performance after 5-year storage when fired within the temperature range of 4.5°C to 32°C (40°F to 90°F) in a vacuum environment. It is manufactured by the Aerojet Solid Propulsion Company.

The apogee motor has a nominal total impulse of 1.822 MN-s (410,700 lb-sec) and a vacuum thrust of 68 kN (15,300 lb) with a burn-time duration of 33 seconds. Figures 55 and 56 are curves of vacuum thrust and chamber pressure vs time. Figure 57 is a plot of spacecraft acceleration.

The propellant and liner system (ANB-3066) is identical to that formulated for INTELSAT II and III and all Minuteman motors produced by Aerojet. The performance of this propellant is fully established for the INTELSAT IV mission and environment. With the 40:1 expansion ratio nozzle, the

*N. R. Lardy is a member of the Technical Staff in the Mechanics Department, Space Segment Implementation Division, COMSAT.*

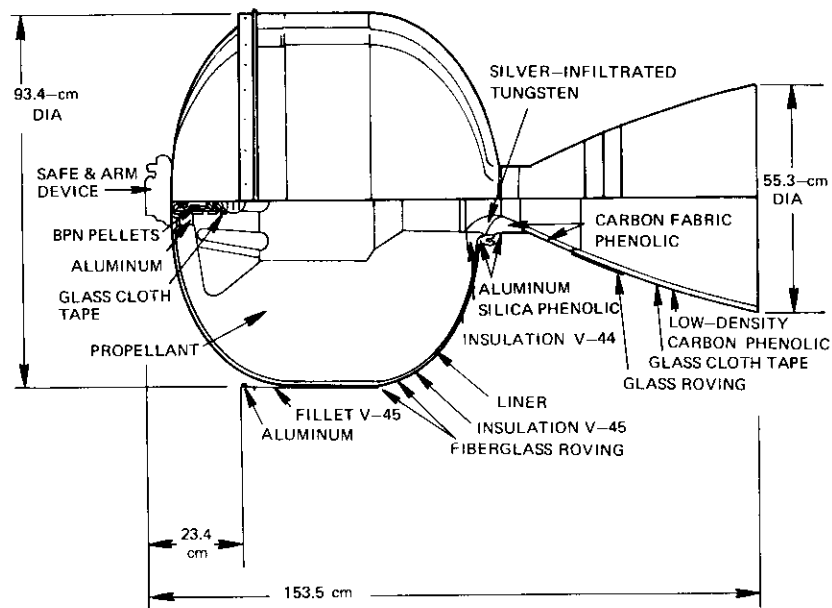


Figure 54. INTELSAT IV Apogee Motor

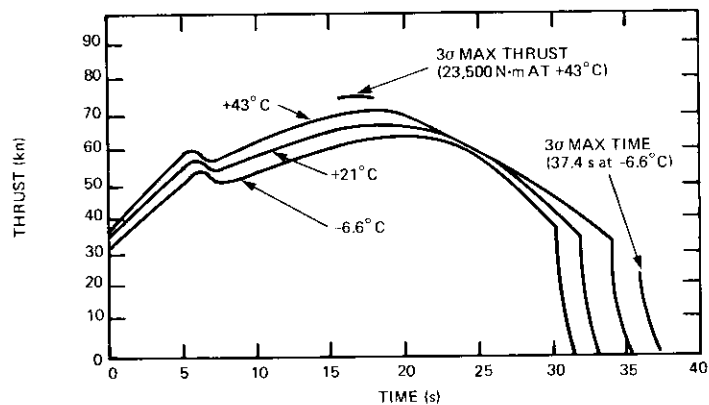


Figure 55. Vacuum Thrust vs Time

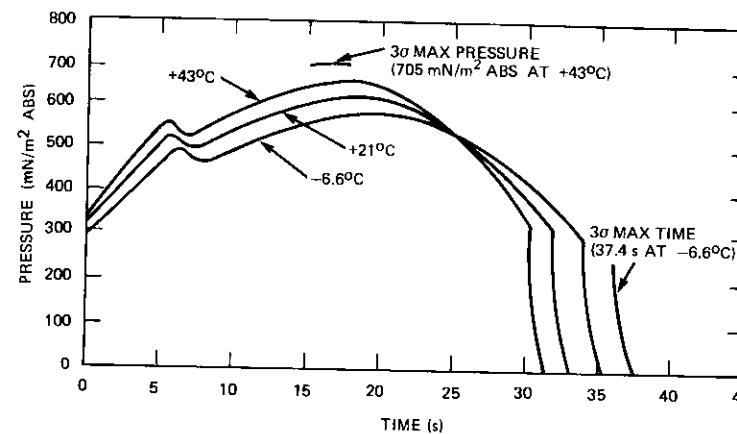
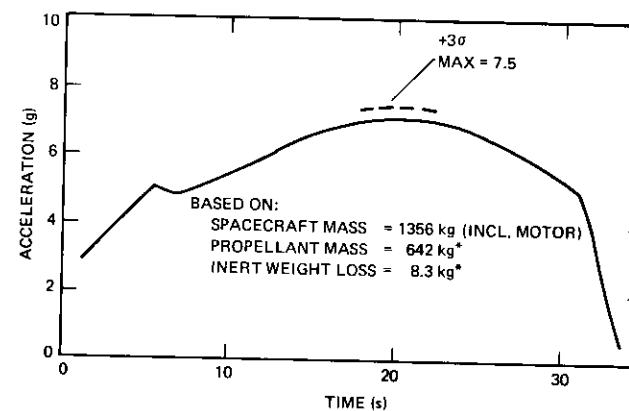


Figure 56. Chamber Pressure vs Time



\*3σ BASED ON D-4, 5, 6, 7 AND QA-1, 2, 3, 4

Figure 57. Nominal Acceleration vs Time at 194°C (90°F)

effective vacuum specific impulse is 286.1 seconds at 21°C (70°F). It is a production carboxy-terminated polybutadiene with a solids content of 88 percent with 15-percent aluminum. Its flame temperature is 3,220°C (5,836°F).

The chamber insulation is a silica-filled polybutadiene rubber whose

erosive and thermal properties have been fully characterized under a variety of actual motor conditions. It was originally developed for a Polaris program about 12 years ago and has been used in many rocket motors to date.

The propellant grain design is a finocyl with eight fins in the forward head and a fully released boot in the aft end. This shape and the fully released aft end provide a desirable thrust/time curve and low stress/strain propellant conditions throughout the full range of temperature operating conditions. The completed motor is Xrayed at 4.5°C (40°F) to shrink the propellant and magnify any cracks or unbonds that may exist in the motor. This careful nondestructive testing procedure is repeated immediately prior to rocket motor installation in the spacecraft.

The motor chamber is a high-performance pressure vessel fabricated from glass filament rovings with a tensile strength of 3.027 GN/m<sup>2</sup> (440,000 psi) in an epoxy resin matrix with an extremely high strength-to-weight ratio. It is wound over its prematched, metal-die-molded insulator and a precision-molded plaster mandrel to ensure precise dimensional control and optimum balance of the finished chamber. This is necessary because the hardware fired by the apogee motor can be a major contributor to the final spacecraft on-station imbalance. The geometry of the chamber is optimized with isotensoid dome contours and a cylindrical center section to produce nearly equal stress in all fibers and to result in maximum load carrying ability with minimum weight.

The nozzle design is a highly reliable conventional concept. It is flush mounted with an aluminum housing supporting a reinforced phenolic entrance section and contoured exit cone with a silver-infiltrated tungsten throat. The tungsten throat precludes erosion and provides precise control of the thrust vector during firing.

The ignition system consists of a perforated glass chamber with boron potassium nitrate (BPN) pellets as the pyrotechnic charge. This charge is initiated with a Bulova safe and arm device.

The inert components prior to propellant casting and the complete and fully flight configured motor are precisely balanced, both statically and dynamically, to ensure spacecraft stability before and after apogee motor firing in orbit.

## ***Nutation damper***

W. A. NAKANO

Nutation damping of the INTELSAT IV spacecraft is provided by two passive eddy current dampers mounted on the despun platform and an active nutation damper (AND) system mounted on the rotor. The dampers are designed to absorb nutational energy during transfer orbit operations, post-apogee boost phase, and normal synchronous orbit operations including spin-up and stationkeeping. The dampers must be effective for various inertial configurations from pre-apogee boost to end-of-life. The eddy current dampers are designed for nutation angles less than 1°, while the AND is designed for angles more than 0.5°.

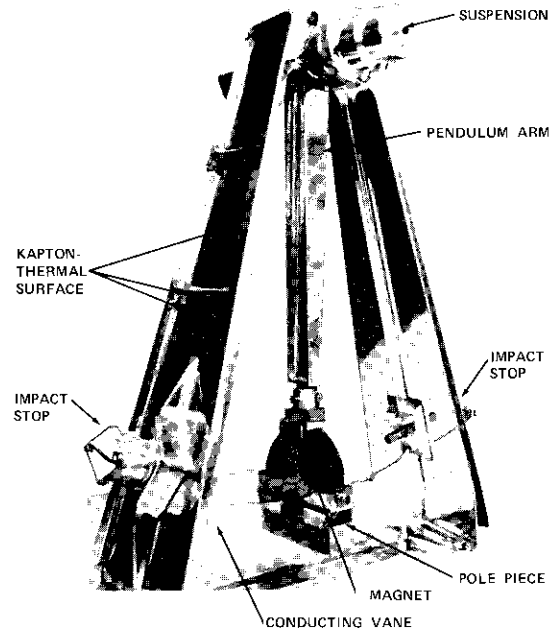
The passive nutation dampers (Figure 58) are pendulous, single-axis, eddy-current-type dampers. Two almost identical dampers are employed high on the antenna mast in orthogonal axes perpendicular to the spin axis. The upper and lower dampers are located 2.55 m (8.37 ft) and 2.00 m (6.55 ft) from the synchronous orbit CG, respectively. The upper damper has a natural frequency of 1.63 rad/s and the lower damper has a natural frequency of 1.89 rad/s.

The basic elements of the damper are the structure, the pendulum suspension system, the magnet and its pole pieces, the eddy current conducting vane, and the impact stops. The structure is basically an equilateral triangle with an eddy current conducting (aluminum) vane as the base, an impact stop mounted on each side, and an apex containing the pendulum suspension system.

The pendulum suspension system is a cantilevered torsion quill shaft. The natural frequency of the pendulum can be controlled by very accurately machining the beryllium copper quill shaft. The quill shaft is tested separately to determine its torsional spring constant and measured for straightness and concentricity. Upon assembly into the damper, it is held in place at one end by a collet end cap, which is in turn screwed on to the structure. Its other end is attached to the rotor (hollow shaft) from which the pendulum is suspended by a cantilever. Both ends of the rotor are caged in a dry lubricated journal bearing designed to operate with a 0.25-mm (0.010-in.) clearance in 0-g damper operation. This clearance prevents

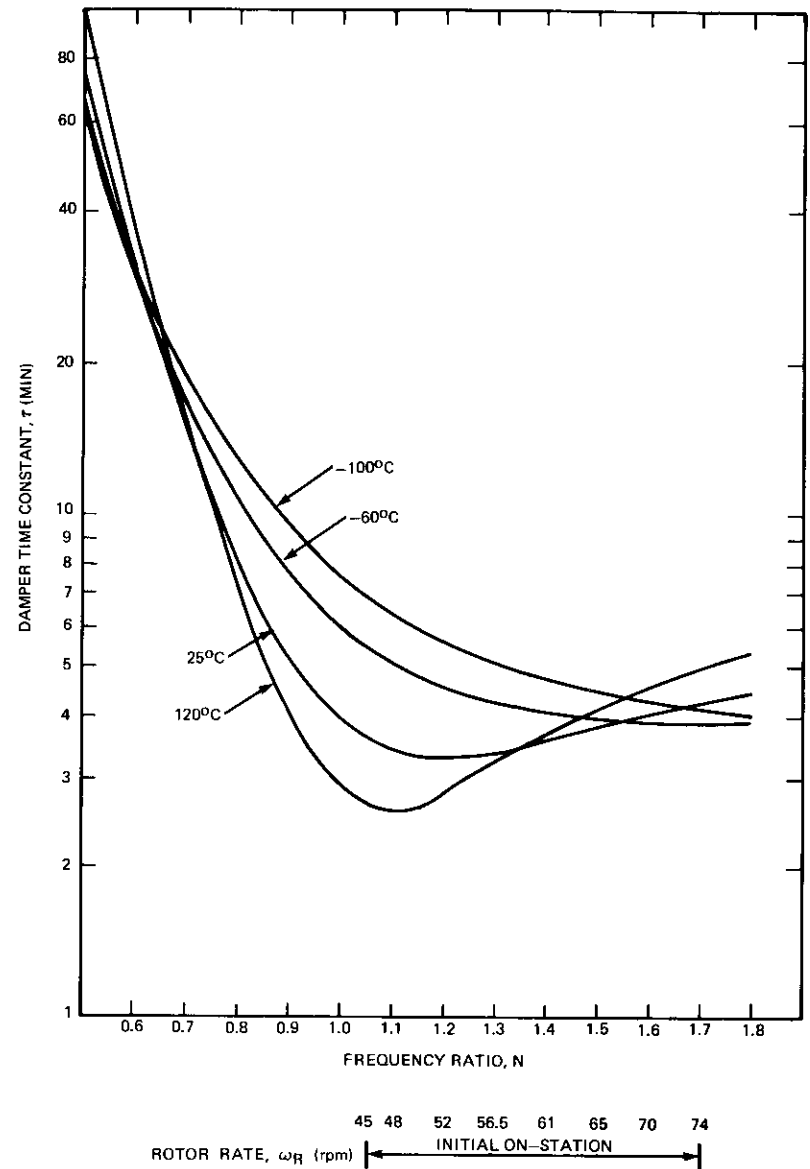
---

*W. A. Nakano is a member of the Technical Staff in the Mechanics Department, Space Segment Implementation Division, COMSAT.*

Figure 58. *Nutation Dampers*

stiction dead band. The journal bearings limit the rotor excursion to prevent excessive load transmission to the quill shaft during launch and apogee motor fire.

The performance criterion for a damper mounted on the despun platform is the effective time constant. The time constants of the upper and lower dampers (which are different) must be combined to yield the total damper time constant. The lower damper is tuned to the synchronous orbit mass properties and the upper damper is tuned to a value that lies between the transfer orbit and synchronous orbit inertial conditions. This is shown in Figure 59, where the damper constant is plotted against the frequency ratio and rotor rate for various temperatures.

Figure 59. INTELSAT IV *Nutation Damper Damping Time Constant vs Frequency Ratio*

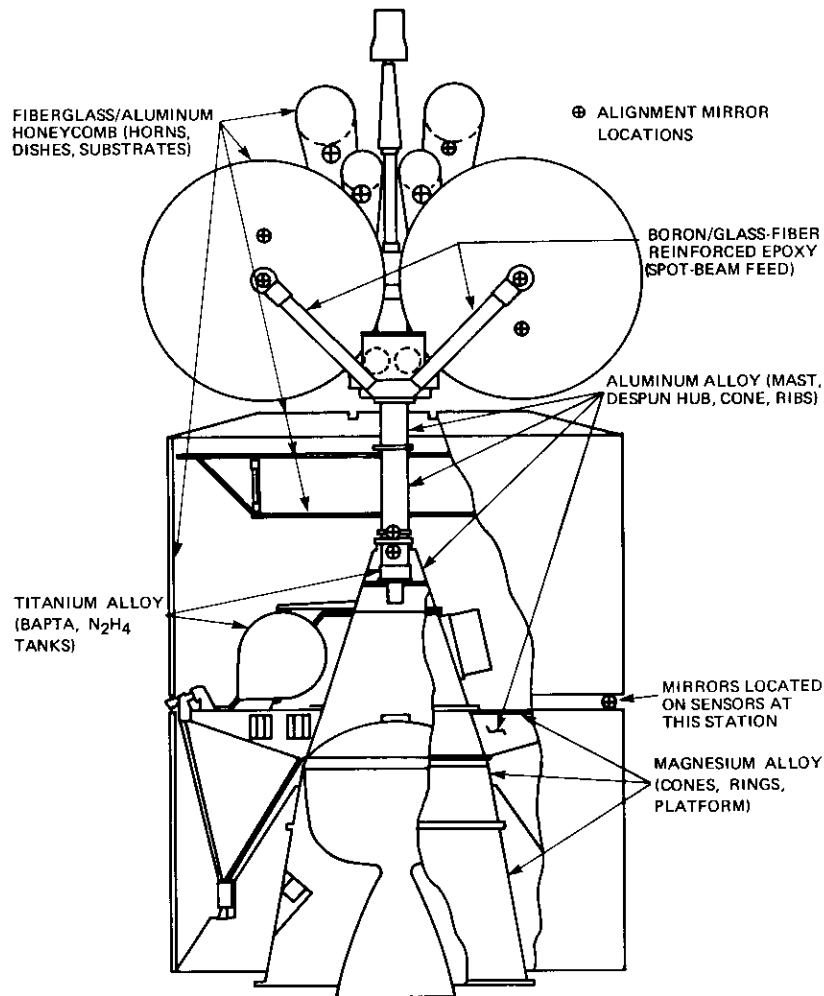


Figure 60. General Distribution of Materials Used in the Spacecraft

## Mechanical design

W. L. DAY

The spacecraft structure or spaceframe can be divided into two major parts: the despun section and the spinning section. The despun section can be subdivided into the despun (or communications) compartment and the mast/antenna subassembly. The spun section can be subdivided into the thrust cone and platform subassembly and the solar substrates. The two major sections, despun and spun, are joined by a rotary interface unit called the bearing and power transfer assembly (BAPTA).

The dual-spin configuration of the spacecraft is based on a symmetrical and balanced weight distribution. Through an efficient use of load paths and materials, the structure constitutes less than 14 percent of the launch payload weight. The selection of materials and manufacturing processes for the structure was influenced by the demand for high reliability and economy. Thus, standard aluminum and magnesium alloys, fiberglass-reinforced epoxy, and aluminum honeycomb sandwich constructions are used extensively. To obtain increased vibration damping characteristics and to minimize distortion, mechanical fasteners, instead of welded joints, are used throughout the relatively large spaceframe. Figure 60 shows the general distribution of materials used in the spacecraft.

The spaceframe was designed to handle the numerous loading conditions imposed on the system during flight. The most significant structural loads acting on the spaceframe occur during lift-off from the launch pad. Other periods of high load on the spacecraft occur during the launch ascent, engine ignitions and cutoffs, separation and jettison of major portions of the launch vehicle, spacecraft separation, and apogee motor firing.

The despun compartment structure is composed of forward and aft aluminum honeycomb shelves separated and stiffened by six radial, machined aluminum ribs, which are in turn riveted to the mast assembly. The aft flange is bolted to the BAPTA shaft with eight high-strength alloy steel bolts. The BAPTA must be thermally and electrically isolated from the structure, which is accomplished by using insulating washers. Components are fastened to the despun shelves by threaded locking inserts molded into shelves in predetermined patterns designed to optimize weight and balance.

*W. L. Day is a member of the Technical Staff in the Mechanics Department, Space Segment Implementation Division, COMSAT.*

The antenna mast assembly supports all antennas, two nutation dampers, and a balance arm. The mast is basically an aluminum tube, concentric with the spin axis, with a tubular aluminum crossarm normal to the mast. The crossarm supports the two spot-beam dishes and the antenna positioning mechanisms. The feed horns for the spot-beam antennas are mounted at the ends of self-supporting elliptical waveguides cantilevered from a bracket near the base of the mast. These waveguides are molded boron filament and fiberglass-reinforced epoxy with a conductive inner surface and aluminum flanges at either end. The spot-beam dishes are fiberglass-reinforced epoxy and aluminum honeycomb sandwich with an RF reflective facing. The four global horns are also honeycomb with aluminum feeds at the base.

The horns are fully gimballed from their bases to the mast feed bracket and are stabilized near the large diameter end by a single-axis gimbal bracket to allow for mast flexure during launch. The nutation dampers are bolted to braced aluminum platforms normal to the mast. A balance arm with adjustable weights is cantilevered normal to and near the top of the mast.

The spinning structure consists of three separable cone assemblies: the booster adapter, intermediate cone and platform, and BAPTA cone. The booster adapter consists of an unstiffened magnesium conical shell riveted at each end to a machined magnesium ring forging. The aft flange contains an 8-bolt hole pattern for attachment to the launch vehicle. The forward flange attaches to the aft flange of the intermediate cone by means of the spacecraft separation system clamp. The booster adapter and separation clamp remain with the launch vehicle after separation of the spacecraft. A conical-shaped charge-destruct package is mounted on a bracket within the adapter.

The intermediate cone consists of three conical magnesium shells joined by two magnesium rings and flanged at the bottom by a magnesium vee-band clamp ring and at the top by an aluminum bolt flange ring. The apogee motor is mounted within the intermediate cone by a circumferential row of 36 shoulder bolts. On the outside of the cone and cantilevered from the two center rings are eight equally spaced, radially projecting ribs. The aluminum ribs are stabilized circumferentially by aluminum intercostals between the outboard rib ends and a thin magnesium shear web riveted across the entire forward surface to form a "platform." The platform supports the positioning and orientation subsystem, sun and earth sensors, and the batteries. The portion of the intermediate cone above the platform contains machined aluminum brackets which support the spin-

ning encoder/decoder stacks, despin control electronics units, squib and solenoid drivers, and battery controllers.

The BAPTA cone is a 1-piece machined aluminum forging, which bolts to the forward flange of the intermediate cone. An integrally machined flange in the middle of the cone provides an attachment for the four radial spokes laterally supporting the aft end of the BAPTA. Since the entire BAPTA unit must be both thermally and electrically isolated, all joints are fully insulated by nonconductive gaskets, washers, and sleeves.

The substrates for solar cell arrays are 1-piece molded aluminum honeycomb and fiberglass cylinders. The two solar panels completely enclose the periphery of the spinning section and are cantilevered fore and aft from the brackets on the spinning platform. The sunshield substrate consists of aluminum honeycomb cone and disc segments with bolted joints. The entire shield assembly is bolted around the outer periphery to the forward edge of the forward solar panel. The spacecraft with the booster adapter is bolted to the launch vehicle by eight 1.27-cm (0.50-in.) diameter bolts. Separation of the spacecraft during the launch sequence occurs at the forward end of the booster adapter.

The spacecraft is secured to the adapter by a vee-band clamp assembly, which is tensioned by two pyrotechnic bolts. When the spacecraft separates from the launch vehicle, the explosive bolts are fired and the band is retracted by springs in two halves, aftward, into catchers located on the adapter. Eight equally spaced separation springs, axially aligned within the interface joint, force the spacecraft forward and clear of the adapter and launch vehicle.

The separation clamp consists basically of two thin half-bands of steel. Upon tensioning, these half-bands apply radial pressure to a number of circumferential, single-vee-grooved steel shoes which are attached to the band, and which in turn clamp the tapered flanges of the thrust cone and adapter together. Strain gauges are attached to each band-half to indicate proper band tension at installation.

The BAPTA clamp prevents rotary motion between the spun and despun sections during vibration testing and launch. More importantly, it prevents high-moment loads, caused by lateral forces, from being passed through the bearings by carrying approximately 90 percent of the load directly through the clamp from shaft to housing. The clamp is similar in construction to the separation band, except that a unique floating center piece causes the shoes to form a double vee to ensure even clamp-up while maintaining the proper gap between flanges. (When unclamped, the gap between flanges is maintained by an axial bearing preload spring.)

The spacecraft is aligned by a combination of mechanical and optical devices, including a precision rotary table (Rotab), dial indicators, and theodolite. The thrust cone apogee motor ring and BAPTA flanges are initially aligned with dial indicators during assembly on a Rotab. The BAPTA is subjected to subsequent optical checks at various stages of assembly and post-test disassembly by means of precision quartz mirrors, aligned to the bearing axis. Boresight mirrors are used to align the sensors. Temporary mandrel-mounted mirrors located on the throat axis are used to align the thrusters.

The global horns, spot-beam dishes, and feed horns are individually aligned by theodolite with the aid of bonded-on mirrors calibrated to the boresights. In addition, these dishes are individually aligned to their respective feed horns by a fixture which is counterbalanced to account for dish gravity sag. Figure 60 gives the locations of permanently attached mirrors.

The despun and spun sections are balanced individually. The despun section is balanced statically on a spin balance machine. Center of gravity, concentricity, and vertical product of inertia are trimmed by adding small weights to the compartment shelf, the lower nutation damper bracket, and the mast balance arm. The spun section is spin balanced at 80 rpm on a Treble machine. Spun section trim balance is achieved by adding small weights at the platform periphery and at the forward and aft ends of the solar panels.

### **Thermal control**

J. A. ROBINSON

Temperature control of the INTELSAT IV spacecraft is essentially a series of subsystem-oriented local heat transfer problems within a bus environment which, except during eclipse (earth shadowing) periods, is a comfortable 10°C (50°F) to 25°C (75°F).<sup>\*</sup> For periods of 45 days centered

<sup>\*</sup> This environment is a fortunate side effect of the spinning cylinder covered with solar cells.

*J. A. Robinson is a member of the Technical Staff in the Mechanics Department, Space Segment Implementation Division, COMSAT.*

about each spring and fall equinox, the spacecraft experiences a daily eclipse lasting up to 70 minutes. Many of the subsystem thermal design characteristics result from the need to maintain desired temperature levels during those periods when the solar array drum drops to temperatures as low as -85°C (-120°F).

Heaters are the only active temperature control elements on the spacecraft. All other components, including surface finishes and wraps, multi-layer insulation blankets (MLI), and conduction filler and isolation materials, are passive. All but one of the heaters used in the system are commandable, resistance-wire-type heaters with fixed power. The only exception is the noncommandable proportional controlled heater circuit, which heats the TDA in the communications receiver unit electronics box. This heater is activated when the receiver is operating and is designed to maintain TDA temperature above 26°C (79°F) at all times. Figure 61 is a cutaway sketch of the spacecraft showing the various subsystems and the temperature control elements.

### **Antenna and mast assembly**

Since the antenna and mast assembly is despun and outside of the spacecraft, it does not benefit from the uniform thermal environment provided to the internal subsystems by the spinning solar array drum. The sun makes one complete rotation relative to the antenna and mast assembly in a 24-hour period. The resulting heat loads consist of daily combinations of direct solar heating, reflected solar heating from other components and the forward end sunshield, and varying degrees of shadowing. None of the equipment is particularly sensitive to the resulting temperature extremes; however, structural distortions caused by large temperature gradients are of concern. Multilayer insulation blankets are used extensively to minimize these gradients. These blankets are made from a combination of aluminized kapton film, fiberglass mat, mylar film, and aluminum foil, and are constructed as described in Table 23.

The blanket external surface has a low solar absorptance-to-emittance ratio ( $\alpha_s/\epsilon \approx 1/2$ ), which helps to minimize the blanket surface temperature when irradiated. Temperature control of the nutation dampers is achieved by conduction coupling to the mast (which experiences relatively small gradients and diurnal variations because of its large mass and conductivity) and by highly polished and aluminized teflon surface coatings to reduce radiation interchange.

The antenna positioner mechanism (APM) motors heat very rapidly

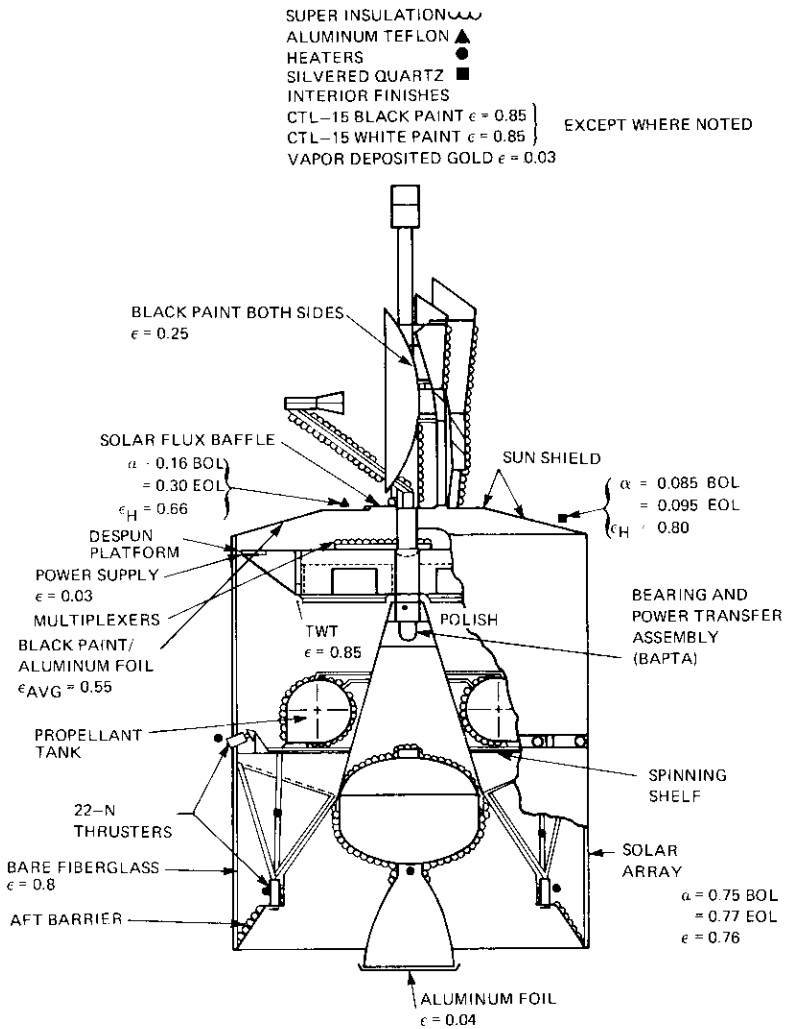


Figure 61. INTELSAT IV Thermal Control Elements

during operation because power dissipated by the windings is trapped inside by the external insulation. To prevent overheating, APM motor operation is limited to a duty cycle of four minutes on in any 30-minute period.

TABLE 23. ANTENNA FARM THERMAL INSULATION SUMMARY

LOCATION	BLANKET LAYER DESCRIPTION	ILLUSTRATION
<ul style="list-style-type: none"> <li>● LOWER MAST</li> <li>● CROSS ARM</li> <li>● ANGLE BRACE</li> <li>● SUPPORT</li> <li>● FEED HORN SUP- PORT MAST</li> <li>● FEED HORN MOUNTING BRACKET</li> <li>● FEED HORN</li> <li>● WAVEGUIDE</li> <li>● GLOBAL HORNS</li> </ul>	<p>ALTERNATE FIVE LAYERS OF FIBERGLASS MAT AND PLASTIC FILM. THE THREE INNER LAYERS OF PLASTIC FILM ARE MYLAR, ALUMINIZED BOTH SIDES. THE FOURTH LAYER OF PLASTIC FILM IS KAPTON, ALUMINIZED BOTH SIDES. THE OUTER LAYER OF PLASTIC FILM IS KAPTON, ALUMINIZED ONE SIDE, KAPTON SIDE OUT.</p>	
<p>FEED HORN SUPPORT TUBE</p>	<p>INNER LAYER - 75-μ ALUMINUM FOIL. THEN ALTERNATE FIVE LAYERS OF FIBERGLASS MAT AND PLASTIC FILM. THE THREE INNER LAYERS OF PLASTIC FILM ARE MYLAR, ALUMINIZED BOTH SIDES. THE OUTER LAYER OF PLASTIC FILM IS KAPTON, ALUMINIZED ONE SIDE, KAPTON SIDE OUT.</p>	

**Despun compartment**

Roughly 90 percent of the spacecraft's internal power dissipation is in the despun compartment (440 watts at beginning-of-life bus voltage). The majority of this power is concentrated at the TWTs and their power supplies. Hence, thermal control in this area involves both local temperature control of the dissipating components and bulk temperature control of the compartment.

Bulk temperature control of the compartment requires dumping the dissipated power from the compartment into space. This function is performed by the forward end sunshield, which also performs the function indicated by its name. The sunshield has two sections. The inboard section is disc-shaped and is covered on the space side with aluminized teflon ( $\alpha_s = 0.16, \epsilon = 0.66$ ). The outboard section is conical and is covered on

the space side with silvered quartz mirrors, which are highly efficient solar reflectors and infrared radiators ( $\alpha_s = 0.085$ ,  $\epsilon = 0.8$ ). The TWTs and power supplies are located toward the outboard edge of the compartment, placing most of the power dissipation under the outboard section of the sunshield. The internal radiation coupling provided by black paint on the compartment shelf ( $\epsilon = 0.85$ ) and a combination of black paint and aluminum foil stripes ( $\epsilon = 0.55$ ) on the inside of the sunshield permits the shield to effectively dump the compartment power dissipation into space.

Local temperature control of the TWTs and power supplies requires simultaneous heat sinking of dissipated power to the mounting surface and protection from eclipse cooling. TWTs and power supplies, as well as all electronics boxes in the compartment, are mounted with RTV filler in the interface to improve contact surface conduction area. The power supplies, communications receivers, and certain other electronics boxes are plated with vapor-deposited gold ( $\epsilon = 0.03$ ) for required radiation isolation during eclipses. The remaining boxes are painted with high-emittance white paint ( $\epsilon = 0.85$ ). Output multiplexers, located atop the compartment under the disc sunshield, are covered with aluminized mylar MLI to decouple them from sunshield cooling during eclipses.

#### **Bearing and power transfer assembly**

Temperature control of the BAPTA is accomplished with a combination of surface finishes, conduction isolation, and heaters. A 1-mm (40-mil) phenolic washer provides some conduction isolation at the BAPTA interfaces with the spinning thrust cone and the despun mast hub. Surfaces of the BAPTA with a view outside the thrust cone or into the mast are wrapped with aluminum foil tape ( $\epsilon = 0.05$ ). The BAPTA clamp support structure is polished aluminum. All of these characteristics are intended to decrease BAPTA cooling during eclipses. Commandable heaters are attached to the spinning housing and despun shaft at either side of the BAPTA forward bearing: two 5-watt heaters on the housing, and one 11-watt heater on the shaft. They can be used to increase the BAPTA steady-state operating temperature level or to provide compensatory heating during eclipse cooling periods.

#### **Thrust cone, spinning shelf, and aft thermal barrier**

Spacecraft components mounted on the thrust cone and spinning shelf include batteries, despin control electronics, squib and solenoid drivers,

spinning encoder/decoder, battery controller, and position and orientation subsystem. (Positioning and orientation will be discussed separately in the next section.) Power dissipation in these units is small; thus they tend to seek thermal equilibrium with their environment, which consists of solar panels and the aft thermal barrier.

As described previously, the solar panel provides a very suitable environment except during eclipses. The aft thermal barrier is a rigid insulation blanket which serves as closure of the aft end of the spacecraft. It is composed of an outer layer of 50- $\mu$  (2-mil) stainless sheet (with black paint on the outside, and vapor-deposited gold on the inside) and one to two layers of 13- $\mu$  (0.5-mil) nickel foil separated by a 50- $\mu$  (2-mil) thickness of glass matting material. The inner nickel foil layer is bare ( $\epsilon = 0.06$ ). In addition to minimizing spacecraft heat losses out the aft end, the aft barrier shields the spacecraft from apogee motor exhaust plume heating and contamination.

Very few special temperature control techniques are used on the equipment in this area. Because of their thermal capacity and conduction to the thrust cone, cone-mounted electronics experience an eclipse cooling that results in acceptable temperatures without additional heaters or insulation. Stacking cone-mounted boxes helps to concentrate thermal capacity and save "floor space." The batteries are mounted on structural ribs about the spinning shelf and experience satisfactory eclipse temperatures because of their thermal capacity.

#### **Positioning and orientation subsystem**

Positioning and orientation subsystem temperature control is designed to prevent hydrazine from freezing in orbit. Hence, heaters and insulative surface wrapping are used extensively. The heaters are resistance wires embedded in rubber molding shaped to fit around lines and valves. All P&O heaters respond to one command and are normally on at all times. To minimize eclipse cooling, lines and valves are conductively decoupled from the spacecraft structure with low-conductivity spacer materials and wrapped with low-emittance aluminum foil tape ( $\epsilon = 0.05$ ) to reduce radiation cooling. Propellant tanks are covered with aluminized mylar MLI.

Thruster temperature control during and after firing is a challenging problem. The spacecraft is shielded from the very high ( $\sim 800^\circ\text{C}$  or  $\sim 1500^\circ\text{F}$ ) thruster firing temperatures by enclosing the thrust chamber assembly in a canister consisting of two concentric shells of stainless

steel separated by refrasil batting. During the firing period, cool flowing fuel maintains relatively low temperatures on all surfaces in contact with it. After thruster firing ceases, the fuel cooling also ceases, and conduction and radiation from the thrust chamber to previously fuel-cooled parts results in heat soakback. Peak soakback temperatures experienced by the valve and fuel distribution manifold are as high as 121°C (250°F) and 343°C (650°F), respectively, for long firings. To prevent potential high-temperature decomposition of hydrazine in the manifold, subsequent firings of a given thruster are not permitted until measured valve and manifold temperatures have cooled to 107°C (225°F) and 177°C (350°F), respectively. This no-fire period lasts up to one hour after firing.

#### Apogee motor

The temperature control requirement for the apogee motor is a propellant and nozzle throat area temperature between 4°C (40°F) and 32°C (90°F) throughout transfer orbit (up to 100 hours). This temperature range is maintained by means of heaters and multilayer insulation. The insulation increases the cooling time constant of the propellant case; the heaters heat the nozzle throat and block that heat loss path from the case. At the throat, four independently commandable heaters provide 70 watts of power in 5- to 15-watt increments. The heat required is a function of transfer orbit sun angles and normally varies from 40 watts when the sun is 65° from the positive spin axis to 0 watts when the sun is 100° off the axis. Post-apogee motor firing heating caused by soakback to the spacecraft is minimized by the MLI case blanket and conduction isolation at the mounting ring.

#### Spacecraft thermal/vacuum testing

The purpose of system-level spacecraft thermal/vacuum testing is to verify spacecraft functional and thermal performance at temperature and vacuum conditions equivalent to those in orbit. The INTELSAT IV spacecraft has three grades of system level thermal/vacuum tests: thermal design verification, qualification, and flight acceptance. Unit and subsystem thermal/vacuum testing is widely practiced on INTELSAT IV, but will not be described here.

**Thermal Design Verification.** Thermal design verification is performed on the thermal test vehicle (TTV) in a vacuum chamber having a solar

simulator. Emphasis is placed on antenna and mast assembly temperature and distortion performance under simulated daily and seasonal solar heating loads. Results of this test are used to establish external surface temperatures (solar panel, sunshield, and aft barrier) to be controlled in qualification and acceptance thermal/vacuum tests without the solar simulator.

**Qualification and Flight Acceptance.** A qualification test is performed on the Y-1 qualification model spacecraft, and flight acceptance tests are performed on each flight model spacecraft as a part of final acceptance procedures. Both tests use the same thermal/vacuum chamber equipment. The test setup is pictured in Figure 62. Without a solar simulator, external heating is accomplished by means of a stationary, narrow, vertical array of infrared lamps. The spacecraft is spinning on a constant-speed spin motor. Adjusting the lamp power makes it possible to achieve various

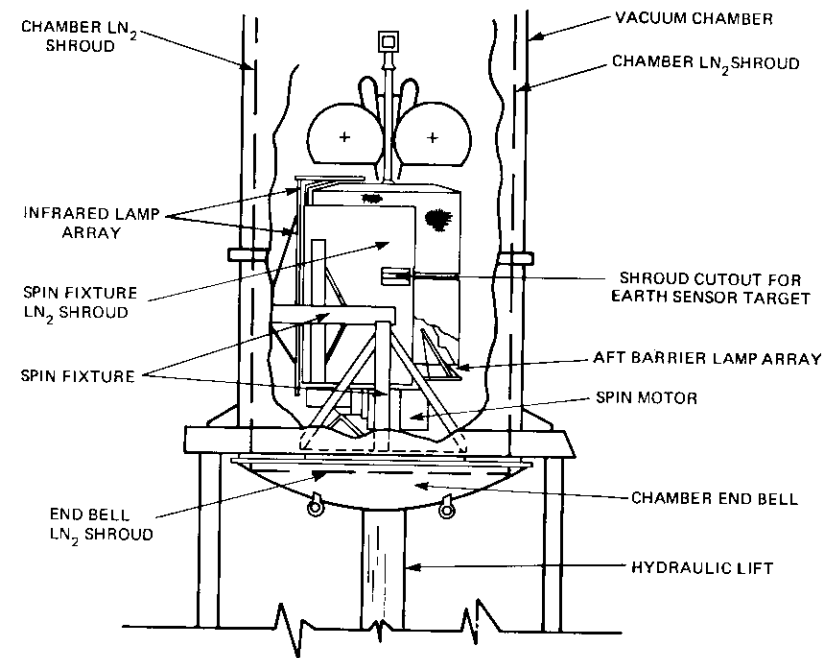


Figure 62. Spacecraft Thermal/Vacuum Test Setup

TABLE 24. FLIGHT ACCEPTANCE THERMAL/VACUUM TEST  
THERMAL CONDITIONS MATRIX

Test Phase	I	II	E1	III	E2	IV	E3	V	E4	VI
Season	Summer	Equinox	Eclipse	Equinox	Eclipse	Equinox	Eclipse	Equinox	Eclipse	Winter
Bus Voltage	← Beginning of Life → 33 V			← End of Life → 23.5 V						
Power	440 W			220 W						
Boundary Temp. Margin	+5.5°C (+10°F)	+5.5°C (+10°F)	+5.5°C (+10°F)	0	0	-5.5°C (-10°F)	-5.5°C (-10°F)	0	0	-10°F
Solar Array Temp.	Forward 20°C (68°F)	30°C (86°F)	—	23°C (74°F)	—	18°C (64°F)	—	23°C (74°F)	—	13°C (55°F)
	Aft 21°C (69°F)	28°C (83°F)	—	23°C (75°F)	—	18°C (65°F)	—	23°C (75°F)	—	16°C (61°F)
Sunshield Temp.	Disc 19°C (67°F)	9°C (48°F)	—	-1°C (30°F)	—	-6°C (20°F)	—	-1°C (30°F)	—	-24°C (-11°F)
	Cone -6°C (20°F)	-11°C (12°F)	—	-22°C (-7°F)	—	-27°C (-17°F)	—	-22°C (-7°F)	—	-37°C (-34°F)
Aft Barrier Temp.	Center -62°C (-80°F)	-68°C (-90°F)	—	-68°C (-90°F)	—	-68°C (-90°F)	—	-68°C (-90°F)	—	+32°C (+90°F)
	Aft -79°C (-110°F)	-84°C (-120°F)	—	-84°C (-120°F)	—	-84°C (-120°F)	—	-84°C (-120°F)	—	+54°C (+130°F)

spacecraft surface temperatures, simulating seasonal and internal power dissipation temperature conditions. To simulate eclipses, the lamps are simply turned off.

Table 24 shows the sequence of thermal conditions used in the 120-hour flight acceptance test. The Y-1 qualification test follows essentially the same sequence, but 11°C (20°F) temperature margins on the boundaries are used instead of the 5.5°C (10°F) margins used in the acceptance tests. Discussion of test temperature results will be foregone in favor of the measured in-orbit temperature data which will be presented in the following section.

#### In-Orbit temperature data

The INTELSAT IV spacecraft telemetry system includes 32 flight temperature sensor channels. Representative flight data for both transfer and synchronous orbits will be presented in the following table and figures. These data summarize INTELSAT IV operating temperatures and demonstrate the results of the temperature control techniques discussed in the preceding paragraphs.

Figures 63 and 64 show the critical transient temperature performance for two key subsystems during transfer orbit: apogee motor and axial thruster. Of interest in Figure 63 is the obvious role of the heaters in

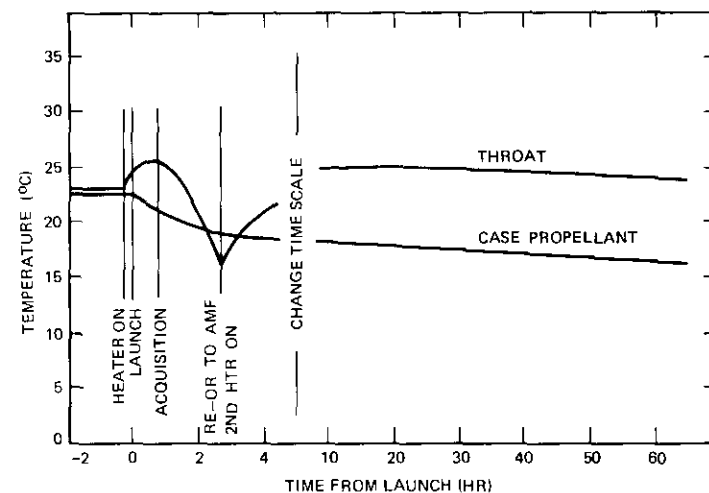


Figure 63. Transfer Orbit Apogee Motor Temperature

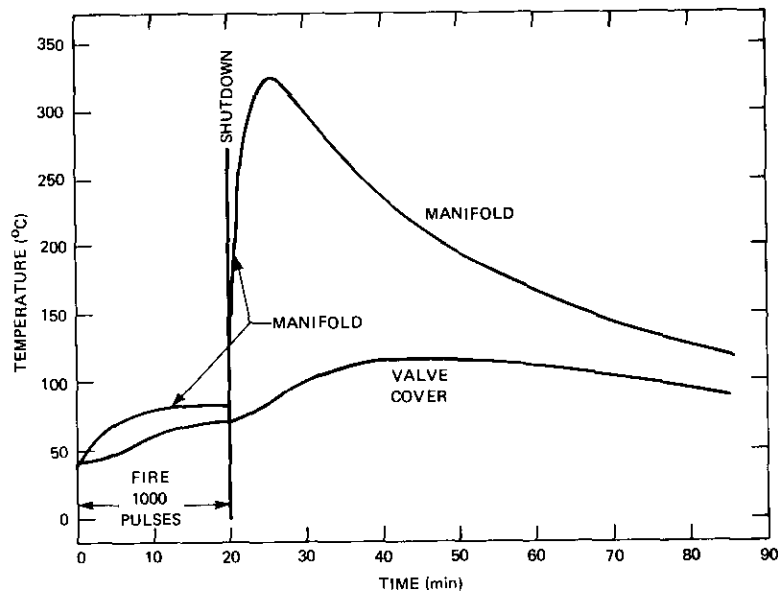


Figure 64. 1,000-Pulse Axial Thruster Firing Post-AMF Reorientation

keeping apogee motor temperatures within the required 4°C (40°F) to 32°C (90°F) band throughout the transfer orbit. The thruster temperature responses in Figure 64 show the tremendous importance of fuel cooling during thrusting maneuvers and the resulting thermal soakback after engine shut-down.

Table 25 summarizes seasonal temperature variations of selected spacecraft external structures and key components in synchronous orbit. Figure 65 is a sample of typical eclipse responses and daily fluctuations for a full 24-hour period at equinox, including a 70-minute eclipse. Of interest in this figure is the daily fluctuation of sunshield temperature and its attenuated effect on internal temperatures of such components as the TWTs. This fluctuation is caused by the varying heat loads resulting from the once-per-day revolution of the sun about the despun antenna and mast assembly. Also of interest are the widely differing temperature responses to eclipse, ranging from the large and rapid response of the solar panel to the much slower and smaller response of the BAPTA, which is a result of its large thermal capacity and high isolation.

TABLE 25. SEASONAL TEMPERATURE VARIATIONS OF SPACECRAFT STRUCTURES AND COMPONENTS IN SYNCHRONOUS ORBIT

	SUMMER SOLSTICE	WINTER SOLSTICE	EQUINOX	ECLIPSE MINIMUM
SOLAR PANEL				
FWD.	14°C	17°C	22°C	53°C
AFT	10°C	17°C	20°C	79°C
SUNSHIELD				
DISC	12°C	-18°C	-4°C	-40°C
CONE	-9°C	-29°C	-19°C	51°C
TWT	36°C	29°C	35°C	10°C
POWER SUPPLY	37°C	31°C	36°C	3°C
RECEIVER				
ON	31°C	30°C	32°C	26°C
OFF	22°C	17°C	22°C	13°C
BAPTA (ON/OFF)*				
HOUSING	31°C/19°C	33°C/21°C	37°C/24°C	27°C/14°C
SHAFT	28°C/22°C	26°C/20°C	32°C/24°C	23°C/16°C
MOTOR	26°C/20°C	29°C/21°C	32°C/25°C	23°C/17°C
BATTERY				
3-CELL	9°C	17°C	22°C	1°C
7-CELL	9°C	17°C	21°C	4°C
P&O TANK	17°C	21°C	21°C	21°C
AXIAL VALVE	24°C	41°C	33°C	19°C
AXIAL MANIFOLD	13°C	44°C	22°C	9°C
RADIAL VALVE	31°C	33°C	38°C	21°C
SPIN VALVE	33°C	36°C	38°C	21°C

\*BAPTA HOUSING HEATERS ON/OFF.

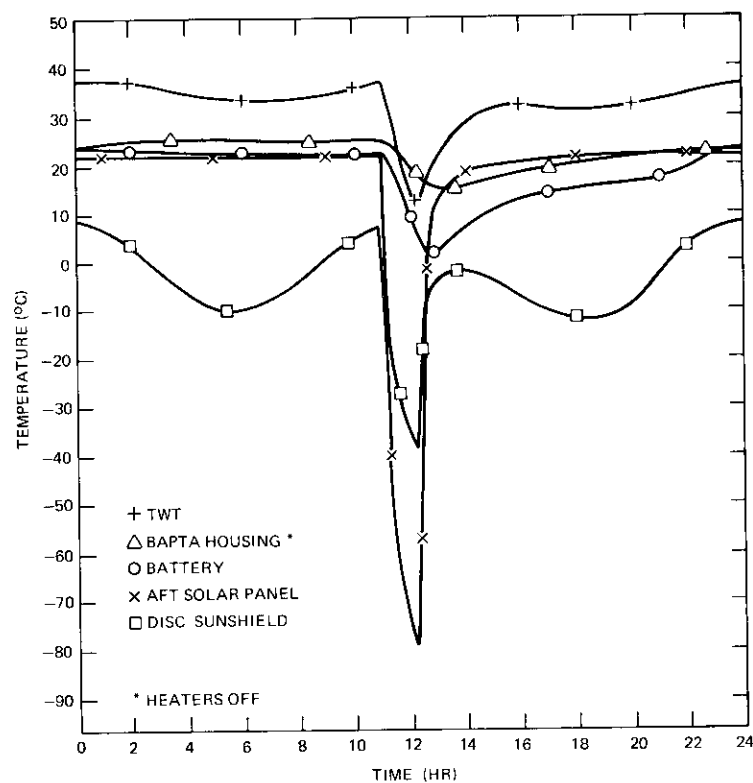


Figure 65. Representative Eclipse and Diurnal Temperature Responses (typical long eclipse day)

### Bibliography

The references below describe subsystems of the INTELSAT IV spacecraft, or of other spacecraft similar to INTELSAT IV.

J. T. Neer, "INTELSAT IV Nutation Dynamics," *AIAA 4th Communications Satellite Systems Conference*, Washington, D.C., April 1972, AIAA Paper No. 72-537.

E. Levy, Jr. and F. S. Osugi, "Design and Performance of the INTELSAT IV Power Subsystem," *7th Intersociety Energy Conversion Engineering Conference*, San Diego, California, September 1972, IECEC Paper No. 729078.

S. Bennett and I. Dostis, "Design of the INTELSAT IV Transponder," *AIAA 4th Satellite Systems Conference*, Washington, D.C., April 1972, AIAA Paper No. 72-535.

J. Dunlop, "Evaluation of INTELSAT IV Nickel-Cadmium Cells," *25th Power Sources Symposium*, Atlantic City, New Jersey, May 1972.

F. A. Glassow, "Despin Bearing Technology and Applications for Communications Satellites," *Communication Satellites for the 70's: Technology*, (AIAA Progress in Astronautics and Aeronautics, Vol. 25), edited by N. E. Feldman and C. M. Kelly, Cambridge, Massachusetts: M.I.T. Press, 1971.

A. J. Gopin and A. S. Friedman, "Thermal Analysis and Control of the Air Force Tactical Communications Satellite," *Communication Satellites for the 70's: Technology*, (AIAA Progress in Astronautics and Aeronautics, Vol. 25), edited by N. E. Feldman and C. M. Kelly, Cambridge, Massachusetts: M.I.T. Press, 1971.

Ernesto R. Martin, "Experimental Investigations on the Fuel Sloss of Dual-Spin Spacecraft," *COMSAT Technical Review*, Vol. 1, No. 1, Fall 1971, pp. 1-20.

B. Agrawal, "Dynamic Analysis of a Spacecraft Structure," presented at the Department of Mechanical and Aerospace Engineering, Syracuse University, July 19, 1971.

F. Glassow, "The INTELSAT IV Antenna Positioner," presented at the 6th Aerospace Mechanism Symposium, NASA Ames Research Center, September 9-10, 1971.

Index: INTELSAT IV, launch vehicle, transfer orbits, spacecraft tracking, synchronous satellites, spacecraft guidance, computerized simulation.

## **Launch and orbital injection of INTELSAT IV satellites**

ALLAN M. McCASKILL, DENNIS V. NEILL  
AND ARNOLD A. SATTERLEE

### **Abstract**

Atlas-Centaur, the INTELSAT IV launch vehicle, and its flight sequence of events are described. The constraints dictating the launch window are listed, and the method of determining the window for the F-2 launch is shown. A discussion of the launch vehicle trajectory characteristics includes the objectives and constraints involved in shaping the launch trajectory. The actual transfer orbit achieved with the INTELSAT IV F-2 launch is presented for comparison with the nominal orbit.

The INTELSAT spacecraft technical control network, including four tracking, telemetry, and command stations and the control center, is also described. Key events following spacecraft separation through the transfer orbit and injection into near-synchronous orbit are delineated.

Finally, the spacecraft guidance technique which is employed to achieve a successful insertion of an INTELSAT IV satellite into a near-synchronous orbit is presented. Particular emphasis is given to the employment and functional significance of the computational procedures used in support of this task.

### **The INTELSAT IV launch**

ALLAN M. McCASKILL

The Atlas-Centaur is the launch vehicle selected for the INTELSAT IV mission. It is produced and launched for NASA by Convair Aerospace

---

*Allan M. McCaskill is Manager, Launch Vehicle Systems, Space Segment Implementation Division, COMSAT.*

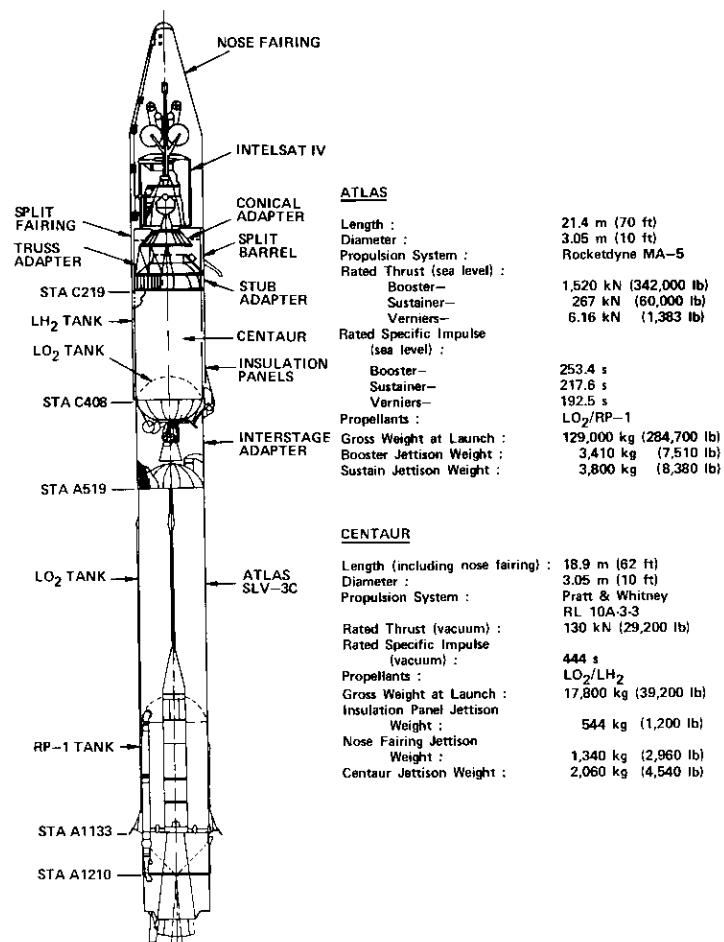


Figure 1. Atlas-Centaur, INTELSAT IV

Division of General Dynamics. The Atlas booster was originally developed by the United States Air Force as a weapon system, but it has evolved into a much used space launch vehicle. The Centaur upper stage was the first launch vehicle developed to use liquid hydrogen as a fuel.

### Atlas

The Atlas booster (Figure 1) is a stage-and-one-half configuration consisting of two booster engines, a sustainer engine, and two vernier engines, all using propellants from a common tank system. The basic Atlas structure consists of a pressure-stabilized, thin-walled, stainless steel propellant tank which provides a low tank-to-propellant weight ratio. The tank is 3.04 m in diameter and is separated into a fuel tank and an oxidizer tank by an intermediate bulkhead. Equipment is mounted in pods on the sides. A helium pressurization system maintains structural integrity and turbopump pressure head during flight.

Thrust is provided by the Rocketdyne MA-5 propulsion system. All of the Atlas engines are ignited prior to lift-off. At about two-and-one-half minutes into flight, the two booster engines are shut down, and they and their associated thrust structure, pneumatic system, and hydraulic system are jettisoned. However, the sustainer engine and two vernier engines continue burning until propellant depletion. A propellant utilization system continuously measures the levels of the propellants in their tanks and adjusts the mixture ratio of the sustainer engine to ensure that both fuel and oxidizer are depleted simultaneously.

Attitude control is accomplished by gimbaling the booster, sustainer, and vernier engines under the direction of the Atlas autopilot and the Centaur guidance system. The vernier engines provide only roll control, and the sustainer engine is gimbaled only after the booster engines are jettisoned.

The Atlas is mated to the upper stage of the Centaur by an aluminum interstage adapter. This adapter remains with the Atlas after Centaur separation.

### Centaur

The Centaur is a liquid-oxygen, liquid-hydrogen-propelled stage designed for use with the Atlas booster. Similar to that of the Atlas, its basic structure consists of a pressure-stabilized, thin-walled, stainless steel propellant tank. The liquid-oxygen and liquid-hydrogen tanks are separated by an insulating bulkhead. The bulkhead is double-walled; when propellants

are loaded, the low temperature of the liquid hydrogen above the bulkhead freezes the air between the walls, thus creating a vacuum which greatly reduces the heat transfer across the bulkhead. Fiberglass insulation panels protect the liquid hydrogen tank from aerodynamic heating during boost through the atmosphere and are jettisoned during the sustainer phase of the Atlas flight. Fixed insulation covers the ends of the tanks. A nose fairing which can be jettisoned is mounted on top of the Centaur stage to protect the spacecraft and components of the launch vehicle during exit through the atmosphere.

Primary thrust is provided by two Pratt & Whitney RL10A-3-3 engines, which produce a total thrust of 130,000 newtons (29,200 pounds). These engines are regeneratively cooled and turbopump fed. Boost pumps powered by hydrogen peroxide increase the total head of the propellants supplied to the engines. Each engine is gimballed by its own hydraulic system to provide vehicle attitude control. A propellant utilization system, consisting of probes, valves, actuators, and associated electronic equipment, continuously measures the amounts of propellant remaining in the tanks and adjusts the engine mixture ratio to ensure simultaneous depletion of both fuel and oxidizer.

During coast flight, attitude control and propellant settling are provided by a hydrogen peroxide reaction control system. This system consists of 14 thrusters (attached to the aft bulkhead), whose thrust levels range from 13.4 to 223 newtons (3 to 50 pounds). Hydrogen peroxide is provided from a common storage sphere to both the reaction control system and the propellant boost pumps.

The inertial guidance system has a gyro-stabilized inertial platform to measure launch vehicle accelerations. These measurements are processed in an onboard computer, which generates appropriate steering signals for the Atlas or Centaur autopilot system. The Centaur autopilot system provides the control signals to both the main engine hydraulic actuators and the reaction control system. These signals are required for vehicle stabilization during powered flight, execution of guidance system steering commands, and attitude orientation during coast phases of flight. In addition, the autopilot system contains timers which provide switching sequences required for programmed flight.

#### **Flight sequence**

The following paragraphs describe the Atlas-Centaur flight sequence. After ignition and thrust buildup of the Atlas engines, the launch vehicle is released and begins a vertical rise. Two seconds after lift-off, it begins

a roll maneuver to the flight azimuth of  $101^\circ$ . Fifteen seconds after lift-off, the roll program is complete and the vehicle begins a programmed pitchover maneuver, which is designed to keep the angle of attack near zero during flight through the atmosphere. At approximately 152 seconds after liftoff ( $T + 152$  s), the axial acceleration has built up to 5.7 g. At this time, the booster engines are shut down and, three seconds later, the entire booster section is jettisoned. The single sustainer engine continues to provide thrust (with roll control furnished by gimbaling of the two vernier engines). At  $T + 196$  s, the insulation panels surrounding the Centaur's liquid hydrogen tanks are jettisoned. At approximately  $T + 241$  s, the Atlas propellants are depleted and the sustainer and vernier engines are shut down. Two seconds later, the Centaur is separated from the Atlas, and eight solid-propellant retrorockets on the Atlas are fired to increase the distance between the two stages. At  $T + 253$  s, the Centaur's main engines are started and, 12 seconds later, the nose fairing is jettisoned.

The first burn of the Centaur engines continues until approximately  $T + 626$  s, when the Centaur and its INTELSAT IV spacecraft are placed in a parking orbit which has a perigee altitude of 185 km (100 nmi) and an apogee altitude of 2,220 km (1,200 nmi). An elliptical parking orbit is utilized instead of a 185-km (100-nmi) circular parking orbit so that the altitude at which the Centaur's second burn takes place is high enough to permit the Ascension Island ground stations to obtain telemetry and metric data during this time period. A 15-minute coast period, required to ensure that injection into the desired transfer orbit to synchronous altitude will take place near the equator, follows shutdown of the main engines. During this time the hydrogen peroxide reaction control system stabilizes the vehicle's attitude and maintains a small continuous acceleration to keep the propellants settled in the tanks.

At  $T + 1,519$  s [at an altitude of 600 km (323 nmi)], the Centaur's main engines are reignited to increase its velocity by 1,970 m/s (6,460 ft/s) and reduce the inclination by about  $1^\circ$ . At  $T + 1,594$  s, the main engines are shut down, since the desired transfer orbit has been achieved. During the next 135 s, the reaction control system allows the Centaur to yaw approximately  $90^\circ$  to align the spacecraft to the desired separation attitude. (The spacecraft's spin axis is normal to the orbital plane.) At  $T + 1,729$  s, the spacecraft is separated.

Following spacecraft separation, the Centaur is again reoriented. The use of the reaction control system permits the residual propellants and gases in the tanks to blow down so that the Centaur's orbit is changed sufficiently to preclude any possible contact with the spacecraft.

### Launch windows

Launch windows are those periods of time when a launch which will satisfy all spacecraft and mission constraints may take place. For INTELSAT IV, these constraints are all expressed in terms of the angle between the spacecraft spin axis and the sun vector. The specific criteria followed in determining these windows are as follows:

a. Sun angles less than  $65^\circ$  or greater than  $100^\circ$  relative to the antenna end spin axis are unacceptable because of spacecraft thermal constraints.

b. Sun interference is not permitted in the north or south earth sensors when the spacecraft is in the apogee motor fire (AMF) attitude. In the orbit normal (injection) attitude, sun interference can be tolerated in either the north or south earth sensor if the spacecraft sequencer has been configured to despin on the sensor not subjected to sun interference. Interference in the equatorial sensor is permitted. The sun interference field of view for an earth sensor is  $\pm 2.5^\circ$ .

c. The orbit normal attitude error, caused by both launch vehicle and spacecraft contributions, is assumed to be no greater than  $\pm 3^\circ$ .

These constraints can generally be satisfied during two periods (approximately 12 hours apart) each day. However, launches around noon GMT are ruled out for a number of reasons, e.g., the possibility that the spacecraft may be eclipsed for long periods near apogee, operational considerations, and spacecraft thermal problems which arise when the launch vehicle coast phase occurs in sunlight.

The derivation of the launch windows for the INTELSAT IV F-2 launch on January 25, 1971, is shown in Figure 2. It can be seen that the first window opens when the injection angle (including a  $3^\circ$  error) exceeds the  $65^\circ$  thermal constraint, and closes because of sun interference in the north earth sensor in the apogee motor fire attitude. The second window opens when the sun leaves the north earth sensor in the apogee motor fire attitude and closes when the sun interferes with the south earth sensor.

Since the INTELSAT IV F-2 launch, the methods used for determining launch windows have been refined. For example, a greater distinction has been drawn between the sun angle at the time of reorientation to the apogee motor firing attitude and the sun angle at the actual time of apogee motor firing. Allowances have also been made for the attitude errors which follow the reorientation maneuver. Thermal constraints are treated as *soft* constraints when they will simplify the formulation and statement of a set of windows covering a series of launch opportunities.

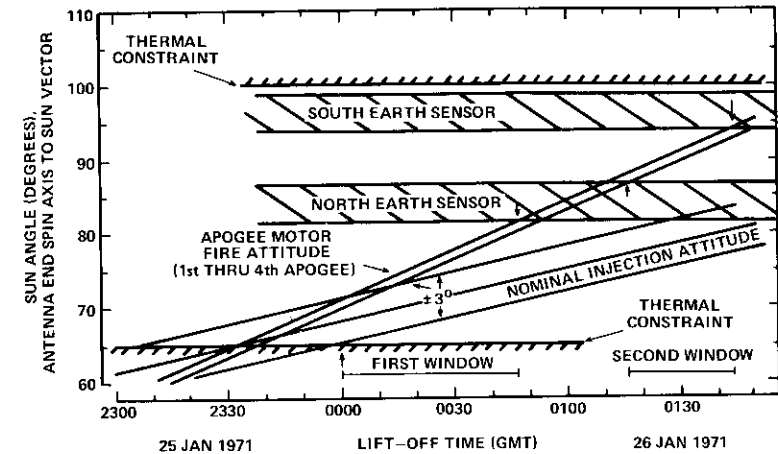


Figure 2. Launch window determination

### Launch vehicle trajectory characteristics

The launch vehicle trajectory is optimized for the generalized stationary orbit problem by utilizing a classical special solution of flight mechanics. The basic conditions of this special solution to the stationary orbit problem are as follows:

- A launch direction that is due east to minimize the parking orbit inclination and obtain maximum assistance from the earth's rotational velocity.
- A circular parking orbit achieved at a minimum altitude, typically about 185 km (100 nmi).
- A coast phase for the launch vehicle and spacecraft in the parking orbit to the first equatorial crossing.
- A restart of the Centaur engines for a second burn to inject into the transfer orbit at perigee over the equator. This second burn also changes the inclination as necessary to match the characteristics of the spacecraft's apogee motor.
- Separation of the spacecraft from the Centaur followed by a coast to the transfer orbit apogee at synchronous altitude over the equator.
- Apogee motor firing at apogee, its fixed impulse providing the velocity required to circularize the orbit and simultaneously reduce its inclination to zero.

The resulting trajectory maximizes the launch vehicle's payload capability, but because of the locations of the Air Force Eastern Test Range downrange installations, it does not provide optimum launch vehicle radar tracking and telemetry reception during flight. In fact, unless one or more range-tracking ships are appropriately deployed, no coverage of the Centaur's second burn is obtained. Radar tracking and telemetry reception during this second burn are highly desirable, however. Therefore, since the INTELSAT IV mission did not require a maximum payload capability, it was decided to shape the launch trajectory so that these data could be obtained by making maximum use of the installations on Antigua and Ascension Island instead of using downrange ships.

The trajectory profile was constrained so that the launch vehicle would be visible from Antigua (elevation angle greater than 5°) until at least two minutes after injection into the parking orbit at first main engine cutoff (MECO 1). This constraint was intended not only to permit telemetry reception during this period, but also to provide sufficient tracking time to allow an accurate determination of the elements of the parking orbit. Visibility from Ascension Island was required from five minutes prior to second main engine start (MES 2) until three minutes after second main engine cutoff (MECO 2). This permitted the reception of telemetry data throughout the prestart sequence, second burn, reorientation, and spacecraft separation, and also provided sufficient tracking time following MECO 2 for an accurate determination of the transfer orbit elements.

TABLE 1. TRAJECTORY CHARACTERISTICS\*

	Nominal Parking Orbit (at MECO-1)	Nominal Transfer Orbit (at spacecraft separation)	Achieved Transfer Orbit, INTELSAT IV F-2 Launch (at spacecraft separation)
Perigee Altitude	185 km (100 nmi)	548.4 km (296.1 nmi)	548.2 km (296.0 nmi)
Apogee Altitude	2,230 km (1,204 nmi)	35,788.4 km (19,324.2 nmi) at apogee	35,797.1 km (19,328.9 nmi) at apogee
Inclination	29.28°	28.23°	28.20°
True Anomaly	357.53°	27.1°	26.9°
Argument of Perigee	129.94°	178.77°	178.76°

\* Launch azimuth = 101°, coast time = 892 s.

The required transfer orbit was given in a targeting specification prepared by COMSAT, based upon preliminary trajectory analyses and upon the best estimates of spacecraft weight and apogee motor performance. (The latter two factors dictated the inclination change during apogee motor firing.) After all of these constraints had been incorporated, the trajectory was optimized by using a computer simulation. The resulting trajectory had the characteristics given in Table 1. Also shown in Table 1 are the characteristics of the transfer orbit actually achieved with the INTELSAT IV F-2 launch.

### Spacecraft technical control network

DENNIS V. NEILL

Primary elements of the spacecraft technical control network include four tracking, telemetry, and command (TT&C) stations, a control center, voice and data communications circuits, and a telemetry and command subsystem (in the spacecraft). Figure 3 is a block diagram which shows the layout of the network.

#### Tracking, telemetry, and command stations

Tracking, telemetry, and command stations are located at Andover, Maine; Fucino, Italy; Carnarvon, West Australia; and Paumalu, Hawaii. These locations were selected by the Interim Communications Satellite Committee of the International Telecommunications Satellite Consortium (INTELSAT) based on the following criteria:

- a. Stations should provide coverage of a satellite in synchronous equatorial orbit above 10° station elevation angles regardless of the satellite's longitudinal position.
- b. Redundant coverage should be provided for satellites positioned at assigned stations for international communications service.
- c. Each TT&C station should be located adjacent to a communications earth station to enhance the reliability of controlling communications.
- d. Readily available resources should be applied to obtain TT&C services. Small antennas [12.8-m (42-ft) Cassegrain folded horns]

*Dennis V. Neill is Manager, System Control, COMSAT.*

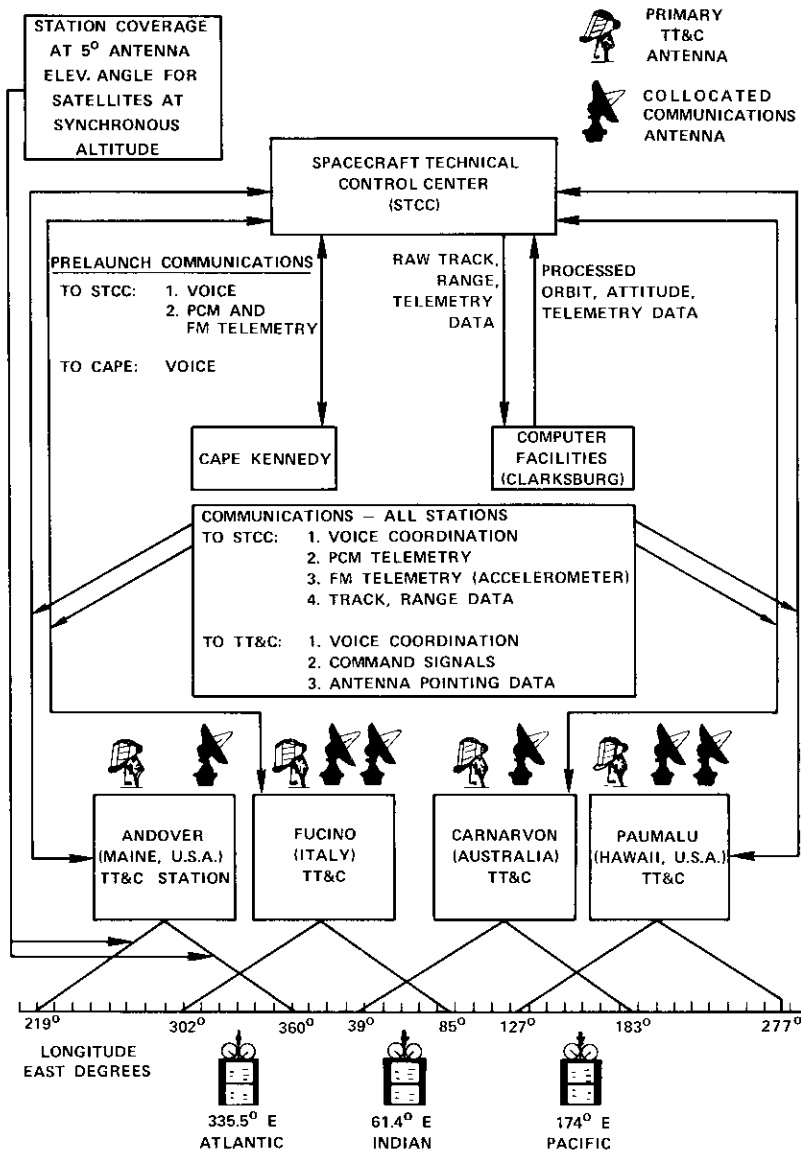


Figure 3. INTELSAT IV spacecraft technical control network

were available from an early INTELSAT II satellite program (NASCOM and commercial service) at Andover, Paumalu, and Carnarvon. A 13.4-m (44-ft) paraboloid antenna was made available at Fucino by Telespazio. Areas of coverage of the TT&C stations are shown in Figure 4.

Each TT&C station contains equipment which permits it to carry out tracking, ranging, telemetry processing, and command functions. Figure 5 is a functional block diagram of a typical TT&C station.

### Antennas

Antennas at Andover, Carnarvon, and Paumalu are Cassegrain horns which have gain performances equivalent to that of a high-efficiency paraboloid with a diameter of 12.8 m (42 ft). Each antenna is mounted on a hydraulically driven azimuth-elevation pedestal, which can be rotated 300° in azimuth and 90° in elevation. The RF feed consists of nine apertures: a center aperture, which transmits at 6,000 MHz and receives the sum signal at 4,000 MHz, and eight horns placed around the center aperture to provide the equivalent of a 5-horn amplitude monopulse tracking feed. The RF feed can radiate up to 10 kW; in combination with the reflector, it will produce an effective isotropic radiated power (e.i.r.p.) of 95 dBW. The transmit beamwidth of the antenna radiation pattern is 0.26°.

The feed can be remotely controlled to receive and transmit left- or right-hand circular polarization as well as rotatable linear polarization. The angle of the linearly polarized wave to and from the spacecraft can be determined by measuring the polarization of the received carrier from the spacecraft beacon signal. The INTELSAT IV beacon signal, when switched to the omnidirectional antenna, is vertically polarized parallel to the spin axis. The command receive antenna in the spacecraft is linearly polarized at 90° from the spin axis.

The antenna reflector at Fucino is a paraboloid with a 13.4-m (44-ft) diameter. An electrical drive system on the azimuth-elevation pedestal is used to point the antenna.

Antenna feeds are designed to transmit and receive over 500 MHz of bandwidth, with frequencies of 6 GHz for transmitting and 4 GHz for receiving. The system noise temperature is lower than 100°K for each station, while the G/T is not less than 33 dB at 10° elevation angles. Antenna gains at 6 and 4 GHz are 55 and 52 dB, respectively.

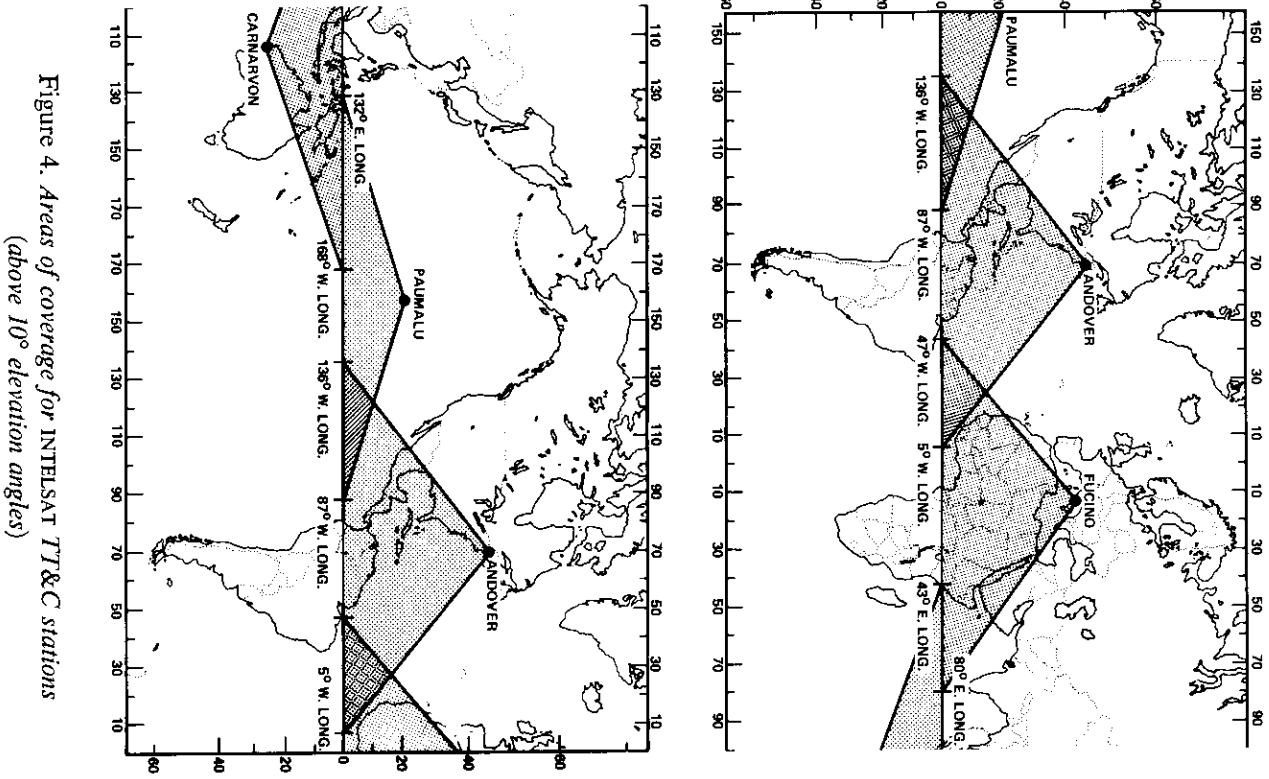


Figure 4. Areas of coverage for INTELSAT TT&C stations (above 10° elevation angles)

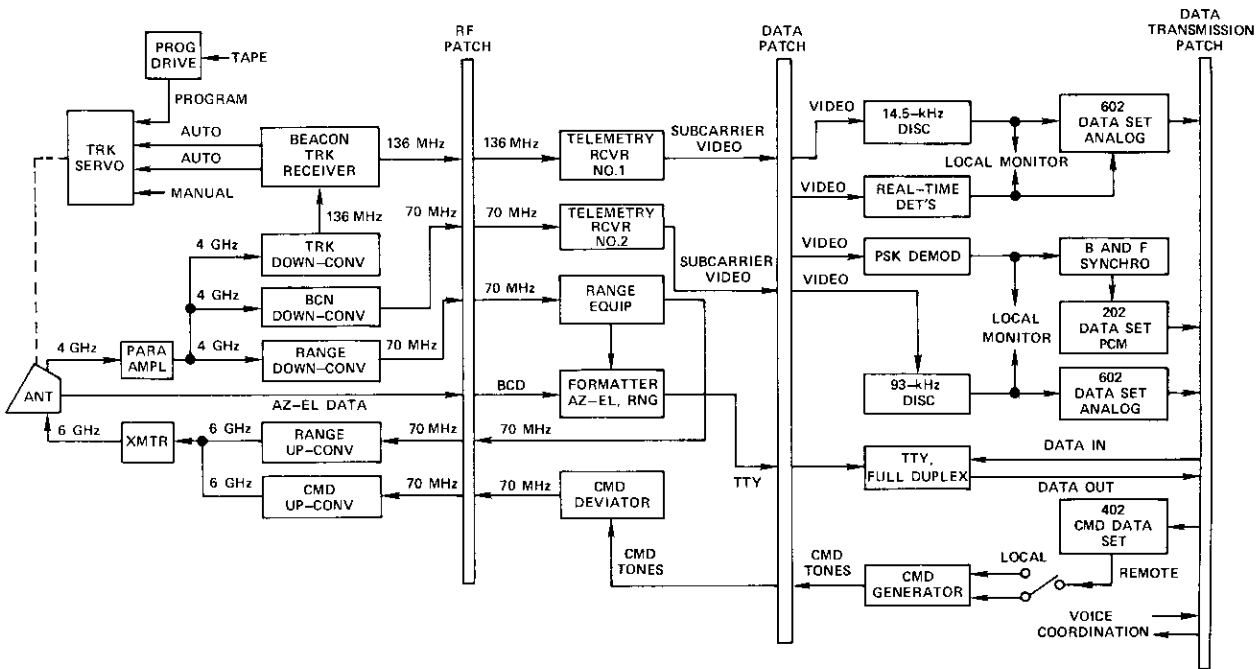


Figure 5. Simplified functional block diagram of a TT&C station

### Tracking

Antenna pointing can be controlled in three modes: autotrack, programmed track, and manual track. Each station is equipped with redundant, low-noise, cryogenically cooled receivers whose noise temperature is approximately 30°K. In the autotrack mode, the output of sum and difference channels is fed through a tracking down-converter (30-MHz bandwidth) to a tracking receiver. The sum signal phase locks the tracking loop upon acquisition of the satellite beacon signal, while the amplitude of the difference channels provides error voltages to be applied through the hydraulic servocontrol network.

The pointing accuracy of the antenna is 0.032° rms. With wind velocities up to 48.3 km/hr (30 mph), an overall tracking accuracy of 0.016° rms can be achieved at the four stations. The maximum rate at which the antenna will autotrack is 1°/s. Readout is accomplished by sampling azimuth and elevation shaft encoders in digital form with a resolution of 0.01°. Data are converted from binary coded decimal (BCD) to Baudot code, commutated, and fed to a tape punch and reader for transmission on a teletype circuit to COMSAT's central computer.

The programmed tracking mode utilizes a tape reader, programmer, interpolator units, and digital-to-analog converter for each axis (azimuth and elevation). Fixed offsets in azimuth, elevation, and time can be applied. Pointing data for programmed tracking (based on predicted or measured orbits) are prepared by COMSAT's central computer and transmitted to TT&C stations on teletype circuits. Antenna search patterns may also be prepared to help a station to follow a planned search pattern when it is attempting to acquire a satellite beacon signal. Pointing accuracy in the programmed drive mode is better than 0.07°, while the 3-dB beamwidth of the antennas is about 0.4° within the receiver bandwidth.

The manual tracking mode employs hand controls which control both the antenna pointing direction and the slew rate. (The maximum slew rate in either axis is 5°/s.) This control is accomplished by applying error offset voltages to both axes in elevation and azimuth. The manual tracking mode is useful when searching for a satellite beacon signal where small offsets from the predicted orbit are apparent. It is also employed to hold the antenna on the satellite beacon signal during a maneuver which is likely to produce signal variations and hence make autotrack maintenance more difficult.

### Ranging

The range to the spacecraft is determined by transmitting four coherent sine wave tones on a loop through the satellite and measuring the shift in phase angle between each transmitted and received tone. A given tone starts a counter at a positive rising zero crossing of the sine wave; then the received tone stops the counter at its positive rising zero crossover point. Each tone provides a range measurement. One cycle of the low tone measures to within 4,545 km (2,454 nmi); the next two successively higher tones resolve ambiguities to within 568.6 km (307 nmi) and 37.0 km (20 nmi), respectively; and the high tone resolves the range to within 5.74 km (3.1 nmi). Measurement of the phase angle displacement is accurate to within 2.6°. When all four tones are measured, the resulting range measurement is accurate to within 30.5 m (100 ft).

Ranging tones are applied continuously while the ranging carrier is illuminating the spacecraft. The tones are processed through a relay multiplexer and applied to a phase meter. Phase differences are converted from analog to digital form through a voltage-to-frequency converter and frequency counter. A commutator then samples the counter measurement and stores it. Each tone measurement is converted from BCD to Baudot code and punched on paper tape for transmission to COMSAT's central computer.

### Telemetry

Each TT&C station is equipped to simultaneously receive pulse-code modulated (PCM) and frequency modulated (FM) telemetry from the satellite. PCM data are processed through a small computer and displayed on a numerical display unit and a stripchart recorder. The PCM signal is relayed to the control center via a C-2 conditioned telephone circuit. FM (real time) or nutation accelerometer traces are processed through a discriminator, which converts the demodulated signal to an output variable voltage which can be displayed on a stripchart recorder or relayed through a data phone to the control center. Figure 6 is a functional block diagram of the spacecraft telemetry and command equipment.

### Command

Commands may be initiated and transmitted to the spacecraft by using command generator units at either the TT&C station or the control center. Command operation consists of the following steps:

- a. The operator selects local control with key switch on, command address, command number, and tone group.
- b. The command tones are transmitted to the spacecraft through an FM deviator and high-power RF amplifier (transmitter).
- c. The command is stored in the spacecraft decoder and detected in the telemetry encoder.

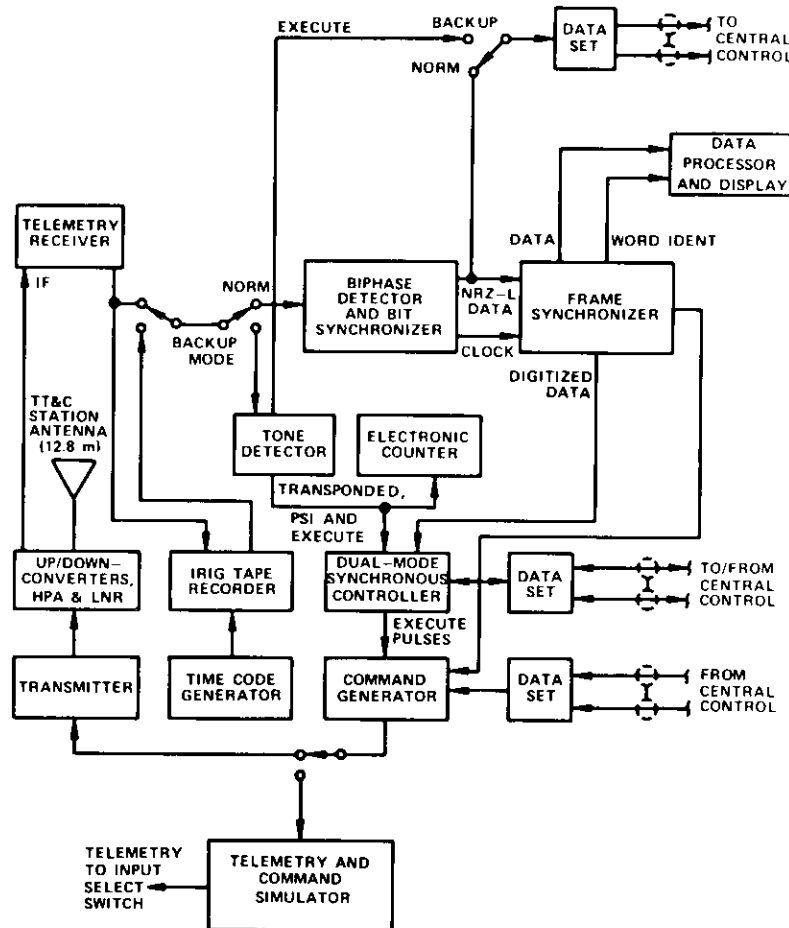


Figure 6. Functional block diagram of INTELSAT IV telemetry and command equipment

- d. The command encoder contents are received and displayed at the command generator, and telemetry is read out.
- e. Through observation, the operator verifies that the selected command is displayed in the command encoder.
- f. The execute signal is transmitted to the spacecraft.
- g. The acknowledgment of execute is received in the spacecraft telemetry.

Commands which require synchronization with spacecraft rotor spin rate and initiation at a specific point in the roll cycle (e.g., satellite maneuvers and station generated pulses for despun platform pointing) are routed at the TT&C station through a synchronous controller. These commands are always executed in local control at the TT&C station rather than at the control center because the time delay in the transmission path between the control center and the TT&C station is unknown. Even if the time delay is known for a given link, it can vary if alternate routing is used in the transmission path.

#### Spacecraft technical control center

Figure 7 is a functional block diagram of the control center. Primary functions of the control center are to assist in controlling the injection of the spacecraft into geostationary synchronous orbit and to maintain the satellite in final orbit. It is equipped to maintain voice and data communications circuits with each of the TT&C stations. It also contains equipment necessary to process telemetry and display selected parameters through a closed-circuit television system and/or manual plotting, to command satellites, and to obtain computational assistance through input-output terminals with an IBM 360/65 computer.

#### Communications network

Figure 8 is a diagram of the communications network. Voice, PCM, teletype, and analog communications links between the control center and each of the four TT&C stations are continuously available. In addition, dedicated voice *hot lines* are installed on a full-time basis between the control center and each TT&C station. PCM data are routed through a type 202 data phone at the TT&C station, and through a C-2 conditioned 4-wire circuit (3-kHz bandwidth) and a receiving 202 data phone at the control center. These data are also routed in parallel to the IBM 360/65 computer.

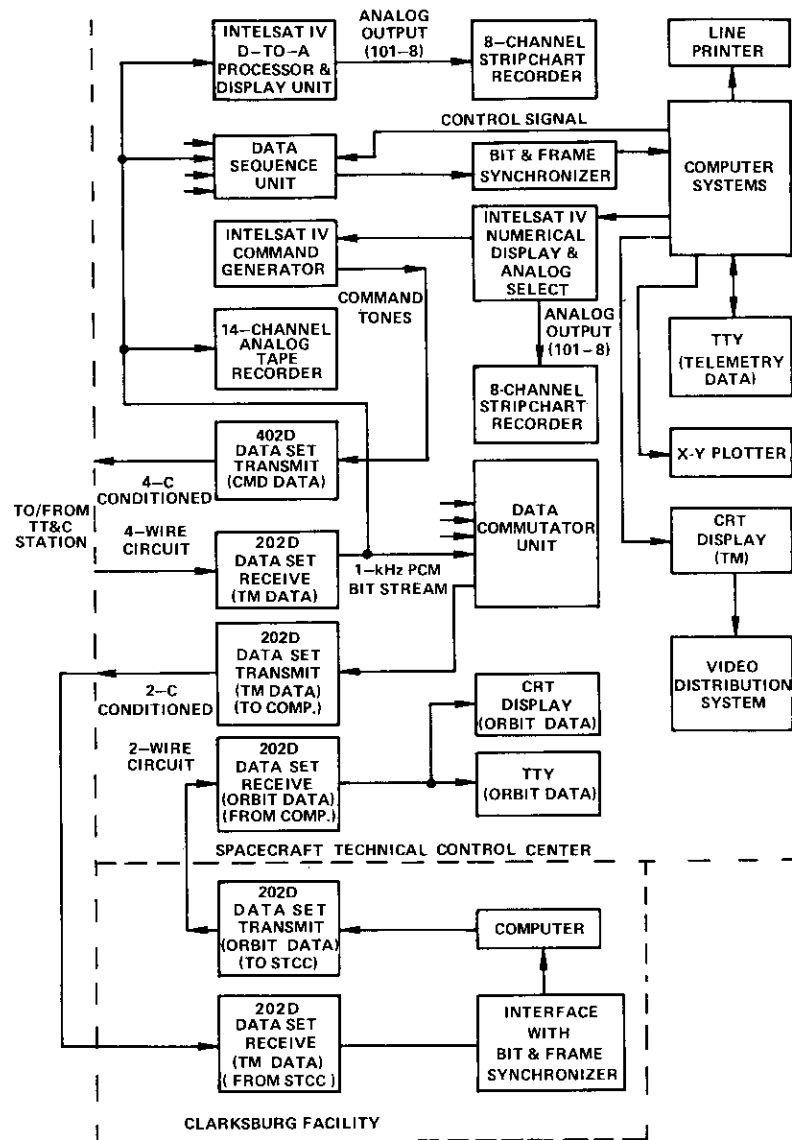


Figure 7. Functional block diagram of the spacecraft technical control center

Commands are transmitted from the control center to the TT&C station via type 402 data phones on the transmit side of the C-2 conditioned circuit. FM (real time), accelerometer, or BAPTA accelerometer data can

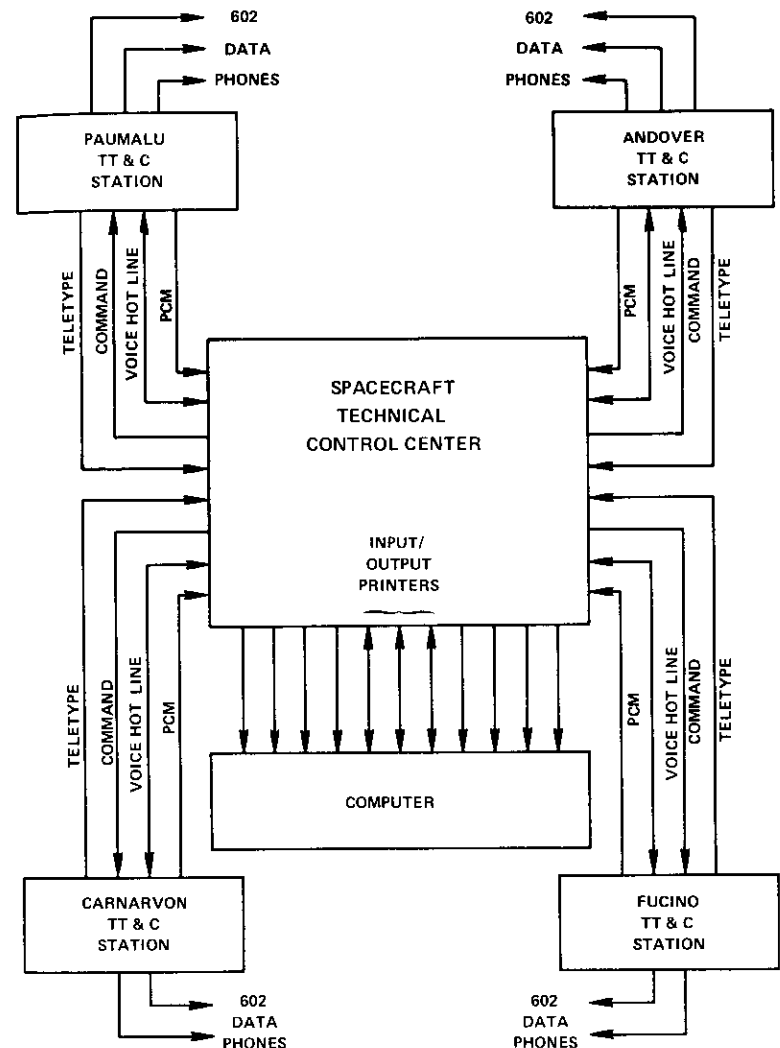


Figure 8. Communications network spacecraft technical control

be routed through a type 602 data phone (1.5-kHz bandwidth) which was previously installed between each TT&C station and the control center for the INTELSAT III satellite system. A teletype circuit to transmit tracking

and ranging data from each TT&C station through the control center to the IBM 360/65 computer is installed on a full-time basis.

### Telemetry processing

PCM telemetry data received from the satellite via the TT&C station are routed from the 202 data set through a bit and frame synchronizer and a Hewlett Packard 2114A computer, which converts the digital and analog parameters to engineering or octal values. The computer output can be displayed on an ASR-35 teletype printer, a stripchart recorder (eight selected words), or through a character generator. The character generator output (which is updated once each second) is displayed on television video monitors (Figure 9). At the same time, telemetry data are processed

```

43-1 133:15:28:09 EX COUNT 0 CMD 30D1 0 33D2 35S1 0 36S2 0
LATCH VLV BUS PRLD BYPAS RY RECEIVER TWT FILS
  1  2  SPN DSPN   1  2  1  2      1-6
CLOS  CLOS NO NO   NORM NORM OFF OFF  1A 2A 3A 4A 5A 6A
TOD HI      DCE 1      MOTOR 1      DSPN REF SUN

T1 SPN  3 ISUN  4 OSUN  5 NEC  6 SEC  7 S-NE  8 S-SE  9 N-SE  10 PNT
1185.3  152.09  163.28  43.81  38.22  399.4  994.9  595.5  96.78

  18    19    20    21    22    23    24    25    26
BUSII  BUSIV  BUS21  BUS2V  BATIV  W.AZ  BAT2V  W.EL  CHGIV
  7.32  32.2  7.00  32.6  33.6  5.29  33.6  4.78  55.6

  27    28    29    30    31    32    33    34    35
BAPST  CHG2V  TWTMT  BAT11  PS/ST  BAT21  RCVRT  BAT1T  PLATT
  74.0  56.0  100.0  -.00  75.0  -.01  72.0  53.0  73.0

  36    37    38    39    40    41    42    44    46
BAT2T  AUXBV  RADJT  E.AZ  AXJT  E.EL  SPNJT  MFLOT  HYD1P
  55.0  0.0  93.0  5.30  85.0  3.20  98.0  55.0  216.0

  48    50    52    54    56    58    60    62
HYD2P  MTRTQ  BAPHT  DSERR  FPNLT  APNLT  APOGT  SUNST
  215.0  -.19  70.0  0.03  62.0  55.0  -20.0  57.0

```

Figure 9. INTELSAT IV telemetry displayed on a television monitor

through the IBM computer and the output can be displayed on an IBM 2741 printer and cathode ray tube (CRT) display unit. Figure 10 is a sample of timing data, including spin rate and attitude information, as printed on the 2741 printer.

```

DOY    HH    MMSS    RPM    SUN
44-1   140   15    5816   51.801  70.919
44-1   140   15    5930   51.801  70.919

ES1AB  ES2AB  SSRES1  SSRES2  ES1A2A
44-1   12.19  12.36  332.56  152.53  179.97
44-1   12.22  12.27  332.82  152.70  179.80

```

LINES REPEATED EVERY 15 SEC (APPROX)

```

44-1   SPACECRAFT IDENTIFIER - INTELSAT IV F-4 ENCODER 1
DOY    DAY-OF-YEAR
HH MMSS  HOURS, MINUTES, SECONDS
RPM      SPIN RATE, REVOLUTIONS PER MINUTE
SUN      SUN ANGLE MEASURED FROM SPIN AXIS, DEGREES
ES1AB    NORTH EARTH SENSOR CHORD, DEGREES
ES2AB    SOUTH (OR CENTER) EARTH SENSOR CHORD, DEGREES
SSRES1   ANGULAR SEPARATION OF SUN AND NORTH EARTH
          SENSOR, DEGREES
SSRES2   ANGULAR SEPARATION OF SUN AND SOUTH EARTH
          SENSOR, DEGREES
ES1A2A   ANGULAR SEPARATION OF NORTH AND SOUTH EARTH
          SENSORS, DEGREES

```

Figure 10. Timing measurements (near real time) readout

### Commands

Commands to the satellite can be formatted in a command generator unit installed in the control center console (Figure 11). The appropriate

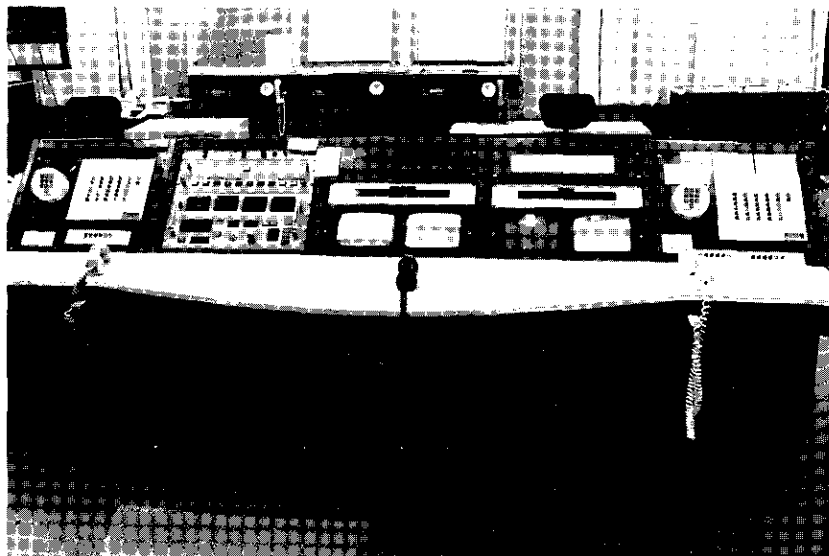


Figure 11. Spacecraft technical control center console

decoder address and command number are selected and transmitted to the TT&C station by coding audio tones through a type 402 data phone, and then applied to discrete tone generators in the command generator unit at the TT&C station. Decoder register contents are contained in the telemetry and displayed in the decoder display at the control center command generator and video monitor (Figure 9). When a command number appears in the telemetry, the 2114A computer is programmed to automatically actuate the ASR-35 printer, and the command is printed so that a record of each command will be available. After verification, the command is executed, the execute return signal is acknowledged, and the appropriate satellite telemetry indicator is checked for a change of status.

During the satellite injection phase following launch, all commands except those requiring synchronization with rotor spin rate and apogee motor firing are initiated and executed at the control center command generator.

#### Transfer orbit

The transfer orbit trajectory is established by the Atlas-Centaur launch vehicle at spacecraft separation (Table 1). At this point, control of the

mission is transferred from the mission director's center at Cape Kennedy to the spacecraft technical control center. The satellite is then controlled through the INTELSAT TT&C stations. The objective at this point is to prepare the spacecraft alignment and configuration for injection into synchronous orbit. A subsatellite ground track, in which station visibility periods are expressed in hours after lift-off, is shown in Figure 12.

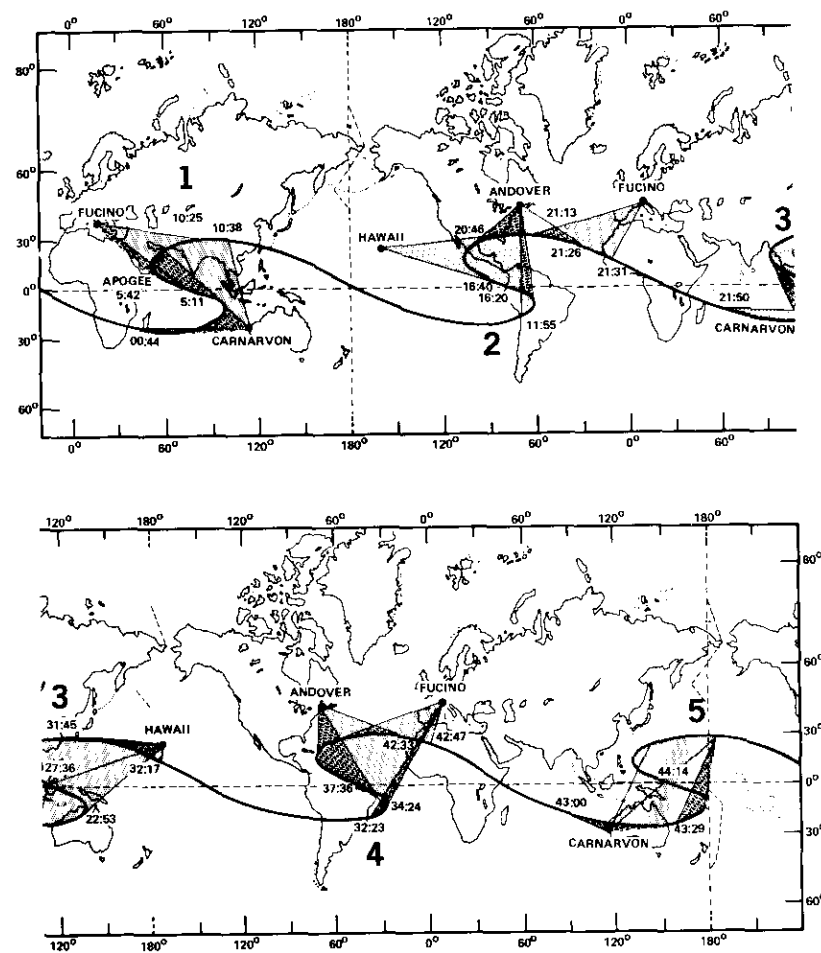


Figure 12. INTELSAT IV subsatellite ground track

Prior to launch, the TT&C stations are given pointing predictions on perforated tape to steer the antennas in the programmed drive mode. Three patterns are provided: a pattern which will track the satellite beacon signal on a nominal orbit; a search pattern, which will enclose the 1-sigma dispersions in the trajectory; and a 3-sigma search pattern.

Before launch, a "sequence of events" is prepared to fit the nominal plan, which assumes that the transfer orbit is within 3-sigma dispersion limits. Table 2 is an outline of significant events for an apogee motor firing (AMF) at third apogee. In this table, the time reference, T, is the time of lift-off.

TABLE 2. OUTLINE OF SIGNIFICANT EVENTS FOR AMF  
AT THIRD APOGEE

Time	Event
T + 28 min, 49 s	Spacecraft separation and spin-up
T + 39 min, 36 s	Initiation of TWT turn-on sequence
T + 44 min	Carnarvon TT&C station acquisition
T + 1 hr, 20 min	Complete review of spacecraft telemetry and command capability
T + 1 hr, 25 min to 2 hr, 10 min	Check of both passive and active nutation control sub- systems
T + 2 hr, 10 min to 3 hr	Despin platform rate memory mode check
T + 3 hr to 4 hr	First reorientation maneuver to align spin axis for AMF*
T + 5 hr, 30 min	First apogee passage
T + 6 hr to 7 hr	Orbit determination
T + 10 hr, 51 min to 11 hr, 13 min	Perigee eclipse and perigee passage
T + 12 hr, 10 min	Andover TT&C station acquisition
T + 13 hr, 15 min	Second reorientation maneuver to align spin axis for AMF
T + 16 hr, 04 min	Second apogee passage
T + 26 hr, 15 min to 27 hr, 10 min	Apogee boost sequence at third apogee
T + 27 hr, 30 min	Post-AMF reorientation to orbit normal
T + 28 hr, 30 min	Spacecraft configuration for in-orbit test phase and attitude touch-up
T + 42 hr to 54 hr	Orbital velocity maneuvers to adjust drift direction and rate

\* This maneuver was completed during the second apogee pass of INTELSAT IV F-2.

#### Separation and spin-up

Upon completion of the yaw maneuver by the Centaur when the spacecraft attitude is normal to the orbit plane, the rotor is spun up to ~51

rpm and the despin reference is switched to either the north or south earth sensor (depending upon the sun's location).

#### Carnarvon acquisition

The Carnarvon TT&C antenna is set at the horizon in the program drive mode on the nominal orbit. At the predicted acquisition time, the antenna is driven in elevation and azimuth. (It rises 14° in elevation in the first five minutes.) Receivers are tuned to the two beacon frequencies with PCM, and the analog output of the accelerometer is patched directly to the control center. At acquisition, engineers in the control center can, in nearly real time, review the telemetry which is presented on TV monitors. The nutation accelerometer trace is presented on a stripchart recorder. In the event that an unstable condition becomes apparent, immediate action can be taken to damp it out by firing axial jets manually if necessary.

When all spacecraft parameters have been checked and found to be nominal, both passive and active nutation control subsystems are tested. Damping time constants of the passive dampers are tested by firing an axial thruster for 500 ms to induce a nutation of approximately 0.3°, which is immediately visible on a calibrated stripchart trace. When passive dampers are found to be acceptable, each of the two automatic nutation damping control units is checked. A nutation of 0.7° is induced by firing two ~800-ms pulses at the nutation frequency. Finally, the automatic nutation damping electronics are energized and the accelerometer-induced jet firings used to damp out the nutation are observed on the stripchart recorder.

Paralleling the action at the control center, the Carnarvon TT&C station transfers its antenna from program drive to autotrack and provides azimuth and elevation data via a teletype circuit to the computer for orbital measurements. Ranging measurements cannot be made until the station gains access to the global-beam pattern, i.e., at about one and one-half to two hours after acquisition, when the platform is despun, pointing at the earth, and at a beam angle of approximately 10° (measured at the satellite).

Before the spacecraft is reoriented to the apogee motor firing attitude it is necessary to ensure that the despun platform will operate in the rate memory mode because there are periods in the transfer orbit when the earth sensors leave the earth and periods during perigee eclipse when the sun reference is not present. This check is accomplished by switching the despin reference to pseudo-earth pulses transmitted by the TT&C station.

The rate at which pseudo-earth pulses are transmitted can be adjusted so that the platform spin rate is set to optimize the damping time constant of the passive dampers. When transmitted pulses are switched off, the phase-locked loop network is fixed on the given frequency and maintains that spin rate. When a satisfactory check of the rate memory mode has been completed, the despin reference is commanded to an earth sensor so that range measurement can be initiated at Carnarvon.

At about three hours after lift-off, the first reorientation maneuver sequence is initiated. The sun sensor reference is used to control the despin platform and to fire the thruster at the calculated sector in the roll cycle. Logic circuits in the spacecraft attitude determination network measure the delay between this reference and the telemetry envelope (frame synchronizing words). This time differential is accounted for in the logic control network by the synchronous controller. Transmission delay and execute angle are then set up to initiate the execute signal at the proper point in the spacecraft.

Changes in sun angle, spin rate, and earth chords to be expected during the maneuver are plotted manually and compared with predictions. The nutation accelerometer trace, with pulses superimposed on it to reflect the sun's position, is displayed on a stripchart. When the thruster is pulsed, the accelerometer is excited and the phasing of pulses can be checked by measuring the interval between sun reference and thruster pulses. At the same time, attitude data are derived by the computer from PCM telemetry and presented in nearly real time on a CRT display. As the axial thruster is pulsed, measurements of sun angle and spin speed are plotted and compared with predictions, and attitude information on the CRT display is checked. If the indicators are satisfactory, the maneuver is completed, and despin control is commanded to the north earth sensor. At this time, a sector change of the platform may be needed to point the antennas at the earth so that range measurements can be resumed.

As the satellite moves in its orbit in the AMF attitude, north and south earth sensors intersect and leave the earth's disc. The despin reference is switched to the appropriate sensor until both earth sensors leave the earth. At that time (approaching perigee), the despin reference is switched to the rate memory mode and automatic nutation control electronic units are energized.

#### **Apogee motor firing**

Prior to launch, a nominal plan for apogee motor firing is prepared. At this point, it is important to determine at which apogee of the transfer

orbit the motor should be ignited. As shown in Figure 12, the first apogee of the transfer orbit is located at 85° east longitude, the second at 285°, the third at 124°, etc. Considerations which affect this decision are as follows:

- a. The level of confidence in the orbit and attitude alignment prior to ignition;
- b. The location of the intended station in synchronous orbit;
- c. Conservation of fuel and minimization of maneuvers, expressed in terms of nominal drift rate, direction, and dispersion which might be expected following apogee motor fire;
- d. The locations of other satellites carrying communications services; and
- e. The time schedule for placing the satellite on station.

According to the nominal plan, a firing at first apogee may be not initiated because there is insufficient confidence that the achieved orbit is known and that the spin axis can be aligned to within acceptable limits ( $\pm 1.0^\circ$ ) prior to first apogee. A change from the injected attitude at an orbit normal of approximately  $36^\circ$  is necessary to align the spin axis for the proper thrust vector. If it can be assumed that there is a 10-percent tolerance the first time a spacecraft is maneuvered in orbit, one maneuver will result in dispersions of  $\pm 3.6^\circ$ . Therefore, two attitude maneuvers should be planned before apogee motor fire. It is also essential to allot sufficient time for spacecraft functional checks, such as testing the nutation damping devices, both passive and active, the platform despin control, and the electronics. Scheduling tasks in the transfer orbit for firing at second and subsequent apogees involves a much smaller risk.

When a satellite is to be positioned over the Pacific Ocean area, the nominal station in synchronous orbit is located at 174° east longitude. From Figure 12, the third apogee of the transfer orbit is located at 124° east longitude, or 50° from the final station, and the fifth apogee is located at 166° east longitude, or 8° from the final station.

For the INTELSAT IV F-4 mission, the apogee motor firing analysis, which considered the mathematical modeling of orbital and spacecraft dynamics, predicted a nominal drift rate following apogee motor firing of 1° per day to the west, with a 1-sigma deviation of +2.0° per day. With an eastward drift requirement and an assumed rate of 2° per day, it would take 25 days of drift with a motor firing at the third apogee and four days with a motor firing at the fifth apogee (Figure 13). The actual transfer orbit trajectory was so nearly nominal that it was decided to ignite the apogee motor at the fifth apogee. The drift following AMF was

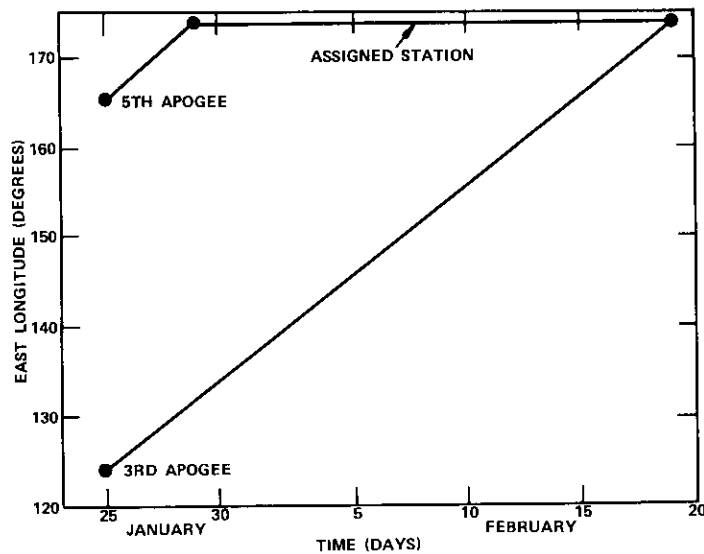


Figure 13. Longitude vs time after launch

0.5° per day to the west. An orbital velocity correction maneuver then changed the drift direction and rate to 1° per day to the east. The satellite was completely tested and placed in commercial service on station within 20 days.

During the apogee boost, it is imperative for the inertial spin rate of the platform to be bounded so that the inherent stability of the dual-spin spacecraft remains intact, the desired thrust vector is maintained, and the effectiveness of the nutation damping devices is not impaired. Extensive analysis revealed that the thrust vector and stability during and after boost were sensitive to variations in the inertial platform rate. It was concluded that, with a rotor rate of 51 rpm, an optimum platform spin rate would be achieved by forward spinning (in the direction of rotor spin) at 2 to 4 rpm. The net effect would be a 50-percent reduction in the thrust vector pointing error which would have been achieved if the platform had been despun at the spin rate.

Prior to apogee motor ignition, the despin platform is set at the desired rate by commanding to the pseudo-earth mode and transmitting pulses using a tone frequency which is different from other command tones. When the desired rate is measured [by counting the master index pulse

interval (platform index)], the input pulses are removed so that the despin platform can be maintained at the desired rate.

Several indicators give an early assessment of apogee boost results:

a. The shift in beacon frequency, as a result of the Doppler effect, is predicted from the satellite motion viewed from the TT&C station. The frequency shifts up or down in relationship to the reference frequency (zero Doppler) as the satellite moves away from or toward the station, respectively. These readings are sent by the TT&C station to a plotter at the control center and plotted manually. The frequency shift can also be detected on a stripchart recorder display at the control center (Figure 14). The signal is processed by the station tracking receiver, a frequency synthesizer, and a 14.5-kHz discriminator which sends variable voltages to the control center via a data phone link.

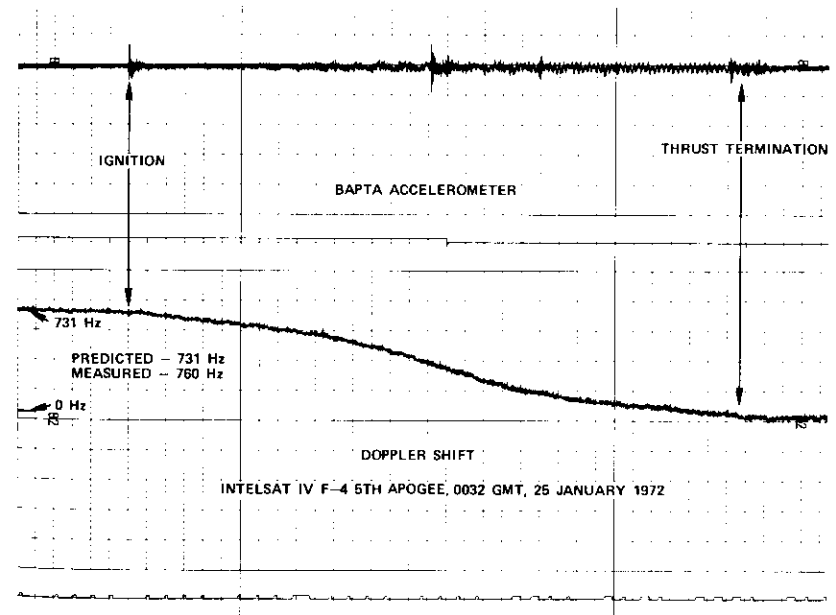


Figure 14. Stripchart sample, BAPTA accelerometer and Doppler shift as viewed from Hawaii

b. Bearing loads on the bearing and power transfer assembly (BAPTA) are disturbed by the force of acceleration during rocket burn. This force is reflected in the indication of torque demand by the despin motor driver, and in the despin position error (Figure 15).

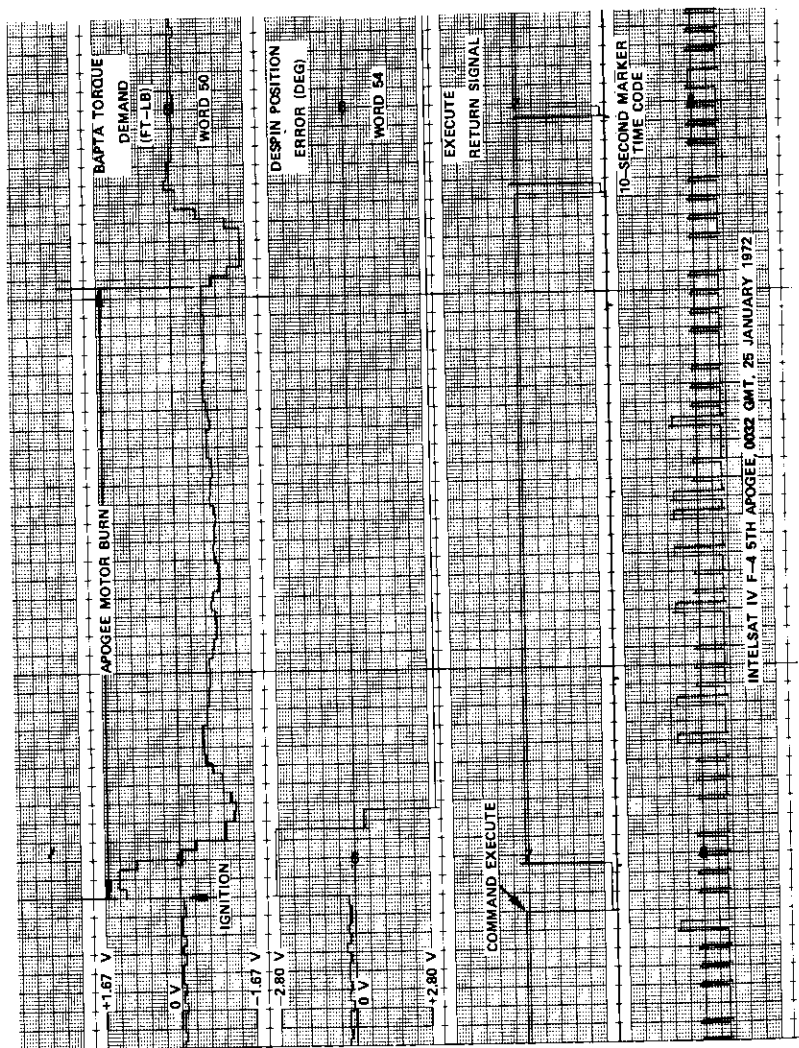


Figure 15. Stripchart sample, BAPTA torque demand and despin position error

c. The BAPTA accelerometer produces increased acoustical noise during thrust (Figure 14).

d. At thrust termination, the buildup in nutation can be measured and the jet firing, which damps the nutation, can be seen on the nutation accelerometer trace (Figure 16).

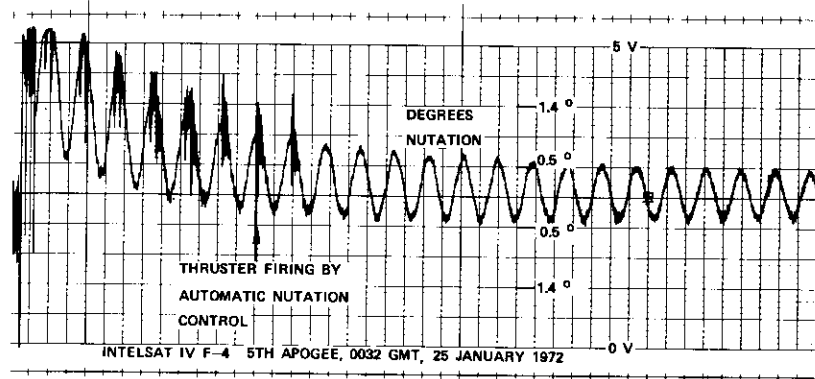


Figure 16. Stripchart sample, nutation accelerometer following apogee boost

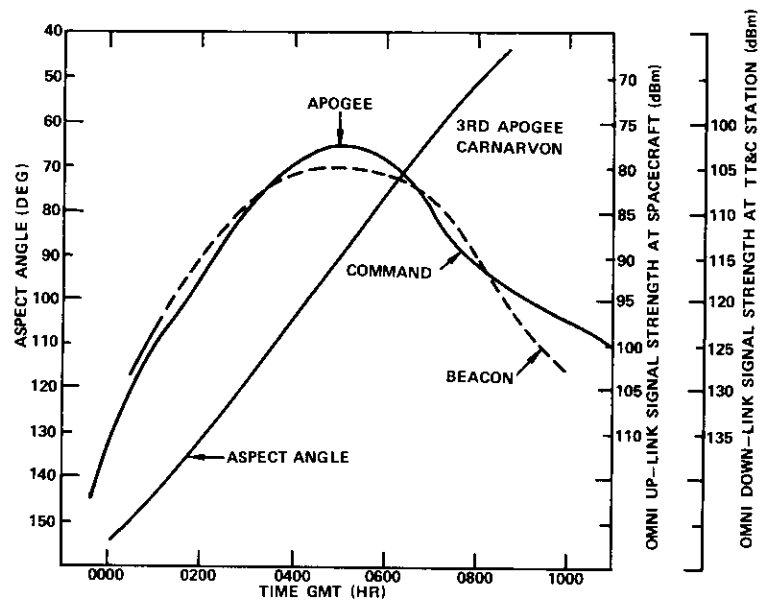


Figure 17. INTELSAT IV postapogee boost orbit signal levels

### Post-AMF erection and drift

Within 30 minutes after AMF, a reorientation maneuver is performed to precess the spin axis approximately  $115^\circ$  so that it is positioned at orbit normal. Figure 17 is a graph which shows received beacon and command signal strengths versus time that the spacecraft is in the AMF attitude. If the erection maneuver is not completed in three hours, it is necessary to wait 10 hours until the command signal to the spacecraft is above threshold. After 12 to 24 hours, an orbital velocity maneuver may be required to adjust the spacecraft drift to the desired rate toward its intended station.

### Mechanics of synchronous orbit insertion

ARNOLD A. SATTERLEE

At the termination of the Atlas-Centaur phase of the mission, the satellite has been established in an elliptical trajectory which is inclined about  $28^\circ$  to the earth's equator (Figure 18). In this transfer trajectory,

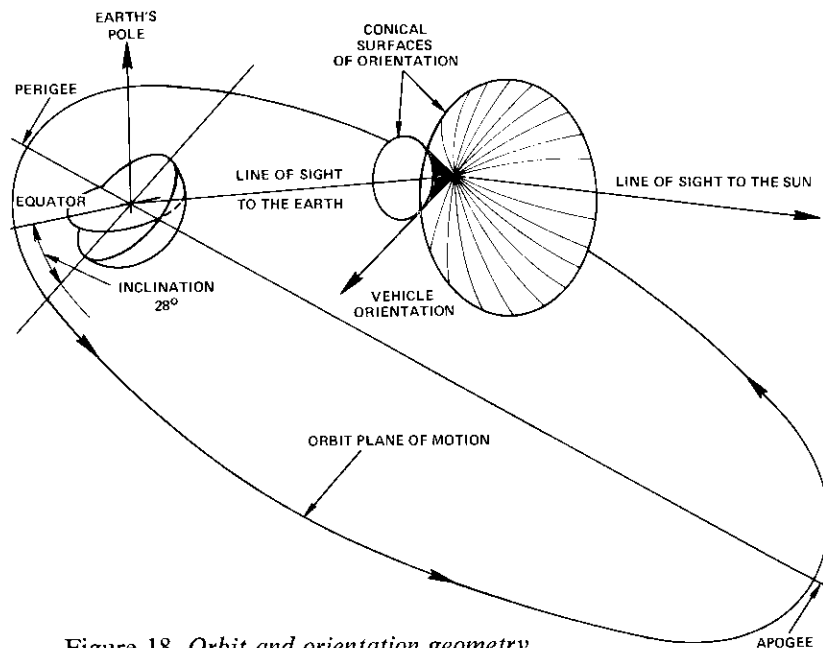


Figure 18. Orbit and orientation geometry

Arnold A. Satterlee is Director, Celestial Mechanics, in System Implementation, COMSAT.

the satellite will, under the influence of the earth's gravitational field, circuit the earth once each 10.67 hours. The position of nearest approach will be approximately 548 km (296 nmi) above the earth's surface. The spacecraft will subsequently rise to an altitude of about 35,788 km (19,324 nmi). If observed from the center of the earth, the angular rate of the satellite's motion will appear to increase uniformly as the satellite approaches the lower altitudes, and decrease as it climbs in height. As a result of this orbital phenomenon, the ground trace of the satellite will form a pattern on the earth's surface similar to that shown in Figure 12.

For the satellite to become an effective communications relay station, its diurnal motion relative to the surface of the earth must be minimized. To control the east-west component of this motion, the orbital period must be synchronized to the period of the earth's rotation, which is about 23 hours and 56 minutes in mean solar time. To ensure that the satellite's motion will nearly coincide with the earth's angular motion, the eccentricity of its orbit must be maintained at a low value. The north-south component of the relative motion originates from the inclination of the orbit plane to the earth's equator. For INTELSAT IV satellites, this daily motion about the equator is limited to  $0.5^\circ$ .

The principal component of the orbit velocity change necessary to achieve the operational orbit is provided by a single-burn, solid propellant rocket motor. This motor delivers an average thrust of 54,478 N (12,480 lb) for a period of 33.8 s. For the INTELSAT IV F-2 spacecraft, this amounts to an incremental velocity change of 1,810.8 m/s (5,941 ft/s). Because the orientation of the operational orbit plane is not coincident with the plane of the transfer orbit, the location of the insertion maneuver is constrained to one of two inertial positions coincident with the intersection of the initial and final orbit planes. Since the plane of the operational orbit is restricted to within  $0.5^\circ$  of arc to the equator, the positions of possible orbit transfer will occur at or near the equatorial crossings of the transfer orbit. Maneuver proficiency is achieved by locating the position of maximum height in the transfer orbit at or near the equatorial crossing defined by the ascending node of the transfer orbit.

The launch or emplacement of a communications satellite into its operational orbit is a 2-phase procedure. The initial Atlas-Centaur boost phase is a self-contained guidance process which, when committed at lift-off, is performed with no external influence from the earth. At the termination of the Centaur-controlled portion of the flight, the spacecraft enters a second or free-flight phase in which control of the spacecraft is transferred to an earth-based control and monitoring network.

During the free-flight phase, emphasis is placed on the preparation of the spacecraft for the single-burn maneuver which will insert the satellite into a near-synchronous orbit. The position and velocity of ballistic trajectories are subject to a degree of uncertainty as a result of inaccuracies associated with the powered-flight portions of the mission. Therefore, because of the limited amount of fuel available, it becomes necessary to provide a form of guidance to ensure that the vehicle does not deviate substantially from the nominal mission profile. The selection of the appropriate course in the presence of these errors requires a measurement of the resulting free-flight trajectories during the period prior to and following the primary insertion maneuver. These measurements provide the reference from which maneuver policies (consistent with the reliable realization of the final operational objectives) are formulated. Prior to the primary insertion maneuver, the principal task required to implement the maneuver policy is that of establishing the required inertial alignment of the insertion engine thrust axis.

The principal navigation measurements necessary to establish the inertial components of the spacecraft trajectory and thrust axis alignment are provided by the INTELSAT TT&C network. These measurements are transmitted directly to a central digital data processor (the IBM 360/65 computer at COMSAT Laboratories in Clarksburg, Maryland). In addition to performing the data collection function, the same computer provides the digital computation capability required to evaluate the geometric and analytical formulations associated with the navigation, guidance, and predicted future orbit operating environment of the spacecraft. A multi-program facility provided by the computer system enables simultaneous operation of the teleprocessing and numerous problem-oriented computer programs. Figure 19 summarizes the functional organization of the computational process.

The principles by which the computer programs were developed permit an interplay between the processing capability of the computer and the reasoning power of the human analysts. In those cases in which rapid response is required to support the responsible operation of the spacecraft, on-line or real-time capability is provided, thus allowing the analyst to direct the operational flow of the computational process. In practice, the mode of operation is a recursive process by which observations are taken, orbit and attitudes are determined, and orbit objectives are analyzed and reviewed, followed by maneuvers which appropriately adjust the spacecraft orbit or orientation. This process continues until the spacecraft is placed at its operational location in an acceptable operational orbit.

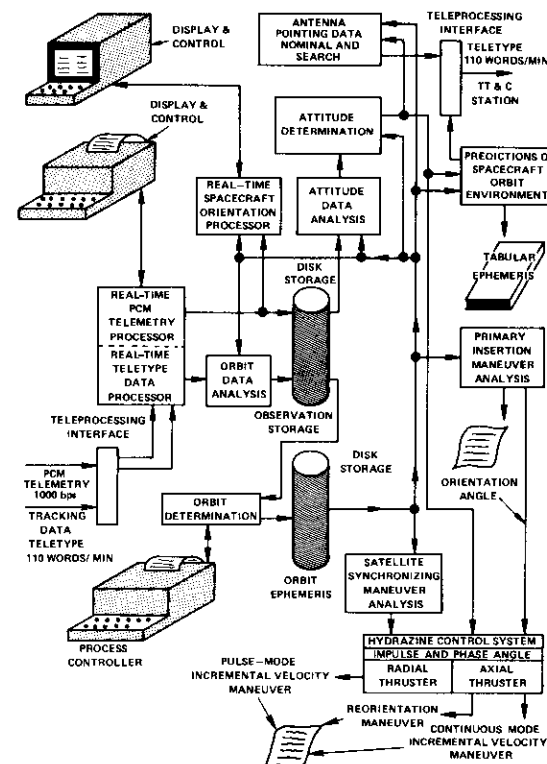


Figure 19. Functional organization of the computational process

### Orbit and orientation parameters

To minimize the complexity of the analytical expressions which describe the free-flight motion of an earth satellite and the alignment of its physical axes, the formulations may be conveniently expressed in an inertial coordinate system for which the origin is the center of the earth and the principal plane of reference is the earth's equator. To evaluate the analytical formulations which describe the motion of the satellite in terms of the inertial coordinate system, six fundamental constants, commonly referred to as the orbit elements, must be known. These elements are the inertial components of the satellite's position and velocity at some epoch time. Since no facility is available to directly measure these elements, it is necessary to rely on tracking station observations measured in coordi-

nates which are different and rotating with respect to the preferred inertial system.

To specify the vehicle orientation, it is convenient to define the components of the vehicle's right ascension and declination in the inertial equatorial reference system. These components are resolved from indirect observations made by sensors on the spacecraft.

As a result of random instrumentation errors, the orbit and attitude parameters determined from the measuring instruments can be interpreted only as estimates of the true values. The use of redundant but time-variant measurements and statistical estimation techniques reduces the degree of parameter uncertainty.

### **Orbit determination**

The determination of the orbital elements of the transfer orbit is a gradually evolving process which continues throughout the launch period. Tracking data which are used in the orbit determination consist of azimuth, elevation, and range data collected during the visibility periods of each TT&C station. The azimuth and elevation data are obtained by tracking the radio frequency beacon transmitted from the satellite through the omnidirectional antenna. These data are available when the satellite is above the station's horizon and the station's line of sight falls within the broad limits of the antenna pattern. In contrast, range measurements are obtained by means of a special ranging carrier transponded through the satellite via the global-coverage antenna. These measurements, in turn, require that the antenna platform be pointed toward the earth and the station's line of sight be within the narrow limits of the global antenna. These conditions are satisfied during only a small portion of each visibility period; therefore, the range data constitute only 30-50 percent of all data collected.

The most important span of tracking data is collected during the first apogee passage of the spacecraft over the Carnarvon and Fucino TT&C stations. Although these data are not sufficient to obtain definitive orbital elements, they are adequate to detect any large deviation from the nominal orbit. The knowledge gained from these data, therefore, plays an important role in determining the future course of the mission.

The first ranging data are received approximately two hours after Carnarvon acquisition, when the orbit determination process begins. Initially the data are processed by the classical Gaussian method of preliminary orbit determination, which determines a purely elliptical orbit

passing through two known spatial positions at known times [1]. One of the positions is computed from a single nearly simultaneous measurement of azimuth, elevation, and range; the other position is initially assumed to be the point of transfer orbit injection determined from the reduction of launch vehicle telemetry data. This method is advantageous because the computation of the orbital elements is straightforward and can be accomplished rapidly. The major disadvantages are that the orbit is assumed to be purely elliptical (and therefore the major perturbations acting on the satellite are not taken into account) and that the orbit exactly matches spatial positions determined from data corrupted by measurement errors. The latter disadvantage is overcome to a large degree by determining numerous orbits, which may or may not include the injection position, from selected pairs of observations. These orbits may be assumed to form an envelope about the true orbit and are valuable in determining whether or not the orbit is nearly nominal.

When sufficient data have been collected (near the time when the spacecraft approaches the first apogee), a more sophisticated orbit determination method of differential correction is used. This method is based upon a comparison of simulated and observed tracking data. The difference between each computed and observed measurement constitutes a measurement residual, and the orbital elements are corrected in an iterative fashion until the weighted sum of the squares of all residuals is minimized. This method, which is the method of weighted least squares invented by Gauss, produces the optimal estimate of the orbital elements when the measurement errors are uncorrelated, normally distributed random variables.

The differential correction method requires an initial estimate of the orbital elements to which the corrections are to be applied. These elements may be the nominal values, or they may be the elements from the preliminary orbit determination previously described. The computed measurements are obtained by calculating the observations which would have been made if the satellite had traveled exactly along the orbit defined by the selected elements. The satellite's position in the assumed orbit is calculated by numerically integrating the differential equations of motion which take into account all of the significant forces acting on the satellite. The initial conditions of the integration are defined by the assumed or corrected values of the orbital elements.

During each continuous period of free flight, the data are processed periodically in increasingly larger batches as new data are collected. Hence, the orbital elements are continually refined, and the orbital elements determined from one set of observations are used as the initial

elements with which the next larger batch is processed. This scheme is continued until no further correction is deemed necessary, or until an orbital maneuver which places the satellite in a new orbit is performed. In the latter case, the whole process is started again, and the predicted postmaneuver elements are the elements to which corrections are applied as new data are received from the tracking stations.

By the time the spacecraft has reached apogee on the third revolution about the earth, the rms uncertainty of its position has been reduced to about  $0.005^\circ$  in angle and 76.2 m (250 ft) in altitude. The rms angular uncertainty of the velocity is also in the neighborhood of  $0.005^\circ$ , with a 0.046-mps (0.15-ft/s) error in its magnitude.

#### Attitude determination

When the spacecraft is inserted into the transfer trajectory by the Atlas-Centaur vehicle, the inertial orientation of the spacecraft is established along an axis normal to the existing orbital plane of motion. Although this alignment is preferred from a communications standpoint, the vehicle must be reoriented to accommodate the thrust axis alignment required for the primary insertion maneuver. The accuracy with which the orientation can be established is directly related to the ability to determine the vehicle's inertial orientation.

Measurements related to the inertial alignment are provided by earth and sun sensing instruments on the rotating portion of the spacecraft. As illustrated in Figure 20, the optical axes of two earth sensors are aligned at an elevation of  $\pm 6.2^\circ$  with a plane normal to the vehicle's spin axis. Within its narrow field of view, the earth sensor detects an infrared radiance variation as it scans the earth's radiation profile during a revolution of the spacecraft. From this radiance variation, the time interval between the apparent leading and trailing edges of the earth's infrared horizon is measured.

Solar detection is provided by a silicon solar cell configuration which is optically arranged as shown in Figure 20. The time interval between successive detections of the sun in the narrow fan-shaped field of view of the  $\Psi$  sensor provides a measure of the rotational period of the vehicle. In addition, from the measured time interval between the detection of the sun in the  $\Psi$  and  $\Psi_2$  sensors, the angle between the sun's line of sight and the spin axes of the spacecraft can be geometrically determined.

In addition to the independent measurements of the earth and sun sensors, the time interval between the detection of the sun in the  $\Psi$  sensor

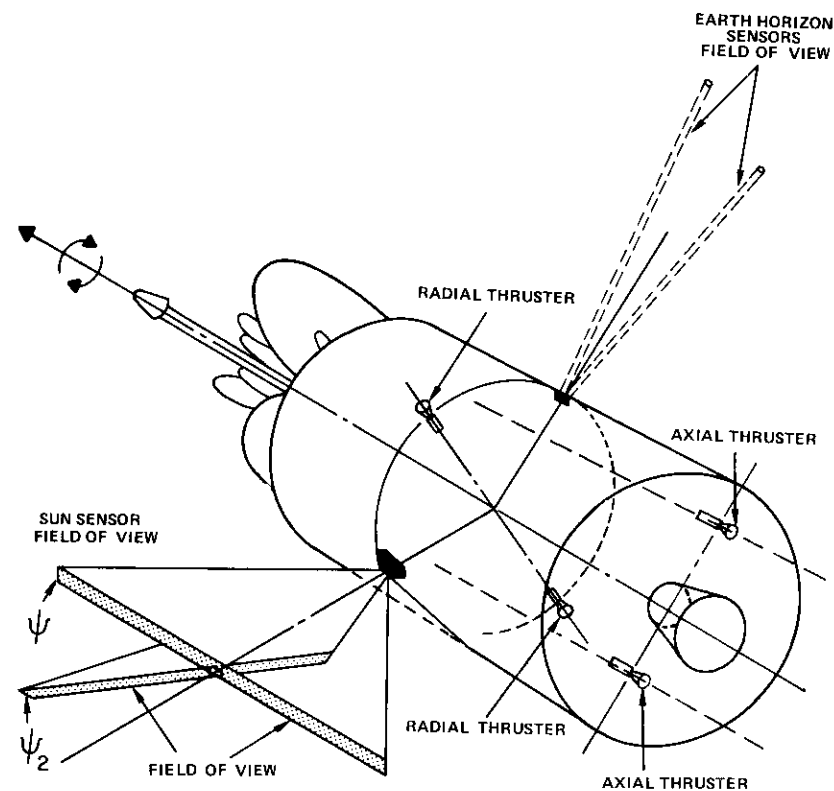


Figure 20. Sensor field of view and primary thrust axis

and the respective electronic pulses representing the detection of the earth's leading edge is measured. The various time interval measurements are sequentially performed in the spacecraft and included in the stream of PCM telemetry data.

Measurement of the subtended angle between the line of sight to the sun and the vehicle's spin axis establishes the spin axis position on the surface of a cone. As indicated in Figure 18, the axis of the cone is in the known inertial direction of the line of sight to the sun. (The apex angle of the cone is defined as twice the measured subtended angle.) Given a second angle measurement to a different inertial body (such as the earth), a second cone of orientation with a different axis and apex angle can be

established. As illustrated in Figure 18, the two cones intersect in two straight lines, one of which is congruent with the spin axis of the vehicle. A third measurement along a different inertial axis will distinguish the correct line. Sometimes the ambiguity can be resolved when the two lines of intersection are widely separated; in this case, an approximate knowledge of the orientation will determine the correct one.

As previously indicated, the angle subtended by the sun is geometrically derived from the telemetered solar timing measurements. The additional cones of orientation are derived from the earth horizon measurements, which are geometrically related to the angle between the spin axis and the known inertial line of sight to the center of the earth.

The axis of the cone of orientation detected by the earth sensors will inertially rotate with the satellite as it moves in its orbit about the center of the earth. When this motion is geometrically combined with the inertially stable orientation of the spin axis, it can result in a dynamic variation of the apex angle of the cone as the satellite revolves about the earth.

In the nominal orientation required for the primary insertion maneuver, the vehicle's spin axis is declined about  $54^\circ$  to the orbit plane of motion. When the vehicle is monitored in this orientation by the tracking network, the earth's horizon can be detected by one or both of the earth sensors only during the period of time when the angle between the spin axis and the line to the earth's center is about  $72^\circ$  to  $105^\circ$ . This results in an earth sensor visibility period of about six hours during each revolution of the satellite about the earth.

A continuous evaluation of the vehicle orientation is available on a real-time monitor as the measured sun and earth horizon data are received at the computer. Each solution is an independent mathematical interpretation of the geometrical intersections of the cones of orientation as characterized by a pair of received sun and earth horizon measurements. In addition, the mathematical derivative of the computed orientation with respect to the apex angle of the cone detected by the earth sensors is provided as an interpretive aid. The time-varying characteristic of the cone detected by the earth sensors can at times result in a poorly defined conical intersection with the solar cone. Thus, the reliability of the solution can be deduced from the computed derivative.

Although the accuracy of this technique is limited in the presence of measurement errors, the running summary is adequate to quickly verify any large deviation which may occur during a major vehicle orientation change. With reasonable conical geometry, accuracies on the order of  $1^\circ$  can be obtained. When the systematic instrumentation errors have been

isolated and taken into account, this uncertainty can be reduced to  $0.3^\circ$  or  $0.4^\circ$ .

Further reduction in the orientation uncertainty is accomplished through the use of the method of differential correction. The mechanics of this technique are essentially the same as those of the technique presented in the discussion of orbit determination. A statistically weighted comparison of the estimated orientation and the redundant but geometrically variant measurements can provide the means of isolating apparent systematic instrumentation errors. To effectively interpret the results of this method, one must be certain that a significant change in the measurement geometry has occurred so that the effect of a fixed measurement error is mathematically perceptible.

In the insertion maneuver orientation, the geometrical variation which can be measured during the initial or final two-thirds of an observable satellite pass is normally sufficient to improve the alignment standard deviation to about  $0.3^\circ$ .

#### **Orbit and attitude corrections**

When the parameters of the spacecraft orbit transfer trajectory have been established, a detailed examination of the probable characteristics of the nominal postinsertion maneuver orbit is possible. Since the impulse capability of the insertion engine is a fixed quantity, the nominal post-maneuver orbit characteristics are controlled by the inertial orientation of the available delta velocity increment. Within the inclination tolerance of the operational synchronous orbit, it is possible to exercise some influence over the component of the available incremental velocity which establishes the orientation of the final orbit plane. Hence, preferred initial orbit orientations, which result in a savings in the fuel required to maintain the inclination of the operational orbit, can be established. The effect on the orientation of the final orbit plane is a variation in the remaining component of the incremental velocity available for the in-plane circularization of the orbit. Consequently, it is possible to interchange the post-maneuver motion of the satellite over the surface of the earth with the amount of preferred orbit plane orientation. The orbit geometry on the third orbit revolution of the INTELSAT IV F-2 vehicle made it possible to achieve the maximum benefits of the final orbit orientation while conforming to the need to attain a nominal westward satellite drift rate.

The predictability of the postinsertion maneuver orbit is contingent on the combined error associated with errors in the inertial orientation of

the vehicle spin axis prior to the maneuver execution; effective thrust pointing errors, which are induced by disturbing torques experienced during the engine burn; and the predictability of the total impulse delivered by the insertion engine. The standard deviation assigned to these error sources at the time of the INTELSAT IV F-2 launch is indicated in Table 3. As a result of these probable errors, the expected standard deviation in the final orbit inclination and resultant satellite drift rate were  $0.13^\circ$  and  $1.9^\circ$  per day, respectively.

TABLE 3. STANDARD DEVIATION OF ERROR SOURCES  
FOR INTELSAT IV F-2

	Standard Deviation	
	Declination	Right Ascension
Spin Axis Alignment Error	$0.3^\circ$	$0.1^\circ$
Thrust-Induced Alignment Error	$0.28^\circ$	$0.28^\circ$
Impulse Predictability	3.96 m/s (13 ft/s)	—

The insertion maneuver was executed on the third orbit revolution of the spacecraft about the earth. At the time of the maneuver execution, the satellite was over the east longitude meridian of  $124.16^\circ$  at an altitude of 35,765.3 km (19,311.7 nmi). Table 4 gives the values of the desired orbit parameters and also includes the corresponding best estimate of the parameters that were achieved. The estimate of the achieved orbit is based on a set of parameters (derived from tracking data) from which the computed effective impulse of the vehicle reorientation to the operational attitude has been subtracted.

An assessment of the maneuver, based on a derived velocity discontinuity between the determined premaneuver and postmaneuver orbits, indicates that an offset from the desired effective thrust orientation was experienced. This offset was equal to  $+0.09^\circ$  in declination and  $+0.12^\circ$  in the right ascension. In addition, there was an excess of 2.8 m/s or 9.2 ft/s (less than 0.2-percent deviation) in the delivered incremental velocity.

As indicated by the characteristics of the postinsertion maneuver orbit, additional incremental velocity corrections are necessary to achieve the desired circular synchronization. The corrections are applied in the classical

TABLE 4. ORBIT PARAMETERS

Parameter	Desired	Achieved
Period	1,440.74 min	1,446.24 min
Eccentricity	0.00265448	0.005797
Inclination	$0.5^\circ$	$0.56^\circ$
Ascending Node	$270.0^\circ$	$265.99^\circ$
Argument of Perigee	$36.07^\circ$	$66.22^\circ$
Mean Anomaly	$0.0^\circ$	$334.06^\circ$
Apogee Altitude	35,989.5 km (19,432.8 nmi)	36,230.5 km (19,562.9 nmi)
Perigee Altitude	35,765.3 km (19,311.7 nmi)	35,739.5 km (19,297.8 nmi)
Drift Rate	$1.14^\circ/\text{day west}$	$2.52^\circ/\text{day west}$

method originally determined by Hohmann [2], in which the points of departure from one orbit to the next are cotangential with the apogee or perigee of the orbits. The sequence and magnitude of the maneuvers are programmed to place the satellite at its geographical location in a circular synchronous orbit in a time period consistent with communications requirements.

The vernier impulse necessary to complete the synchronization is derived from a monopropellant hydrazine propulsion system located on the spinning portion of the spacecraft, as shown in Figure 20. As indicated, the axes of the thrusters are arranged to provide their primary components of force either parallel to (axial) or perpendicular to and through (radial) the vehicle spin axis. Under the control of a TT&C station, the radial thruster is programmed on and off to produce an incremental impulse which is synchronized and phased to the detection of the sun in the  $\Psi$  sun sensor. Via ground control of the phase, the primary incremental velocity derived from a radial impulse can be directed along a selected inertial line normal to the vehicle spin axis. When the vehicle is aligned in its operational orientation normal to the orbit plane, the orbit velocity becomes nearly normal to the vehicle spin axis and, hence, can be influenced by a radial thruster.

In addition to the known transmission delay, the computed ground-controlled phase angle accounts for the known relative alignment of the sun sensor to the thruster and the previously measured centroid of the impulse. The number of impulses necessary to achieve a given incremental velocity change is derived from models of the propulsion characteristics.

These characteristics are based on performance parameters determined during the thruster acceptance test program.

In a similar manner, the axial thruster operating in the pulse mode makes it possible to vary the orientation of the vehicle. As the spacecraft is spin stabilized, the moment produced by the incremental axial thrust will result in a precession of the angular momentum axis. When the incremental thrust is synchronized and phased to the solar detector, the direction of the precession will always be a fixed angle measured from a plane defined by the spin axis and the line of sight to the sun. On a unit sphere, for which the sun line is defined as the pole, the locus of the spin axis will describe a rhumb line for which the direction of motion is constrained to cross the meridian lines at a fixed angle. To control the precession between two known inertial points, the required fixed torque angle can be analytically derived. Under normal operating conditions, the additional precession required by this technique as compared to that required by the great circle route is only slight.

In addition, the axial thruster can be programmed to provide continuous thrust. Under normal circumstances, this capability is not required during the launch phase. Instead, this continuous mode of operation is provided for future maintenance of the operational orbit inclination.

#### **Predictions of orbit operating environment**

The course of events experienced during the launch phase is dictated by the time-variant geometrical relationship between the spacecraft in its orbit and its spin-stabilized orientation as viewed by the earth-based monitoring and control network. Because of the geometrical complexity of the various physical relationships, it is difficult to anticipate the future value of many parameters related to the satellite orbit. To evaluate these parameters and to provide an aid to the orderly organization of the launch activity, a sequential ephemeris of all orbit related launch parameters are computed. For the earth station, some of the parameters which are included are the following:

- a. acquisition and loss of visibility,
- b. azimuth,
- c. elevation,
- d. range,
- e. received signal strength (omni-antenna),
- f. received signal strength (global antenna) despun on earth sensor 1,

- g. received signal strength (global antenna) despun on earth sensor 2,
- h. polarization angle, and
- i. Doppler shift.

For the satellite, the following parameters are included:

- a. sun angle,
- b. time and duration of solar eclipse,
- c. earth sensor measurements,
- d. possible sun interference in an earth sensor,
- e. position over the surface of the earth,
- f. received signal strength (omni-antenna), and
- g. angle between the spin axis and the line to the center of the earth.

These predictions are periodically updated to reflect current knowledge of the vehicle orbit and orientation.

To facilitate the expedient acquisition of the spacecraft as it enters the visibility of the earth station, predictions of the expected azimuth and elevation as functions of time are provided. These predictions are transmitted from the computer to the station via teletype in a format compatible with the paper tape input of the antenna driver.

For the initial acquisition of the vehicle and at the time of the insertion maneuver, the tracking antennas are provided with alternate pointing profiles which are used in the event of an initial failure to acquire. Two patterns are normally provided; the first covers expected 1-sigma variations in the orbit, while the second extends the search through 3-sigma limits.

During the course of a satellite maneuver, certain significant parameters can be monitored via the telemetry network. When possible, appropriate predictions of the parameter variation are provided as an aid to maneuver monitoring. Predictions of the data detected by sun and earth sensors are of particular significance during the execution of a major vehicle orientation change. From measurements of the observed deviation from nominal, one can detect errors which may become unacceptable if the maneuver is allowed to continue.

#### **References**

- [1] R. M. L. Baker, *Astrodynamics—Applications and Advanced Topics*, Academic Press, 1967, p. 64.
- [2] W. Hohmann, *Die Erreichbarkeit der Himmelskörper*, Munich, Oldenburg Publishing Corp., 1925.

Index: INTELSAT IV, communications satellites, telecommunications, radio transponders, earth terminals, mathematical models, simulation, frequency division multiplexing, time-division multiplexing, multiple access.

## ***The Intelsat IV communications system***

P. L. BARGELLINI, EDITOR

### ***Abstract***

This paper presents various aspects of the INTELSAT IV communications system. Following an outline of possible system approaches, transponder configurations and characteristics, earth stations, transmission analyses and simulations, field tests, and operational procedures are described.

### ***Introduction***

While it is possible to compound in a single equation all of the significant parameters of a space link, the design of a satellite communications system is complicated by the imperfections of the transponders, the multiple-access constraints, and the traffic distribution.

Both channel capacity and connectivity contribute to the total communications system capacity. The former can be defined in terms of communications theory (bps), or more practically, by the number of channels provided by a given spacecraft, while the latter can be formulated in terms of traffic matrices. The following interacting parameters affect the communications capacity:

- a. traffic requirements (type of traffic, number of earth stations, locations, desired connectivity, and traffic growth predictions),

---

*P. L. Bargellini is Senior Scientist, COMSAT Laboratories.*

- b. earth station characteristics (e.g., antenna G/T and transmitter power),
- c. operational constraints,
- d. spacecraft design (configuration, weight, power, and stability),
- e. allocated frequency bands,
- f. antenna characteristics,
- g. transponder characteristics (configuration, number, and interconnections), and
- h. methods of multiplexing, modulation, and multiple access.

The useful lifetime and reliability of the spacecraft, which contribute to the engineering and economics of a system, are also significant.

Overall parametric studies can provide useful guidelines for defining satellite systems which can meet the traffic requirements of a network model over a given time period. The adoption of technologies available at a given time or expected to become available in the future also has a significant impact on the configuration and choice of the system. On the other hand, any theoretical system approach must be strengthened with data gathered through experience. For instance, when a series of new satellites is introduced within an existing operational system, certain problems arise which can be resolved only by compromise. Thus, new generations of spacecraft can be defined through a combination of parametric studies and the pragmatic method of introducing gradual changes into an existing system.

The INTELSAT IV spacecraft and system characteristics were obtained in this manner. By late 1967, it became clear that a new satellite with a large capacity would be needed to meet the needs of the increased traffic requirements expected in the near future. A single design capable of providing service to three regions (i.e., the Atlantic, the Pacific, and the Indian Ocean areas) was desirable. The main objective was an average communications capacity of about 5,000 telephone circuits per satellite achieved by using the frequency-division multiplex/frequency modulation/frequency-division multiple-access (FDM/FM/FDMA) mode and standard size earth stations (30-m or 97-ft parabolas with a G/T ratio of 40.7 dB/°K).

Since operational flexibility was a requirement, efficient utilization of the 500-MHz total available bandwidth (around 6 GHz for the up-link and 4 GHz for the down-link) favored a multiple repeater approach in combination with global- and spot-beam antennas. Twelve transponders, each having a 36-MHz usable bandwidth, in combination with two global receive antennas (one redundant) and four transmit antennas (two for global- and two for spot-beam coverage), provide the required capacity.

Each transponder has a saturated RF power output of 6 W. Because of the backoff required to keep the intermodulation noise down, the global transmit antennas (17° beamwidth, 20-dB on-axis gain) provide a nominal e.i.r.p. (equivalent radiated power with reference to isotropic) of 22 dBW; spot-beam antennas (4.5° beamwidth, 31.7-dB on-axis gain) provide a nominal e.i.r.p. of 33.7 dBW.

As a result of the combined use of the global- and spot-beams, the actual satellite communications capacity in each case varies from around 4,000 to 6,000 telephone circuits. In addition, although FDM/FM/FDMA and standard earth station antennas are currently used, the design of the INTELSAT IV spacecraft provides flexibility to adapt to a variety of modulation techniques and multiple-access modes while accommodating earth stations with G/T values ranging from 5 to 41 dB/°K.

### **Systems planning**

J. L. DICKS, P. H. SCHULTZE, AND C. H. SCHMITT

#### **Communications subsystem tradeoff studies**

This section will describe the considerations that led to the choice of many of the characteristics which were introduced into the satellite specification.

**Antenna Coverage. Global Beam.** The beam that covers approximately one-third of the earth's surface as seen from a geostationary satellite is designated as the "global beam." The angle subtended from the edge of the earth to the subsatellite point is approximately 8.67°. Therefore, for the radiation in this direction to be no more than 3 dB down from beam center, the antenna beamwidth must be greater than 17.3°. Figure 1 shows

---

*J. L. Dicks is Manager, Systems Utilization, Systems Division, COMSAT Laboratories.*

*P. H. Schultze is Manager, Engineering Economics, Systems Division, COMSAT Laboratories.*

*C. H. Schmitt is a Technical Staff Member, Spectrum Utilization, Systems Division, COMSAT Laboratories.*

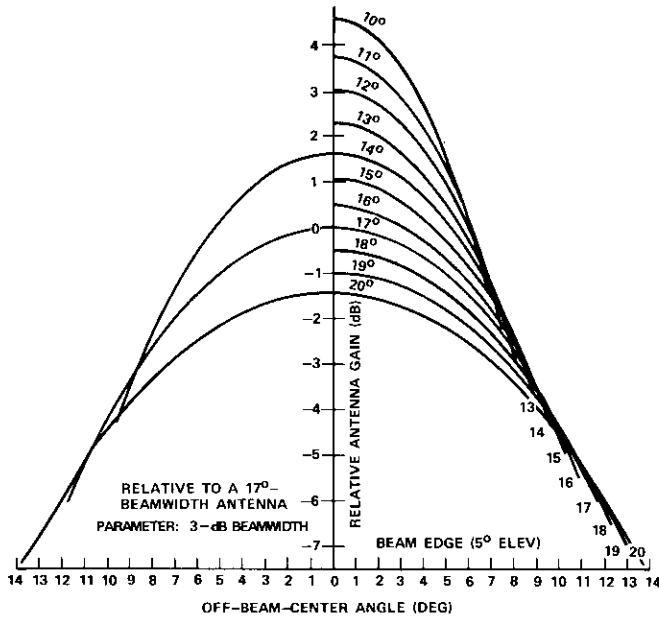


Figure 1. Antenna Gain vs Off-Beam Center Angle

typical antenna gains versus offset angles from beam center for 3-dB beamwidths from 10° to 20°. In this figure, the beam center gain of an antenna with a 17° beamwidth was arbitrarily chosen as the reference (0 dB). Figure 2 indicates that the highest antenna gain at 8.64° from beam center (as seen by earth stations with an elevation angle of 5° to the satellite) is obtained by using an antenna with a 3-dB beamwidth of 15.5°. The maximum of this curve is quite broad; a loss of only 0.5 dB is experienced with beamwidth variations from 12.2° to 19.2°.

Figure 2 makes it possible to read the variation of antenna gain with pointing errors. Maximum antenna gain variations, caused by satellite pointing errors of  $\pm 0.5^\circ$  as seen by earth stations with a 5° elevation angle to the satellite, are listed in Table 1. The  $\pm 0.5^\circ$  error is assumed to be caused by combined effects of maximum spin axis orientation errors and despin errors of 0.35° each.

In addition, system implementation considerations affect the satellite specification. For example, on multidestinational carriers, earth stations

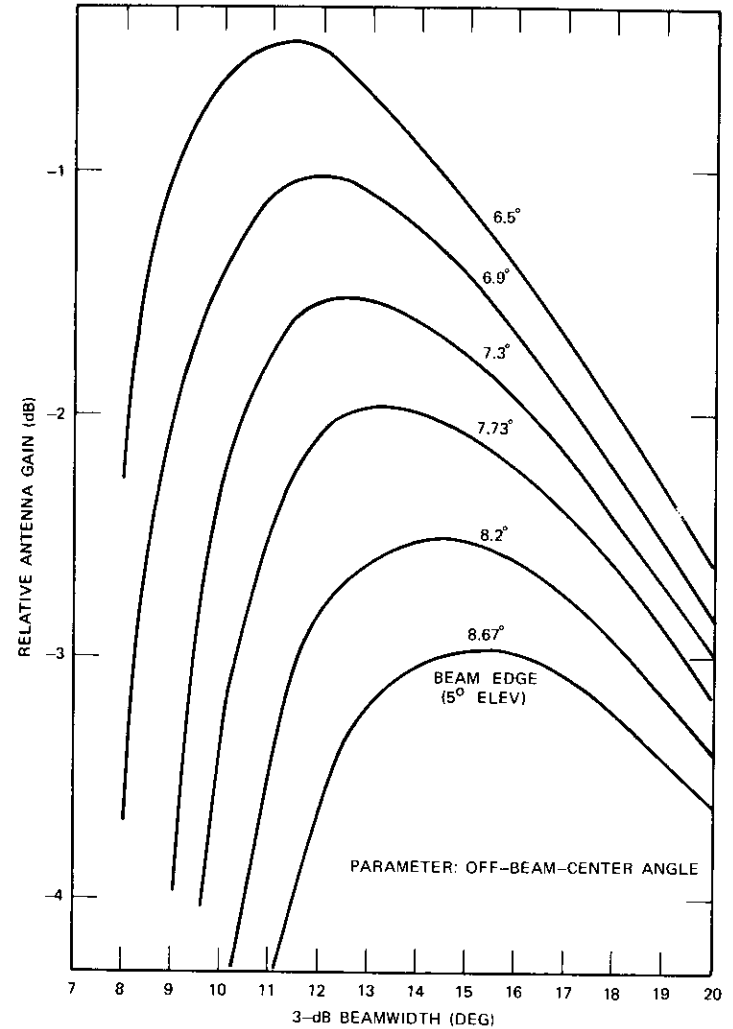


Figure 2. Antenna Gain Relative to a 17° Beamwidth

located at or near beam edge determine the required satellite e.i.r.p. While the use of this type of carrier favors wider beamwidths, carriers received nearer the beam center favor the use of narrow beamwidths. The beamwidth selected was therefore approximately 15°. Figure 3 shows the normal

relative antenna gain for some earth stations and the maximum gain variation corresponding to errors of  $\pm 0.35^\circ$  in the north-south and east-west directions.

TABLE 1. GLOBAL-BEAM ANTENNA GAIN VARIATION

3-dB Beamwidth (degrees)	Maximum Peak-to-Peak Antenna Gain Variation for Pointing Errors of $\pm 0.5^\circ$ (dB)
12	2.25
13	1.8
14	1.5
15	1.25
16	1.1
17	0.95
18	0.85
19	0.75
20	0.65

*Spot Beams.* In the case of spot beams, coverage was selected primarily on the basis of the Atlantic traffic forecasts. The northwest spot beam was intended to cover Mill Village, Canada; Andover, Maine; Etam, West Virginia; and Cayey, Puerto Rico. The northeast beam was intended to cover Goonhilly Downs, U.K.; Pleumeur Bodou, France; Raisting, Germany; Buitrago, Spain; Fucino, Italy; and other stations in the same general area.

The primary criterion for selecting the beamwidth for spot-beam coverage was the desire to achieve a high antenna gain for the spot-beam earth stations over the probable range of longitude for Atlantic INTELSAT IV satellites with small variations in antenna gain caused by satellite pointing error. In terms of these considerations, an antenna beam with a 3-dB beamwidth of  $4.5^\circ$  was found to be nearly optimum for northwest Atlantic coverage.

Table 2 lists relative antenna gains and maximum peak-to-peak antenna gain variations caused by satellite antenna pointing errors at the nominal satellite longitude of  $335.5^\circ$  east for some of the earth stations within the  $4.5^\circ$  spot-beam coverage. Although a slightly narrower antenna beam would have provided an acceptable coverage for the European stations

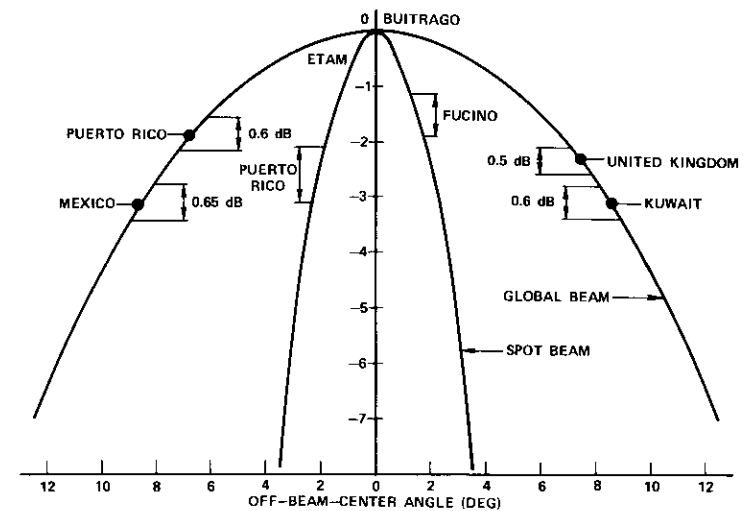


Figure 3. Spot and Global Beams

TABLE 2. SPOT-BEAM ANTENNA GAIN VARIATION

Earth Station	Relative Antenna Gain with Nominal Pointing (dB)	Maximum Range of Relative Antenna Gain Caused by Pointing Errors of $0.35^\circ$ (dB)	Maximum Peak-to-Peak Gain Variation (dB)
Mill Village	-2.1	-1.1 to -3.3	2.2
Andover	-1.6	-0.8 to -2.6	1.8
Etam	-0.3	-0.1 to -0.8	0.7
Cayey	-2.8	-1.8 to -4.2	2.4
Goonhilly Downs	-0.5	-0.2 to -1.2	1.0
Pleumeur Bodou	-0.4	-0.1 to -0.8	0.7
Raisting	-0.5	-0.3 to -1.1	0.8
Buitrago	-0.3	0 to -0.5	0.5
Fucino	-1.5	-0.8 to -2.5	1.7

indicated in Table 2, it was decided to specify a  $4.5^\circ$  beamwidth for the northeast Atlantic spot beam for the following reasons:

- The  $4.5^\circ$  beam could provide satisfactory coverage for potential earth stations in the same geographical area.

b. A narrower beam would require a larger satellite antenna reflector, which would result in a small (but not insignificant) reduction in the spacecraft weight available for power generation.

c. Values of e.i.r.p. higher than those achieved with a beamwidth of  $4.5^\circ$  would result in a relatively small increase in channel capacity since the transponder would operate in a bandwidth-limited mode.

d. System operation would be simplified if identical parameters were used for transmissions through both spot beams.

Figure 4 shows the spot-beam coverage with perfect antenna pointing for the nominal Atlantic satellite position of  $335.5^\circ$  east. The nominal relative antenna gain for some earth stations in the spot beams and the maximum gain variation corresponding to errors of  $\pm 0.35^\circ$  in the north-south and east-west directions are also plotted in Figure 3.

It was found that if the spot beams could be made fully steerable, their usefulness would be increased in the Pacific and Indian Ocean areas. Table 3 lists some of the earth stations that could be covered by  $4.5^\circ$  spot beams. According to initial traffic projections, spot-beam operation would not be required in the Pacific Ocean until the late 1970s. Nevertheless, this fully steerable operation, which was initially considered to be an option, was later made mandatory to accommodate future traffic projections.

*Other Antenna Configurations.* Elliptical spot-beam antennas with major axes in a north-south direction would have offered a slightly higher e.i.r.p. However, for reasons of simplicity, the more easily implemented circular pattern was retained. In addition, excessive ellipticity could have diminished the usefulness of the antenna in other regions of the world.

*Spot-Beam Receive Antennas.* The use of spot-beam receive antennas on the spacecraft would have reduced the requirements for earth station transmit power (e.i.r.p.). However, it was found that receive spot beams would result in the following disadvantages:

a. Reduction of satellite capacity. The west spot-beam receive antenna would be connected to the east spot-beam transmit antenna, and the east spot-beam receive antenna would be connected to the west spot-beam transmit antenna. This arrangement would not permit the use of spot-beam transmit antennas for traffic between stations within the same spot-beam coverage area (e.g., between North America and Puerto Rico) or for traffic from any country outside the spot beams to earth stations which are covered by the transmit spot

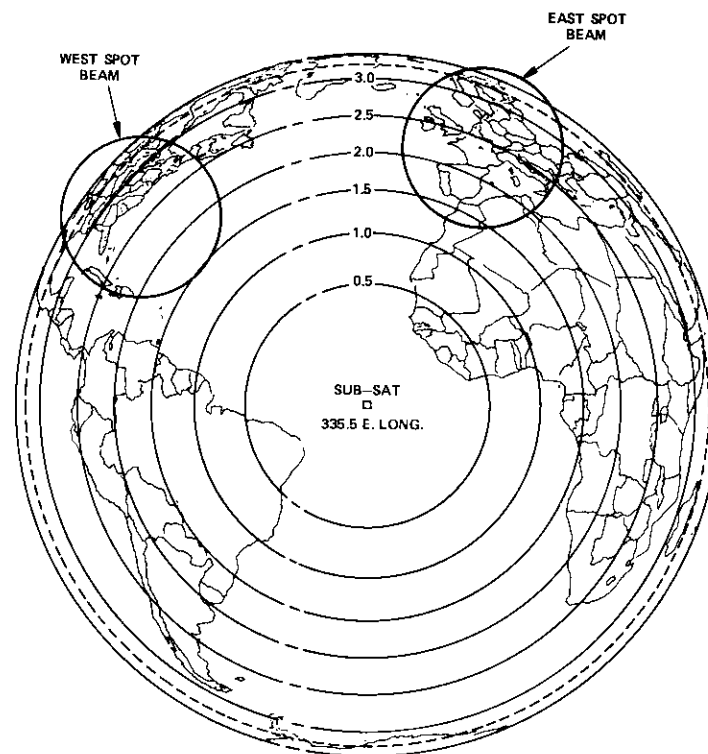


Figure 4. Spot- and Global-Beam Gain Contours in the Atlantic Region

beams unless special switching facilities were also to be added. Thus, a large percentage of traffic would have to be transmitted through the global-coverage antennas. This would reduce the capacity in the Atlantic area by 10 to 15 percent.

b. Increased satellite complexity. Spot-beam operation would require additional spot-beam receive feeds or antennas, additional redundant preamplifiers, and an additional receive multiplexer and switches to the spacecraft.

c. Increased susceptibility to interference. The receive carrier-to-noise ratio for spot-beam transmissions is on the order of 25 to 30 dB.

TABLE 3. COVERAGE OF PACIFIC AND INDIAN OCEAN AREAS

Region	East Spot Beam		West Spot Beam	
	Potential Earth Stations in 3-dB Beamwidth	Beam Direction	Potential Earth Stations in 3-dB Beamwidth	Beam Direction
Pacific Ocean Satellite Longitude 174° East	Brewster, Washington	5.0° East	Kum San, Korea	5.3° West
	Jamesburg, California Paumotu, Hawaii	5.2° North	Ibaraki, Japan Taiwan Hong Kong	4.1° North
Indian Ocean Satellite Longitude 62.5° East	Yamaguchi, Japan	6.3° East 3.6° North	Pleumeur Bodou, France	5.3° West
	Sri Racha, Thailand Hong Kong East Pakistan Tanay, Philippines		Fucino, Italy Buitrago, Spain Goonhilly Downs, U.K.	6.2° North

This means that the carrier-to-interference noise ratio would have to be considerably higher. Increasing the satellite receive antenna gain would increase the risk of interference in the up-link.

For these reasons, the INTELSAT IV design provides only global-coverage receive antennas.

**Number of Transponders.** After the beamwidths of the antennas have been selected on the basis of coverage considerations, the number of transponders per satellite must be determined. For a given satellite power and weight budget allocated to communications capability, tradeoffs can be established in terms of the power and bandwidth allotted to each transponder. Figures 5, 6, and 7 show typical results obtained from basic configurations which were developed to permit realistic estimates to be made. Figure 5 shows the total RF power per satellite. This power is highest for a configuration with only one transponder per satellite. The total RF output power of a 16-transponder configuration is nearly 3 dB lower than that of a 12-transponder configuration. This reduction of output power precludes the use of many more than 12 transponders.

Figure 5 also gives the total usable bandwidth per satellite as a function of the number of transponders. The bandwidth decreases with an increasing number of transponders because a larger number of guardbands is required. This consideration militates against the use of a very large num-

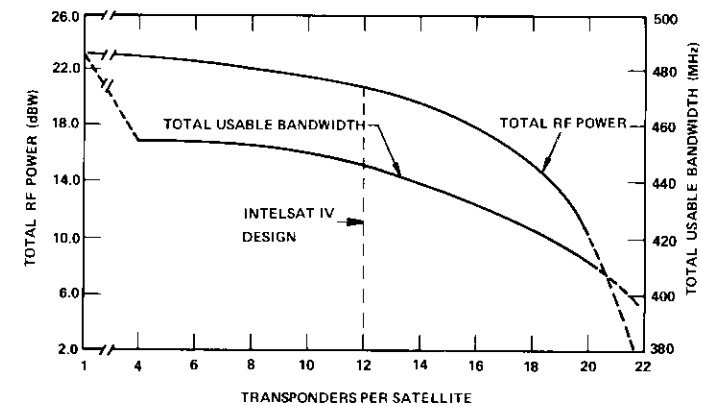


Figure 5. Total Power and Usable Bandwidth vs Number of Transponders

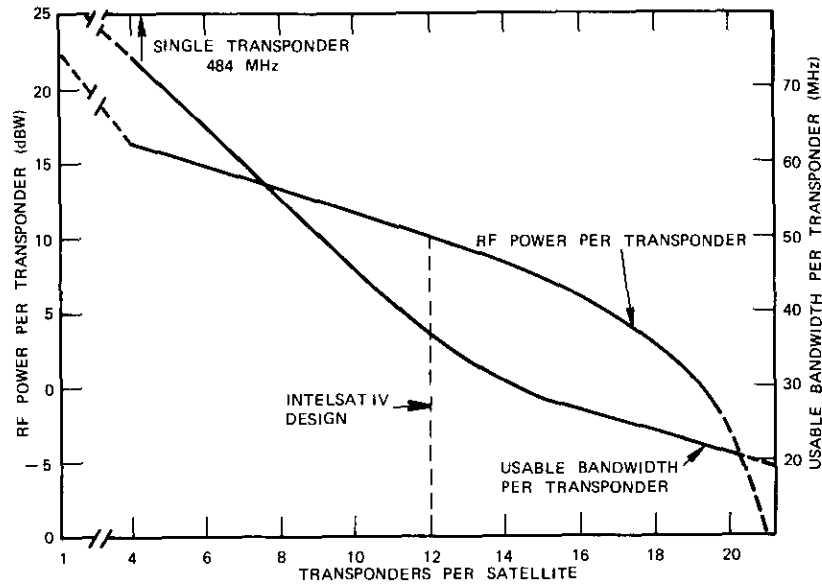


Figure 6. RF Power and Usable Bandwidth per Transponder vs Number of Transponders

ber of transponders, but its effects are not significant below 18 transponders.

Figure 6 shows the RF output power and usable bandwidth per transponder as functions of the number of transponders per satellite. Figure 7 indicates the approximate channel capacity per transponder for single-carrier FDM/FM transmission with global- and spot-beam coverage. The total satellite channel capacity in the FDM/FM mode is also shown as an example for different numbers of transponders and global coverage. It can be seen that the total capacity remains reasonably constant up to 12 transponders, but falls quite rapidly beyond that point.

It would be desirable to use more transponders, each with a smaller number of channels (e.g., 300 to 600) so that many of the large satellite users could transmit single carriers per transponder. However, spot-beam operation would require approximately 20 transponders per satellite to provide a capacity of 600 channels, and approximately 22 transponders per satellite to provide 300 channels. Hence, these configurations, which would result in approximately 11 and 20 dBW less available RF power, respectively, than the 12-transponder configuration, would no longer be advantageous.

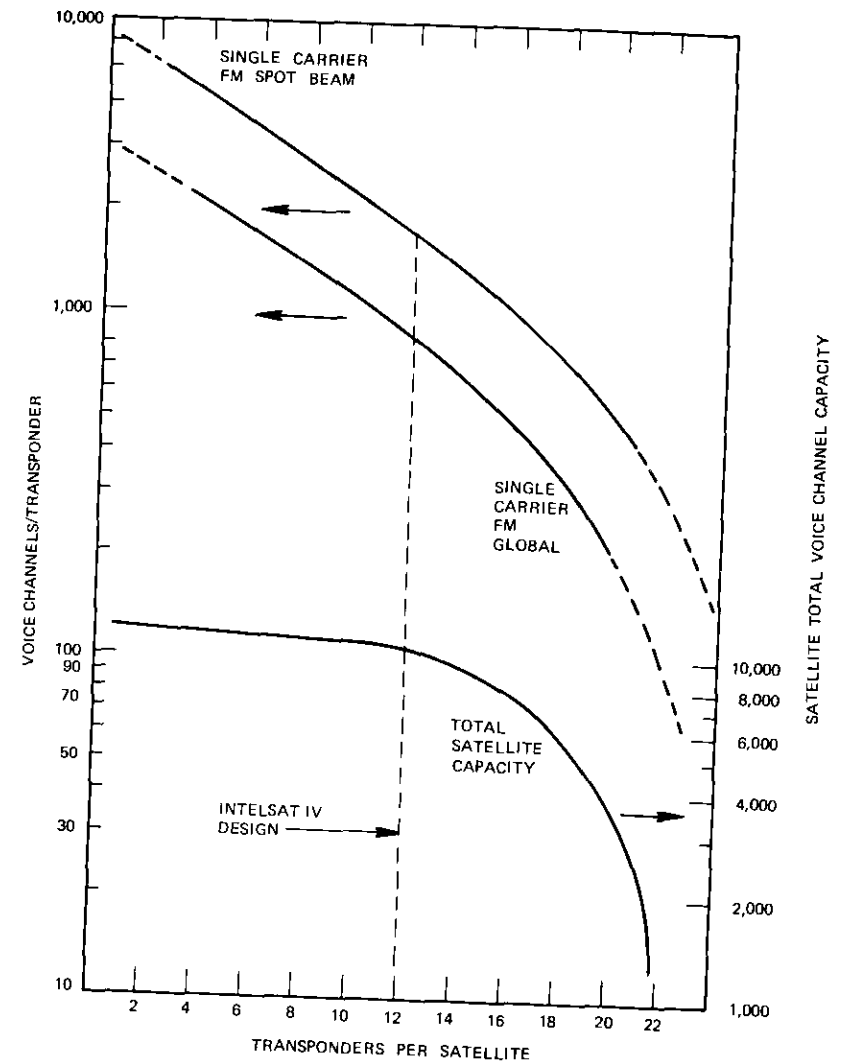


Figure 7. Channel Capacity vs Number of Transponders

Interference considerations rule out configurations with only a few transponders, since each transponder is expected to include a mixture of TV and FDM/FM carriers with time-division multiple-access (TDMA)

carriers. Such wideband transponders will also experience higher levels of satellite intermodulation than a 12-transponder configuration.

**Redundancy Considerations.** A study was undertaken to determine the requirements for redundancy. This study essentially consisted of a comparison of the following configurations:

- 12 transponders and full redundancy for all active elements,
- 12 transponders and no redundancy, and
- 24 transponders and no redundancy.

Probability of survival calculations were based on the best information currently available. The validity of some of the failure rates for space applications was uncertain due to the lack of data. An example of the 12-transponder, fully redundant configuration is shown in Figure 8. (Full redundancy for all active components was made mandatory.)

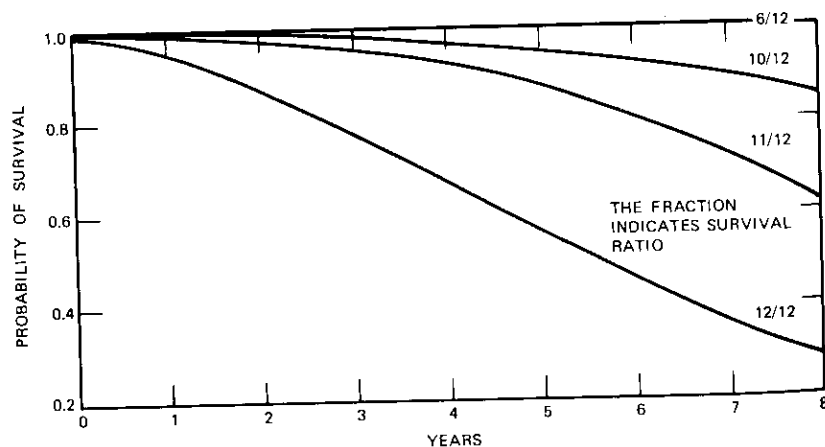


Figure 8. *Survival Probability for 12-Transponder Redundant Communications Subsystem*

**Impact of Traffic Distribution Patterns.** Unequal transponder bandwidths could be advantageous for certain applications. For these applications, several transponders might be allocated to each of the following bandwidths:

- a bandwidth adequate for TV transmission;

- a bandwidth which is optimized for time-division multiplex (TDM) applications, but could also be used for multiple-carrier FDM/FM transmission; and
- a smaller bandwidth for single-carrier FDM/FM transmission.

To implement this scheme, however, it would be necessary to predict the relative requirements of each type of application and design the satellite accordingly. Even if this could be done, the requirements for the three coverage zones (Atlantic, Pacific, and Indian Ocean) would probably be different; hence, it would be difficult to provide spare or replacement satellites. For the Atlantic, it would also be necessary to switch the transponders used for TDM and multiple-carrier FDM/FM transmissions and single-carrier FDM/FM transmission between global-coverage and spot-beam antennas. Apart from these difficulties, providing some transponders with smaller bandwidths would increase the total number of transponders and significantly decrease the available total RF power per satellite. Filtering and multiplexing problems would also be aggravated.

Specific studies were conducted to determine if transponders with unequal bandwidths would provide more channel capacity. Three transponder configurations were considered:

- communications option no. 1: 12 transponders, each having a 36-MHz bandwidth;
- communications option no. 2: 16 transponders (eight transponders with 36-MHz bandwidths and eight transponders with 16-MHz bandwidths); and
- twelve transponders with unequal bandwidths.

The traffic forecast for the Atlantic area at the end of 1976 was used to determine the multiple-carrier FDM/FM channel capacity for each transponder configuration when different sets of carrier assignment rules are used. From this study, the following conclusions were drawn:

- For the Atlantic traffic forecast, a mixture of spot- and global-beam transponders may be used. This will result in an available satellite capacity of approximately 12,000 channels and a usable satellite capacity of approximately 10,000 channels. (The difference between these two numbers corresponds to an average carrier fill factor of approximately 80 percent.)
- There is no significant difference between the number of available channels and the number of usable channels for the three communications configurations.

c. Some difference in capacities results from the application of different carrier assignment rules.

For these reasons, transponders with equal bandwidth and power were proposed. In this case, any transponder would be equally suitable for any of the anticipated transmissions. There would be sufficient flexibility to meet changing traffic needs in any region, and the same satellite could be used in all three ocean areas.

**Single Versus Dual Polarization for the Up-Link.** Opposite senses of polarization could have been used on the up-link for adjacent transponders so that filter requirements for out-of-band rejection would be reduced. This reduction would generally appear to be advantageous in terms of spacecraft design.

If dual polarization had been used for INTELSAT IV, a large number of earth stations would have been required to simultaneously transmit both polarizations at different frequencies. On the other hand, if only global-beam transmission had been employed in the satellite, some earth stations might have transmitted only into transponders with left-hand circular polarization, while other earth stations might have transmitted only into transponders with right-hand circular polarization. In this case, since spot-beam transmission would be used in the Atlantic area, many earth stations would have had to transmit carriers into two or three transponders (for example, into one global-beam transponder, one east spot-beam transponder, and one west spot-beam transponder). Because of this requirement and because traffic on individual links could not be accurately predicted, it was nearly impossible to work out a transmission arrangement in which most earth stations would have been required to transmit only one sense of polarization. Hence dual polarization was rejected.

Finally, it must be remembered that satisfactory operation of a system with dual polarization requires all earth stations to maintain a good axial ratio for their transmit antennas at all times. Degraded axial ratios of any earth station could cause serious interference in adjacent transponders.

#### Transmission system planning

After the essential satellite characteristics of INTELSAT IV had been determined and the satellite specification developed, it was possible to prepare detailed transmission plans and standards for earth stations to work with INTELSAT IV. The objective was to achieve the maximum channel capacity and specified channel performance within the constraints imposed by

satellite and earth station characteristics. For the initial planning stage, only conventional multiple-access FDM/FM was considered. This limitation was necessary to provide a gradual transition, in terms of operational considerations and equipment changes, from INTELSAT III to INTELSAT IV satellites. Transmission characteristics for the more advanced techniques such as TDMA and a SPADE-type system were developed later.

**Telephony Performance Objectives.** The INTELSAT IV system has been designed to meet all C.C.I.R. and C.C.I.T.T. recommendations applicable to satellite communications. For example, the C.C.I.R. recommendation on channel noise performance (Rec. 353-2 [1]) states that the noise power in a telephone channel should not exceed the following values:

- a. 10,000-pW psophometrically weighted mean power in any hour,
- b. 10,000-pW psophometrically weighted 1-minute mean power for more than 20 percent of any month,
- c. 50,000-pW psophometrically weighted 1-minute mean power for more than 0.3 percent of any month, and
- d. 1,000,000-pW unweighted (with an integrating time of 5 ms) for more than 0.03 percent of any month.

This recommendation obviously had a direct impact on the design of the transmission parameters. In line with this recommendation, the following noise breakdown was adopted for the design of the INTELSAT IV satellite communications link:

thermal noise at the satellite (up-link) + thermal noise at the earth station (down-link) + satellite intermodulation noise:	7,500 pWp
earth station out-of-band intermodulation:	500 pWp
interference noise:	1,000 pWp
earth station equipment noise:	1,000 pWp
total	10,000 pWp

The appropriate recommendations for intelligible crosstalk and impulse noise were considered in the design of carrier sizes and their arrangement in the transponder, as well as in the selection of earth station IF filters. Other factors which had a direct impact on the design of the transmission parameters were group-delay distortion, multipath transmission, and adjacent transponder intermodulation.

**Typical INTELSAT IV Transponder Operating Characteristics.** Transmission characteristics and FDM/FM channel capacities of an INTELSAT IV transponder are largely a function of its mode of operation. For example, the use of a single carrier to access the transponder permits full utilization of the transponder output power and hence maximum channel capacity. However, if the transponders are accessed by multiple FM carriers, traveling wave tube (TWT) nonlinearities will produce intermodulation noise. To limit the intermodulation noise at which the transponder must be operated, an appropriate input backoff, resulting in a less efficient utilization of transponder output power, is employed. Table 4 has been prepared for both spot- and global-beam operation to demonstrate the impact of single- and multiple-carrier operation on transponder operating parameters and achievable channel capacities.

TABLE 4. TYPICAL INTELSAT IV TRANSPONDER OPERATING CHARACTERISTICS

Operating Characteristics	Global Beam		Spot Beam	
	Single Carrier	Multiple Carriers	Single Carrier	Multiple Carriers
Satellite e.i.r.p. at Beam Edge (dBW)				
Specified	22.0	22.0	33.7	33.7
Expected Average	22.5	22.5	34.2	34.2
Satellite Receive G/T (dB/°K)				
Specified	-18.6	-18.6	-18.6	-18.6
Expected Average	-17.6	-17.6	-17.6	-17.6
Selected Gain Setting No.	2	4	4	7
Saturation Flux Density at Beam Edge (dBW/m <sup>2</sup> )	-73.0	-67.0	-66.0	-57.0
Optimum TWT Operating Point (dB)	0	-11.0	0	-16.0
Total Carrier-to-Noise Density Ratio, (C/N <sub>0</sub> ) <sub>T</sub> (dB-Hz)	94.6	88.1	105.1	96.0
Total Carrier-to-Noise Ratio, (C/N) <sub>T</sub> (dB)	19.0	13.0	29.5	20.9
Transponder Capacity (channels)	960	500	1,800	900

In Table 4, it should be noted that an increase in satellite e.i.r.p. of approximately 12.0 dB when switching from the global-beam mode to the spot-beam mode results in a capacity increase of only 3 dB. This indicates

that the achievable transponder capacity is not merely a function of the available satellite e.i.r.p., but that it is also a function of the achievable total carrier-to-noise density ratio and the available transponder bandwidth.

#### Optimization of Carrier-to-Noise Density Ratio for Multicarrier FDMA.

The impairments suffered by FDM/FM carriers passing through a transponder operating in the multiple-access mode are caused by a number of factors. The nonlinear characteristic of the satellite TWT will create an intermodulation spectrum which causes interference noise in the wanted carriers. The amount of intermodulation noise encountered in a telephony channel is primarily a function of the TWT operating point, the level and composition of the RF spectrum, and the relationship of the RF spectrum to the wanted carrier spectrum. Extensive studies have been performed at COMSAT Laboratories to accurately calculate and predict the intermodulation noise in a telephony channel. From these studies, a computer model has been developed which has been successfully verified in a laboratory simulation test program.

In systems calculations, it is useful to express the channel intermodulation noise as an equivalent carrier-to-intermodulation noise density, (C/N<sub>0</sub>). Hence, the equivalent average intermodulation noise density in the transponder and the appropriate carrier power level adjustment for equalization of the channel noise performance can be determined. Figure 9 shows the RF intermodulation spectrum for a typical frequency plan, the computed equivalent carrier-to-noise density ratio for each carrier, and the

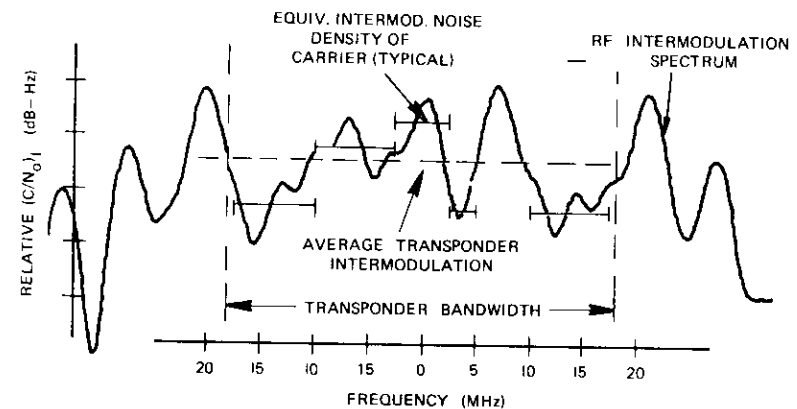


Figure 9. Intermodulation Spectrum of Typical Frequency Plan

corresponding average transponder intermodulation. Figure 10 shows the typical variation of the intermodulation as a function of the TWT operating point. The total intermodulation carrier-to-noise density ratio is a composite of intermodulation noise caused by amplitude and phase nonlinearities of the satellite TWT.

The total carrier-to-noise density ratio,  $(C/N_o)_T$ , as a function of the TWT operating point is the sum of thermal up-link noise, thermal down-link noise, and satellite intermodulation noise:

$$\frac{1}{\left(\frac{C}{N_o}\right)_T} = \frac{1}{\left(\frac{C}{N_o}\right)_U} + \frac{1}{\left(\frac{C}{N_o}\right)_D} + \frac{1}{\left(\frac{C}{N_o}\right)_I} \quad (1)$$

The carrier-to-noise density ratio in the up-link is

$$\left(\frac{C}{N_o}\right)_U = W_s + \left(\frac{G}{T}\right)_s - 10 \log \frac{4\pi}{\lambda^2} - 10 \log k - BO_i \quad (2)$$

where  $W_s$  = saturation flux density at beam center, in dBW/m<sup>2</sup>

$\left(\frac{G}{T}\right)_s$  = gain-to-noise-temperature ratio of the satellite at beam center, in dB/°K

$10 \log \frac{4\pi}{\lambda^2}$  = gain of 1-m<sup>2</sup> aperture at the transponder center frequency, in dB

$10 \log k$  = Boltzmann's constant (-228.6 dBW/°K - Hz)

$BO_i$  = TWT input backoff relative to single-carrier saturation, in dB.

The carrier-to-noise density ratio in the down-link is

$$\left(\frac{C}{N_o}\right)_D = e.i.r.p._{sat} - PL_{4GHz} + \left(\frac{G}{T}\right)_E - \Delta D - 10 \log k - BO_o \quad (3)$$

where  $e.i.r.p._{sat}$  = satellite e.i.r.p. at beam center and single-carrier saturation, in dBW

$PL_{4GHz}$  = 195.6-dB path loss from the satellite to the sub-satellite point at 4 GHz

$\left(\frac{G}{T}\right)_E$  = 40.7-dB/°K earth station gain-to-noise temperature ratio at 4 GHz

$\Delta D$  = average down-link adjustment factor for path loss and antenna gain in dB

$BO_o$  = TWT output backoff relative to single-carrier saturation in dB.

Since path loss and earth station antenna gain have the same frequency dependence, equation (3) can be applied to frequencies other than 4 GHz.

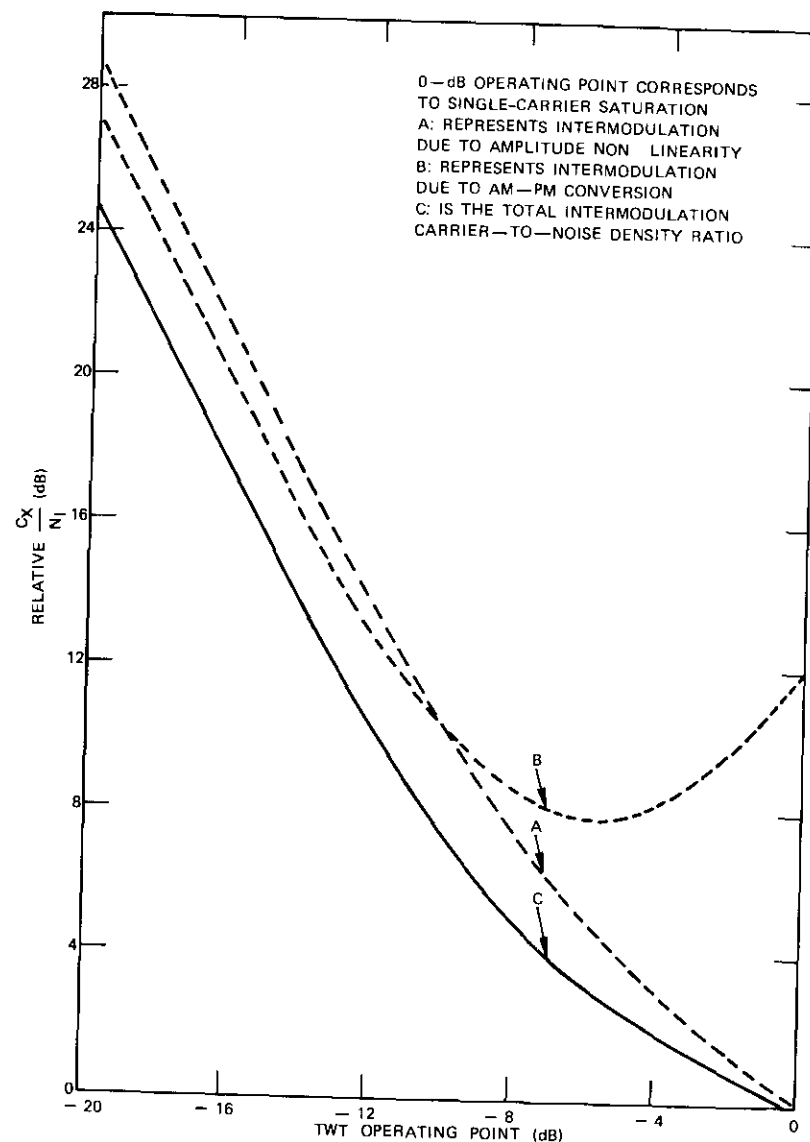


Figure 10. Relative Carrier-to-Intermodulation Noise Ratio vs TWT Operating Point

Figure 11 is a graphical presentation of the resulting  $(C/N_o)_T$  as a function of the TWT operating point. [The optimum TWT operating point is defined as the point where  $(C/N_o)_T$  reaches its maximum.]

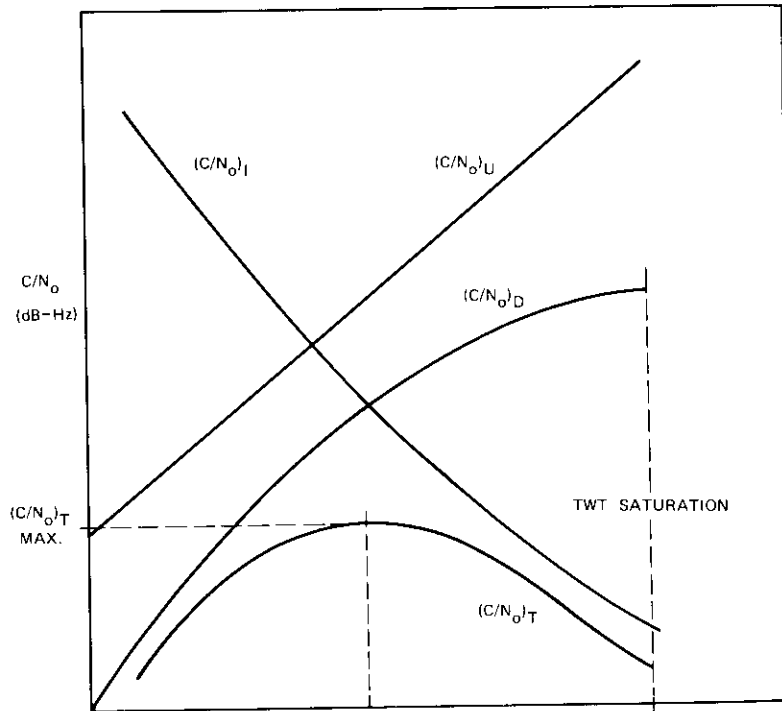


Figure 11. Optimum TWT Operating Point

**Transponder Gain Settings.** Switchable attenuator settings in the INTELSAT IV satellite make it possible to vary the saturation flux density in discrete steps. If the gain of the satellite is reduced, the earth station transmit power must be increased, resulting in a better up-link carrier-to-noise density ratio. An attenuation range of 24 dB makes it possible to adjust the up-link noise for various modes of operation so that it does not become the noise-limiting factor.

Figure 12 shows a typical gain setting tradeoff for global-beam multicarrier operation. It can be seen that reducing the gain from gain setting

no. 1 to gain setting no. 4 results in a capacity increase of 25 percent, whereas a further gain reduction will have no significant impact on the transponder capacity. Once thermal down-link and satellite intermodulation noise become the limiting factors, a further reduction of thermal up-link noise becomes relatively inconsequential.

The required earth station power per channel was used as a criterion for selecting the appropriate gain settings for a particular mode of operation. Power requirements of approximately 1 to 2 watts/channel yield a

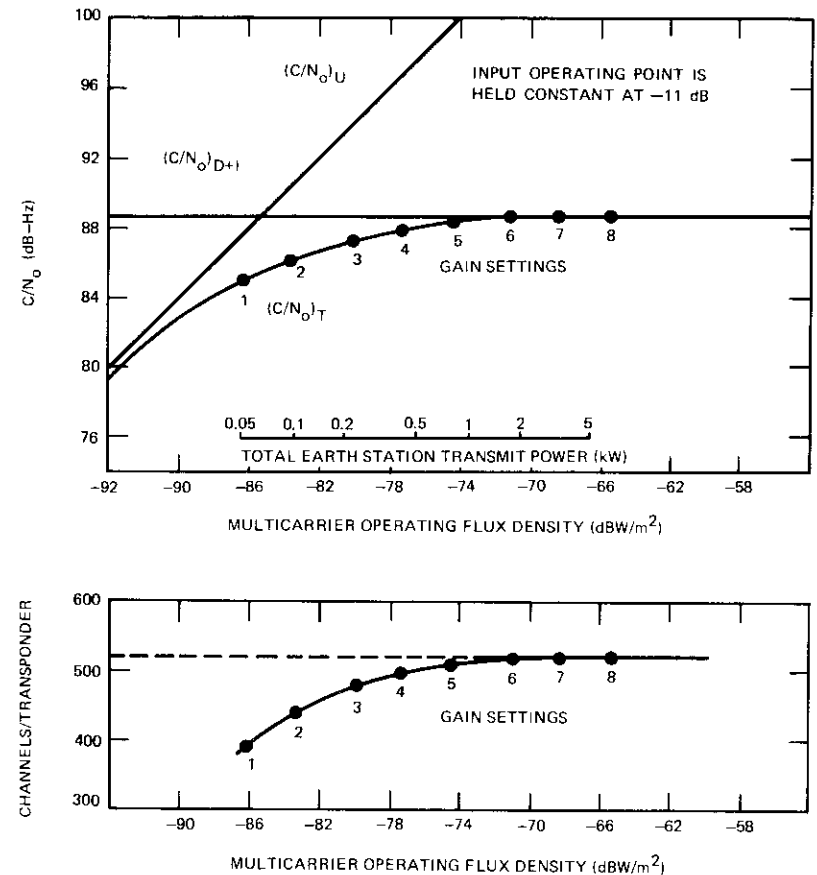


Figure 12. Carrier-to-Noise Density Ratio and Channel Capacity as a Function of Flux Density (Global Beam)

reasonable tradeoff between satellite capacity and earth station power requirements.

**Selection of Carrier Sizes and Parameters.** Because of the traffic requirements in the global network, a wide range of carrier capacities had to be accommodated by the satellite. Hence, it was necessary to introduce a large number of carrier sizes in reasonable increments so that a reasonable ratio between available and actual used capacity, or fill factor, could be achieved. Bandwidth units of multiples of 2.5 MHz were selected to allow a flexible interchange of carriers within a given frequency range without requiring frequency changes among adjacent carriers. Furthermore, it was desirable to obtain the carrier sizes from multiples of channel groups and supergroups.

The transmission parameters for each carrier size were calculated by using the standard FM equation and Carson's Rule of bandwidth,

$$\left[ \frac{S}{N} \right] = \left[ \frac{C}{N} \right] \frac{B}{b} \left[ \frac{f_r}{f_m} \right]^2 P \cdot W$$

$$B = 2[3.16 g f_r + f_m]$$

where  $\left[ \frac{S}{N} \right]$  = weighted signal-to-noise ratio at the 1-mW test-tone level = 51.2 dB for 7500-pWp channel noise

$\left[ \frac{C}{N} \right]$  = carrier-to-noise ratio over the Carson's Rule bandwidth, B

$b$  = channel bandwidth = 3.1 kHz

$f_r$  = rms test-tone deviation

$f_m$  = maximum baseband frequency  $\approx 4.2 \times n$ , in kHz

$n$  = number of telephone channels

$P$  = psophometric weighting factor = 2.5 dB

$W$  = pre-emphasis weighting factor = 4 dB

$g$  = antilog  $\left[ \frac{L}{20} \right]$

$L = -15 + 10 \log n$ ,  $n \geq 240$  channels,

$= -1 + 4 \log n$ ,  $n < 240$  channels.

Once the number of channels per carrier and the desired signal-to-noise ratio,  $S/N$ , are fixed, the carrier-to-noise temperature ratio,  $C/T$ , can be traded for RF bandwidth, B. The only constraint in this tradeoff is that

the carrier-to-noise ratio,  $C/N$ , should not fall below a minimum of 13 dB to avoid operation in the threshold region of the demodulator.

Figure 13 shows the number of channels per carrier as a function of RF bandwidth for spot- and global-beam operation, a noise allocation of 7,500 pWp, and guardbands of 10 and 20 percent. These curves and the points discussed previously were used to select the INTELSAT IV carrier sizes. Tables 5 and 6 show the transmission parameters for all spot- and global-beam carrier sizes selected for use on INTELSAT IV satellites.

**Transmission Impairments.** As shown in Table 7, transmission impairments in a communications satellite link can be classified according to the sources of degradation. These impairments can occur in the satellite or at the earth stations, or they can be caused by linear or nonlinear devices in the communications link. In addition, there can be dual-path transmissions, in which signal transmitted through two independent paths, produces interference noise. More specifically, the various sources of transmission impairments which can be encountered in a communications satellite link are

- a. thermal up-link and down-link noise,
- b. group-delay noise,
- c. intelligible crosstalk,
- d. dual-path transmission,
- e. impulse noise, and
- f. RF out-of-band intermodulation.

Thermal up-link noise, thermal down-link noise, and satellite intermodulation noise have already been considered in the carrier-to-noise density optimization procedure and will therefore be excluded from this discussion.

Group-delay noise caused by the nonlinear phase characteristics of the transmission path can occur at the earth stations as well as in the satellite. The use of group-delay equalization at the transmitting earth station makes it possible to keep the group-delay noise in a link within the 500-pWp allowance. (See Fig. 25.)

Intelligible crosstalk is caused by nonlinearities in the gain-frequency response of a transmission path which includes an active device such as an earth station high-power amplifier (HPA) or a satellite TWT with inherent AM/PM conversion characteristics. Intelligible crosstalk can be kept at an acceptable level by equalizing the gain-frequency response or, in the case of nonlinearities in the satellite, by predistorting the gain-frequency response at the transmitting earth station.

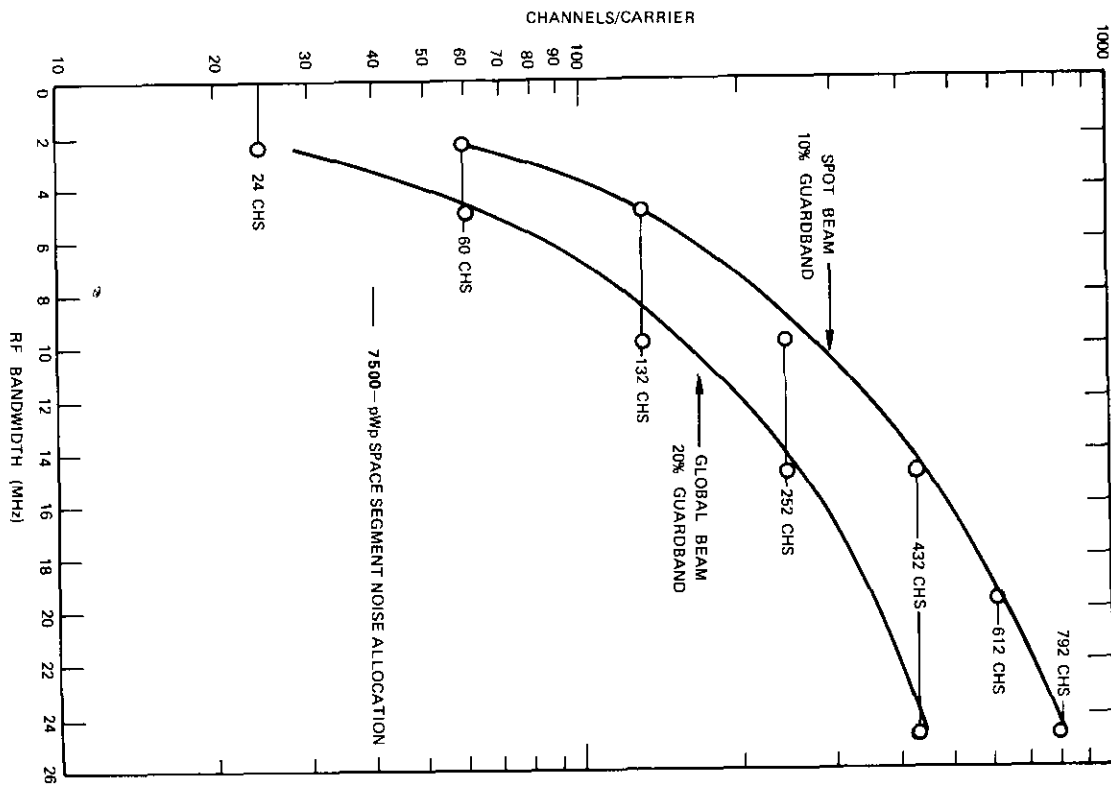


Figure 13. Channel Capacity per Carrier as a Function of RF Bandwidth

TABLE 5. GLOBAL-BEAM INTELSAT IV TRANSMISSION PARAMETERS (8,000 pWp) FOR STANDARD AND EXPANDED CARRIERS

Channels/Carrier, n	Top Baseband Frequency, $f_m$ (kHz)	Allocated Satellite BW Unit (MHz)	Occupied BW (p) (F at Earth Station) (MHz)	rms Multicarrier Deviation, $f_{rms}$ (kHz)	Carrier-To-Total Noise Temp Ratio, (C/T) <sub>T</sub> (dBW/°K)	Carrier-To-Noise Ratio in Occupied BW, C/N (dB)	Satellite e.i.r.p. at Beam Edge (dBW)	Earth Station e.i.r.p. at 10° Elevation (dBW)
24	108.0	2.5	2.00	275.0	-153.0	12.7	5.8	74.7
36	156.0	2.5	2.25	307.0	-150.0	15.1	8.8	77.7
60	252.0	2.5	2.25	276.0	-144.0	21.1	14.8	83.7
60	252.0	5.0	4.00	546.0	-149.9	12.7	8.9	77.8
72	300.0	5.0	4.50	616.0	-149.1	13.0	9.7	78.6
96	408.0	5.0	4.50	584.0	-145.5	16.6	13.3	82.2
132	552.0	5.0	4.40	529.0	-141.4	20.7	17.4	86.3
96	408.0	7.5	5.90	799.0	-148.2	12.7	10.6	79.5
132	552.0	7.5	6.75	891.0	-145.9	14.4	12.9	81.8
192	804.0	7.5	6.40	758.0	-140.6	19.9	18.2	87.1
132	552.0	10.0	7.50	1020.0	-147.1	12.7	11.7	80.6
192	804.0	10.0	9.00	1167.0	-144.4	14.7	14.4	83.3
252	1052.0	10.0	8.50	1009.0	-139.9	19.4	18.9	87.8
252	1052.0	15.0	12.40	1627.0	-144.1	13.6	13.9	82.8
312	1300.0	15.0	13.50	1716.0	-141.7	15.6	16.3	85.2
432	1796.0	17.5	15.75	1919.0	-138.5	18.2	18.0	88.0
432	1796.0	20.0	18.00	2276.0	-139.9	16.1	17.7	86.6
432	1796.0	25.0	20.70	2688.0	-141.4	14.1	16.2	85.1
972	4028.0	36.0	36.00	4417.0	-135.2	17.8	22.4	90.1
1092	4892.0	36.0	36.00	4118.0	-132.4	20.7	23.7	93.6

TABLE 6. SPOT-BEAM INTELSAT IV TRANSMISSION PARAMETERS (8,000 pWp)  
FOR STANDARD AND EXPANDED CARRIERS

Channels/Carrier, n	Top Baseband Frequency, f <sub>b</sub> (kHz)	Allocated Satellite BW Unit (MHz)	Occupied BW (MFE at Earth Station) (MHz)	rms Multicarrier Deviation, f <sub>mc</sub> (kHz)	Carrier-To-Total Noise Temp. Ratio, (C/T) <sup>T</sup> (dBW/K)	Ratio in Occupied BW, C/N (dB)	Satellite E.I.P. Beam Edge (dBW)	Earth Station e.I.P. at 10° Elevation (dBW)
60	252.0	2.5	276.0	-144.0	21.1	15.2	81.4	
72	300.0	2.5	261.0	-141.7	23.4	17.5	83.7	
132	552.0	5.0	529.0	-141.4	20.7	17.7	83.9	
192	804.0	5.0	459.0	-136.3	25.8	22.8	86.0	
192	804.0	7.5	758.0	-140.6	19.9	18.5	84.7	
252	1052.0	7.5	733.0	-137.1	23.2	22.0	88.2	
252	1052.0	10.0	1009.0	-139.9	19.4	19.2	85.4	
312	1300.0	10.0	1005.0	-137.1	22.0	22.0	86.2	
432	1796.0	15.0	1479.0	-136.2	21.2	22.2	88.4	
612	2540.0	20.0	1996.0	-134.2	21.9	23.9	90.1	
792	3284.0	20.0	1784.0	-129.9	26.2	28.2	94.4	
792	3284.0	25.0	2494.0	-132.8	22.3	25.3	91.5	
972	4028.0	25.0	2274.0	-129.4	25.7	28.7	94.9	
1872	8120.0	36.0	3181.0	-123.5	29.5	34.2	98.6	

TABLE 7. CLASSIFICATION OF TRANSMISSION IMPAIRMENTS

Transmission Path	Satellite		Earth Station
	Single Transponder	Two Transponders	
Linear	Thermal Noise (up-link)	Dual-Path Group-Delay Distortion	Thermal Noise (down-link)
	Group-Delay Distortion		Group-Delay Distortion (envelope distortion)
Nonlinear			Amplitude/Frequency Distortion
			Impulse Noise
	Intermodulation	Adjacent Transponder Intermodulation	Out-of-Band Emission due to HPA multicarrier operation
	Intelligible In-Band Crosstalk	Intelligible Out-of-Band Crosstalk	

Dual-path transmission occurs when a signal near the band edge of a transponder is also transmitted through the adjacent transponder at a reduced level. This impairment source will introduce phase nonlinearities in the wanted signal path and can be treated as group-delay noise. The amount of noise encountered is primarily a function of the filter response of the adjacent transponder, the gain difference between the two transponders, and the mode of operation of the two transponders (spot or global beam). The dual-path transmission effect was one of the major inputs to the INTELSAT IV filter specification and it is one of the factors which must be considered in the development of frequency plans.

Impulse noise is formed in the demodulator when the instantaneous noise or interference power level equals or exceeds the carrier power level. This impairment may be caused by the threshold effect at low carrier-to-noise ratios (not expected to be encountered on INTELSAT IV operation), bandlimiting within a carrier selection filter, or adjacent carrier interference. Thus, the major factors controlling impulse noise are carrier arrangements, relative power levels resulting from different carrier sizes and geographical advantages, frequency deviations, and filter performance. These factors and their variations must be considered in the development of frequency plans. The transmit and receive IF filter specifications for INTELSAT IV carriers were primarily based on impulse noise considerations.

RF out-of-band intermodulation in the satellite and earth station occurs when a number of carriers are transmitted through the same nonlinear amplifier. The RF out-of-band emission from the earth station is caused by the transmission of two or more carriers through the same HPA.

A noise allowance of 500 pWp for RF out-of-band emission restricts the earth station HPA drive to a level which will produce a power flux density of 26 dBW/4 kHz at a 10° elevation angle. At higher angles, the flux density should be reduced by the empirical factor of 0.06 ( $\alpha - 10$ ). RF out-of-band emission in the satellite is a function of the frequency plan, the TWT operating point, the gain-frequency response of the satellite output multiplexer, and finally the relationship between the wanted and interfering spectra, which determines the amount of noise in a baseband channel.

In developing the satellite filter specifications it was found that for typical frequency plans the RF out-of-band intermodulation noise could be neglected. Except in cases in which two large carriers are transmitted through a transponder, the interference noise into the adjacent transponder must be carefully evaluated.

Before the INTELSAT IV carriers were introduced into the operational system, a laboratory transmission simulation was performed through INTELSAT IV transponders. The purpose of this system simulation program was to ensure that all transmission impairments had been properly considered in the design of the system and that the overall systems performance would be as expected. Mathematical models were developed for individual transmission effects and then verified by measurements. The results of the simulation program indicated that all transmission impairments were within the expected limits.

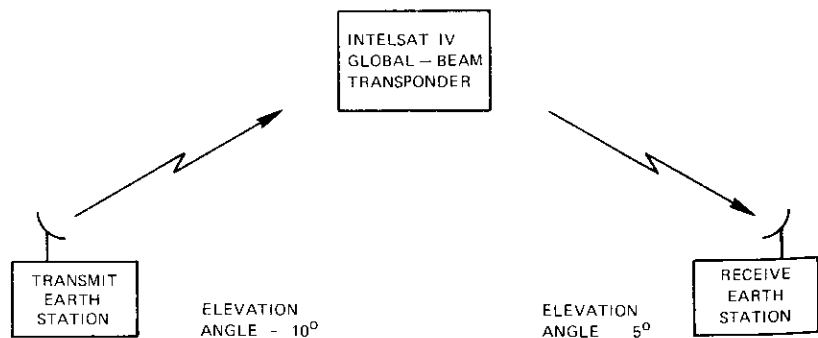


Figure 14. INTELSAT IV Television Reference Link

**Television Performance.** The transmission parameters and performance objectives for the INTELSAT IV television channel are described in Ref. 2. It is convenient to apply these parameters and objectives to a hypothetical earth station-to-earth station link, which will be called the INTELSAT IV television reference link. Such a link, which is shown in Figure 14, is consistent with the transmit earth station elevation angle of 10° and the reference receive station elevation angle of 5° for television.

The television signal-to-noise ratio can be written as

$$\frac{S}{N} = \frac{3}{2} d^2 \frac{C}{T} \frac{1}{f_{v_n}} \frac{1}{k} \quad (4)$$

where  $S$  = sinusoidal signal average power

$N$  = noise power in the video noise bandwidth.

$d = f_a/f_v$  = peak FM deviation index

$C$  = received carrier power, in  $W$ , over the video noise bandwidth

$T$  = system noise temperature, in °K

$k = 1.38 \times 10^{-23}$ , in  $J/^\circ K$

$f_v$  = highest modulating frequency, in Hz

$f_a$  = peak frequency deviation, in Hz

$f_{v_n}$  = video noise bandwidth, in Hz.

The C.C.I.R. recommends that the signal-to-noise ratio for TV signals be expressed in terms of the ratio:

$$\frac{\text{peak-to-peak luminance signal}}{\text{weighted rms noise}} \quad (5)$$

Since for a sine-wave the (power) ratio of the peak-to-peak and rms values is eight, and since the peak-to-peak value of the luminance component is 0.707 of the peak-to-peak value of the composite video signal, the above-mentioned (power) ratio must be halved.

Substitution into equation (4) yields

$$\frac{\text{peak-to-peak luminance signal}}{\text{average noise power}} = \frac{S_{p-p}}{N} = 6d^2 \frac{C}{T} \frac{1}{f_{v_n}} \frac{1}{k} \quad (6)$$

If pre-emphasis of the video signal is not employed, the noise can be assumed to be triangular in shape and a weighting improvement,  $w$ ,\* can be included in equation (6). Thus,

$$\frac{\text{peak-to-peak luminance signal power}}{\text{weighted average noise power}} = \frac{S_{p-p}}{N_w} = 6d^2 \frac{C}{T} \frac{1}{f_{v_n}} \frac{1}{k} w \quad (7)$$

If pre-emphasis of the video signal is employed, the complementary de-emphasis network,  $d$ , will modify the noise spectrum and  $q(w,d)$  will be the weighting improvement after de-emphasis. Therefore,

$$\frac{\text{peak-to-peak luminance signal power}}{\text{weighted average noise power}} = \frac{S_{p-p}}{N_q} = 6d^2 \frac{C}{T} \frac{1}{f_{v_n}} \frac{1}{k} q \quad (8)$$

When equation (8) is expressed in dB,

$$\left[ \frac{S_{p-p}}{N_q} \right]_{dB} = 236.4 + 20 \log d + \left[ \frac{C}{T} \right]_T - 10 \log f_{v_n} + Q \quad (9)$$

In equation (9), it was assumed that the bandwidth allocation of a TV carrier would have the value listed in Table 8. The signal-to-noise ratios,  $S_{p-p}/N_q$ , for the various systems are plotted in Figure 15 as a function of  $(C/T)_T$ .

TABLE 8. BANDWIDTH AND FREQUENCY ALLOCATIONS FOR ONE VIDEO CARRIER AND TWO AUDIO CARRIERS

Carrier	Bandwidth (MHz)	Frequency Allocation for Transponder No. 12 (MHz)
Video Carrier	30	$f_c = 4178 \pm 15$
Audio Carrier No. 1	2.5	$f_c = 4158.25 \pm 1.25$
Audio Carrier No. 2	2.5	$f_c = 4160.75 \pm 1.25$

\* Weighting networks as per C.C.I.R. rec. 421-1 and 451 [3], [4]

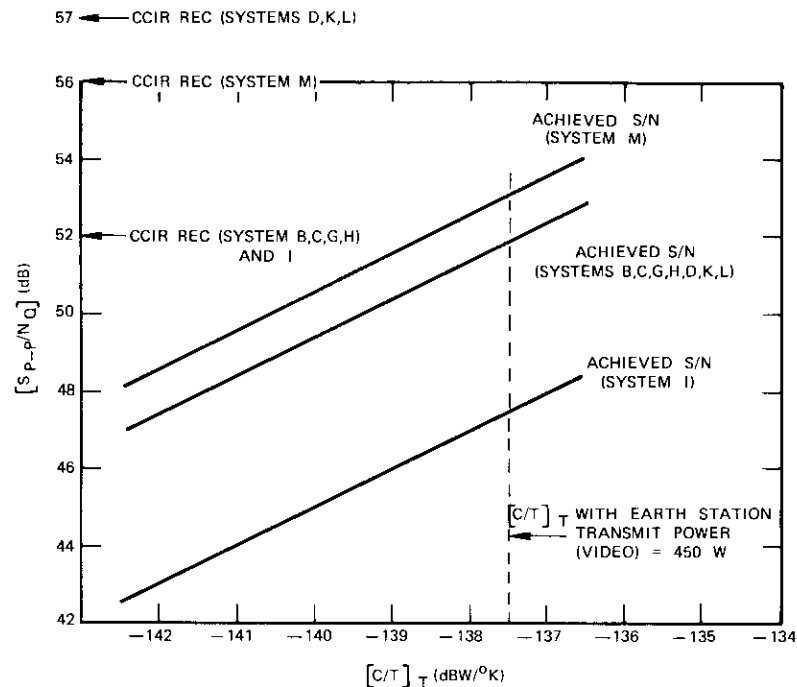


Figure 15. Video Channel S/N as a Function of  $[C/T]_T$

### System evaluation and analysis

To utilize the satellite system efficiently several factors must be considered. In frequency planning, transponder and carrier configurations must be optimized to minimize transmission impairments while maximizing capacity.

Computer techniques have been developed to determine the optimum performance for a given FM multicarrier configuration. To verify overall system performance and transmission impairment models, in-orbit multicarrier field tests have been conducted. These tests show good agreement between system models and laboratory simulation. In addition, a continuing evaluation program has been implemented for assessing and predicting system performance under actual operating conditions. This program uses a computer model to predict out-of-band noise performance for single- or multiple-carrier FM configurations, based on reported earth station or satellite radiated power. At the earth station, out-of-band performance is

monitored and recorded for later statistical analysis to determine trends and to more closely verify and optimize the operating system and noise budget predictions.

**Frequency Plan Evaluation.** The complexity of traffic requirements in the INTELSAT system make frequency planning an extremely difficult task. The ultimate aim in frequency planning is to provide for the most efficient use of the space and earth segments, while minimizing cost, inconvenience, and service discontinuities. Many operational factors and constraints must be considered in developing such a frequency plan.

In general, a number of tentative frequency plans are developed and evaluated for their technical feasibility until a plan is ultimately approved and can be put into operation. A detailed discussion of this topic will be included in a later section of this paper.

After a frequency plan is developed from traffic requirements, it is important to evaluate this plan in terms of total power requirements and achievable system noise performance and to arrive at the optimum transmission parameters required for implementation. To facilitate this step, a computer program has been developed to efficiently evaluate and optimize these parameters.

Figure 16 shows the major input and output parameters of the program. Given a frequency plan with a number of FM carriers, the program calcu-

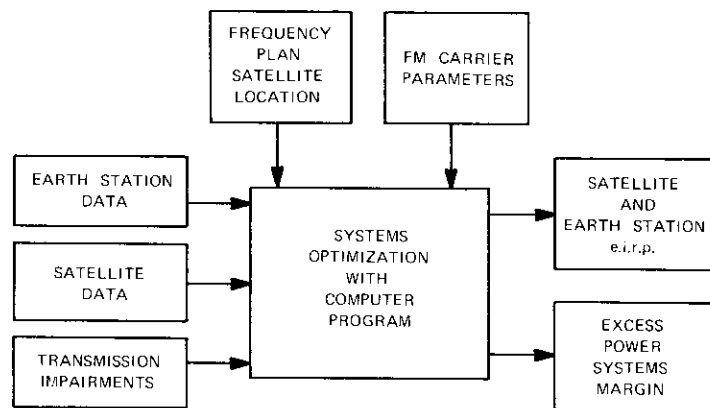


Figure 16. *Input and Output Parameters of the Program Used to Evaluate and Optimize Transmission Parameters*

lates intermodulation noise caused by amplitude and phase nonlinearities of the satellite TWT, optimizes the TWT operating point, and selects the appropriate gain setting. For each carrier the satellite and earth station e.i.r.p. levels are calculated and adjusted for intermodulation and up- and down-link noise so that specified channel noise performance will be achieved for all carriers in the transponder. The resulting satellite power budget will determine the excess power in the transponder, as well as the system margin. Figure 17 shows a typical INTELSAT IV frequency plan, which has been evaluated by using the computer program.

Figure 18 shows the input parameters to the computer program. These parameters can be divided into three categories:

- satellite parameters, including satellite position, spot-beam pointing directions, and antenna patterns;
- transponder characteristics which specify its communications performance, and
- the frequency plan, which specifies the carrier parameters, the carrier frequencies, and the transmit and receiving stations.

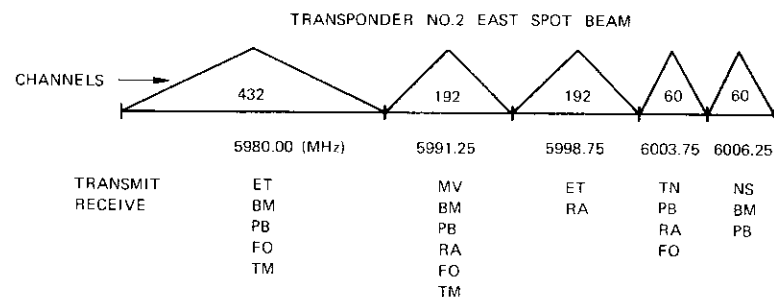


Figure 17. *Typical Frequency Plan for INTELSAT IV*

Figure 19 shows the program output parameters. The optimum traveling wave tube amplifier (TWT) operating point, total carrier-to-noise density ratio  $(C/N_o)_T$ , and achievable systems margin are computed for all gain settings. Satellite and earth station e.i.r.p. and the actual noise breakdown for each carrier are computed for the selected gain settings only.

Figure 20 is a computer plot of  $(C/N_o)_T$  as a function of the TWT operating point with the gain setting as a varying parameter. It should be noted that the optimum operating point is a function of the gain setting used in the satellite. In the example shown in the figure, positive systems margins are achieved for gain settings 6, 7, and 8.

SATELLITE PARAMETERS

..... INTELSAT IV F-2 1972 ATLANTIC FREQUENCY PLAN .....

POSITION OF SATELLITE (EAST LONG.) 335.50

DIRECTION OF SPOT-BEAM POINTING

WEST BEAM	5.15	WEST	4.95	NORTH
EAST BEAM	3.15	EAST	6.75	NORTH

SPOT-BEAM AVERAGE ANTENNA PATTERN

GLOBAL-BEAM AVERAGE ANTENNA PATTERN

TRANSPONDER CHARACTERISTICS

TRANSPONDER NO. 2 EAST S BEAM CENTER FREQUENCY 3765.0

SATURATION e.i.r.p. (dBW) 37.9

G/T OF SATELLITE (dB/K) -13.2

(C/N<sub>0</sub>)<sub>1</sub> AT 0 dB BOI (dB-Hz) 89.0

FLUX DENSITY -57.6 -61.0 -64.5 -67.9 -71.5 -75.0 -78.4 -81.8

SELECTED GAIN SETTINGS 1 2 3 4 5 6 7 8

FREQUENCY PLAN

CARRIER SIZE	BANDWIDTH AVAILABLE	BANDWIDTH USED	G/T REQUIRED	DEVIATION FR	TOP BASEBAND FREQUENCY
432	15.0	13.0	-135.9	1479.0	1796.0
FREQUENCY	TRANSMIT STATION	RECEIVING STATIONS			
5980.00	ET	BM,PB,FO,TM			
CARRIER SIZE	BANDWIDTH AVAILABLE	BANDWIDTH USED	G/T REQUIRED	DEVIATION FR	TOP BASEBAND FREQUENCY
192	7.5	6.4	-140.3	757.9	804.0
FREQUENCY	TRANSMIT STATION	RECEIVING STATIONS			
5991.25	MV	BM,PB,RA,FO,TM			
5998.75	ET	RA			
CARRIER SIZE	BANDWIDTH AVAILABLE	BANDWIDTH USED	G/T REQUIRED	DEVIATION FR	TOP BASEBAND FREQUENCY
60	2.5	2.25	-143.7	275.5	252.0
FREQUENCY	TRANSMIT STATION	RECEIVING STATIONS			
6003.75	TN	PB,RA,FO			
6006.25	NS	BM,PB			

Figure 18. Program Input Parameters

**System Performance Evaluation.** To utilize the INTELSAT IV most efficiently, it is necessary to evaluate the system under actual operating conditions and to compare the realized communications performance with the developed engineering design models. Various performance data are gathered from many sources over the useful lifetime of the satellite. Evaluation of these data is a massive task in the global network; therefore, it is performed by using various computer-aided techniques.

A satellite system performance evaluation program has been developed to calculate the noise performance of an FM multicarrier system. Unique features of the program allow predictions to be based on actual or design earth station G/T as a function of elevation angle, actual or design earth station equipment, out-of-band emission, and interference noise budgets. Hence, top channel and upper out-of-band channel performance can be calculated for both design models and actual systems.

Figure 21 shows the required input data, functions of the program, and the output of the program. Given a frequency plan and either earth station and/or satellite e.i.r.p., the program calculates the expected signal-to-noise and out-of-band noise for each carrier's receive location. The satellite TWTA operating point is determined by a reiteration process using a typical input-output multicarrier transfer curve in conjunction with the intermodulation analyzer program. Figure 22 is a sample output for a transponder and one of its carriers.

System noise performance is monitored by measuring the out-of-band slots of receive carriers at the earth stations. Short- and long-term programs for out-of-band statistical evaluation have led to the development of a computer program to evaluate and display out-of-band data on a monthly basis. During a measurement program, out-of-band data are recorded every two hours. This time interval provides a good approximation to evaluate long-term statistics and trends and to assist in determining system variations such as propagation anomalies or spacecraft antenna pointing variations.

The programs described in the previous paragraphs have been useful in comparing performance with system design and are being used to improve the performance of the operating system.

GAIN SETTING	OPTIMUM INPUT BACKOFF (dBW/m <sup>2</sup> )	OPTIMUM OUTPUT BACKOFF (dB)	SAT. E.I.P.D. AVAIL. (dBW)	(C/N <sub>0</sub> ) <sub>U</sub> (dB-Hz)	(C/N <sub>0</sub> ) <sub>D</sub> (dB-Hz)	(C/N <sub>0</sub> ) <sub>1</sub> (dB-Hz)	(C/N <sub>0</sub> ) <sub>T</sub> (dB-Hz)	(C/N <sub>0</sub> ) <sub>T</sub> (dB-Hz)	SYSTEMS MARGIN (dB)	TOTAL EARTH ST. E.I.P.D. (dBW)	W/CH	
	57.60	14.30	7.45	30.45	106.50	103.11	104.57	99.74	95.83	3.909	33.76	2.551
	-61.00	13.60	6.89	31.01	103.80	103.67	103.35	98.83	95.83	2.968	31.08	1.370
	-64.50	12.70	6.20	31.70	101.20	104.37	101.86	97.50	95.83	1.670	28.48	0.753
	-67.90	11.70	5.43	32.47	98.80	105.14	100.23	95.90	95.83	0.061	26.08	0.433
	-71.50	10.20	4.37	33.53	96.70	106.20	97.99	94.02	95.83	-1.819	23.98	0.267
	-75.00	8.10	3.15	34.75	95.30	107.41	95.43	92.22	95.83	-3.615	22.58	0.194
	-78.40	4.90	1.92	35.98	95.10	108.64	92.88	90.77	95.83	-5.067	22.38	0.185
	-81.80	2.50	1.65	36.25	94.10	109.91	91.52	89.56	95.83	-6.277	21.38	0.147

TRANSMISSION PARAMETERS FOR CARRIERS IN TRANSPONDER 2

TRANSMIT FREQUENCY (MHz)	RECEIVE FREQUENCY (MHz)	BANDWIDTH UNIT (MHz)	NUMBER OF CHANNELS	REQUIRED (C/T) <sub>T</sub> (dBW/K)	TRANSMIT STATION	ELEVATION ANGLE (DEG)	UP LINK VARIATION (dB)	WORST LOCATED RECEIVE STATION	ELEVATION ANGLE (DEG)	DOWN-LINK VARIATION (dB)	
5980.00	3755.00	15.00	432	-135.90	ET	17.91	4.06	TM	16.55	1.73	
5991.25	3766.25	7.50	192	-140.30	MV	25.37	3.60	TM	16.55	1.73	
5998.75	3773.75	7.50	192	-140.30	ET	17.91	4.06	RA	25.15	0.97	
6003.75	3778.75	2.50	60	-143.70	TM	56.31	1.28	FO	28.13	1.65	
6006.25	3781.25	2.50	60	-143.70	NS	43.40	2.25	FB	30.47	1.23	
WEIGHTED AVERAGE UP-LINK VARIATION							3.88	WEIGHTED AVERAGE DOWN-LINK VARIATION			1.96

SATELLITE POWER BUDGET USING GAIN SETTING 6, SAT. FLUX DENSITY OF -64.50 dBW/Hz

TRANSMIT FREQUENCY (MHz)	INTERMOD. INC.(CS)	ACTUAL UP (dBW/K)	ACTUAL DOWN (dBW/K)	(C/T) INT. (dBW/K)	TOTAL (dBW/K)	SATELLITE TRANSMIT FOR AVG INT. (dBW)	E.I.P.D. (BEAM CENTER) ADJUSTED FOR INTERMOD. (dBW)	REQUIRED EARTH STATION TRANSMIT E.I.P.D. (dBW)
5980.00	-61.3	-132.7	-129.1	-130.0	-135.6	26.9	26.9	498.3
5991.25	-59.3	-136.2	-132.6	-135.6	-139.8	22.5	22.1	163.7
5998.75	-62.2	-137.5	-133.2	-134.0	-140.1	22.0	22.1	80.1
6003.75	-64.9	-141.5	-137.8	-135.2	-143.7	15.1	15.1	75.3
6006.25	-64.0	-141.4	-137.3	-136.1	-143.7	15.0	15.2	72.5
Avg. Int. (C/N <sub>0</sub> ) <sub>T</sub>	-61.3	TOTAL SATELLITE POWER USED			30.0	30.0	1018.2	73.5
	101.7	ACTUAL OUTPUT BACKOFF (dB)			7.9			0.37
		ACTUAL INPUT BACKOFF (dB)			15.0			

Figure 19. Program Output Parameters

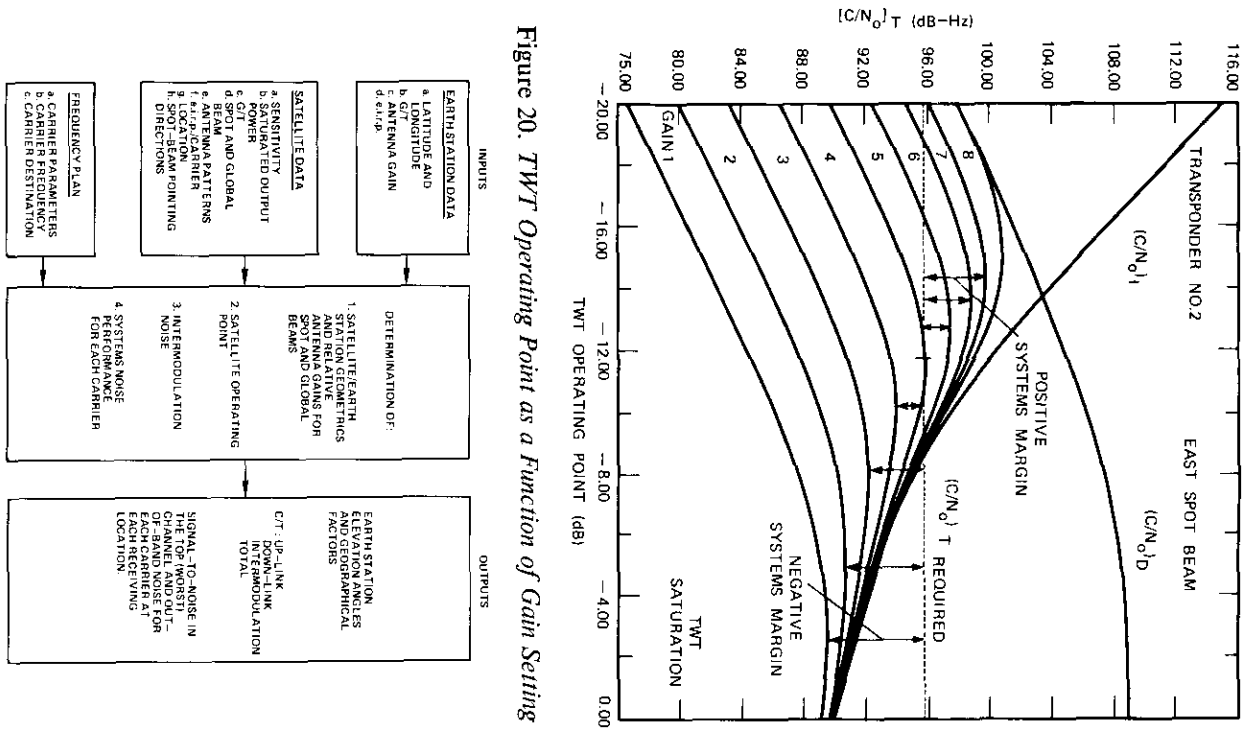
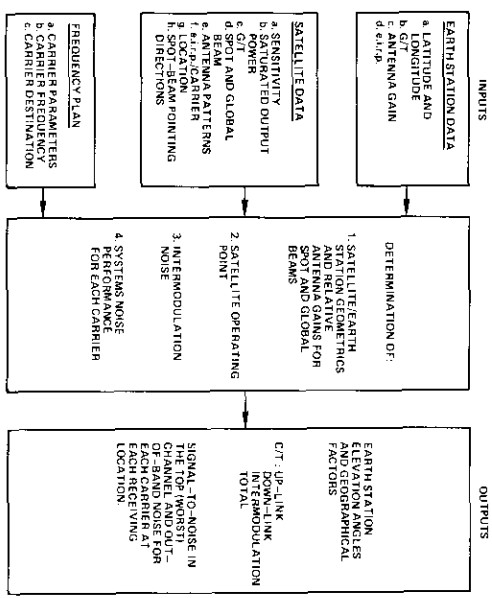


Figure 20. TWT Operating Point as a Function of Gain Setting

Figure 21. Input and Output Parameters Used to Determine System Noise Performance



TRANSPONDER NO. 2		EAST SPOT		CENTER FREQUENCY 3765 MHz													
SATURATION e.i.r.p. (dBW)		37.90		G/T OF SATELLITE (dB/K) 13.60													
INPUT BACKOFF (dB)	14.08	OUTPUT BACKOFF (dB)	5.77	SAT. POWER AVAILABLE (dBW)	37.90	AVERAGE INTERMOD LEVEL	0.0	ADDED NOISE (dBW)	2500	SATURATION FLUX (dBW/m <sup>2</sup> )	-82.10	UNIT GAIN (dB/m <sup>2</sup> )	37.01				
CARRIER NO.	1	CARRIER SIZE	797	FREQUENCY UP (MHz)	4056.25	FREQUENCY DOWN (MHz)	4056.25	BANDWIDTH AVAILABLE (MHz)	20.00	TOP-BB FREQUENCY (kHz)	3284.00	FREQUENCY DEVIATION (MHz)	1.78				
TRANSMIT STATION	TU	ELEVATION ANGLE (DEG.)	6.52	UP-LINK ANT. FACTOR	-4.56	UP-LINK LOSS	200.86	ASPECT ANGLE	8.65	EARTH STATION UP-LINK e.i.r.p. (dBW)	84.08	SATELLITE e.i.r.p. (dBW)	32.13				
RECEIVE STATIONS	RA-1	ELEVATION ANGLE	25.15	DOWN-LINK ANT. FACTOR	-0.97	DOWN-LINK LOSS	196.45	IG/TIE (dB/K)	40.79	ACTUAL C/T (dBW/K)	-123.73	SYSTEMS/N (dBmop)	52.38				
***** ACTUAL G/T VALUES WERE USED AS A FUNCTION OF ELEVATION ANGLE *****																	
												NOISE (pWp)	5781	S/N WITH ADDED NOISE	50.82	ORR (dBmcp)	50.42

Figure 22. Sample of Transponder Output Data

## Earth stations

C. A. BLACKWELL

When INTELSAT I was launched and placed in service in 1965, there were only six earth stations. Two were located in North America (Andover, Maine, and Mill Village, Nova Scotia) and four were in Europe (Goonhilly Downs, U.K.; Raisting, Germany; Pleumeur Bodou, France; and Fucino, Italy). Most of these stations were not originally designed as part of the INTELSAT system. For example, the Andover station, built before the decision to utilize synchronous satellites, was designed and used for the TELSTAR experiment (see Figure 23). The ability to track, control, and communicate with a satellite in a low orbit was a fundamental requirement. In addition to the severe tracking problem, the maser front end amplifier, used to obtain the lowest possible noise temperature and hence the maximum earth station antenna gain-to-noise temperature ratio, G/T, made it necessary to sacrifice economy and serviceability [5].

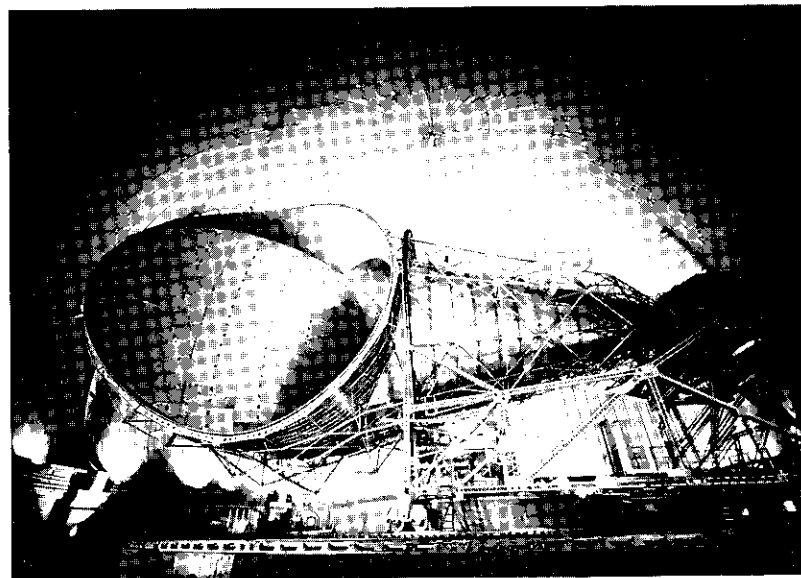


Figure 23. Andover Earth Station Horn Antenna

C. A. Blackwell is Manager, Systems Engineering, Systems Division, COMSAT Laboratories.

Several significant changes have been made since the design of the early earth stations. For example, the original antennas were approximately 26 m (85.3 ft) in diameter, whereas today, the majority of the new antennas have diameters around 28–30 m (91.8–98.4 ft), as shown in Figure 24. In addition, the attempt to achieve the absolute minimum noise temperature has been greatly de-emphasized. The increase in gain resulting from the larger aperture has made it possible to substitute wideband (500-MHz) parametric amplifiers for very-low-noise narrowband (25-MHz) maser amplifiers.

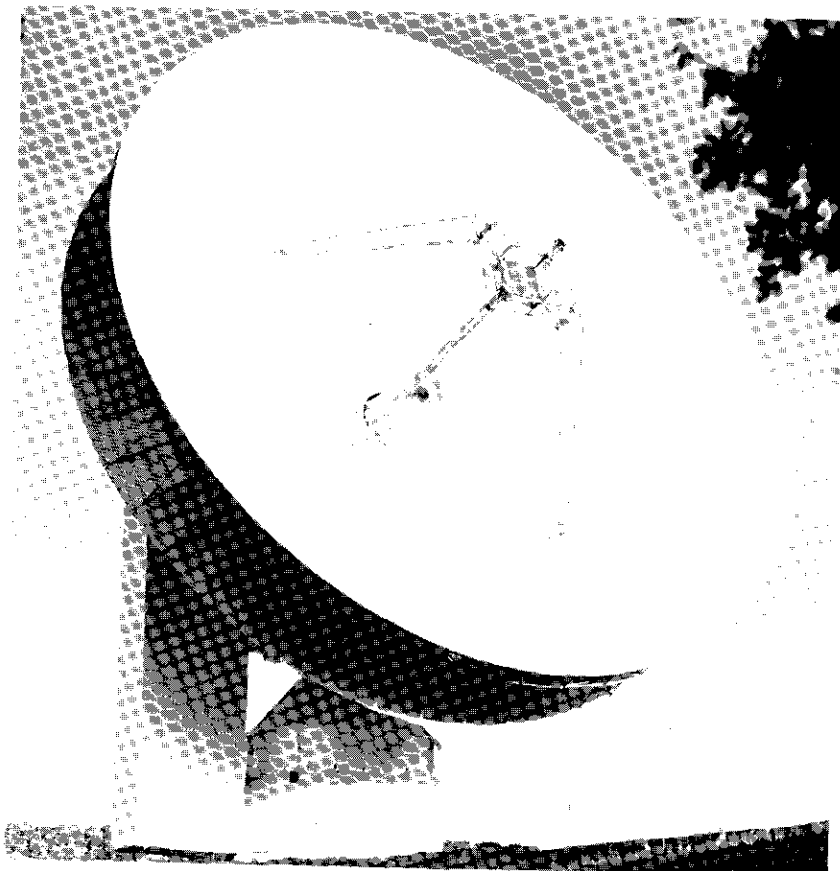


Figure 24. Typical 29.5-m (nominally 97-ft) Antenna

The antenna is not the only element in which significant changes have been made. However, since the antenna and the associated HPAs and low-noise receivers are unique to a satellite system, changes in these areas are more significant. In the remaining portion of the earth station, changes are not significantly different from those associated with 4-/6-GHz ground-based microwave facilities [6].

The number of earth stations in the INTELSAT system has increased to more than 70 in 1972 and should approach 80 by 1974. These are currently providing approximately 6,500 telephone channels (4 kHz), as well as global television coverage. Communications are currently being handled through four basic modes of transmission:

- a. FDM/FM with top baseband frequencies from 108 to 8,120 kHz;
- b. FM for video basebands, including both 625-line/50-frame/s and 525-line/60-frame/s transmission;
- c. PCM/PSK channels available on either a preassignment or a demand-assignment basis (using the SPADE system);
- d. digital/PSK channels for transmission of data, e.g., 50-kbps data.

Earth stations in the system utilize one or a combination of these modes depending on the particular traffic requirements and bilateral agreements between cooperating administrations. In the future, new types of modulation and multiple-access techniques, such as TDMA and digital television (DITEC), may be employed.

#### **Mandatory performance characteristics**

Table 9 is a partial list of the more important mandatory performance characteristics. Earth station e.i.r.p. varies from approximately 75 dBW for small capacity carriers to as much as 95 dBW for some of the larger capacity carriers. The required power stability has been significantly improved. For example, for a typical antenna having a gain of 62 dB and a feed loss of 2 dB, 33 dBW of power is required to achieve an e.i.r.p. of 95 dBW. Thus, HPA capabilities around 2,000 watts are common. Since several carriers must often be handled and since backoff from saturation is frequently in the neighborhood of 7 to 9 dB, the total power capacity of the transmitters is significant.

The noise budget allocates 1500 pWp of noise to the earth station equipment, including the equipment required to provide equalization for satellite group delay. To meet this noise budget, earth station designers allocate various amounts of noise to the subsystems which make up the

TABLE 9. MANDATORY PERFORMANCE CHARACTERISTICS OF EARTH STATIONS IN THE INTELSAT IV SYSTEM

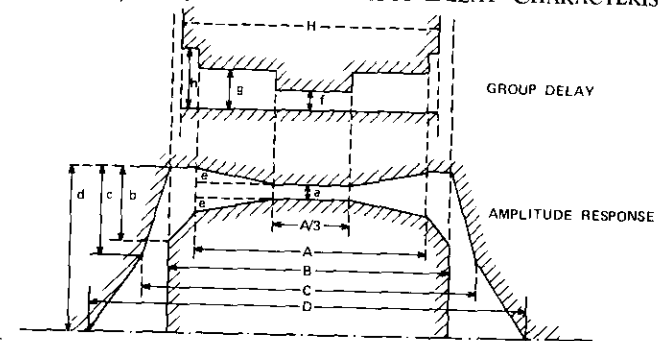
Gain-to-Noise Temperature Ratio at 4 GHz	$\geq 40.7 \text{ dB/}^\circ\text{K}$
at Other Frequencies within the 3.705- to 4.195-GHz Band	$\geq 40.7 \text{ dB/}^\circ\text{K} + 20 \log_{10} f/4$ (f is the receive frequency in GHz)
Antenna Receive Gain at 4 GHz	$\geq 57 \text{ dB}$
at Other Frequencies within the 3.705- to 4.195-GHz Band	$\geq 57 \text{ dB} + 20 \log_{10} f/4$ (f is the receive frequency in GHz)
Transmit Antenna Sidelobes ( $\geq 1^\circ$ away from the main lobe center)	$\geq 29 \text{ dB}$ below the main lobe maximum
Feed Polarization	circular with a voltage axial ratio not exceeding 1.4:1
Antenna Steerability	compatible with satellites having $\leq 5^\circ$ orbit inclination, $\pm 10^\circ$ longitudinal drift
System Bandwidth Receiving	3.7-4.2 GHz
Transmitting	5.925-6.425 GHz
Required e.i.r.p. Stability	$\pm 0.5 \text{ dB}$
RF Out-of-Band Emission in Any 4-kHz Band	
Spurious	$< 4 \text{ dBW}$
Intermodulation	$< 26 \text{ dBW}$
Carrier Frequency Stability	
FM Carriers Above 5 MHz	$\pm 150 \text{ kHz}$
FM Carriers at or Below 5 MHz	$\pm 80 \text{ kHz}$
SPADE and PCM/PSK Single-Channel-per-Carrier Preassigned Carriers	$\pm 200 \text{ Hz}$
Sense of Video Modulation	positive
RF Energy Dispersal on FM Telephony Carriers	low-frequency triangular dispersal waveform calculated so that the maximum e.i.r.p. per 4 kHz of the fully loaded carrier is $\leq 2 \text{ dB}$
Pre-emphasis for Telephony, Television, and Program Sound Channels	in accordance with C.C.I.R. and C.C.I.T.T. recommendations
Residual Amplitude Modulation, rms Value within Any 4 kHz	$\leq -20 (1 + \log_{10} f) \text{ dB}$ referred to the RF carrier level (f is the carrier frequency, in GHz, of the 4-kHz slot)
> 500 kHz	-74 dB

transmitting and receiving portions of the overall link. The typical noise budget given in Figure 25 is intended for design purposes only.

Important elements of the performance specifications are the group delay and the selectivity characteristics of the overall earth station equipment. As shown in Table 10, the upper portion of the mask specifies the group-delay requirements over the entire frequency band of each carrier, whereas the lower portion of the mask indicates the gain-frequency response.

Special filters are designed in accordance with the specifications of Table 10. Significant development was required to adequately equalize filters so that they could meet the required noise objectives for the INTELSAT IV system. Improved utilization of the frequency spectrum was made possible by reducing interference among the carriers sharing a common satellite transponder. Filters generally operate at an intermediate frequency of 70 MHz within both the receive and transmit portions of the earth station.

TABLE 10. GAIN/FREQUENCY AND GROUP-DELAY CHARACTERISTICS



- NOTES:  
 (1) FIGURES ARE SYMMETRICAL RELATIVE TO CENTER FREQUENCY  
 (2) FIGURES ARE NOT DRAWN TO SCALE  
 (3) AMPLITUDE SCALE IS LINEAR IN dB  
 (4) FREQUENCY SCALE IS LINEAR IN MHz

CARRIER SIZE (MHz)	A (MHz)	B (MHz)	C (MHz)	D (MHz)	H (MHz)	a (MHz)	b (dB)	c (dB)	d (dB)	e (dB)	f (ns)	g (ns)	h (ns)
2.5	1.8	2.25	2.75	8.0	2.1	0.7	1.5	2.5	25	0	16	16	20
5.0	3.6	4.5	5.25	13.0	4.1	0.5	2.0	3.0	25	0	12	12	20
7.5	5.4	6.75	7.75	17.0	6.2	0.4	2.5	4.0	25	0	12	12	20
10.0	7.2	9.0	10.25	19.0	8.3	0.3	2.5	5.0	25	0.1	9	9	18
15.0	10.8	13.5	15.5	25.0	12.4	0.3	2.5	5.5	25	0.1	6	6	15
20.0	14.4	18.0	20.5	28.0	16.6	0.3	2.5	7.5	25	0.1	4	4	15
25.0	18.0	22.5	25.75	34.0	20.7	0.3	2.5	8.0	25	0.2	3	3	15
36.0	28.8	36.0	42.25	60.0	33.1	0.6	2.5	10.0	25	0.3	3	3	15
VIDEO	24.0	30.0	--	--	30.0	0.5	2.5	--	--	0.3	5	5	15

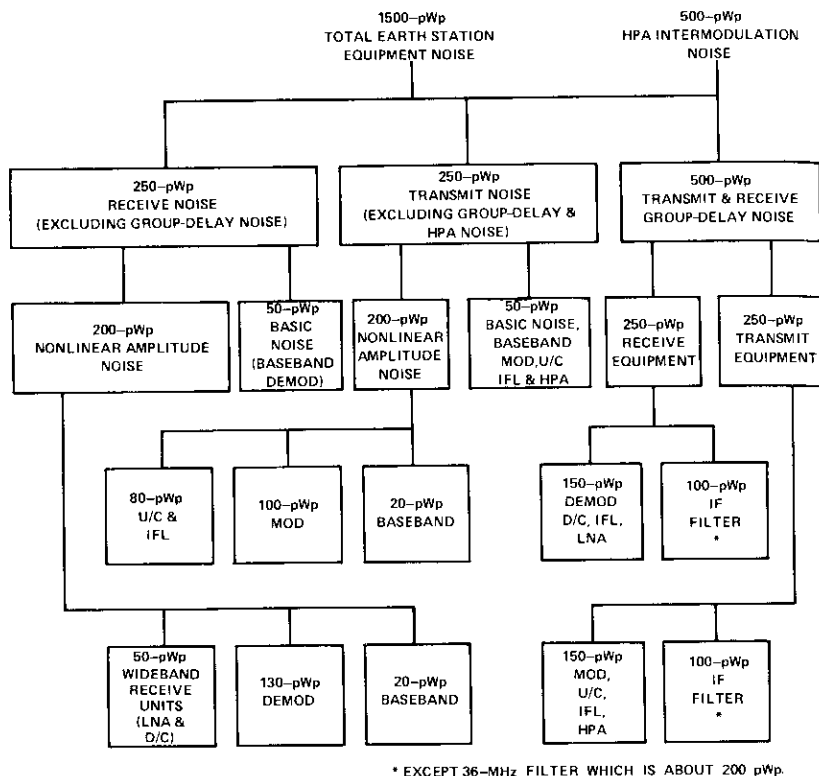


Figure 25. Typical Earth Station Noise Budget

#### Gain-to-noise temperature ratio and antenna receive gain

To ensure the maximum flexibility in the global network and the best utilization of the space segment, it has been attempted to achieve a receive system  $G/T$  of 40.7 dB at a  $5^\circ$  elevation angle under clear sky conditions, and an antenna gain,  $G$ , greater than 57 dB measured at 4 GHz at the input to the low-noise amplifier. This original design requirement was obtained by constructing a 26-m (85.3-ft) antenna with 50-percent efficiency, yielding a corresponding gain of approximately 57.7 dB. This gain and a system noise temperature of  $50^\circ\text{K}$  resulted in a  $G/T$  of 40.7 dB. In some recent designs, however, 29.5-m (96.7-ft) reflectors with 70-percent efficiency and system noise temperatures of about  $78^\circ$  at a  $5^\circ$  elevation angle have been used.

The importance of the earth station  $G/T$  is illustrated by the well-known relationship

$$C/T = \text{satellite e.i.r.p.} - \text{path loss} + G/T$$

where  $C/T$  is the down-link receive carrier-to-noise ratio. Clearly, for given values of satellite e.i.r.p. and path loss,  $C/T$  is directly dependent upon the earth station  $G/T$ .

It is preferable to obtain the actual value of the  $G/T$  from radio star measurements (either Y-factor or radiometric) [7]. When possible, these measurements are made at the elevation angle and direction to be employed during actual operation. Cassiopeia A, Taurus A, and Cygnus A have been used as radio stars, although Cassiopeia A is the preferred source for the northern hemisphere. For antennas which cannot be adequately measured by using a radio star, gain can be measured by using a satellite carrier whose e.i.r.p. is carefully calibrated by a separate monitoring station. Temperature measurements are then taken to obtain the actual earth station  $G/T$ .

#### Polarization and axial ratio requirements

Linear polarization was originally employed on the INTELSAT I and II satellites. However, for INTELSAT III and IV, various reasons dictated the use of left-hand circular polarization for transmission from the earth station and right-hand circular polarization for reception by the earth station.

The use of circular polarization makes it unnecessary to rotate the position of the feed to coincide with the polarization orientation of the satellite. In addition, since diurnal variations associated with Faraday rotation and simulation periods involve angular changes of the vertical and horizontal polarizations, it is generally impossible to align both the transmit and receive polarizations.

The axial ratio for transmissions from the earth stations in the direction of the satellite must not exceed a value of 1.4:1 (3 dB). Since the polarization axial ratio of the INTELSAT IV spacecraft antenna does not exceed 3 dB, the total system polarization loss will not exceed 0.5 dB.

#### Low-noise amplifiers

Since the INTELSAT IV satellite utilizes both global- and spot-beam antennas, investigations were carried out to determine the earth station low-

noise amplifier modifications needed to ensure satisfactory intermodulation performance.

For an earth station with a net receive antenna gain of 58 dB, the following typical receive power levels have been calculated in the 500-MHz bandwidth:

- a. -69 dBm for earth stations within the zone of the spot-beam antenna, and
- b. -76 dBm for earth stations outside the zone of the spot-beam antenna.

These values will increase if the receive antenna gain is increased, or if the mode of operation of the satellite is changed (particularly if more transponders are operated in a single-carrier mode). Furthermore, INTELSAT may decide to change the pointing directions of the spot-beam antennas because of changing traffic requirements. Hence, earth stations must be designed to permit certain maximum receive carrier power levels.

Within these power levels, the intermodulation noise produced in typical parametric amplifiers can be kept at a negligible value in all cases. However, subsequent stages of amplification can contribute to intermodulation noise. For earth stations within the spot-beam coverage, a typical tunnel diode amplifier (TDA) produces about 200 pWp of intermodulation noise; hence, TDAs should be avoided in these earth stations. A low-level (10-mW) receiving TWT produces about 100 pWp of noise, while an intermediate-level (0.8-W) receiving TWT yields measurable intermodulation noise. As a result, the design emphasizes the selection of a relatively high output power (0.1 to 1 W), a low noise figure (8 to 10 dB), and a relatively low gain (30 dB) for the stages following the parametric amplifier.

#### **e.i.r.p. stability**

To maintain uniform performance, earth stations must ensure that the e.i.r.p. of carriers in the direction of the satellite is within  $\pm 0.5$  dB of the nominal value. This tolerance is intended to include all factors causing variation, e.g., transmitter RF power level instability, antenna transmitting gain instability, and antenna beam pointing error.

Antenna gain instability may be a long-term effect or a short-term effect. Long-term instability results from creep deformation of the structure, distortions caused by thermal effects, snow loading, and other similar effects. Short-term instability results from wind gust structure deformation and from pointing errors and corrections, which are also caused by wind. Antenna pointing errors, except those caused by wind gusts, can result from

autotracking limitations and, in program or manual steering systems, from small operation errors.

To meet the e.i.r.p. stability requirements, the contribution of each of these sources of instability can be budgeted as follows:

transmitter RF power level instability:	0.2 dB
antenna gain instability:	0.15 dB
antenna pointing error:	0.15 dB
Total	0.5 dB

#### **RF out-of-band emission**

For multicarrier transmissions through a single wideband high-power amplifier, intermodulation products may occur within the satellite frequency bandwidth, resulting in interference to other carriers. This type of interference is commonly referred to as RF out-of-band interference, since there is usually no interference to the responsible carrier(s).

For purposes of system design, 500 pWp of noise have been allocated to out-of-band interference. Hence, wideband power amplifiers, e.g. TWTs, must be operated well below saturation. Studies carried out in the early planning stages of the INTELSAT IV system resulted in the recommendation that earth station TWTs should be operated with a minimum output power backoff of 7 dB. However, this objective can also be met by utilizing separate HPAs for each of the various carriers transmitted. Some earth stations within the INTELSAT system have utilized this approach by employing klystrons in lieu of wideband TWTs.

When only one or two carriers are radiated, klystrons offer an attractive solution, since two units can be operated in the single-carrier mode at or near saturation. Even if a 3-dB loss is added to the outputs of the two klystron units, the total prime-power requirement is considerably less than that of a single TWT.

#### **Energy dispersal for telephony carriers**

In the INTELSAT IV system, earth stations are required to provide energy dispersal for both telephony and television carriers by inserting a low-frequency symmetrical triangular waveform in the baseband signal prior to the FM modulator. This procedure ensures that the C.C.I.R. limit of  $-152 + \theta/15$  (the working elevation angle) in dBW is met in any 4-kHz frequency band. However, the major benefit to the INTELSAT system is

that the intermodulation noise is reduced over the 500-MHz frequency spectrum. The frequency of this dispersal waveform is in the range of 20 to 150 Hz. The inclusion of this low-frequency waveform also helps to spread the RF energy. The magnitude of the spreading waveform is determined so that the maximum e.i.r.p. per 4 kHz will not exceed the corresponding full load value by more than 2 dB. This procedure prevents a concentration of carrier energy near the center frequency during periods of light loading. Hence, it significantly reduces the amount of intermodulation which would otherwise be present in the system.

#### **Transmission modes**

The satellite system is designed to accommodate all classes of telecommunication services, ranging from public message services (telephony and multichannel telegraphy on voice bearers) through voice band and wide-band data transmission, facsimile, TV video, and sound programs.

For FDM/FM telephony carriers, the baseband constituents (groups and supergroups) are arranged in accordance with the INTELSAT recommendations and the bilateral or multilateral agreements between the earth station administrations. The multiplex equipment may be located at the earth stations or at the outgoing international exchange. The earth stations and the international centers are in most cases interconnected via microwave radio links.

In some cases, a satellite radio link is composed of two satellite hops via one or more intermediate stations by a patch connection at or below baseband (channel level). This link could be effected at one station if the transmit and receive intermediate stations were collocated, or it could be provided via one or more international maintenance centers.

For PCM/PSK demand-assignment operation (SPADE) [8] and pre-assignment PCM/PSK operation, each carrier will carry only one telephony channel. As a result, blocks of frequency-division multiplexed voice channels received at the earth station from the international maintenance center must be divided into single channels. Each of these channels is then PCM encoded, PSK modulated, and transmitted through the satellite to its destination. At the destination earth station, the received channels may be multiplexed into groups or any other required form and sent to the international maintenance center.

For television transmissions, many earth stations provide multiple-standard interface equipment to accommodate both 525- and 625-line color and monochrome requirements. This interface equipment may some-

times include video standards converters to convert the received signals from the satellite to the national standard. It is expected that the use of video standards converters on international satellite transmissions will rapidly increase. Accordingly, international agreements have recommended that the use of standards conversion should be restricted to the receive side of the satellite system. Hence, double conversion, which could be required for multiple-destination transmissions, causing unnecessary signal degradation, could be eliminated.

A high-quality sound program channel is provided in conjunction with a television transmission. Often it is necessary to supplement this channel with additional channels for multilingual multiple-destination transmissions. These channels are usually frequency-division multiplexed to form one or more telephony groups so that they can be packaged within the regular telephony baseband which is exchanged with the national terrestrial system.

#### **Data transmission**

Although the demand for international transmission of medium- and high-speed data has been rapidly increasing, the INTELSAT system continues to provide excellent performance. At present, data signals are received from the terrestrial systems in the form of analog signals occupying standard bandwidths of the FDM hierarchy, e.g., 4-kHz voice channels and 48-kHz group bands. Recent measurements have demonstrated virtually error-free transmission: bit-error rates of better than  $1 \times 10^{-7}$  are typically achieved on earth station-to-earth-station transmission of 4,800-bps voice band data and 50-kbps group band data. The phase jitter which often degrades data transmission on terrestrial systems is virtually nonexistent on satellite transmissions because of the excellent spectral purity of the earth station carrier supplies, the small number of frequency translations, and the low level of additive thermal noise.

The digital satellite transmission systems of the near future will provide a more efficient method of data transmission. For example, a group band (50-kbps) data channel could be demodulated at the transmit earth station and transmitted over a single PCM/PSK channel, thus displacing only one voice channel rather than 12. Alternatively, the demodulated data signal could be time-division multiplexed with other data signals and with PCM telephony signals to form high-speed digital basebands for TDMA carriers.

Error control systems used on satellite data circuits should allow a high throughput for the inherent delay of satellite links.

### Earth station performance

Satellite system performance, as measured by continuity of service figures from earth station to earth station, has shown continuous improvement over the years. For the first five months of 1972, the earth station-to-earth station continuity of service was at a level of 99.86 percent. For all earth stations, the continuity of service averaged 99.94 percent; for a number of individual stations, it exceeded 99.99 percent. These outages correspond to less than one hour per year. Earth station outages, which are attributable to equipment failure, human error, and necessary downtime for preventive maintenance, accounted for the bulk of the total system circuit-hours of outage during this period.

The remaining circuit-hours of outage are attributable to atmospheric effects and system reconfiguration. Satellite outages may also contribute to total system circuit-hours of outage; however, no outages of this type have been experienced by an INTELSAT IV during 1972. Although detrimental effects of atmospheric phenomena on system continuity of service were thought to be a potential source of service interruption in the early days of the INTELSAT system, they have proven to be relatively insignificant. Rain attenuation has been negligible, but outages have been caused by other severe weather phenomena. On a few occasions, antennas have been stowed and secured against high winds during the typhoon season [9].

Interference between the sun and received down-link signals from the satellite has also resulted in service interruptions. This interference occurs during the spring and autumn equinoxes, when the sun crosses the equator and is sufficiently aligned with the satellite, as viewed from the earth station, to enter the earth station receive antenna pattern and increase the antenna noise temperature beyond operating levels. The duration of sun interference outages is usually between two and six minutes a day over a 2- to 4-day period. Future system operation techniques such as the utilization of satellite diversity may reduce these types of outages significantly.

As indicated previously, earth stations are responsible for the major portion of the outages. The broadband elements in the earth terminal are generally redundant and provide protection against outages. A notable exception, however, is the antenna; a second major contributor is primary power. In most cases, primary power is derived from commercial sources with standby diesel generators for use in the event of a commercial power failure. Use of various uninterruptible power supplies helps to minimize the effects of power failures, but outages occur as a result of malfunctions of switching logic and component failure.

Another major contributor to earth station outages is the high-power-amplifier (HPA) subsystem. A large number of HPA interruptions stem from the complex protective arrangements provided to protect relatively expensive tubes in a high-voltage, high-power application. Many HPA interruptions are a result of switching redundant equipment in response to protective circuit alarms. These outages are of very short duration (usually a second or less). Component failures are fewer than are indicated by the number of interruptions, and tube lifetimes of three years of continuous operation are now achievable. It is interesting to note that the relatively complex, cryogenically cooled, low-noise receivers are responsible for a small percentage of the equipment-related circuit-hours of outage.

### Transmission modeling

A. L. BERMAN, C. MAHLE, AND M. R. WACHS

#### Typical signal path

Figure 26 will be used to model the INTELSAT IV communications system. Initially, one carrier will be traced from the modulator, through the spacecraft transponder, to the demodulator to define the distortion effects encountered in this case. Subsequently, the additional distortion effects caused by multicarrier operation will be presented, and finally, the detailed modeling of each of these effects will be described.

#### Single-carrier operation

At baseband, a stack of FDM telephone channels is represented by the equivalent white noise load from  $f_a$  to  $f_b$  (see Figure 27). After pre-emphasis, this composite signal band frequency modulates an IF carrier. The process is essentially distortion-free up to this point. A transmit filter following the modulator limits the out-of-band spectrum of the modulated carrier. Out-of-band attenuation, which is dictated by adjacent channel

---

*A. L. Berman is Manager, Transponders Department, Technology Division, COMSAT Laboratories.*

*C. Mahle is Manager, Transponders Design, Technology Division, COMSAT Laboratories.*

*M. R. Wachs is a Technical Staff Member, COMSAT Laboratories.*

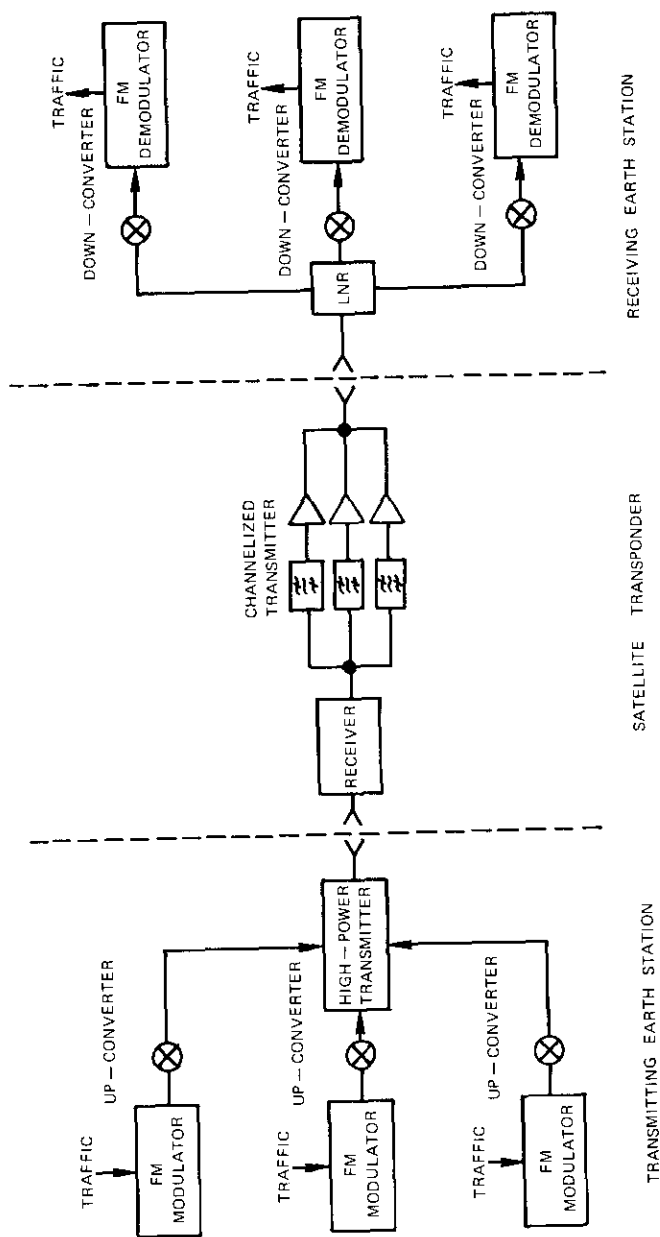


Figure 26. Block Diagram of INTELSAT IV Communications System

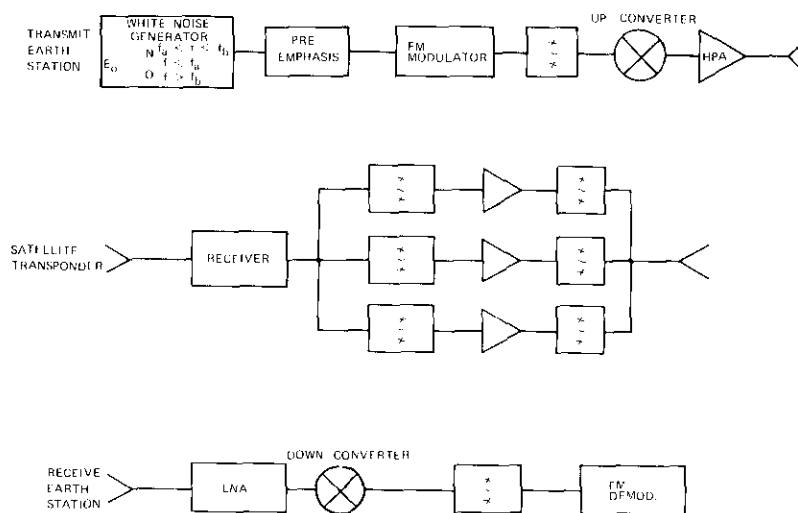


Figure 27. Single-Carrier Path

considerations, will be described further in the discussion of dual-carrier operation.

The ideal in-band characteristics of the filter are flat amplitude and group delay over the largest bandwidth which will satisfy the attenuation requirements in the adjacent band. With a realizable filter, several distortion components of the signal will exist at the output of an "ideal" frequency demodulator:

- a. intermodulation noise at baseband caused by finite residual group-delay variation across the Carson's Rule bandwidth [10], [11],\*
- b. truncation noise at baseband caused by the abrupt rise of either group delay or attenuation at the filter band edge [12],
- c. an increase in the onset of the impulse threshold caused by momentary suppressions of the modulated carrier when detection is performed in the presence of noise, and
- d. amplitude modulation (AM) components in the carrier envelope that are coherent with the original baseband modulation because of their finite amplitude slope. These typically low-level AM compo-

\* To compute the intermodulation distortions across the baseband, it is sufficient to resolve the group-delay variation into linear, parabolic, and ripple components and to utilize the formulas given in References 10 and 11.

nents are of interest primarily because they produce crosstalk onto other carriers in subsequent common path amplifiers exhibiting AM/PM conversion effects. (These effects will be described in the discussion of dual-carrier operation.)

The signal path through the up-converter, high-power transmitter, and satellite receiver can be made essentially distortion free for single-carrier operation. [The illumination level and satellite G/T determine the up-link carrier-to-noise temperature ratio (C/T), and requirements for multiple-carrier operation determine the other major performance characteristics.] At the input to the channelized satellite transmitter, two signal paths are possible:

- a. a path through the intended input channel filter, TWT, output combining filter, and antenna to the receiving earth station at approximately zero relative attenuation, or
- b. a path through the adjacent channel filters, TWT, and antenna to the receiving earth station at a relative attenuation determined by the skirt selectivity of the adjacent channel filters across the desired channel bandwidth.

The sum of the microwave carrier vectors (i.e., the vector of the intended path plus the vector of the adjacent channel path at a reduced level and different phase) results in the well-known multipath ripple, with overall effect of amplitude and group-delay distortion. The dual-path effect is most severe at the band edge and drops to negligible levels toward mid-band as the attenuation of the adjacent channel increases. This effect cannot be equalized because of the rapid variations of the undesired channel path length with illumination in that channel, filter tuning variations with temperature, and pointing variations of the spacecraft.

At the input to the earth station receiver, the distortion levels previously described for the single carrier are increased as a result of dual-path and unequalized residual group-delay contributions of the channelizing filters. At this point, the down-link C/T is determined by the received illumination and the earth station G/T. Again, the signal path through the earth station receiver and down-converter may be made essentially distortion free for a single carrier. The function of the receive filter (in conjunction with the transmit filter of the adjacent channel) is primarily that of reducing adjacent channel interference. In the absence of adjacent channel considerations, the receive filter will define a bandwidth just wide enough to be essentially transparent to the modulated carrier while minimizing the total

noise presented to the demodulator. This will provide a composite (carrier plus noise) signal that can be used to derive the automatic gain control at the detector input.\*

The distortion components at the output of the receive filter are identical to those described previously for the transmit filter.

The state of the art in demodulator design [13] permits an essentially linear detection of all signals with intermodulation contributions of less than 100 pWp.

### Multicarrier operation

In addition to the baseband distortion components of each single carrier (primarily in-band linear, parabolic, and ripple group-delay coefficients), three other components have a significant effect on multicarrier operation of the INTELSAT IV satellite: adjacent channel interference, RF intermodulation distortion (caused by nonlinear  $P_{out}$  vs  $P_{in}$  and  $\Delta\phi_{out}$  vs  $P_{in}$  characteristics), and coherent crosstalk.

**Adjacent Channel Interference.** To achieve the maximum channel capacity in a bandwidth-limited mode such as that encountered by the INTELSAT IV satellite, the number of channels within each bandwidth unit is maximized, and the guardband between adjacent channels is reduced until the resulting distortions rise to a level of several hundred picowatts. † In the case of FDM/FM telephony transmissions, two interference effects occur as the guardband is reduced:

- a. Spectrum overlap giving rise to "convolution" noise in the baseband (measured in pWp). For purposes of computation, this noise component, calculated from the convolution of two spectra, may be assumed to have a Gaussian amplitude distribution in the baseband.
- b. Impulse noise caused when the resultant RF vector at the demodulator input undergoes an abrupt rotation of  $2\pi$  radians as the

\* In the case of phase-lock demodulators, a constant level into the phase detector is required to achieve a constant loop gain. For conventional detection above threshold with a limiter discriminator, the filter bandwidth will determine the C/N ratio.

† This would provide a reasonable margin (3-6 dB) against accidental overdeviation.

adjacent carrier momentarily deviates into the desired channel bandwidth. This effect produces impulses at baseband, similar to those observed at the onset of the FM threshold, which can be measured as average noise in a 4-kHz voice channel and on a counter to determine the number of impulses above the  $-22\text{-dBm0}$  reference level in one minute.

For FDM/FM telephony, the multiplexed baseband has a Gaussian amplitude statistic (i.e., links are tested with bandlimited white noise); therefore, large deviations for small periods of time are inherent. In this case, receive filters alone are insufficient to control the interference effects described in the preceding paragraph. As noted previously, a combination of a transmit filter on the interfering channel (to limit its instantaneous frequency excursions and spectrum) and a receive filter on the "desired" channel (to limit the spectrum presented to the demodulator) are required.

For INTELSAT IV, representative adjacent channel cases were selected. (A 10-MHz carrier positioned next to a 2.5-MHz carrier was assumed to be a practical worst case before frequency plan readjustment.) Each of the transmit/receive filter pairs was then narrowed until the effects of in-band distortion were balanced against adjacent channel interference. In this tradeoff, the ultimate limit of in-band noise caused by the truncation effect was used [14] with the understanding that the group-delay response of the filters would be equalized [15] so that truncation noise would be the dominant contributor.

**RF Intermodulation Caused by Multicarrier Operation.** Analysis and experimental confirmation of RF intermodulation levels produced by amplitude and phase nonlinearities typical of traveling wave tubes have been previously published [16-19]. A brief summary of the base model used for computation, the series representations of the nonlinearities, and the logic algorithm used to sort the products will be given in a subsequent subsection.

**Crosstalk Caused by FM/AM/PM Conversion.** The modeling technique presented here was originally developed to determine the extent to which the transponder channelizing filters could be permitted to have rounded corners caused by finite Qs and still meet the multicarrier crosstalk specifications. To evaluate this effect for more than two carriers, a statistical approach was used to compute the AM component, and the 2-carrier AM/PM conversion coefficient was replaced by a direct computation of the crosstalk term of interest from the series representation of  $\Delta\phi_{out}$  vs  $P_{in}$ .

### Description of the individual distortion effects

For convenience, the distortion components in this subsection will be grouped into several relatively independent effects:

- a. multipath considerations (satellite transmitter channelizing filter selection),
- b. TWT nonlinearities resulting in RF intermodulation products,
- c. crosstalk considerations, and
- d. adjacent channel interference (balancing of in-band and adjacent channel effects).

**Multipath.** The dual path under consideration is shown in Figure 28. The basic procedure for evaluating the distortion consists of computing the desired (intended path) vector and adding it to the unwanted (adjacent channel) vector. The resultant vector across the band of interest gives the channel amplitude response. Differentiating\* the phase response with respect to frequency makes it possible to obtain the group delay. In this case, with the unwanted path length independent of the desired path length, the computation has been performed for initial mid-band phase differences of  $0^\circ$  to  $360^\circ$  in increments of  $30^\circ$ .

To optimize the INTELSAT IV satellite, the following constraints were assumed at the beginning of the study:

- a. no more than 21 microwave cavities per channel should be used for the input filter, output filter, and input filter equalizer because of weight budget limitations;
- b. the center-to-center spacing between channels should be 40 MHz, with full communications performance over the center 36 MHz for an arbitrary mixture of RF carriers; and
- c. the loss in the output combining network (multiplexer) should be no more than 0.5 dB.

An examination of microwave filters potentially capable of meeting the gain slope requirements (typically 0.01-dB Tchebycheff filters) leads to the following initial configurations:

\* High-resolution differentiation may be performed efficiently on a digital computer by computing a set of phase values typically every 100 kHz, determining a corresponding second set of phase values displaced by 1 kHz from the first set, and then forming  $\bar{\tau}(\omega) = \Delta\phi/\Delta\omega$ .

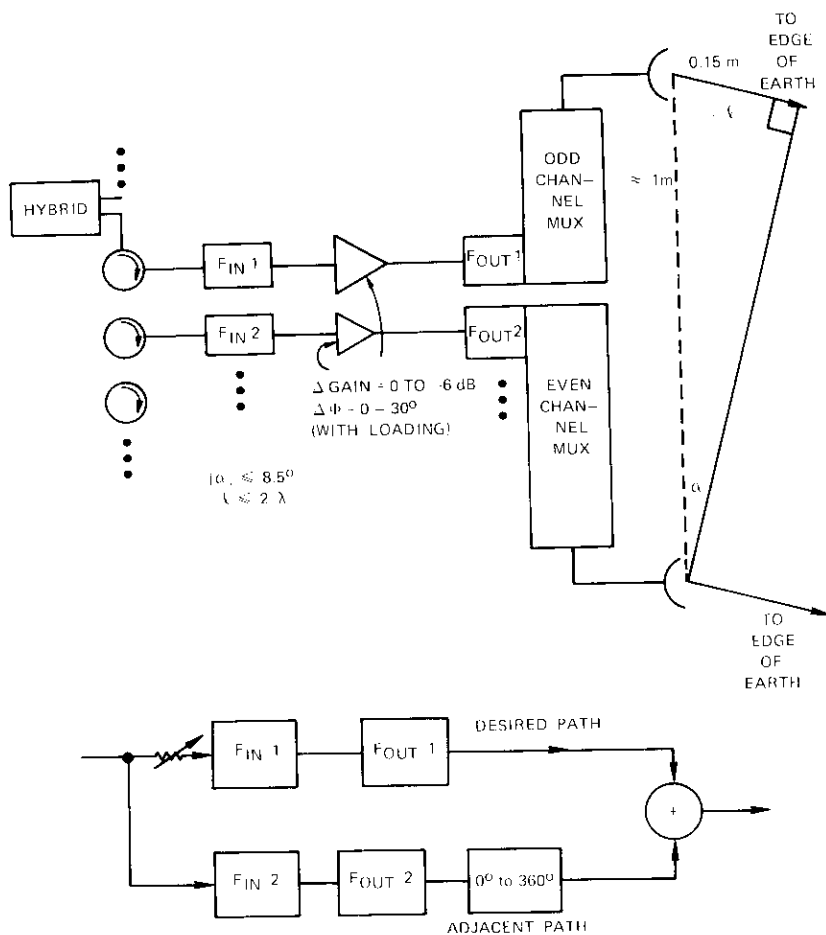


Figure 28. Multipath Diagram

a. For realizable unloaded  $Q_s$  of 7,000 to 10,000, the loss in the output section can be met with six sections or less. Two output multiplexers and antennas (one set for even channels and one for odd channels) are required to successfully combine the required output with the selectivity available from 6-pole filters. Initial computations of required intermodulation product suppression in the adjacent channel indicated that the output filter should have six sections.

b. Again, based on unloaded  $Q_s$  of 7,000 to 10,000, the rate of attenuation at the band edge of the adjacent channel reaches the point of diminishing returns for filters with 9 to 11 sections.

c. Since elliptic function filters were not realizable at microwave frequencies in the early stages of the project, only Tchebycheff filters were considered.

d. A minimum of five equalizer poles is required to achieve equalization over most of the 36-MHz band.

On the basis of these assumptions, a set of multipath calculations was performed for the two most probable filter configurations:

- a. a 10-pole input filter, a 5-pole equalizer, and a 6-pole output filter; and
- b. a 9-pole input filter, a 6-pole equalizer, and a 6-pole output filter.

For both input filter configurations, the equiripple bandwidths were set at 35, 36, 37, 38, and 40 MHz. In addition, for each of these cases, the output filter bandwidth was initially 2 MHz wider than that of the input filter\* (to limit the number of cases studied), and the equalizer poles were set to give the best equalization over the center 36 MHz.

The results for the nominal case of a 38-MHz input filter and a 40-MHz output filter are presented in Figures 29-32. The other cases, which are summarized in Tables 11 and 12, show that, for each of the filter sets, the use of a 40-MHz equiripple bandwidth yields a very low inherent group delay (caused only by the filters) across the center 36 MHz. However, the multipath contribution (indicated by the spreading of the curves as the initial phase of the adjacent channel is varied) severely limits the channel

\* As previously mentioned, because of initial loss and design complexity considerations, there is one output multiplexer for the even channels, and another one for the odd channels. Hence, the diplexer at the output is no longer required to provide total reflection at the edge of the adjacent channel. Instead, it must provide "total reflection" of other signals at least one channel bandwidth (40 MHz) from band edge.

The major factor in determining the output filter bandwidth was the tradeoff between the rapid rise of group delay over the last 10 percent of its equiripple bandwidth (leading to widening of the filter to facilitate equalization) and the requirement for attenuating those intermodulation products falling into the adjacent channel. For the input filter selected, further computations showed a broad maximum of system performance, varying slowly with the choice of output filter equiripple bandwidth.

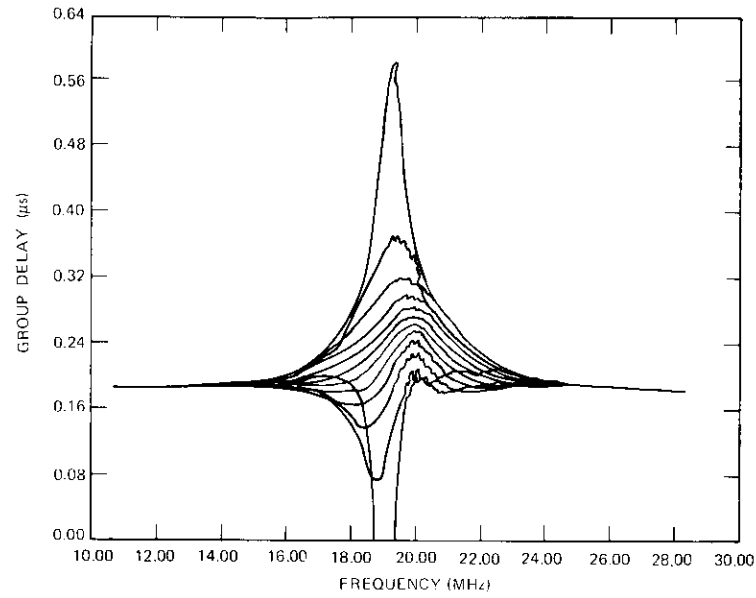


Figure 29. Sample Output, Group Delay (9-section input filter)

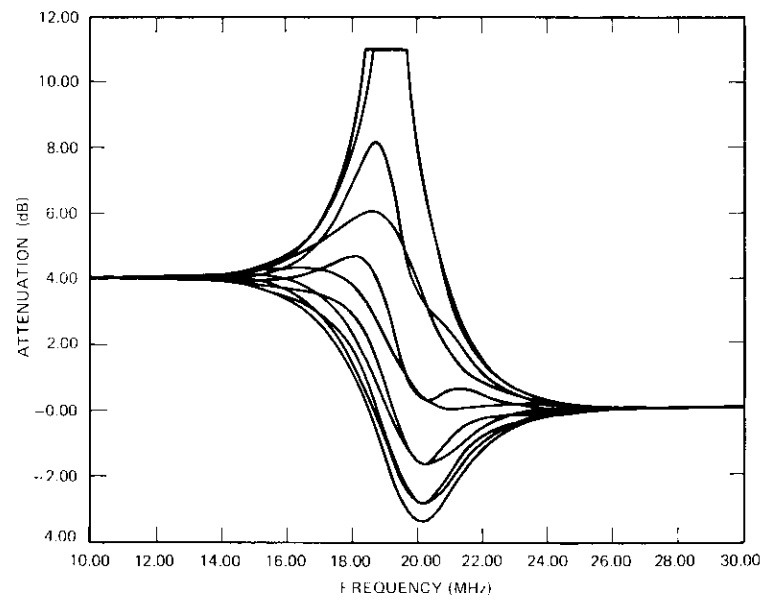


Figure 30. Sample Output, Attenuation (9-section input filter)

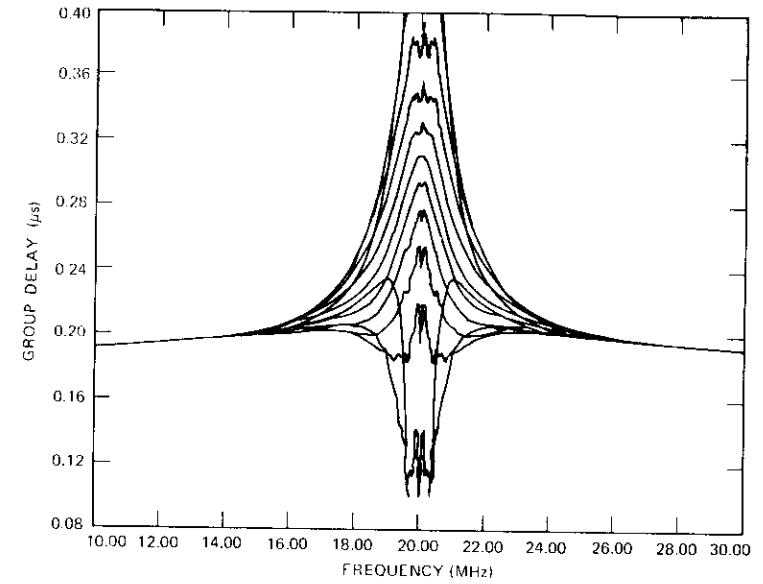


Figure 31. Sample Output, Group Delay (10-section input filter)

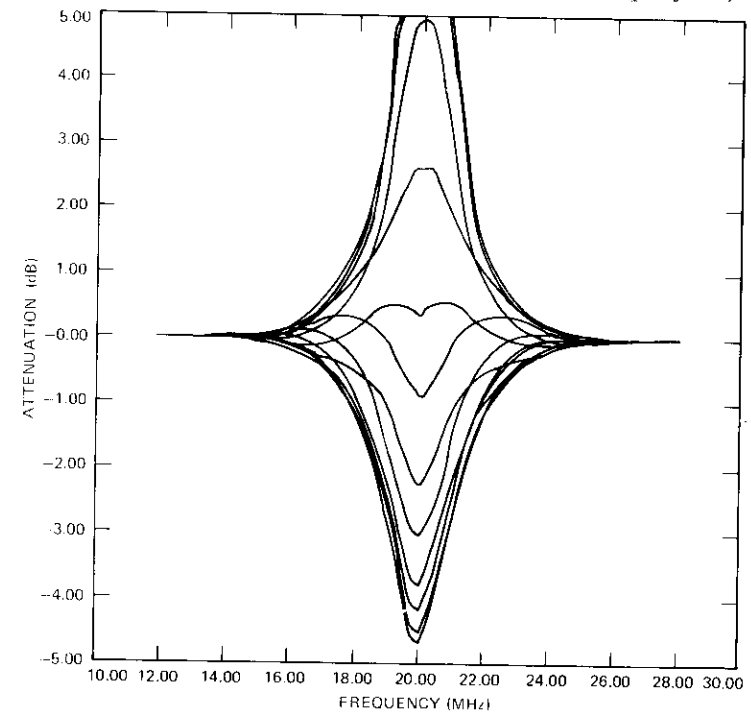


Figure 32. Sample Output, Attenuation (10-section input filter)

TABLE 11. MULTIPATH RESULTS FOR A 9-SECTION TCHEBYCHEFF INPUT FILTER AND A 6-SECTION TCHEBYCHEFF OUTPUT FILTER (6-SECTION NETWORK DELAY EQUALIZER)

Filter Bandwidths (MHz)	Percent of 36-MHz Bandwidth	Additional Group Delay (ns)		Gain Slope (dB/MHz)	
		Maximum	Minimum	Maximum	Minimum
Input = 38.9, Output = 41	70	0.6	-0.6	0.0354	-0.0302
	80	2.68	-2.69	0.14	-0.154
	90	11.1	-11.7	0.59	-0.697
	100	22.4	-55.6	1.9	-4.17
Input = 37, Output = 39	70	0.209	-0.209	$0.932 \times 10^{-2}$	-0.0135
	80	0.947	-0.947	0.0518	-0.0517
	90	4.56	-4.6	0.236	-0.267
	100	18.1	-21.5	1.03	-1.33
Input = 35, Output = 36.9	70	0.0667	-0.0667	$-0.161 \times 10^{-2}$	$-0.89 \times 10^{-2}$
	80	0.292	-0.292	0.0198	-0.0121
	90	1.48	-1.48	0.074	-0.883
	100	8.48	-8.66	-0.314	-1.25
Input = 33.1, Output = 34.8	70	0.0215	-0.0215	$-0.114 \times 10^{-2}$	$-0.349 \times 10^{-2}$
	80	0.09	-0.09	$-0.176 \times 10^{-2}$	$-0.116 \times 10^{-1}$
	90	0.443	-0.443	0.046	$-0.242 \times 10^{-2}$
	100	5.82	-5.84	-5.25	-5.89

TABLE 12. MULTIPATH RESULTS FOR A 10-SECTION TCHEBYCHEFF INPUT FILTER AND A 6-SECTION TCHEBYCHEFF OUTPUT FILTER (5-SECTION NETWORK DELAY EQUALIZER)

Filter Bandwidths (MHz)	Percent of 36-MHz Bandwidth	Additional Group Delay (ns)		Gain Slope (dB/MHz)	
		Maximum	Minimum	Maximum	Minimum
Input = 38.9, Output = 41	70	0.266	-0.266	0.025	$-0.416 \times 10^{-2}$
	80	1.33	-1.33	0.0658	-0.0794
	90	6.57	-6.68	0.351	-0.379
	100	26.4	-39.2	1.63	-2.66
Input = 37, Output = 39	70	0.0863	-0.0863	0.0127	$-0.33 \times 10^{-2}$
	80	0.0432	-0.0432	0.014	-0.0333
	90	2.36	-2.36	0.13	-0.128
	100	12.4	-13	0.685	-0.74
Input = 35, Output = 36.9	70	0.0256	-0.0256	$-0.224 \times 10^{-3}$	$-0.302 \times 10^{-2}$
	80	0.123	-0.123	$0.663 \times 10^{-2}$	$-0.684 \times 10^{-2}$
	90	0.696	-0.696	0.025	-0.0511
	100	4.91	-4.94	-1.06	-1.6
Input = 33.1, Output = 34.8	70	$0.769 \times 10^{-2}$	$-0.769 \times 10^{-2}$	-0.0104	-0.0113
	80	0.0351	-0.0351	$0.643 \times 10^{-2}$	$0.26 \times 10^{-2}$
	90	0.191	-0.191	0.0428	0.022
	100	4.15	-4.15	-8.13	-8.58

capacity. As the equiripple bandwidth is narrowed, the multipath effect is reduced, and it becomes more difficult to equalize across the center 36 MHz. For both filter sets, the optimum bandwidth choice (where inherent group-delay and multipath effects are approximately equal and their sum is a minimum) is a bandwidth between 37.5 and 38.5 MHz, and the 10-cavity filter yields slightly better results.

### Amplitude and phase nonlinearities

For the purpose of discussion, the traveling wave tubes (earth station HPA, satellite receiver driver, and satellite transmitter) will be assumed to dominate the nonlinear amplitude and phase behavior of the INTELSAT IV system.\*

In general, a traveling wave tube may be represented by cascaded filters and two nonlinear effects, as shown in Figure 33.† Since the nonlinear

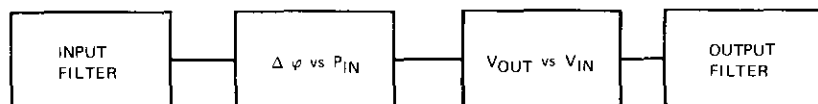


Figure 33. Simplified Model of Helix TWT

element (the beam interacting with the helix) has a bandwidth which is much larger than the possible rates of change of the envelope, the nonlinearities are assumed to be memoryless and are represented by a series expansion. To choose a series expansion, several factors were considered. First, the series approximation of measured single-carrier behavior should provide high accuracy over the range of output drive from zero to the drive required for saturation, reasonable accuracy for inputs up to twice the drive required for saturation, and bounded values (for which the magnitude of the computed value should not exceed the saturated value) for inputs from twice to at least four times the drive required for saturation.

\* Detailed measurements of individual circuits have shown that C/I contributions of the 6- and 4-GHz TDAs in the satellite receiver may not be neglected. However, the bandwidth of the nonlinear element (the diode) is large enough so that the instantaneous (memoryless) modeling developed for the TWTs may also be used to predict their low-level nonlinear performance.

† The present state of the art in traveling wave tubes makes it possible to omit the filters in the case of the satellite tubes, and to reduce them to input and output linear slopes for a majority of the HPAs.

Second, the series selected should be suited to efficient solution by computer and should typically yield closed-form algorithm solutions.

**Amplitude Nonlinearity.** As shown in Figure 34 and Reference 16, the amplitude nonlinearity is characterized by

$$e_{out} = c_1 \sin(ae_{in}) + c_2 \sin(2ae_{in}) + c_3 \sin(3ae_{in}) + c_5 \sin(5ae_{in})$$

where the coefficients are determined graphically from the measured single-carrier data.

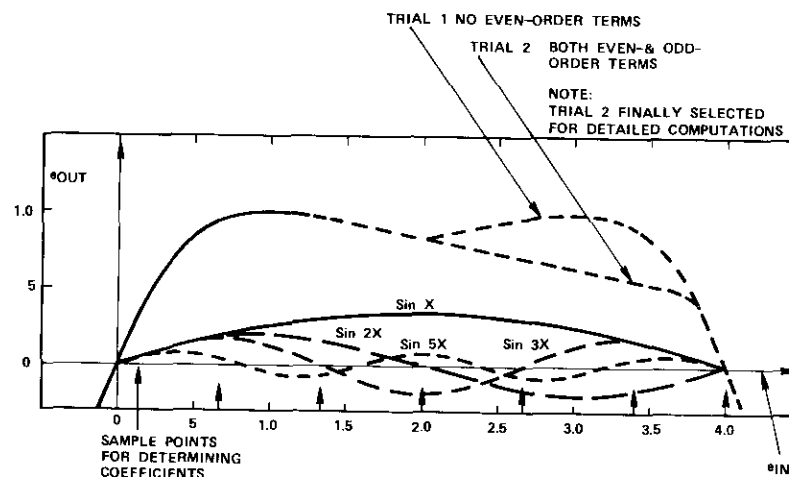


Figure 34. Instantaneous Voltage Transfer Characteristic

For the general case of an arbitrary set of inputs,

$$e_{in} = \sum_{i=1}^n A_i \sin \left[ \omega_i t + \int \psi_i dt \right]$$

where  $A_i$  = amplitude of the  $i$ th carrier

$\omega_i$  = center frequency of the  $i$ th carrier

$\psi_i$  = rms value of the frequency deviation when the RF carrier is modulated with a noise-like baseband signal.

The output,  $e_{outs}$ , may be written as

$$e_{out} = c_1 \sin \left[ \alpha \sum_{i=1}^n A_i \sin \omega_i t + \int \psi_i dt \right] + \dots$$

The output of any terms may be obtained by appropriately manipulating the subscripts; i.e.,

$$e_{out} = k_1 \sum_a \sum_b \sum_c \dots \sum_d J_a(\alpha A_1) \cdot J_b(\alpha A_2) \\ \cdot J_c(\alpha A_3) \dots J_d(\alpha A_n) \\ \cdot \cos [(a\omega_1 + b\omega_2 + c\omega_3 + \dots d\omega_n)t \\ + \int \psi_r dt] + \dots$$

where  $\psi_r = \sqrt{(a\psi_1)^2 + (b\psi_2)^2 + (c\psi_3)^2 + \dots (d\psi_n)^2}$

in the case of high-index noise modulation. If the *i*th subscript is assumed to be 1 (and all others are assumed to be 0), the useful power output of the *i*th carrier may be computed. Similarly, if the remaining subscripts are appropriately evaluated, all of the output products can be computed. For certain applications with small numbers of carriers, the useful power output and product heights are utilized directly. However, in the general multicarrier case, it is desirable to use an appropriate algorithm to further process the products before the computer prints out the final values.

For the INTELSAT IV multiple-carrier computations, the following sorting modes have been provided:

- classifying product types, with options to compute or neglect (see Table 13),
- sort/store by frequency,
- product spreading caused by modulation, and
- coherence between products [19].

TABLE 13. CLASSIFYING PRODUCT TYPE

Subscript Forms	Type
1,0,0, . . . , 0	1st-Order Desired Carrier Output
2,1,0,0, . . . , 0	3rd-Order A <sup>2</sup> B Intermodulation Product
1,1,1,0,0, . . . , 0	3rd-Order ABC Intermodulation Product
1,1,1,1,0, . . . , 0	5th-Order ABCDE Intermodulation Product
2,2,1,0, . . . , 0	5th-Order A <sup>2</sup> B <sup>2</sup> C Intermodulation Product
3,1,1,0, . . . , 0	5th-Order A <sup>3</sup> BC Intermodulation Product
3,2,0, . . . , 0	5th-Order A <sup>3</sup> B <sup>2</sup> Intermodulation Product
4,1,0, . . . , 0	5th-Order A <sup>4</sup> B Intermodulation Product

In the sort/store by frequency mode, the 500-MHz communications band is subdivided into 5,000 cells. For each product type, an algorithm gives the frequencies of the product (i.e., an  $A_i^2 A_j$  product falls at  $|2\omega_i - \omega_j|$ ), enters the product into the appropriate cell, and keeps a running power total for each of the cells. A plot of the total in the cells yields the intermodulation density.

In the case of FDM/FM telephony (sorting mode c), the spectrum of an RF carrier is approximately Gaussian, with an rms value equal to the rms deviation of the baseband noise load.\* For any product of the form  $A_i^m \cdot A_k^n$  (rigorously obtained from the multiple convolution of the carriers comprising it), the spectral shape will be Gaussian with an rms index given by

$$\sigma^2 = (m\sigma_i)^2 + (n\sigma_j)^2 \dots (p\sigma_k)^2.$$

The spectral density of each product is computed, and the portion falling into each frequency cell is entered into the total of that cell (sorting mode b).

It should be noted that, for other forms of modulation, the spectral shape must be computed only once for each product type; it can then be stored as a "library" function.

If a significant number of carrier pairs have instantaneous difference frequencies that are smaller than the baseband widths of other large carriers within the multiple-access community, the fourth sorting mode should be used to properly interpret the intermodulation noise density when deriving the resulting baseband (detected) noise spectrum.

For FM carriers, products having the form  $\dagger \omega_i \pm (\omega_i - \omega_j) = \omega_i \pm \Delta\omega$  will appear as an amplitude modulation about  $\omega_i$ . If  $\Delta\omega$  is less than the Carson's Rule bandwidth of  $\omega_i$ , the product pair is discarded. On the other hand, if  $\Delta\omega$  is greater than the Carson's Rule bandwidth of  $\omega_i$ , then each of the individual terms will appear as an unrelated intermodulation product about some other carrier; each term must then be retained and added (in power) to the appropriate cell (sorting mode b).

\* To compute the spectral density of the intermodulation products, the Gaussian approximation is sufficiently accurate for the range of rms indexes encountered by the INTELSAT IV system.

† For most cases of interest, only ABC products are significant; fifth-order products may be neglected entirely.

**Phase Nonlinearity.** The single-carrier phase nonlinearity curve is shown in Figure 35. The curve is approximated by the series [17]

$$\phi = k_1[1 - \exp(-k_2 P_{in})] + k_3 P_{in}$$

where  $k_1, k_2, k_3 =$  tube constants  
 $P_{in} =$  normalized input power  
 $\phi =$  relative phase shift.

With an arbitrary set of input carriers,

$$e_{in} = \sum_{i=1}^p A_i \cos \omega_i t$$

The squared envelope is given by

$$\overline{[e_{in}(t)]^2} = \sum_{i=1}^p A_i^2 + 2 \sum_{i=1}^{p-1} \sum_{k=i+1}^p A_i A_k \cos(\omega_i - \omega_k)t$$

leading to output terms of the form

$$e_{out} = \sum_{i=1}^p A_i \sum_{j=1}^{p-1} \sum_{k=j+1}^p \prod_{m=1}^{\infty} \sum_{n_{mik}=-\infty}^{+\infty} J_{n_{mik}}(\alpha_{mik}) \cdot \cos [\omega_i + mn_{mik}(\omega_i - \omega_k)]t$$

where

$$\alpha_{mik} = 2k_1 \exp\left(-k_2 \sum_{i=1}^p A_i^2\right) \cdot I_m(2k_2 A_i A_k) + \begin{cases} 2k_3 A_i A_k, & m = 1 \\ 0, & m \neq 1 \end{cases}$$

As in the case of the AM nonlinearities, sorting modes a through c, listed previously, are used.

For phase nonlinearity, sorting mode d is altered as follows. Products of the form  $\omega_i \pm \Delta\omega$  produce coherent phase modulation about  $\omega_i$ . Since the output of the computations is a spectral density which will be added to other noise densities during the course of system computations, the product value is doubled (in power) before it is added to the totals in the cells if  $\Delta\omega \leq$  Carson's Rule bandwidth of  $\omega_i$ . Then, the amplitude intermodulation density and the thermal noise density are added in power.

Subsequent work in this area has shown that the effects of both phase and amplitude nonlinearities can be derived from a single nonlinear

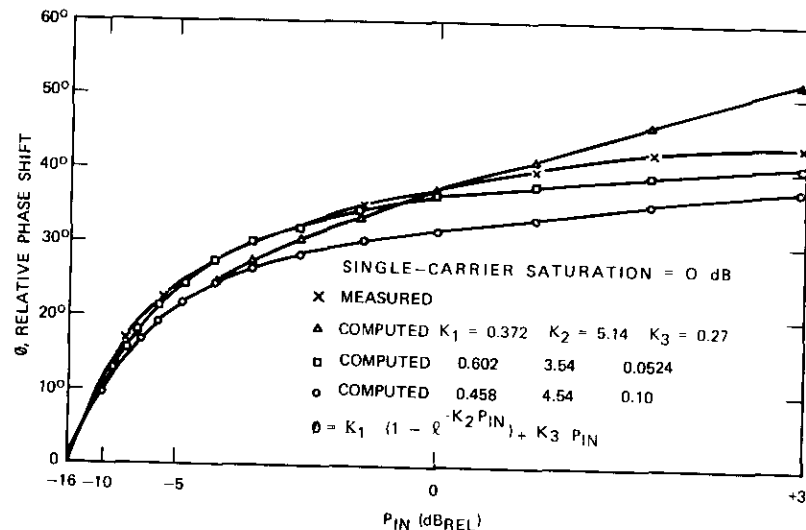


Figure 35. Measured and Computed Phase Shift Transfer Function

transfer function expanded as a series with complex coefficients. This characterization has resulted in a unified formulation which allows convenient sorting for coherence relationships, and direct computation of baseband noise for a variety of modulation types.\*

**Crosstalk computations**

In multicarrier FM systems, crosstalk results from a sequence of two phenomena: first, an amplitude response which varies with frequency, producing amplitude modulation coherent with the original frequency modulation of an RF carrier (FM/AM transfer); and secondly, a coherent amplitude modulation, which phase modulates all carriers in a subsequent traveling wave tube amplifier exhibiting AM/PM conversion.

For those cases in which the gain slope is small and may be characterized by a linear coefficient (in dB/MHz), and the phase shift vs drive may be represented by an average conversion coefficient (in deg/dB), accurate results may be obtained from Reference 20. However, several cases of in-

\* This work will be reported in a forthcoming paper.

terest in the INTELSAT IV system required further refinement. For example, in the satellite transmitter (and again in the earth station transmitter), signals intended for channel II were slope detected on the skirt of channel I, producing coherent AM components and crosstalk in channel I. In this case, the use of an unmodified gain slope (in dB/MHz) resulted in grossly inaccurate predictions of the AM produced in channel I. As a second example, when two or more carriers were located within one input filter bandwidth, the carrier near band edge experienced a high-order unsymmetrical gain slope because of the filter's finite unloaded Q (and consequent rounded corners). In this case, the use of either an instantaneous gain slope or an average chord would yield predictions of the coherent AM component that may be in error by as much as a factor of 2 to 5.

In addition, when there is a wide variety of carrier combinations, the use of an average AM/PM conversion coefficient results in a poor correlation between predicted and measured results. The latter problem is readily overcome (once the AM component is known) by using the phase non-linearity series described previously\* to directly compute the one term of interest.

To compute the resulting AM component, a test tone inserted into the top baseband telephone channel is represented by a pair of low-index sidebands about the carrier. The remainder of the multiplex signal (having an average frequency lower than that of the top baseband signal) is assumed to be a low-frequency slewing signal with a Gaussian probability density. To provide computational assistance, a program has been written to slew the carrier and sideband pair across a given filter response (one of the program inputs) in small increments. For each position, the imbalance in sideband heights is resolved into an AM component and multiplied by the probability that the carrier is in that position (determined from the Gaussian statistic of the noise load). The probabilistic weighted sum over all positions gives the average AM component that would cause crosstalk into another 4-kHz voice channel.

Experimental verification of this model, detailed in the following, indicates good agreement with theory over a large range of rms indexes ( $\geq 0.5$ ), gain slopes ( $\geq 0$ ), and locations on the filter curve.

\* To simplify the computations, the AM component is represented at the input to the phase shift program as a small carrier next to the AM producing carrier; the spacing is set to yield the desired rate, and the height of the small carrier is set to yield the desired AM index.

### Verification of the crosstalk model

**Theoretical Model.** Figure 36 is a 2-block model used to represent the satellite repeater. The first block of Figure 36 contains the amplitude and group-delay frequency response of the communications path up to the input of a TWT. The second block models the AM/PM conversion exhibited by a TWT or other active device.

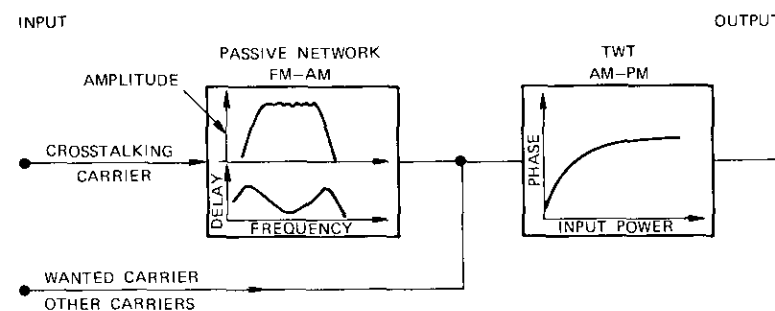


Figure 36. Model of a Satellite Repeater

In this analysis, the crosstalking carrier bears a multicarrier frequency modulation, the wanted carrier is an unmodulated carrier, and other carriers (with arbitrary angle modulation) are inserted to achieve the actual operating conditions for the TWT characteristic. The intelligible crosstalk originates from a baseband channel on the crosstalking carrier and is transferred onto the wanted carrier. In this case, only the crosstalking carrier must pass through the FM/AM conversion block of the model. The wanted carrier and the other carriers are injected at the input of the AM/PM converter so that any frequency response in their path may be neglected.

For this analysis, intelligible crosstalk is defined as a performance requirement specified in terms of the ratio between wanted and unwanted levels of a sine wave test tone inserted into the baseband channel of interest. The actual level used to represent an average talker is not significant in the computations; however, this level must be taken into account when comparing experimental results measured with an NPR test set with theoretical predictions referenced to a 0-dBm0 test tone.

It is well-known that the intelligible crosstalk increases proportionally with the baseband frequency. Therefore the worst case can be expected to occur at the high-frequency end of the baseband spectrum of a multichannel signal. For system performance evaluation, the worst case is usually of

interest; consequently, the frequency of the test tone can be restricted to the high end of the baseband spectrum. This restriction leads to a significant simplification of the analysis; i.e., the test tone can be represented in the RF spectrum by a low index modulation, and the noise loaded baseband including the test tone can be represented by a high index modulation. Figure 37 shows the baseband and RF spectrum for this situation.

For clarity, the analysis has been divided into two parts. The first part follows the path through the model for the simple case of a single tone-

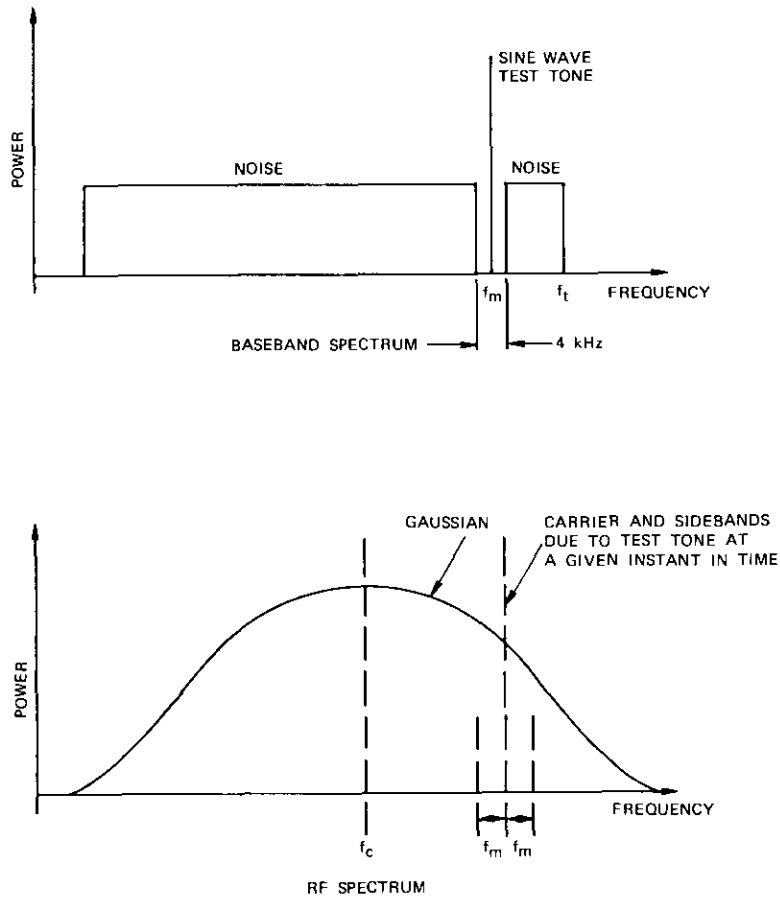


Figure 37. Baseband and RF Spectrum Representation of Crosstalking Carriers

modulated crosstalking carrier. The second part leads to an equation which allows computation of intelligible crosstalk for the noise loaded case.

Consider a crosstalking carrier modulated by a sine wave of frequency  $f_m$ , where  $\beta_c$  is the modulation index. In the time domain, this can be expressed as

$$A_c \sum_{n=-\infty}^{+\infty} J_n(\beta_c) \cdot \cos 2\pi(f_c + n f_m) t \quad (10)$$

where  $A_c$  is the carrier amplitude and  $f_c$  the carrier frequency.

The carrier and sidebands described by equation (10) will be modified in accordance with the transfer characteristic of the passive network at the particular carrier and sideband frequencies. For the simple case of a carrier with only two sidebands and a passive network with amplitude response  $G(f)$  and constant group delay, this process is shown in Figures 38 and 39. After passing through the amplitude response  $G(f)$ , the carrier and its sidebands will have new amplitudes:

$$\begin{aligned} \text{carrier amplitude} &= A_c \cdot G(f_c) \\ \text{upper sideband amplitude} &= A_c \cdot G(f_c + f_m) \cdot J_1(\beta_c) \\ \text{lower sideband amplitude} &= A_c \cdot G(f_c - f_m) \cdot J_1(\beta_c) \end{aligned} \quad (11)$$

where it is assumed that  $J_0(\beta_c) \approx 1$ .

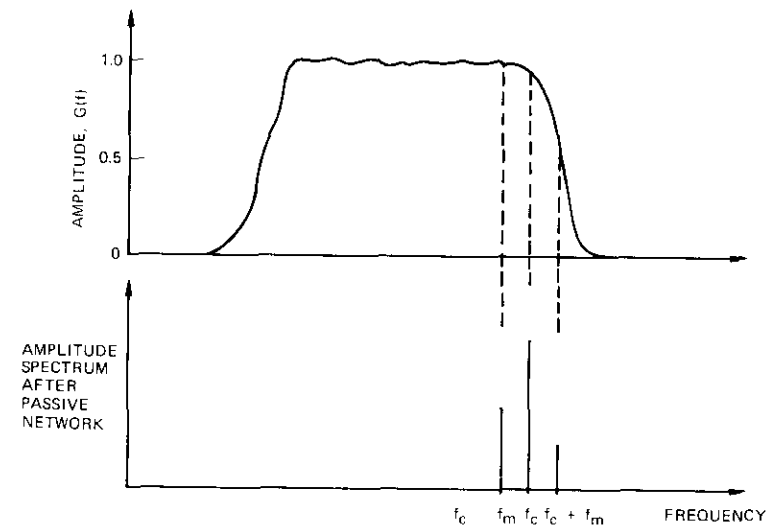


Figure 38. Amplitude Response and Spectrum at Output of Passive Network

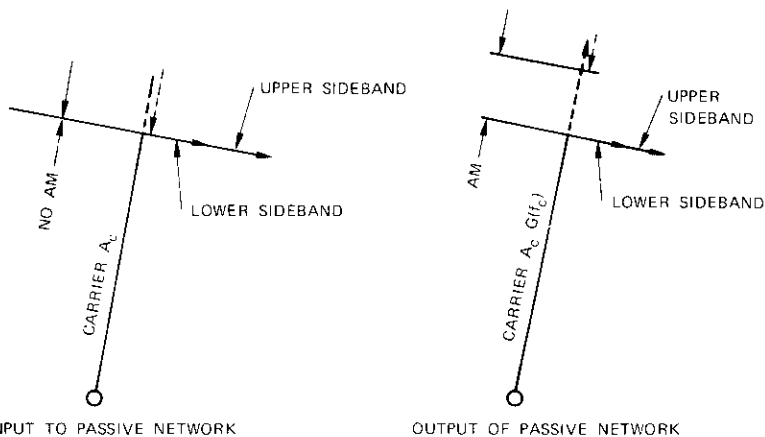


Figure 39. Vector Diagram of the Crosstalking Carrier

It is apparent that the sidebands become unbalanced so that AM is generated. In this simple case, the amount of AM generated is proportional to the amplitude difference of the two sidebands, which can be expressed as

$$A_c \cdot J_1(\beta_c) \cdot D \tag{12}$$

where  $D = [G(f_c + f_m) - G(f_c - f_m)]$ . The AM index can be obtained by dividing equation (12) by the actual carrier amplitude, i.e.,

$$m = \frac{J_1(\beta_c)}{G(f_c)} \cdot D. \tag{13}$$

On the crosstalking carrier in the subsequent AM/PM converter, amplitude modulation or envelope fluctuations coherent with  $f_m$  are the only components of interest. The crosstalking carrier at the output of the passive network can therefore be expressed as

$$A_c \cdot G(f_c) [1 + m \cos(2\pi f_m t)] \cdot \sin 2\pi f_c t. \tag{14}$$

This carrier, the wanted carrier, and other eventual carriers are fed to the AM/PM converter. The AM on the crosstalking carrier then gives rise to PM at the same rate on all other carriers passing through the AM/PM converter.

For clarity, the pertinent results of Reference 18 will be summarized in the following. Assume that there are three carriers, described by their amplitudes  $A_1, A_2, A_3$ , and their frequencies  $f_1, f_2, f_3$ , at the input of the AM/PM converter. For illustrative purposes, also assume that  $f_1 < f_2$  and  $f_2 \approx f_3$ . After the AM/PM converter, carrier  $A_1$  will bear sidebands at the rate of  $|f_2 - f_3|$ . Each sideband will consist of two components; i.e.,

$$SB = A_1 \cdot J_1\{2k_1 e^{(-k_2 P_{in})} \cdot I_1(2k_2 A_2 A_3) + 2k_3 A_2 A_3\} \cdot \cos 2\pi [f_1 - (f_2 - f_3)]t + A_1 \cdot J_1\{2k_1 e^{(-k_2 P_{in})} \cdot I_1(2k_2 A_1 A_2) + 2k_3 A_1 A_2\} \cdot \cos 2\pi [f_1 + (f_2 - f_3)]t \tag{15}$$

where  $k_1, k_2, k_3$  are constants characterizing the AM/PM converter,  $P_{in}$  is the input backoff (input power to the AM/PM converter normalized with respect to the saturation power), and  $\sum_i A_i^2 = P_{in}$ .

For this part of the analysis, the AM on the crosstalking carrier can be represented by a carrier whose amplitude =  $A_c \cdot G(f_c)$  and one sideband whose amplitude =  $A_w J_1(\beta_c) D$ . If these amplitudes are substituted into equation (15), the amplitude of the PM sidebands generated on the wanted carrier is

$$SB = A_w J_1\{2k_1 e^{(-k_2 P_{in})} \cdot I_1[2k_2 A_c^2 G(f_c) J_1(\beta_c) D] + 2k_3 A_c^2 G(f_c) J_1(\beta_c) D\} + A_w J_1(\beta_c) D \cdot J_1\{2k_1 e^{(-k_2 P_{in})} \cdot I_1[2k_2 A_c G(f_c) A_w] + 2k_3 A_c G(f_c) A_w\}. \tag{16}$$

This PM sideband amplitude will be much smaller than the wanted carrier amplitude,  $A_w$ . Therefore, the approximation  $J_1(x) = x/2$  is valid and the modulation index of the interfering PM on the wanted carrier is

$$\beta_i = \frac{2SB}{A_w}. \tag{17}$$

The crosstalk ratio for this simple case can now be calculated as

$$IXTR \text{ (single-tone FM)} = 20 \log \frac{\beta_i}{\beta_w} \tag{18}$$

where  $\beta_w$  is the modulation index of a similar test tone of frequency  $f_m$  on the wanted carrier. In satellite systems,  $\beta_c$  and  $\beta_w$  may or may not be the

same. For example, for a 432-channel carrier crosstalking into a 252-channel carrier, the highest  $f_m$  of interest is obviously that of the 252-channel carrier, and depending on pre-emphasis,  $\beta_c \neq \beta_w$ .

For the general case of a noise loaded baseband, the same procedure will be followed. The baseband of the crosstalking carrier is as shown in Figure 37. If the quasi-stationary FM model is used and a Gaussian probability density is assumed, the RF spectrum can be written as

$$S(f) = \frac{1}{\sqrt{2\pi} f_{rmsc}} \cdot \exp - \left\{ \frac{(f - f_c)^2}{2f_{rmsc}^2} \right\} \cdot \sum_{n=-\infty}^{+\infty} A_n J_n(\beta_c) \cdot \cos 2\pi(f_c + nf_m)t \quad (19)$$

where  $f_{rmsc}$  is the rms deviation of the crosstalking carrier.

In a practical situation, the passive network given by the amplitude and group-delay response may contain sharp filters. Hence, if a polynomial representation is used, several higher order terms will be required.

The approach presented here uses directly measured responses. The envelope of the crosstalking carrier will contain a broad spectrum after passing through the passive network. For calculations of intelligible crosstalk, the envelope components at rates of  $f_m$  and integer multiples of  $f_m$  are of interest, and a Fourier series is an adequate representation. Since the energy of the crosstalking carrier is spread out over a bandwidth approximately equal to the Carson's Rule bandwidth, the coefficients of the Fourier series are functions of the instantaneous carrier frequency. This Fourier series can be pictured as a carrier amplitude modulated by a time-varying complex wave with a fundamental frequency  $f_m$ . All other envelope components may be neglected.

The amplitude modulated carrier, wanted carrier, and other carriers are fed to the AM/PM converter. At the output, all carriers will bear a similarly complex wave phase modulation, which, after demodulation, will result in a baseband complex periodic wave. The phase modulation sidebands on the wanted carrier can be calculated according to Reference 18, regardless of any angle modulation this carrier might bear before entering the model. The complex wave at baseband can be developed into another Fourier series, in which the coefficient of the fundamental represents the instantaneous amplitude of the crosstalking signal. A time average of this amplitude can then be calculated and compared with the level of a similar test tone on the wanted carrier, and the intelligible crosstalk ratio can be determined.

For engineering purposes, this process can be simplified considerably without appreciably degrading the accuracy of the results. First, the series describing the angle modulation of the test tone on the crosstalking carrier may be truncated so that only one pair of sidebands is considered, i.e.,  $n = \pm 1$  in equation (19). Hence, a Fourier analysis of the envelope of the crosstalking carrier after the passive network is no longer necessary. Although the AM of interest is still a complex wave, the amplitude of the first pair of AM sidebands can be calculated by using equation (11). This approximation is valid for  $\beta_c \ll 1$ . (For  $\beta_c = 0.9$ , the amplitude error is 1.5 dB; for  $\beta_c = 0.6$ , it is less than 0.7 dB.)

In addition, since experimental data indicate that, in practical networks such as microwave filters, group delay is only a minor worst-case contributor to the FM/AM conversion, it can usually be neglected. As a further simplification, the series describing the complex periodic AM wave may be truncated. Omitting the higher order ( $2f_m, 3f_m, \dots$ ) AM sidebands does not introduce any significant error, at least for all practical cases of interest. Since the transfer from AM to PM is small in practical communications systems, this approximation makes it possible to calculate the PM sidebands on the wanted carrier by using an expression similar to equation (16). A Fourier development of the wanted carrier's complex periodic wave at baseband is no longer necessary, and the time average can be taken directly on the PM sidebands. As a result of these three simplifications, the time-averaged PM sideband amplitude on the wanted carrier can be expressed as

$$\overline{SB} = \frac{1}{\sqrt{2\pi} f_{rmsc}} \int_{-\infty}^{+\infty} \left[ A_w J_1 \{ 2k_1 e^{(-k_2 P_{in})} \cdot I_1 [ 2k_2 A_c^2 G(f) J_1(\beta_c) D ] + 2k_3 A_c^2 G(f) J_1(\beta_c) D \} + A_w J_1(\beta_c) D \cdot J_1 \{ 2k_1 e^{(-k_2 P_{in})} \cdot I_1 [ 2k_2 A_c G(f) A_w ] + 2k_3 A_c G(f) A_w \} \right] \cdot \exp - \left\{ \frac{(f - f_c)^2}{2f_{rmsc}^2} \right\} df \quad (20)$$

The intelligible crosstalk ratio can now be calculated by using equations (17) and (18):

$$IXTR = 20 \log_{10} \frac{\overline{SB}}{A_w \beta_w} \quad (21)$$

This equation, which has been slightly modified by using a finite sum of samples at equidistant frequencies covering the Carson's Rule bandwidth,

has been programmed on a digital computer. The spacing between samples is selected according to the frequency-response of the passive network.

Equation (21) describes the most common process involved in the generation of intelligible crosstalk in satellite repeaters. Actually, intelligible crosstalk can also be produced by more elaborate processes. An example that has been observed experimentally is as follows. Assume that a non-linear amplifier passes two carriers at  $f_1$  and  $f_2$ , generating a third-order intermodulation product at  $2f_1 - f_2$ . This product falls on a steep amplitude or group-delay slope of a passive network following the amplifier. It can be shown that, at the output of this passive network, the intermodulation product contains amplitude modulation coherent with the frequency modulation of both  $f_1$  and  $f_2$ . Amplifying this intermodulation product and one of the two carriers in a subsequent AM/PM converter will result in intelligible crosstalk. This process can be calculated by modifying the model described here to achieve a 3-block model.

**Comparison with Previous Results.** The intelligible crosstalk ratio has previously been calculated by Chapman and Millard [21]; i.e.,

$$\text{IXTR} = 20 \log 2K_1 A_c^2 g f_m$$

where  $K_1$  is a tube constant related to the phase shift and the input power of the TWT by their equation (56):

$$\phi = \frac{K_1 P_{in}}{2} \quad (22)$$

$A_c^2$  is the power of the crosstalking carrier referenced to single-carrier saturation,  $g$  is the gain slope defined by

$$G(f - f_i) = 1 + g(f - f_i) \quad (23)$$

and  $f_m$  is the baseband frequency under consideration.

It can be shown that Chapman and Millard's result is a special case of the foregoing analysis. If the operating range of the TWT is restricted to low input power, and small signal approximations are used, both results become identical.

For low input power, it can be assumed that  $J_1(x) \approx x/2$ ,  $I_1(x) \approx x/2$ , and  $\exp(-k_2 P_{in}) \approx 1$  in equation (20). Furthermore, according to Reference 18, the phase-input power characteristic of a TWT can be described as

$$\phi = k_1 [1 + e^{(-k_2 P_{in})}] + k_3 P_{in} \quad (24)$$

which, for  $P_{in} \ll 1$ , reduces to

$$\phi = (k_1 k_2 + k_3) P_{in} \quad (25)$$

A comparison of equations (22) and (25) indicates that

$$k_1 k_2 + k_3 = \frac{K_1}{2} \quad (26)$$

These approximations can be used to simplify equation (21) as follows:

$$\text{IXTR} = 20 \log_{10} \frac{2 \int_{-\infty}^{+\infty} K_1 A_c^2 A_w G(f) J_1(\beta_c) D \cdot \exp - \left\{ \frac{(f - f_c)^2}{2f_{rmsc}^2} \right\} df}{\sqrt{2\pi} A_w \beta_w f_{rmsc}} \quad (27)$$

Assuming a linear gain slope as in equation (23), where  $f - f_i = f_m$  and  $G(f) \approx 1$ , makes it possible to simplify equation (27):

$$\text{IXTR} = 20 \log_{10} \frac{2K_1 A_c^2 J(\beta_c) 2g f_m}{\beta_w} \cdot \frac{1}{\sqrt{2\pi} f_{rmsc}} \int_{-\infty}^{+\infty} \exp - \left\{ \frac{(f - f_c)^2}{2f_{rmsc}^2} \right\} df \quad (28)$$

The integral with the preceding factor  $1/\sqrt{2\pi} f_{rmsc}$  is equal to 1. With further simplification, equation (28) can be expressed as

$$\text{IXTR} = 20 \log_{10} \frac{2K_1 A_c^2 g f_m \beta_c}{\beta_w} \quad (29)$$

For equal modulation parameters, equation (29) can now be reduced to yield the result of Chapman and Millard.

### Experimental results

The objective of the experimental work was to verify specific parts of the model for which a correlation between experiment and analysis had not yet been established instead of using a baseband-to-baseband measurement of intelligible crosstalk to verify the overall model. Such an overall crosstalk measurement presents many possibilities for error that cannot be recognized as easily as in a part-by-part verification of the model.

Since the validity of the model for the AM/PM conversion mechanism had already been established, the experimental work concentrated on the first part of the model, the FM/AM conversion. The first objective consisted of matching measurements and computed predictions of AM at the output of a linear network. For convenience, the AM index was measured for three values of  $\beta$ . The test object was a filter characterized by the measured responses shown in Figure 40. A carrier was frequency modulated with a single tone at 100 kHz and fed through the filter; the AM index was then measured at the output of the filter. The results for three modulation indexes (Figures 41-43) show excellent agreement with computed data. These computations included up to seven pairs of FM sidebands, and both amplitude and group-delay responses. The AM index was

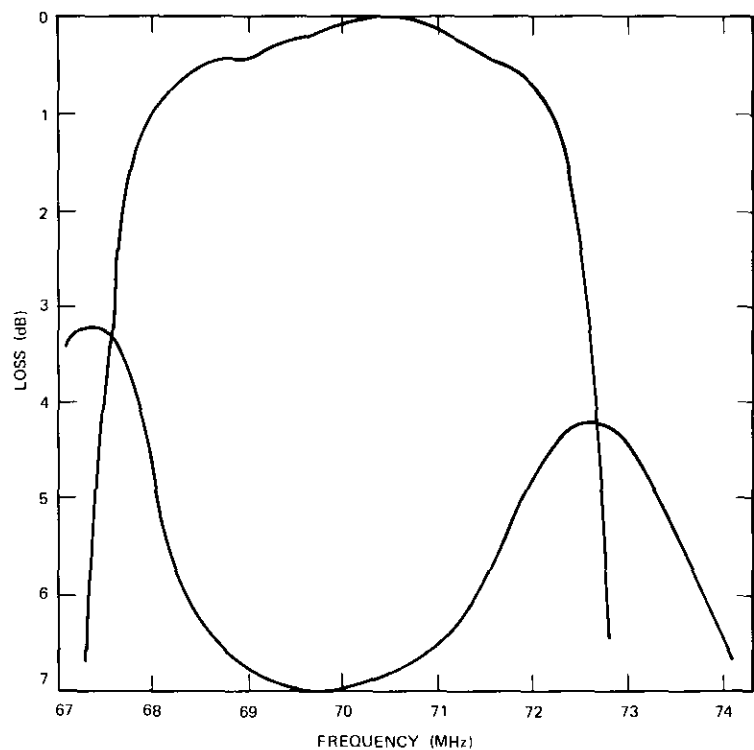


Figure 40. Frequency Response for 5-Pole, 5-MHz, Elliptic Function Filter

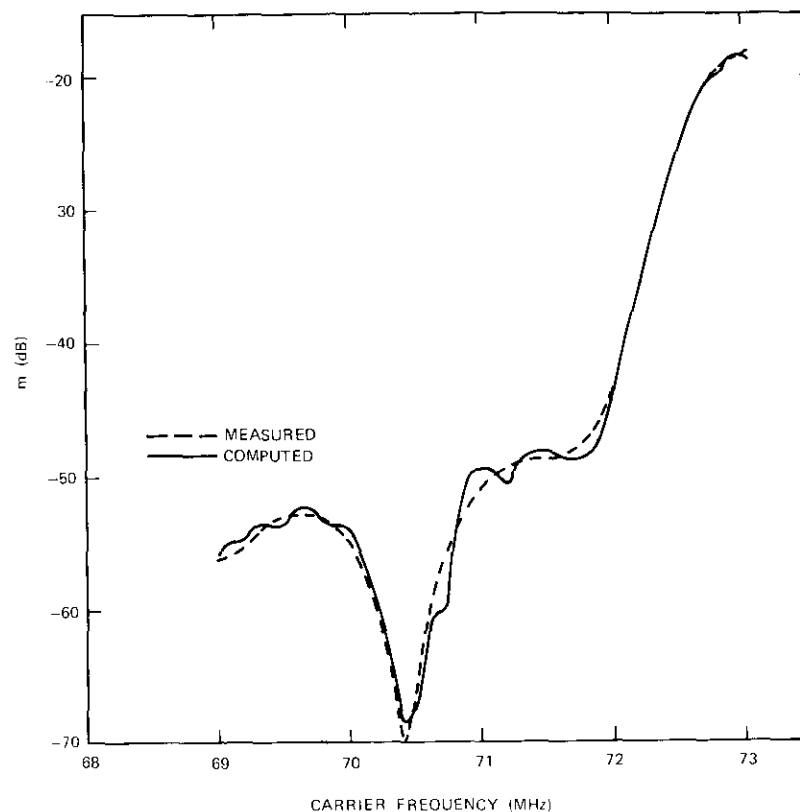
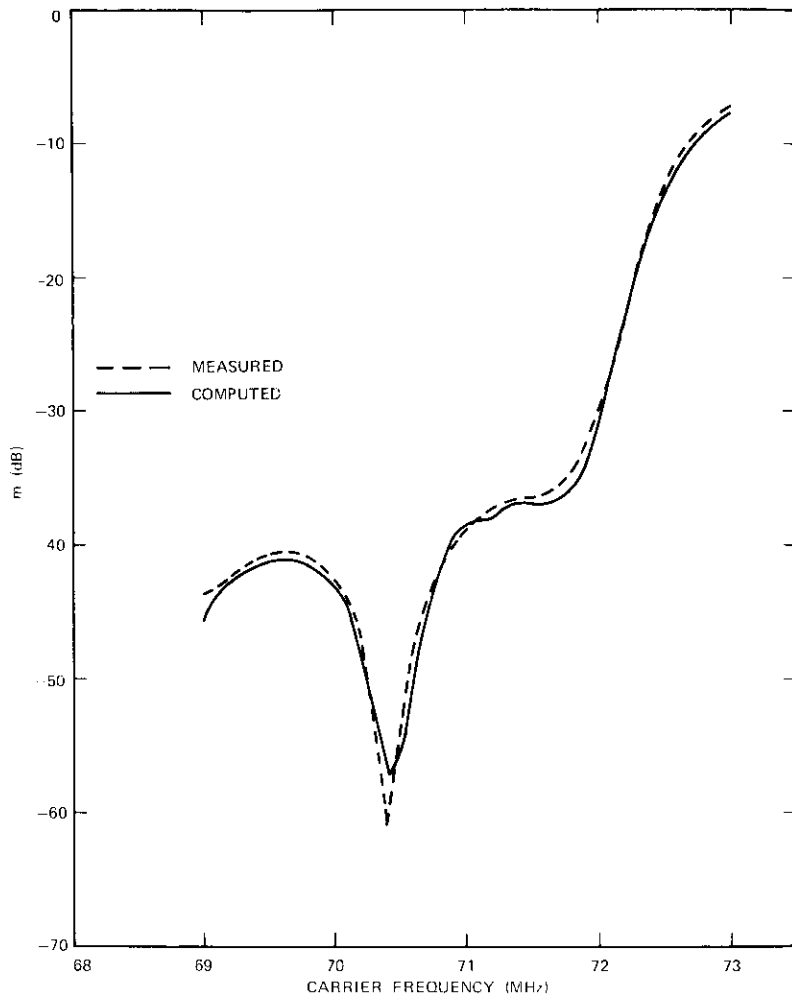


Figure 41. AM Index for  $\beta = 0.5$

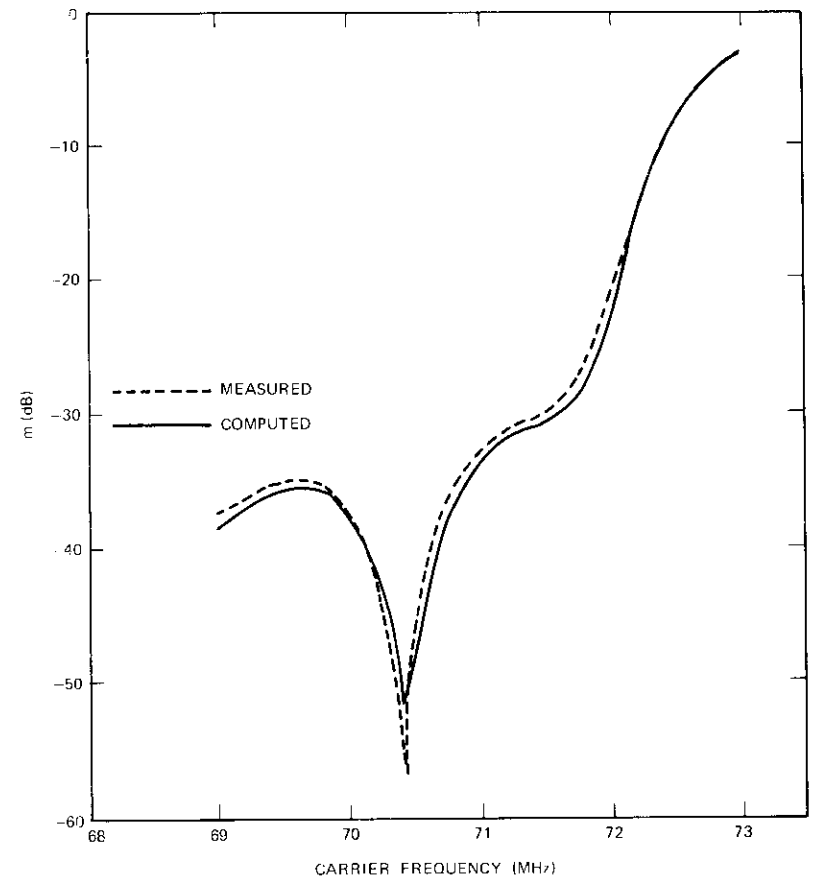
obtained from a Fourier evaluation of the envelope at the output of the filter.

Omitting the group delay in these computations affected only the AM close to the sharp dip occurring around 70.4 MHz; where the AM index peaks (for instance, at 69.7 MHz and above 71 MHz), no appreciable group-delay effect could be detected.

These single-tone measurements were used as a basis for two of the approximations made in the analysis. Another assumption used in the model, namely, the assumption that the test tone is represented by a low index modulation and the noise loading by a high index modulation, was verified as follows. A carrier was frequency modulated by a 1002-kHz sine wave with an index of 0.14, and a triangular wave with a peak deviation of

Figure 42. *AM Index for  $\beta = 2.0$* 

$\pm 3$  MHz. (The triangular wave was chosen because it has a constant probability density so that the RF spectrum of the modulated carrier can be easily calculated.) This composite signal was fed through a 10-section Tchebycheff filter with the carrier placed close to the sharp dropoff in amplitude response. The triangular wave frequency could be varied from 20 to 100 kHz without appreciably changing the AM index measured at the output of the filter.

Figure 43. *AM Index for  $\beta = 4.0$* 

Next, noise loading was measured for a 252-channel carrier using standard parameters and a 1002-kHz test tone. The modulated carrier was fed through the same 10-section filter used previously, and a weighted AM index was measured at the output of the filter and compared with computed data (Figure 44). The computations omitted group delay and included only one pair of FM sidebands on the carrier. The weighted AM index was computed as follows:

$$M = \frac{J_1(\beta_c)}{\sqrt{2\pi} f_{rmsc}} \int_{-\infty}^{+\infty} D \cdot \exp \left\{ -\frac{(f - f_c)^2}{2f_{rmsc}^2} \right\} df. \quad (30)$$

To verify that the probability approach to the problem was correct, the noise baseband spectrum width was varied from about 252 kHz to above 2 MHz, while the rms deviation was kept constant. The modulation index,  $M$ , varied less than  $\pm 0.5$  dB over this range.

These measurements complete the verification of the first block of the model. Additional corroboration was obtained from a baseband-to-baseband measurement of a 132-channel carrier. The test setup, the measured filter response, and the computed intelligible crosstalk ratio are shown in Figure 45. Discrepancies, caused by an imperfect test setup, occur in the case of low crosstalk. In addition, the measurement accuracy for crosstalk ratios greater than 70 dB degrades very rapidly because of noise. Otherwise, the agreement between predictions and measurements is considered to be good.

**Adjacent channel interference**

Adjacent FDM/FM telephony channels are characterized as shown in Figure 46 [14]. At the output of the desired channel receive filter, two effects are noted. First, there is a spectral density caused by modulator 2 (modified by filters  $G_I$  and  $G_{RD1}$ ) at the output of  $G_{RD}$ . It can be shown that, after demodulation, the resulting phase noise at baseband is given by the convolution of the desired spectrum with the residual adjacent channel spectrum (both referenced to the output of  $G_{RD}$ ). The only restriction on this derivation is that the instantaneous complex amplitude of the desired carrier must always be greater than that of the interfering carrier.

Secondly, when viewed in the time domain (i.e., at output  $R_1$ ) with a detector having a video bandwidth  $\approx 10$  times greater than the top baseband frequency of the interfering modulation,  $M_2$ , the instantaneous amplitude of the waveform caused by  $M_2$  is greater than the amplitude of the waveform caused by the desired modulation,  $M_1$ , for short random time periods. This random impulse interference was the limiting factor in the guardband and filter requirements determined for the cases of interest in the INTELSAT IV system.

It can be shown [14] that the rate of impulses is

$$\text{rate} = \int_{-\infty}^{+\infty} |F_o - f'| \cdot p(f') \cdot p[A_D(f) < A_i(f')] df'$$

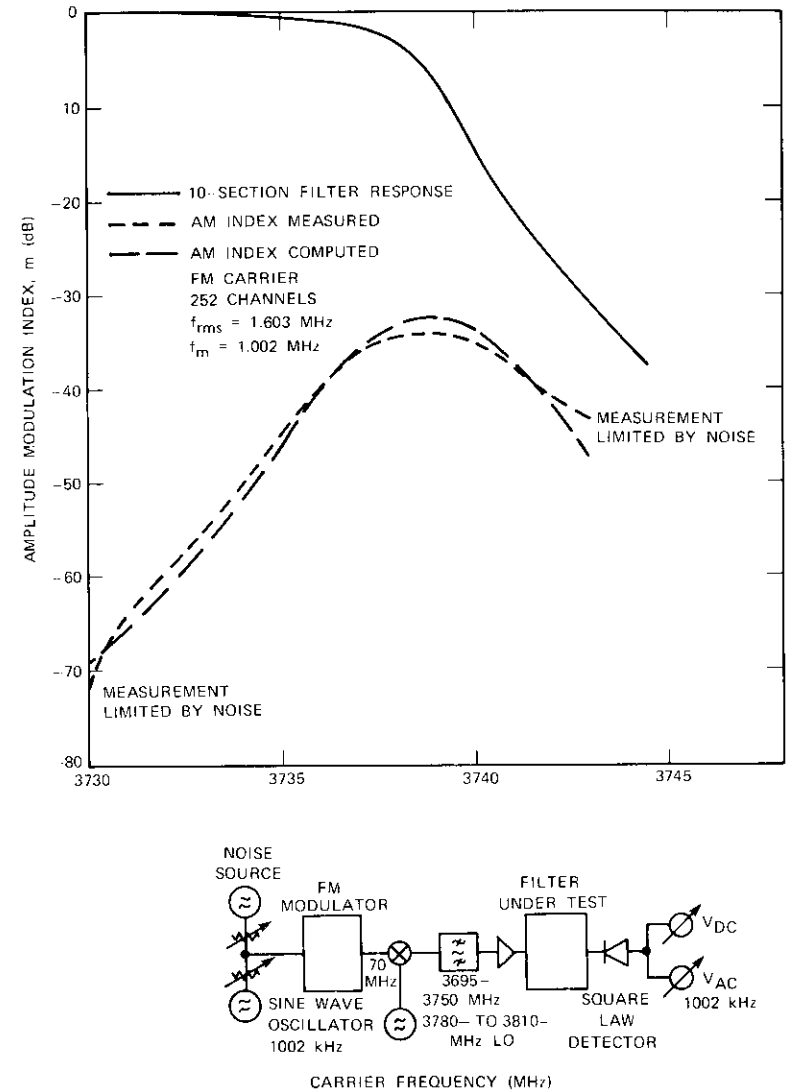


Figure 44. AM Index Measurement with Noise Loading

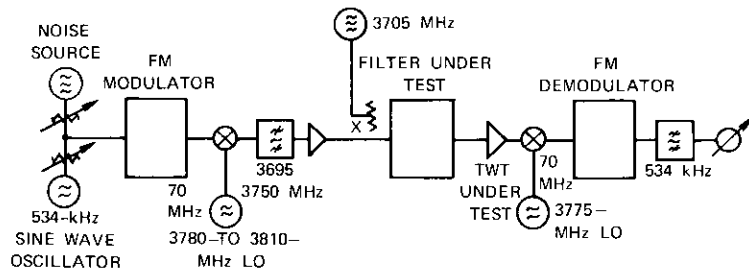
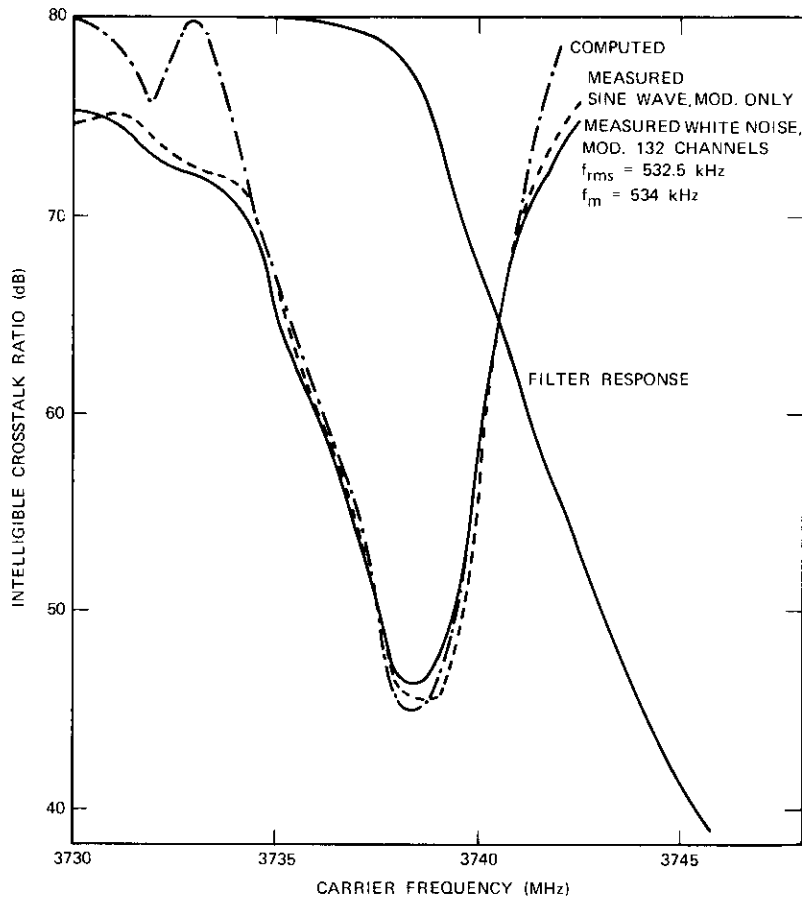


Figure 45. Baseband-to-Baseband Measurements

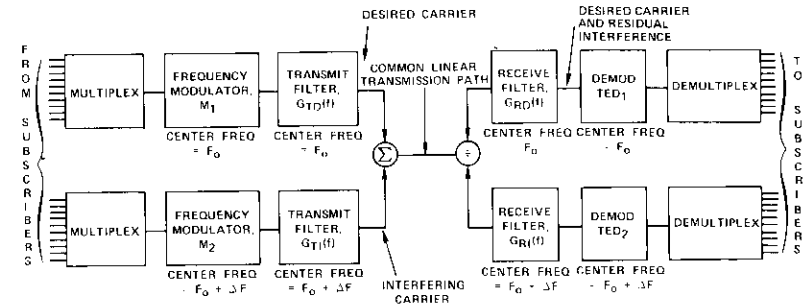


Figure 46. Adjacent Channel Interference

where  $F_0$  = center frequency of the desired carrier  
 $f'$  = frequency variable of integration  
 $P(f')$  = probability density for the interfering carrier at frequency  $f'$   
 $P[A_D(f) < A_i(f')]$  = probability density when the amplitude of the desired carrier is less than that of the interfering carrier and the interfering carrier is at frequency  $f'$ .

In a bandwidth-limited mode, the system capacity increases in proportion to the useful bandwidth. To increase the useful bandwidth while maintaining the impulse interference at an acceptable level, all adjacent channels should have transmit filters with very high rates of attenuation for the initial 10 to 15 dB, and bandwidths as narrow as possible without distorting the modulation in the adjacent channel. Companion studies [15] have shown that elliptic function filters with up to seven poles may be used at intermediate frequencies (typically 70 MHz) before the achievable unloaded Q's begin to limit the achievable rate of attenuation. It has also been shown that these filters may be group-delay equalized over their full equiripple bandwidth.

For the case of interest, the residual ripple component of group-delay was set to contribute  $\approx 100$  pWp to the overall noise budget, and the performance limit was determined by truncation noise caused by the abrupt attenuation at the filter band edge. In the adjacent channel interference study, the filter characteristics (summarized in Table 10) were set to balance the in-band impulse effects caused by truncation noise against the impulse effects caused by the adjacent channel.

For the entire range of parameters in the INTELSAT IV system, the con-

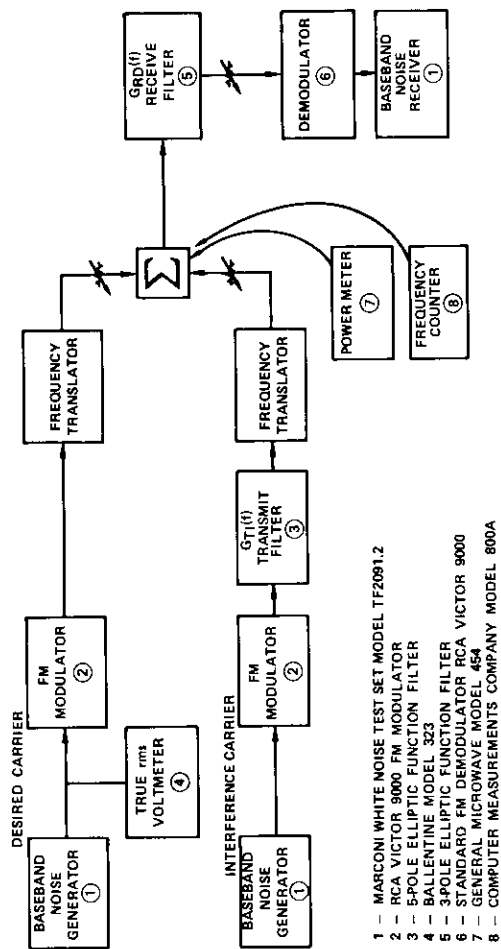


Figure 47. Measurement Setup

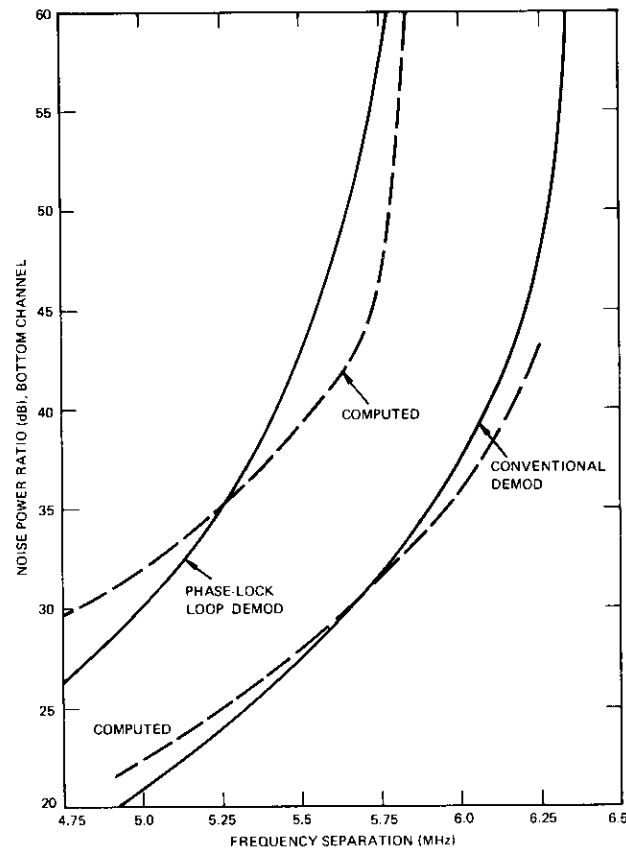


Figure 48. Comparison of Measured and Computed Adjacent Channel Interference Performance

cept of instantaneous frequency was used to predict the number of impulses. In addition, a phase-lock loop was modeled as a single-pole tracking filter (whose bandwidth was set approximately equal to the closed-loop bandwidth of the receiver), and a statistical distribution of center frequency was determined from the modulation statistics. The validity of this modeling for engineering purposes was confirmed by the accuracy with which the modeling predicted the onset of impulses as the adjacent carrier and its transmit filter were translated in frequency toward the desired carrier and its receive filter, and the statistical improvement offered by the use of a threshold extending receiver that could be logically characterized as a "narrow" tracking filter (see Figures 47 and 48).

## Transmission simulations

N. K. M. CHITRE

### Purpose

The individual mathematical models which adequately define the transmission impairments have been described in the previous section. However, it was necessary to ensure that the individual impairments were properly added before predicting the overall degradation. It was therefore deemed prudent to perform a transmission simulation of the INTELSAT IV communications system during the summer of 1970 to confirm its ability to meet the predicted performance requirements and to support the traffic for which it was designed. Additional objectives of the simulations program were to investigate the range of operating parameters over which the system could meet its performance objectives and to generate overall systems models.

### Test plan and simulation setup

In the overall system noise budget, thermal noise is the major component. Therefore, in an overall system test, all other impairments will be masked by noise and only gross errors in transmission modeling will be detected. Hence, this simulation has emphasized the importance of isolating and measuring the individual impairments through the INTELSAT IV transponder before performing the overall tests. The transmission impairments can be classified, as shown in Table 14, according to whether or not they are produced in the satellite, whether or not they are generated by one transponder in use, and whether the linear or nonlinear transfer characteristics of the transponder are involved.

**Simulation Test Setup.** An engineering model of the transponder assembled by the RF Transmission Laboratory at COMSAT Labs was used for this simulation. The transponder assembly basically consisted of one quadrant of the INTELSAT IV communications platform. In addition to the common low-noise receiver and driver TWT, it had three output TWTAs and associated filters. The three transponders were tuned to

*N. K. M. Chitre is Manager, Systems Simulation Department, Systems Division, COMSAT Laboratories.*

TABLE 14. TRANSMISSION IMPAIRMENTS

Transfer Characteristic	Satellite		
	Single Transponder	Two Transponders	Out of Satellite
Linear	Thermal Noise (up-link) Group-Delay Distortion	Multipath Group-Delay Distortion	Thermal Noise (down-link) Adjacent Carrier Interference
Nonlinear	Intermodulation Intelligible Crosstalk (in-band)	Adjacent Transponder Intermodulation Intelligible Cross-talk (out-of-band)	

channels 2, 3, and 4 of the INTELSAT IV frequency plan. A command console, which allowed external control of the gain settings, and transmission configurations of the transponders completed the assembly.

**Simulation Equipment.** The transmit side simulation equipment is shown in Figure 49. It was capable of generating and combining up to eight up-link, crystal-controlled carriers in the 6-GHz band. The level of each carrier was individually controlled and the total level of the carriers could be set by a separate control. Three of these carriers, which were generated by using standard earth station modulator up-converter chains, represented high-quality "wanted" and "interfering" carriers. The other five carriers, which were generated by directly modulating solid-state RF sources with bandlimited noise, represented the "loading" carriers.

On the receive side (Figure 50), two parallel receivers were available; both receivers were standard earth station down-converter demodulator chains. A calibrated IF noise generator was used to insert the down-link equivalent noise for the overall NPR tests.

### Frequency plans

For the FDM/FM tests, two representative frequency plans, each including the associated spot- or global-beam operating parameters, were used during the simulation. Figure 51 shows the carrier arrangements chosen for the two plans. The baseband frequencies, multichannel and test-tone deviations, and relative carrier levels, listed in Table 15, were in

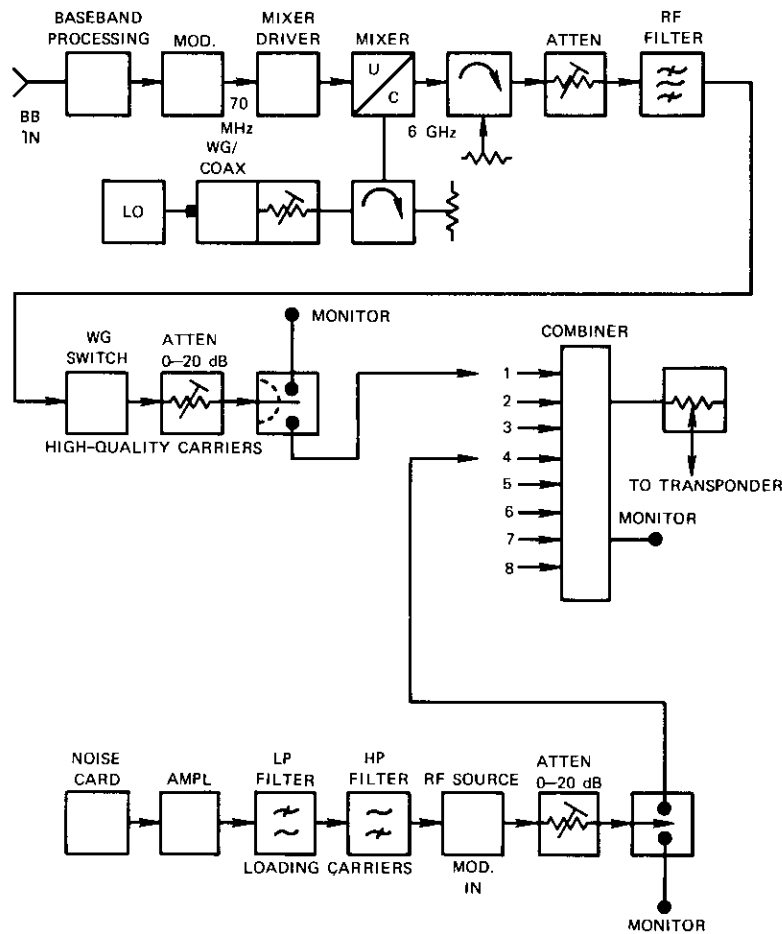


Figure 49. Simulation Equipment, Transmit Side

accordance with the INTELSAT IV transmission standards. The complete video reference link, with its associated audio and return audio channels, was simulated in accordance with the third frequency plan given in Table 15. Pre-emphasis and de-emphasis networks were in accordance with C.C.I.R. rec. 275-1 [22] for FDM/FM tests and C.C.I.R. rec. 405, curve B, for video tests [23].

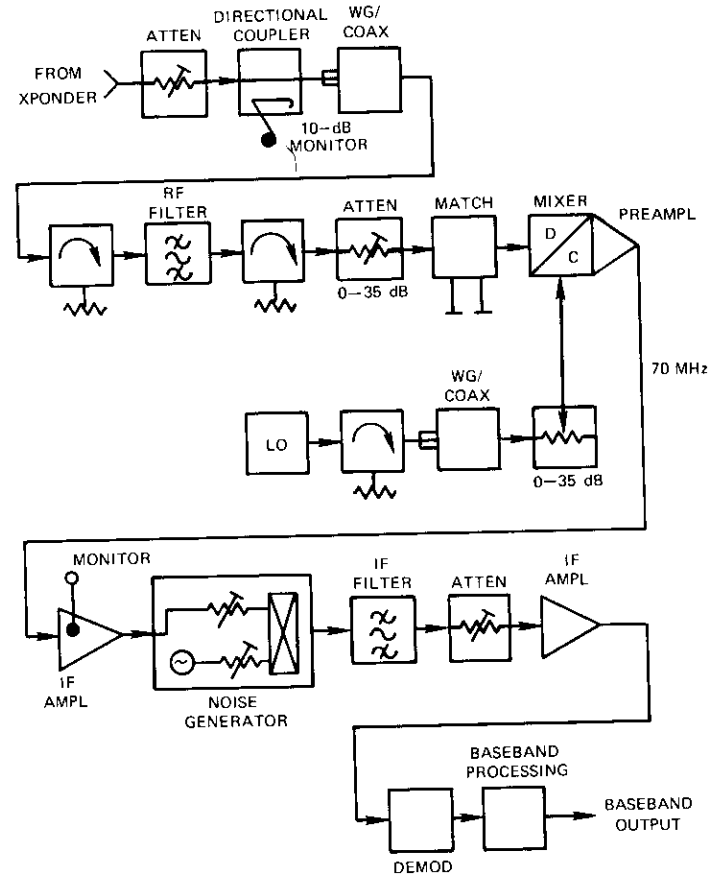


Figure 50. Simulation Equipment, Receive Side

**Results of measurements**

**In-Band Intermodulation Products. RF Levels.** To locate the frequencies and normalized output levels of the third-order intermodulation products (and some of the larger fifth-order intermodulation products) generated in the output TWTA, the unmodulated input carriers were inserted at the correct relative levels. Figure 52 shows the output spectrum, referenced to the output level of a single carrier at saturation, for the frequency plans of simulations 1 and 2. The levels of the output carriers and the

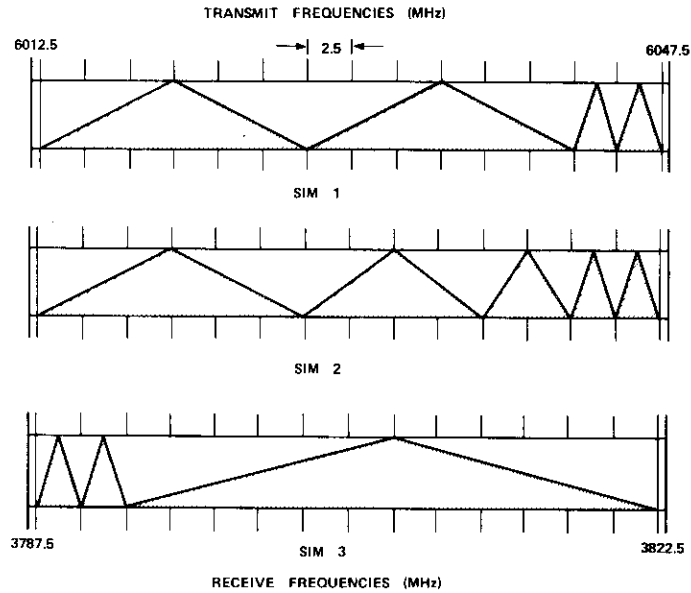


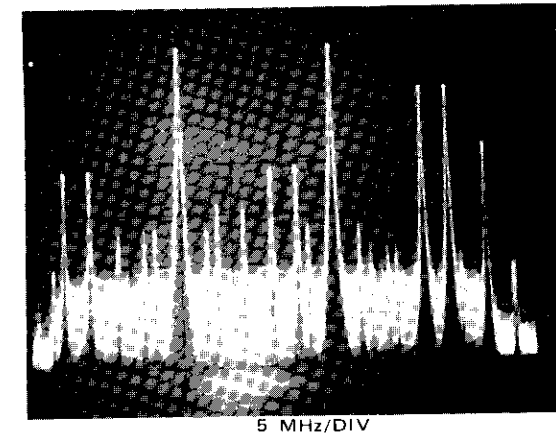
Figure 51. Frequency Plans

intermodulation products were measured at various input backoffs and compared with the levels predicted by using a computer program based on the principles included in the previous section. This comparison, shown in Figure 53, indicates a close agreement between the predicted and measured levels of all carriers and intermodulation products except those at levels which were too low to measure accurately.

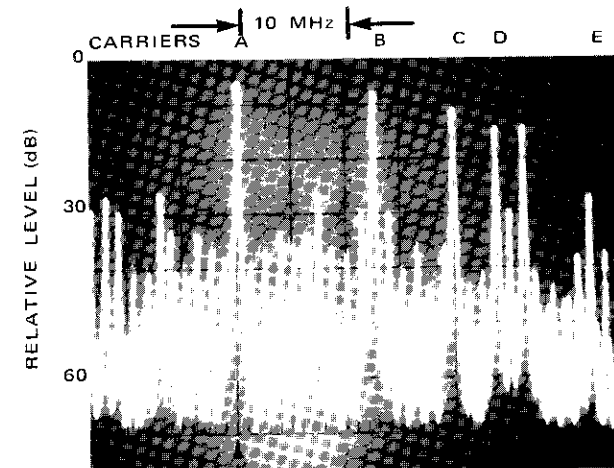
**Baseband Distortion.** To evaluate the baseband distortion produced by intermodulation products generated in a TWTA operating in a multi-carrier mode, an overall system model was assembled by using the principles outlined in the previous section. The inputs to this model were the frequency plans and transmission parameters of Table 15, and the outputs were the NPR and baseband noise (expressed in pWOp) in the top slot on each carrier. The calculated distortion for the simulation 2 frequency plan at nominal operating levels is indicated in Table 16.

It is interesting to note that the distortion is distributed quite unevenly and that carrier A in the global-beam configuration has very little distortion. The latter effect is partly caused by the preponderance of symmetrical twin intermodulation products of the type  $A \pm (X - Y)$  in the

CARRIERS: A B C D



FREQUENCY PLAN: SIMULATION 1, INPUT BACKOFF = 6 dB



FREQUENCY PLAN: SIMULATION 2, INPUT BACKOFF = 6 dB

Figure 52. Output Spectrum

TABLE 15. FREQUENCY PLANS AND TRANSMISSION PARAMETERS FOR SIMULATIONS

a. Frequency Plan 1					
Parameters	Carrier Designation				
	A	B	C	D	
Transmit Frequency (MHz)	6020.00	6035.00	6043.75	6046.25	
Receive Frequency (MHz)	3795.00	3810.00	3818.75	3821.25	
Nominal Bandwidth (MHz)	15.0	15.0	2.5	2.5	
Global Beam					
Number of Channels	252	252	24	24	
Baseband (kHz)	12-1052	12-1052	12-108	12-108	
rms Deviation (kHz)	1627	1627	274.7	274.7	
Test-Tone Deviation (kHz)	577	577	164	164	
Relative Carrier Input Levels (dB)	0.0	0.0	-8.1	-8.1	
Spot Beam					
Number of Channels	432	432	60	60	
Baseband (kHz)	12-1796	12-1796	12-252	12-252	
rms Deviation (kHz)	1479	1479	275.5	275.5	
Test-Tone Deviation (kHz)	401	401	136	136	
Relative Carrier Input Levels (dB)	0.0	0.0	-7.0	-7.0	
b. Frequency Plan 2					
Parameters	Carrier Designation				
	A	B	C	D	E
Transmit Frequency (MHz)	6020.00	6032.50	6040.00	6043.75	6046.25
Receive Frequency (MHz)	3795.00	3807.50	3815.00	3818.75	3821.25
Nominal Bandwidth (MHz)	15.00	10.00	5.00	2.50	2.50
Global Beam					
Number of Channels	252	132	60	24	24
Baseband (kHz)	12-1052	12-552	12-252	12-108	12-108
rms Deviation (kHz)	1627	1019	545.80	247.70	247.70
Test-Tone Deviation (kHz)	577.00	430.00	270.00	164.00	164.00
Relative Carrier Input Levels (dB)	0.0	-2.2	-5.0	-8.1	-8.1

TABLE 15. FREQUENCY PLANS AND TRANSMISSION PARAMETERS FOR SIMULATIONS (continued)

Parameters	Carrier Designation				
	A	B	C	D	E
Spot Beam					
Number of Channels	432	252	132	60	60
Baseband (kHz)	12-1796	12-1052	12-552	12-252	12-252
rms Deviation (kHz)	1479.00	1009.00	528.00	275.50	275.50
Test-Tone Deviation (kHz)	401.00	358.00	236.00	136.00	136.00
Relative Carrier Input Levels (dB)	0.0	-3.0	-4.5	-7.0	-7.0
c. Frequency Plan 3					
Parameters	Channel/Carrier Designation				
	Audio/A	Return Audio/B	Video/C		
Transmit Frequency (MHz)	6013.25	6015.75	6033.00		
Receive Frequency (MHz)	3788.25	3790.75	3898.00		
Nominal Bandwidth (MHz)	2.5	2.5	30.0		
Number of Channels	24	24	Video		
Baseband (kHz)	12-108	12-108	DC-4200		
rms Deviation (kHz)	275.5	275.5	—		
Peak-to-Peak Test-Tone Deviation (MHz)	—	—	21.0		
Relative Carrier Input Levels (dB)	-12.6	-12.6	0.0		

TABLE 16. BASEBAND DISTORTION CAUSED BY INTERMODULATION PRODUCTS (simulation 2 frequency plan)

Carrier Designation	Calculated Intermodulation Distortion (pW0p)	
	Global-Beam Parameters (nominal input backoff = 11 dB)	Spot-Beam Parameters (nominal input backoff = 16 dB)
A	173	523
B	1000	998
C	266	274
D	450	331
E	520	373

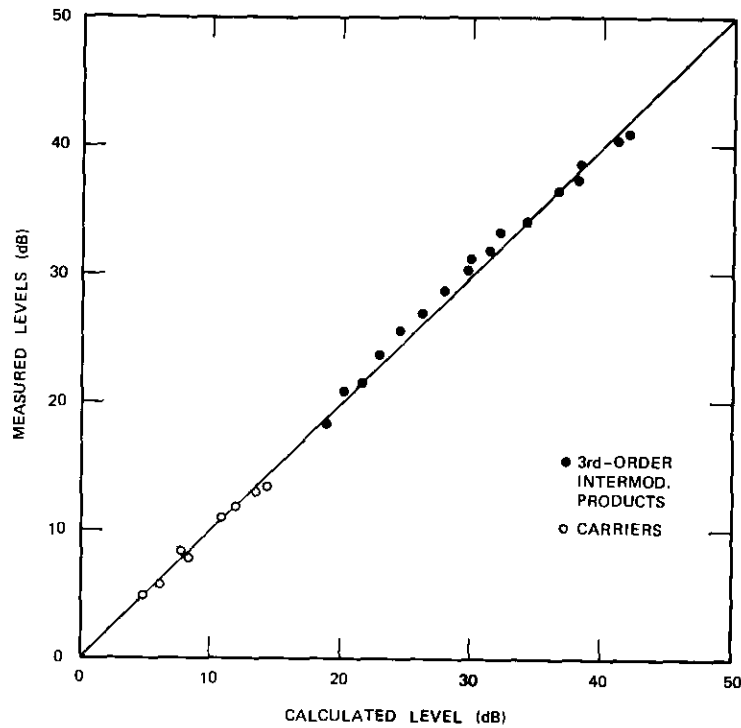


Figure 53. Comparison of Calculated and Measured Intermodulation Levels

vicinity of carrier A. As discussed in the previous section, the in-phase components of these products do not contribute to baseband distortion.

Many distortion contributors are included in an NPR measurement. Furthermore, under "nominal" conditions the intermodulation noise is only a fraction of the total. It is thus necessary to deviate from nominal operating conditions to isolate the NPR resulting from intermodulation. This was accomplished by reducing the thermal noise to a minimum and measuring the NPR of each carrier under both single- and multiple-carrier conditions with the TWTA operated closer to saturation.

Figure 54 summarizes the comparison of measured and calculated NPR caused by intermodulation products for some of the carrier configurations. In view of the average tube constants used in the calculations and the margin which had to be included for measurement errors, the agreement between the measured NPR and the predictions is quite good.

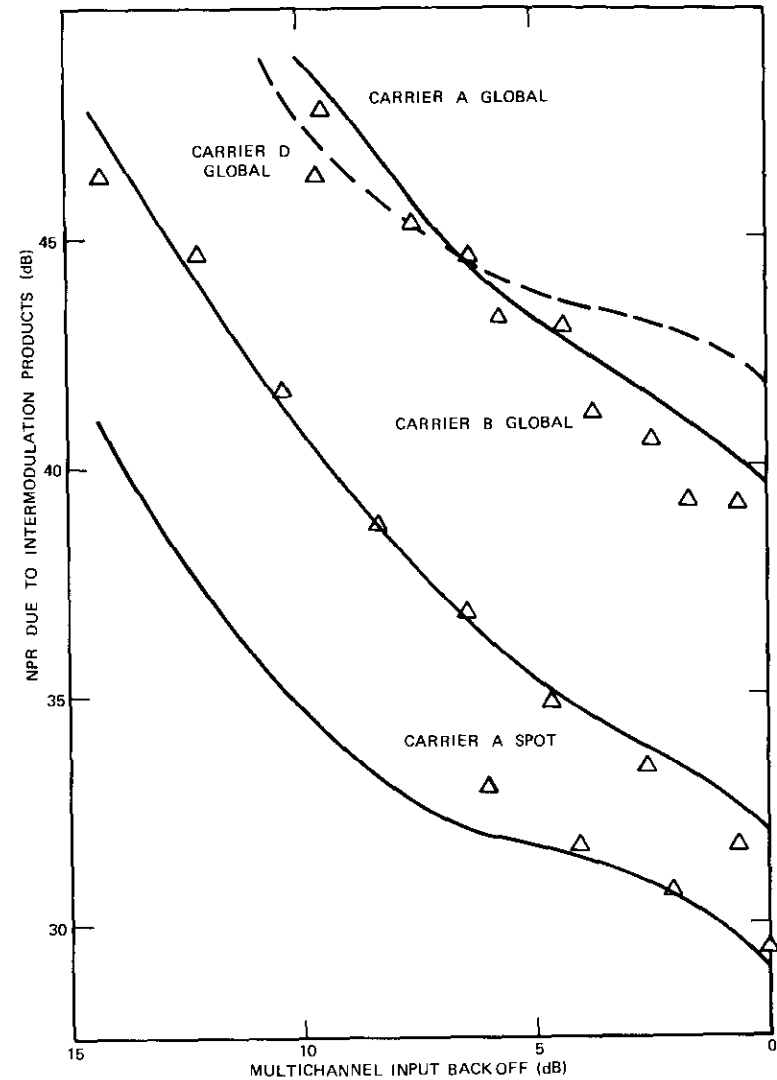


Figure 54. NPR vs Input Backoff

**Out-of-Band Intermodulation Products.** The intermodulation products generated by nonlinear amplification of multiple carriers in a transponder occupy a frequency band approximately three times the width of one transponder channel. Thus some of the intermodulation noise spills over

into the adjacent transponder channels, where protection is provided by only the output multiplexer filters.

To evaluate the degradation caused by this out-of-band intermodulation, it was assumed that transponder 3 was loaded with the frequency plan of simulation 2. The first step was to calculate and measure the intermodulation noise spectral density falling in transponders 2 and 4. This is plotted in Figure 55, where the noise density is measured in a 100-kHz

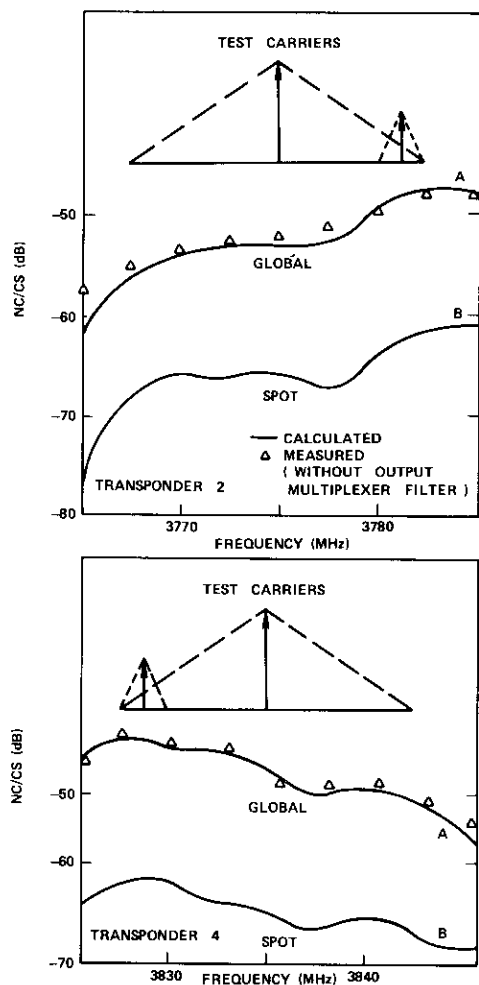


Figure 55. NPR vs Input Backoff for Transponder no. 3

band and normalized to the single-carrier saturated output of the TWTAs. Curves A and B refer to global carrier loading with 16-dB backoff. Without the output multiplexer filters, the noise density decreases slowly across the band; with the filters, it decreases at about 2 dB per MHz.

The size and capacity of the carriers located at the edge of the band in transponders 2 and 4 determine the amount of degradation which will be produced. The small carriers with nominal bandwidths of 2.5 MHz are located in regions of high intermodulation noise density and will therefore be particularly susceptible to degradation.

The measured and calculated NPR caused by adjacent transponder intermodulation in a global 2.5-MHz carrier is plotted in Figure 56 as a function of the TWTA backoff in transponder 3 with and without a typical output multiplex filter. Table 17 gives the NPR resulting from out-of-band intermodulation for various carriers. It should be noted that, when two adjacent transponders are connected to global- and spot-beam antennas, respectively, the degradation depends on the relative gain through the two beams at the location of the earth station. Table 17 assumes that the gain in the spot beam is 11 dB higher than that in the global beam.

TABLE 17. NPR IN A TEST CARRIER IN THE ADJACENT TRANSPONDER \*

Loading in Transponder 3	Test Carrier	Nominal Bandwidth (MHz)	Noise Power Ratio (dB)	
			Transponder 2	Transponder 4
Global Frequency Plan 2	Global	2.5	48.0	47.5
	Spot		46.3	45.8
	Global	15	59.7	57.2
	Spot		60.2	57.7
Spot Frequency Plan 2	Global	2.5	51.0	50.5
	Spot	15	49.3	48.8
	Global		60.2	57.7
	Spot		60.7	58.2

\*Nominal operating parameters and suppression resulting from the use of a typical output multiplexer filter are assumed.

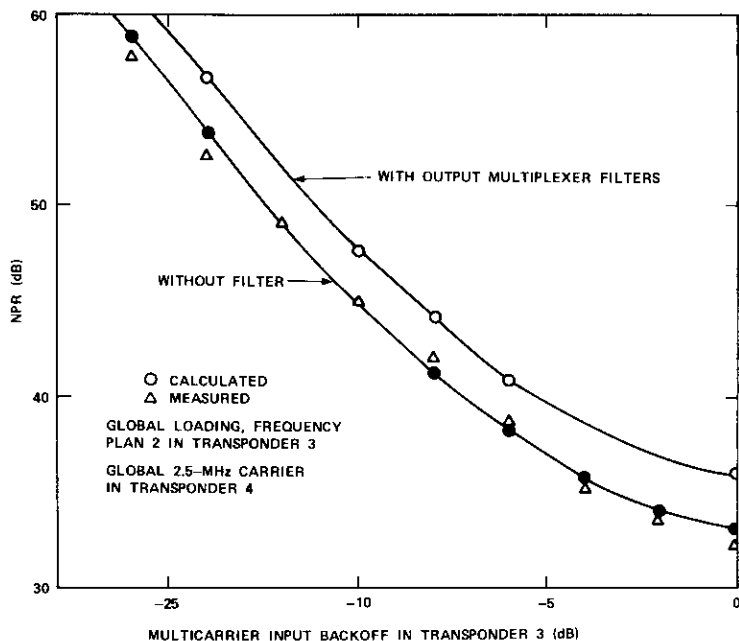


Figure 56. Measured and Calculated NPR vs TWTA Backoff for Transponder no. 3 with and without a Typical Output Multiplex Filter

Degradation of the smaller carriers at the transponder edges as a result of adjacent transponder intermodulation is significant enough to be considered during the frequency planning and allocation phase.

**Intelligible Crosstalk. Worst Crosstalk Configuration.** The INTELSAT IV system parameters have been used to calculate the carrier combination which results in the worst crosstalk for a given input gain slope. For the global-beam configuration, the worst crosstalk configuration consisted of two 252-channel carriers; for the spot-beam configuration; it consisted of two 432-channel carriers.

**Crosstalk Measurements.** Since all other carrier configurations can be related to the worst crosstalk configurations through the adjustment factors given in Table 18, laboratory measurements of only the worst crosstalk cases were conducted.

The crosstalking carrier was noise modulated in the conventional

manner using the appropriate INTELSAT IV parameters, but the top base-band channel was replaced by a 0-dBm0 test tone. A measurement of the test tone transferred from the crosstalking carrier to the wanted carrier indicated the amount of crosstalk produced.

TABLE 18. ADJUSTMENT FACTORS IN CROSSTALK RATIOS FOR OTHER THAN WORST-CASE CARRIER SIZES

a. Global-Beam Configuration					
Crosstalking Carrier Size (channels)	Wanted Carrier Size (channels)				
	24	60	96	132	252
Adjustment in Crosstalk Ratio (dB)					
24	-35	-34	-35	-36	-38
60	-30	-22	-21	-21	-22
96	-23	-20	-15	-14	-13
132	-22	-18	-13	-9	-7
252	-16	-12	-10	-7	0

b. Spot-Beam Configuration					
Crosstalking Carrier Size (channels)	Wanted Carrier Size (channels)				
	60	132	192	252	432
Adjustment in Crosstalk Ratio (dB)					
60	-31	-30	-31	-33	-33
132	-27	-19	-19	-18	-18
192	-24	-18	-14	-14	-11
252	-22	-17	-14	-11	-8
432	-15	-11	-10	-8	0

Measurement results of the worst-case crosstalk configuration are plotted in Figures 57 and 58 for the global- and spot-beam configurations, respectively. For the global-beam configuration, the worst measured in-band crosstalk is -58 dB, which barely meets the appropriate C.C.I.T.T. specification. However, this configuration of two 252-channel global carriers in a transponder is certainly not typical. A more realistic operational worst-case configuration will result in an expected crosstalk ratio

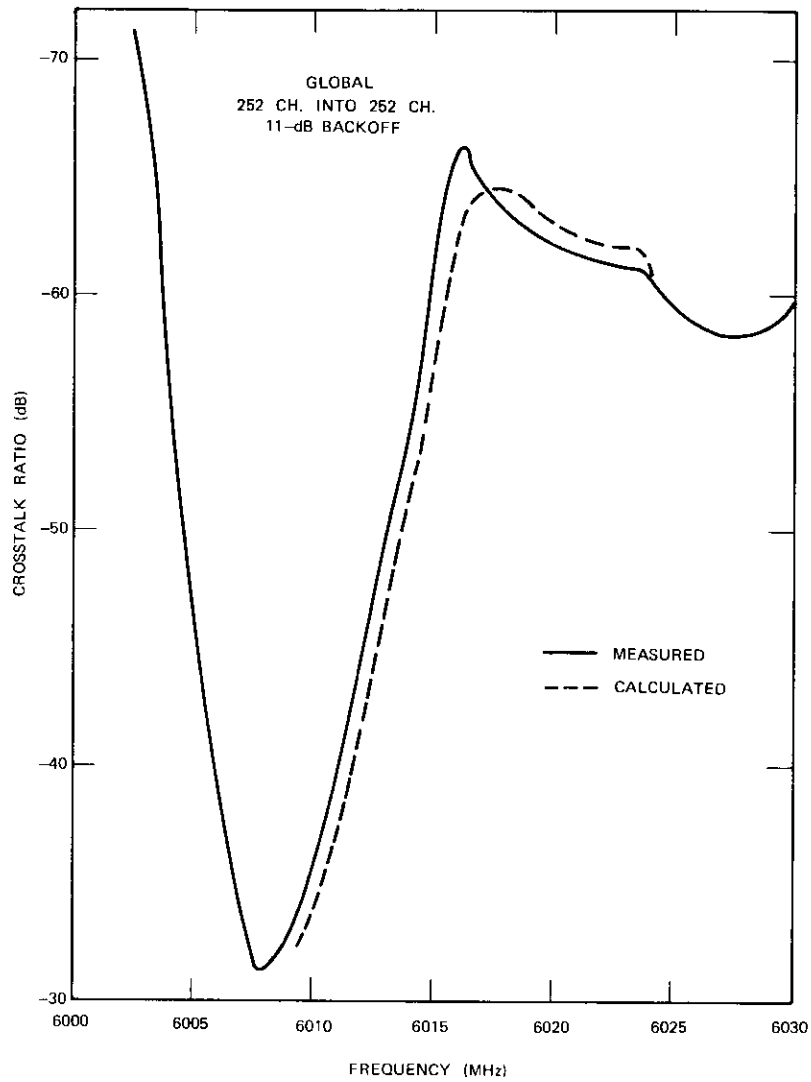


Figure 57. Worst Global-Beam Crosstalk

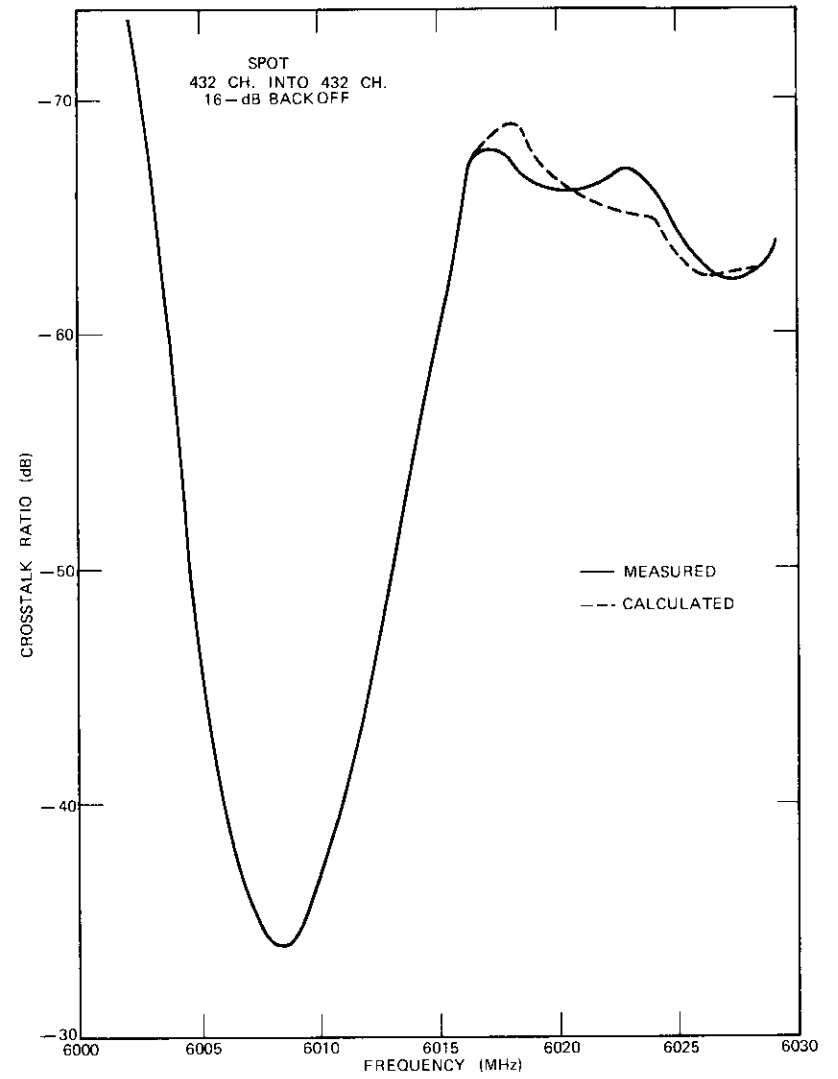


Figure 58. Worst Spot-Beam Crosstalk

of about  $-65$  dB, which is well within the  $-58$ -dB specification (see Table 19). These calculated values were derived from the model described in the previous section, which included Gaussian power averaging over the first two AM sidebands and a weighted TWTA gain response to take into account any additional AM generated within the TWTA.

It is apparent from this study that the out-of-band crosstalk, which monotonically decreases as the crosstalking carrier is moved further out-of-band, is less than  $-70$  dB for a nominal carrier location in the adjacent channel. Even if a spot-beam carrier is positioned next to a global-beam transponder on one occasion, less than  $-70$  dB of crosstalk can be expected, since the adjustment in the carrier sizes more than compensates for the higher input level of the adjacent channel spot carrier. Therefore, it appears that the in-band entry will be the dominant contributor to crosstalk in the INTELSAT IV system.

The intelligible crosstalk ratio is dependent on the total amplitude responses of the earth station equipment, the satellite receiver, the input multiplexer and its associated equalizer, and the TWTA. The major contribution to crosstalk appears to be the first derivative of the gain variation or gain slope. It has been experimentally verified that the addition of a simple gain-slope equalizer at the transmit side leads to a considerable reduction in the crosstalk ratio.

**Linear Dispersion.** The transmission distortion caused by group-delay and amplitude transfer responses across the transponder frequency band was evaluated first for the responses assumed during the planning stage (ICSC/T-33-10 [24]) and then for the measured responses of transponder 3 in the simulation setup. In both cases, the distortion was computed for the maximum carrier displacement from the transponder center frequency. The results are listed in Table 19. Since no group-delay equalization was assumed, there was a high value of distortion in the case of the large carrier.

The overlap in the filter skirts of the input and output multiplexers, resulting in imperfect isolation between adjacent transmission channels, causes dual-path transmission and modifies the overall transfer response. Laboratory measurements of distortion were made for the 24-channel global-beam carrier and the 60-channel spot-beam carrier with the adjacent transponder set for equal gain but variable phase. The dual-path distortion was measured as a function of the carrier center frequency for the worst phase difference. The results of the dual-path distortion (NPR) are plotted in Figure 59 and compared with the calculated values.

TABLE 19. TRANSMISSION DISTORTION (SINGLE PATH)

Carrier Designation	Maximum Frequency Displacement (MHz)	Assumed Responses from ICSC/T-33-10		Measured Responses of Transponder 3	
		NPR in the Top Channel (dB)	Transmission Distortion, $N_p$ (pW)	NPR in the Top Channel (dB)	Transmission Distortion, $N_p$ (pW)
G 24	16.25	70.5	4	66.7	11
G 60	15.00	62.5	16	60.1	29
G 96	13.75	59.5	24	60.7	19
G 132	12.50	59.5	20	59.6	20
G 252	10.00	56.5	30	52.2	80
G 432	5.00	52.8	70	50.0	133
G 900	0	36.8	2,780	43.3	622
G 960	0	37.3	2,480	42.9	685
<hr/>					
S 60	16.25	63.3	14	59.3	4
S 132	15.00	55.1	55	53.6	78
S 192	13.75	54.3	53	54.9	47
S 252	12.50	54.3	50	53.6	59
S 432	10.00	52.8	70	48.3	196
S 612	7.50	47.8	224	45.7	356
S 792	5.00	48.0	212	45.0	420
S 1,500	0	34.3	5,000	40.7	1,055
S 1,800	0	34.3	4,790	39.3	1,495

For the 24-channel global-beam carrier and the 60-channel spot beam carrier at nominal carrier locations, the distortion contributions are 35 and 180 pW0p, respectively; however, the distortion rises very steeply as the carriers are offset.

**Adjacent Carrier Interference.** Adjacent carrier interference tests were conducted for a 132-channel carrier interfering with a 24-channel carrier having a relative carrier power of 8.9 dB, which is 3 dB higher than that specified for the INTELSAT IV system. NPR and impulse rates were measured as the desired channel C/N and carrier separation were varied. The impulse counter was set to count whenever the voltage in the 34-kHz slot exceeded  $-22$  dBm0. Test were performed on both the IF and transponder loops.

Results indicate that, for transmission through the transponder or

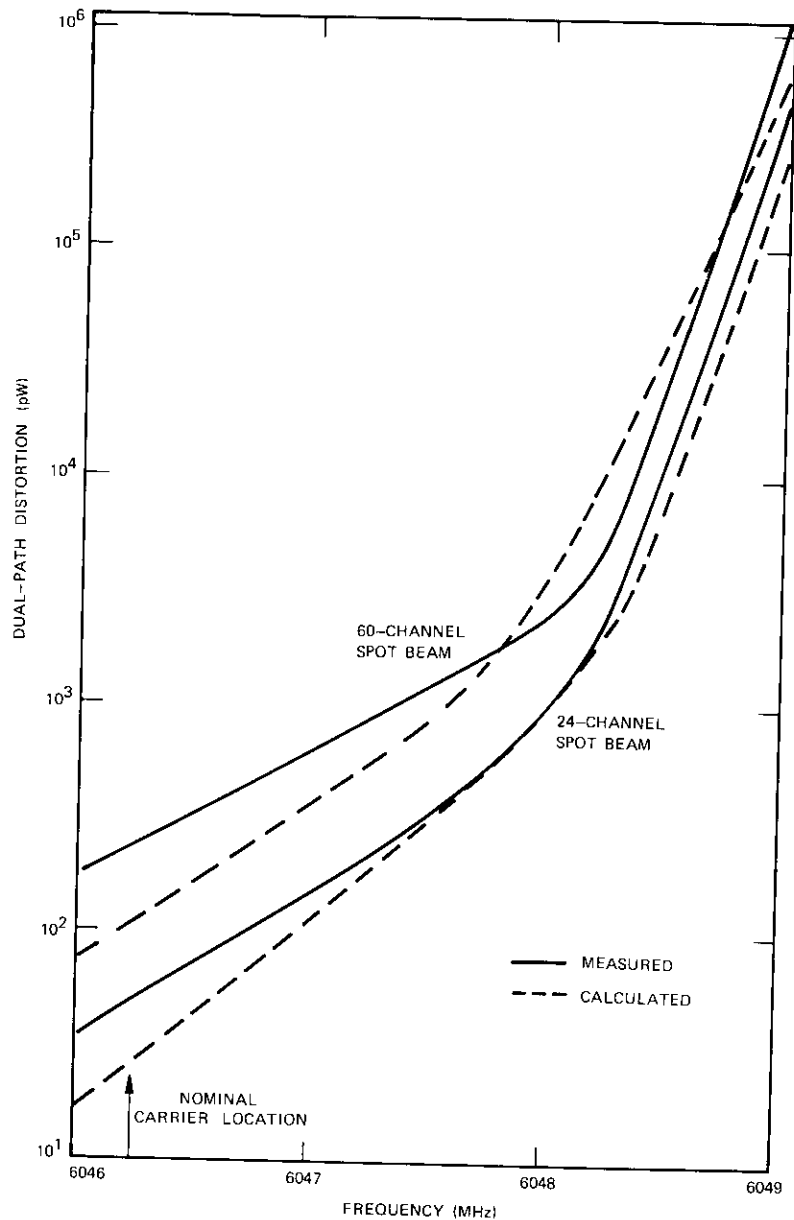


Figure 59. Worst Phase Dual-Path Distortion

IF loop, the NPR contributions as functions of C/N and carrier separation are essentially the same, at least for values of C/N above threshold. Above threshold the NPR contributions from adjacent channel interference and thermal noise are essentially independent; the total impairment is simply the sum of the individual impairments.

As shown in Figure 60, below threshold, cross products arise and the NPR caused by adjacent channel interference is a function of both carrier separation and C/N. A similar effect is observed in the impulse rate test (see Figure 61).

**Overall Impairments.** It appeared to be more fruitful to depart from nominal conditions to determine the effect of changes in some parameters on the total measured NPR. The basic tradeoff between down-link thermal noise and intermodulation noise was experimentally determined to establish a range of parameters over which the system could meet its performance objectives.

Although the final objective of a frequency plan evaluation is the adjustment of the relative carrier levels until all carriers exhibit a relatively uniform degradation (in picowatts), this was not attempted here. Instead, it was attempted to map the resulting measured noise performance for a range of multichannel input levels and transponder gain settings. Hence, lines of constant crosstalk could be shown.

Representative results of such measurements are shown in Figure 62 for the largest carrier in a 5-carrier frequency plan in the spot-beam configuration. The effect of intermodulation noise on carrier A, as noted earlier, is considerably less than the effect which may have been predicted by the prevalent intermodulation theory. Therefore, the noise can be considerably reduced if the multicarrier input power is increased from nominal and the optimum transponder attenuator setting is used.

Also shown in Figure 62 are lines corresponding to combinations of input power and transponder gain setting which result in constant crosstalk. The crosstalk values correspond to the worst-case conditions discussed earlier, and the factor A represents the adjustment factor for the worst-case configuration.

#### FM/video transmission

The frequency plan of simulation 3 was used to evaluate FM/video transmission in the INTELSAT IV system. During these tests, only transponder 3 was activated; its transmission parameters are listed in Table 20.

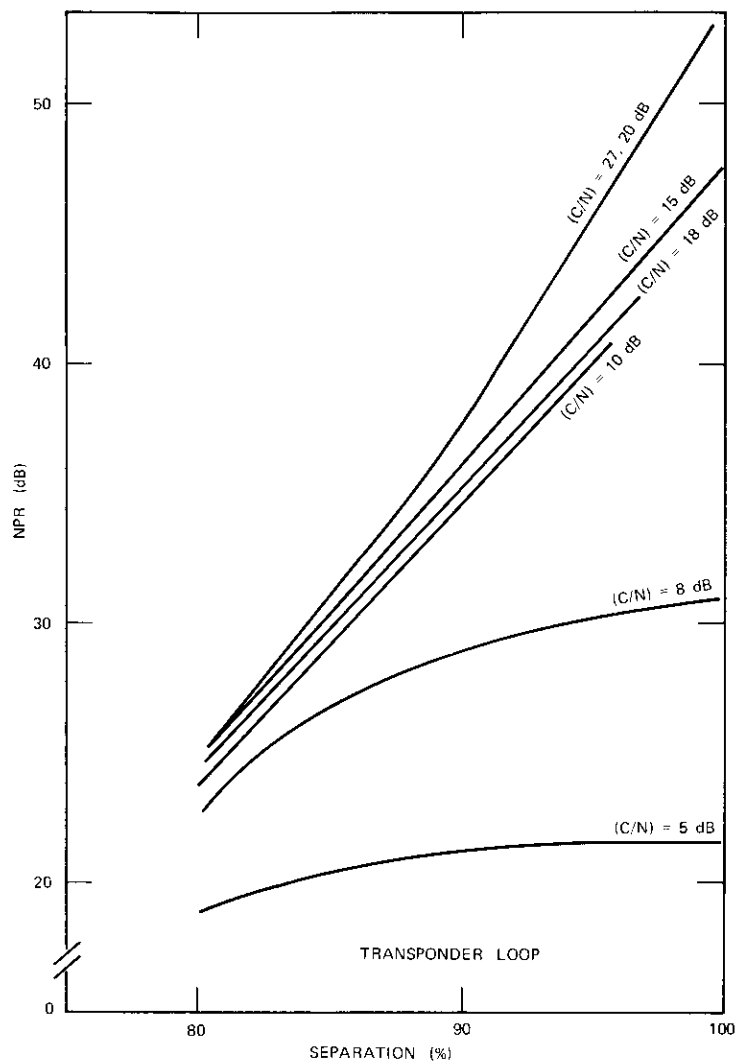


Figure 60. NPR Caused by Adjacent Channel Interference vs Channel Separation

Intermediate-frequency filters with nominal bandwidths of 2.5 and 30.0 MHz for the audio and video carriers, respectively, were used on the receive side. These filters meet the "preferred" requirements of ICSC/T-45-13

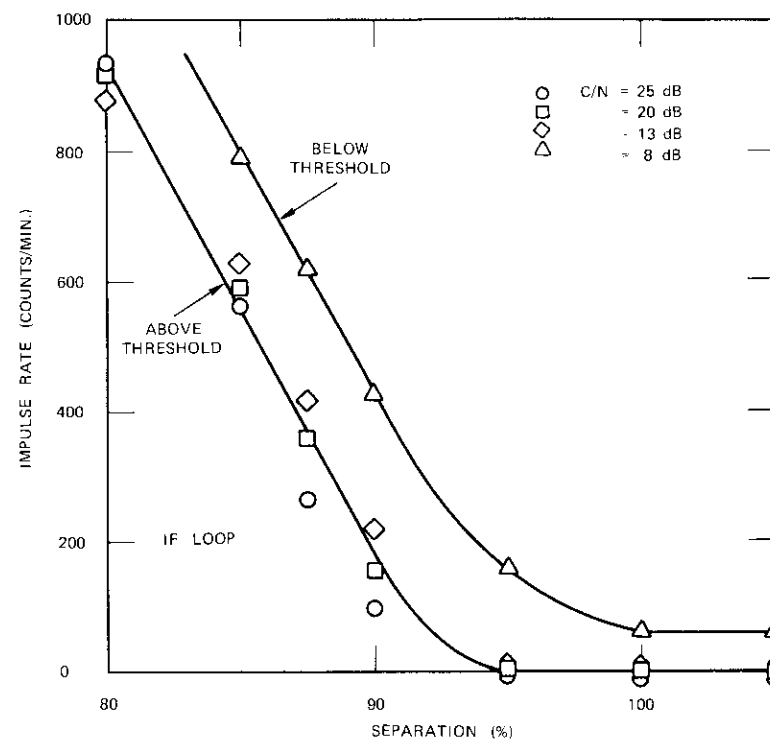


Figure 61. Impulse Rate vs Channel Separation

[25]. A noise weighting network in accordance with C.C.I.R. recommendation 421-1 [3] for system M was used to measure the weighted signal-to-noise ratio  $(S/N)_w$  in the video channel.

The intermodulation products causing the most degradation in the video channel were expected to be twin  $C \pm (B - A)$  products whose

TABLE 20. TRANSMISSION PARAMETERS FOR TRANSPONDER 3

Gain Setting	1
Input for Single-Carrier Saturation	-82.5 dB (W)
Noise Temperature	44.2 dB ( $^{\circ}$ K)
C/T Up-Link at Single-Carrier Saturation	-130.1 dB (W/ $^{\circ}$ K)

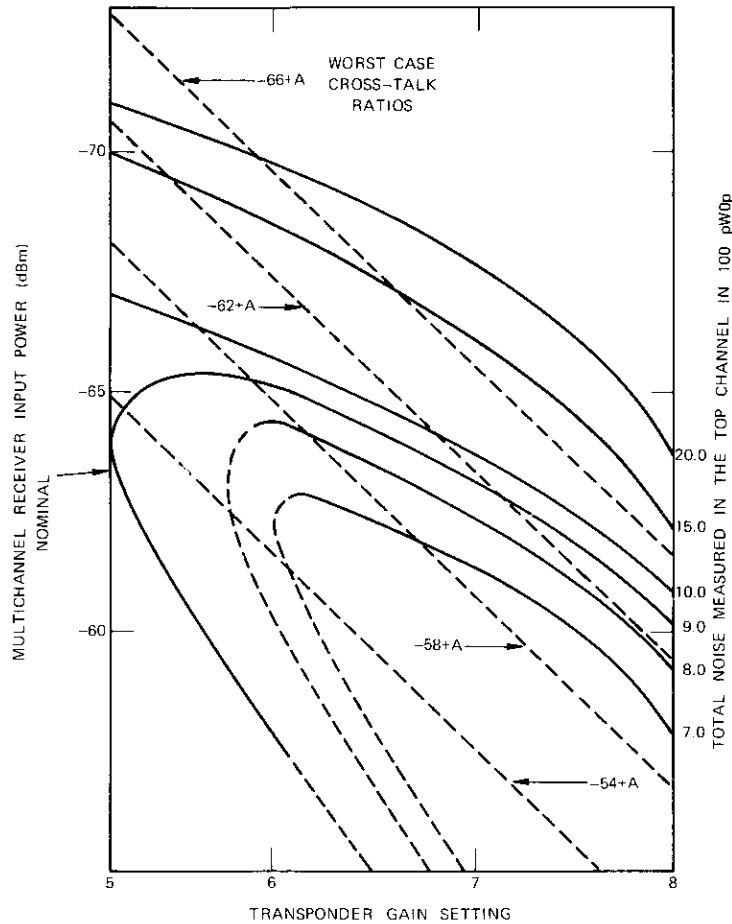


Figure 62. Noise Contours for Channel A, Simulation 2, Spot Beam

measured RF level was only 31 dB below the video carrier. However, only the phase quadrature component of the intermodulation products appears at the demodulated output; consequently, very little degradation results. Table 21 summarizes the various contributions of weighted noise over the video link. The initial estimate of the total  $(S/N)_w$  was approximately 1.4 dB larger than the simulation measurement because it included a slightly higher up-link thermal noise and an allowance for in-phase intermodulation product contributions. Further tests confirmed that the

TABLE 21. CONTRIBUTIONS TO  $(S/N)_w^a$

Source	C/T (dBW/°K)		$(S/N)_w$ (dB)	
	Initial Estimate	Simulation Measurement	Initial Estimate	Simulation Measurement
Up-Link Thermal Noise	-132.8	-132.5	58.4	58.6
Down-Link Thermal Noise	-134.4	-134.4	56.8	56.8
Amplitude Nonlinearity	-131.1 <sup>b</sup>	-	60.1	-
Intermodulation	-	-	-	-
Phase	-125.1 <sup>b</sup>	-122.6	66.1	68.6
Total	-138.0 <sup>b</sup>	-136.6	53.2	54.6

<sup>a</sup> Input transponder backoff = 2.4 dB, output transponder backoff = 0.1 dB.  
<sup>b</sup> Equivalent carrier-to-noise temperature ratio.

degradation in  $(S/N)_w$  caused by the presence of two audio carriers was less than 0.1 dB for all values of transponder backoff.

The differential phase and gain of the overall simulation link were initially measured without group-delay equalization; a linear group-delay equalizer (-0.65 ns/MHz) was later added to the transmit side. The measured results are compared with the INTELSAT IV video link objectives in Table 22. During these tests, although the two audio carriers were present in the transponder, they were unmodulated.

TABLE 22. DIFFERENTIAL PHASE AND DIFFERENTIAL GAIN

Amplitude and Phase Linearity	INTELSAT IV Video Link Objectives	IF Loop Measurements	Simulation Link	
			Unequalized	Equalized
Differential Phase				
10%	±3°	Negligible	+1.5°	<1°
50%	±3°	Negligible	+4.1°	<1°
90%	-	+0.5°	+5.2°	+1.4°
Differential Gain				
10%	10%	Negligible	+4.5%	-
50%	10%	Negligible	+3.0%	-
90%	-	2%	+3.0%	+3.0%

### Remarks

The results of the simulations indicated that the INTELSAT IV transmission system would exceed its performance objectives for both telephony and video transmissions. During the course of these simulations a major effort was expended to generate overall transmission systems models which could directly predict the baseband (or video channel) distortion from various impairment mechanisms in the earth station to satellite to earth station link.

These overall models, which proved very useful during the field tests described in the following section, have been integrated into the planning models. The promising results obtained from the laboratory simulations and the subsequent field test also led to increased interest in a tradeoff between performance and capacity. The simulations and the overall models have thus contributed to the proposed capacity increase per transponder by making possible the use of expanded capacity carriers.

### Field tests

P. H. SCHULTZE AND B. A. PONTANO

During the months of June and July of 1971, FM multicarrier telephony testing was conducted on transponder no. 5 of INTELSAT IV F-2, the Atlantic primary satellite, from the Cayey, Puerto Rico, earth station. The primary purpose of the testing program was to acquire sufficient data to permit a thorough assessment of the system models under operational conditions. A combination of INTELSAT IV carrier sizes, including some expanded carriers, was devised for the test programs. One of these frequency plans was used in the laboratory simulation studies to provide a common bridge between laboratory, theoretical, and field test results. The field test program was also intended to determine the extent to which the INTELSAT IV satellite system could be loaded without sacrificing C.C.I.R. performance quality in the worst channel for each carrier. In

*P. H. Schultze is Manager, Engineering Economics, Systems Division, COMSAT Laboratories.*

*B. A. Pontano is Manager, Laboratory Simulation, Systems Division, COMSAT Laboratories.*

addition, transmission impairments, including intermodulation in the satellite traveling wave tube amplifiers (TWTAs) and dual-path transmission through adjacent transponders, and the extent to which crosstalk might limit the use of large carriers were investigated.

The frequency plans implemented in the field are shown in Figure 63. The frequency plan for case 1 was used in the laboratory simulation and is included here to provide a comparison with these measurements. The original frequency plan for case 2 included carriers which were larger than had been planned so that a heavy load could be placed on the transponder's available power. The frequency plan for case 3 was intended to test spot-beam

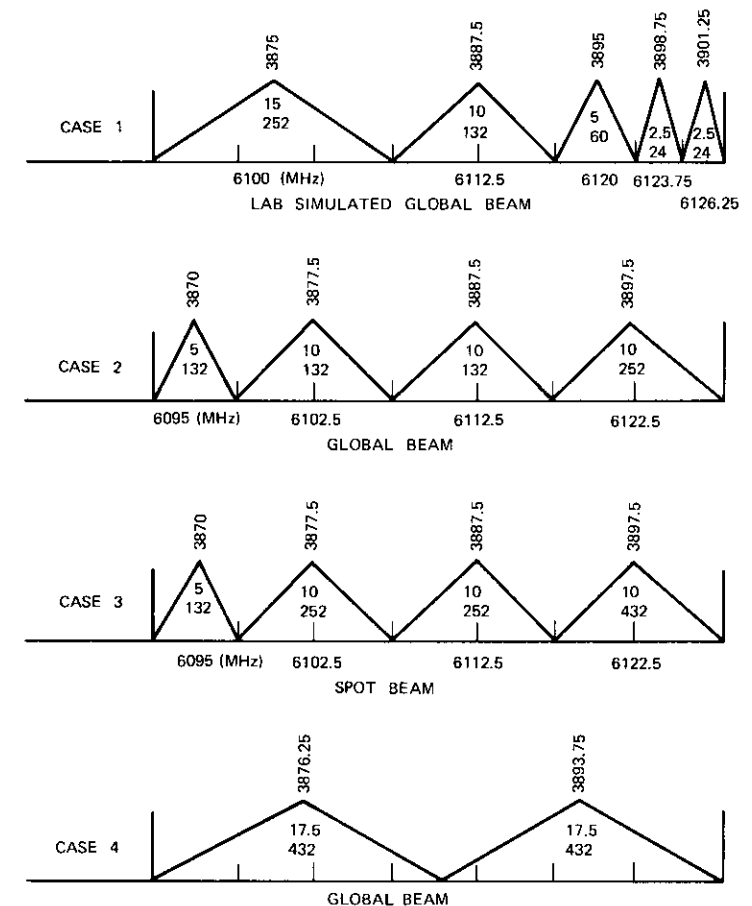


Figure 63. Test Frequency Plans

operation, and the case 4 frequency plan was a dual-carrier plan developed for contingency traffic restoration. These plans were tested at the nominal TWTA operating points shown in Table 23 as well as at regular increments which were above and below these points, but within equipment limitations and thresholds.

**Intermodulation noise**

To estimate the expected performance of the various frequency plans tested, the satellite system noise was calculated for the worst (top) telephony channel as a function of the satellite operating point. The computer model used to calculate the expected values of the NPR in the top channel included the three major sources of noise and interference:

- a. up-link thermal noise, governed by satellite sensitivity, G/T, and up-link power;
- b. down-link thermal noise, governed by earth station G/T and satellite e.i.r.p.; and
- c. intermodulation noise, governed by TWTA amplitude and phase nonlinearities.

Although other smaller noise sources, such as out-of-band emissions caused by the transmit chain nonlinearities of 13 earth station amplifiers, receiver impairments, and adjacent channel interference, are an inherent part of the measured data, they were not included in the model because their contributions were minimal. Other tests for crosstalk, group delay, and dual-path transmission were used to isolate additional transmission impairments. System noise components were computed by using a computer model similar to the one used for the previous system evaluation.

The results of these calculations give the NPR for each of the carriers in the test plans as a function of transponder operating point and gain setting. Figures 64 to 68 show calculated and measured performance for each carrier of test case I. Note that measured data are in good agreement with calculations over a wide range of operating points.

In addition to the loading tests discussed in the previous paragraphs, tests on carrier crosstalk and dual-path transmission effects were performed.

**Intelligible crosstalk**

Intelligible crosstalk is generated when two or more angle-modulated carriers are passed through any nonlinear (phase) device. In an operating

TABLE 23. TRANSMISSION PARAMETERS AND TEST RESULTS OF THE FREQUENCY PLANS TESTED

Case Car- No. rier	Transmit Freq (MHz)	Receive Freq (MHz)	Bandwidth Unit (MHz)	Chan-nels	TWT Operat-ing Point (dB)	Satel-ite e.i.r.p. (dBW)	Cavey Earth Station e.i.r.p. (dBW)	C/T (dBW/°K)	S/N Nom-inal (dB)	NPR Non-inal (dB)	NPR Mea-sured (dB)	Δ NPR (dB)
1	6100	3875	15	252		18.7	79.1	-141.4	53.7	35.0	35.3	+0.3
	6112.5	3887.5	10	132		16.3	76.9	-144.8	53.7	36.3	36.4	+0.1
	6120	3895	5	60	-11	13.4	74.1	-146.8	54.2	38.8	39.0	+0.2
	6123.75	3898.75	2.5	24		10.3	71.0	-150.1	53.7	40.8	40.4	-0.4
	6126.25	3901.25	2.5	24		10.3	71.0	-150.2	53.7	40.8	41.4	+0.6
2	6095	3870	5	132		19.4	82.3	-142.0	50.1	32.7	32.5	-0.2
	6102.5	3877.5	10	132		16.6	79.7	-147.8	50.5	33.1	33.4	+0.3
3	6112.5	3887.5	10	132	-6	16.6	79.7	-147.9	50.3	32.9	32.4	-0.5
	6122.5	3897.5	10	252		20.6	83.3	-140.5	49.9	31.3	31.8	+0.5
4	6095	3870	5	132		22.9	82.1	-141.2	46.1	28.7	29.5	+0.8
	6102.5	3877.5	10	252		24.9	84.1	-139.7	47.3	28.5	29.2	+0.7
	6112.5	3887.5	10	252	-12	25.2	84.4	-139.5	47.7	28.9	28.4	-0.5
	6122.5	3897.5	10	252		30.4	89.3	-131.4	44.5	25.8	25.7	-0.1
4	6101.25	3876.25	17.5	432		22.8	84.2	-138.5	53.4	34.7	34.9	+0.2
	6118.75	3893.75	17.5	432	-2	22.8	84.2	-138.5	53.4	34.7	34.9	+0.2

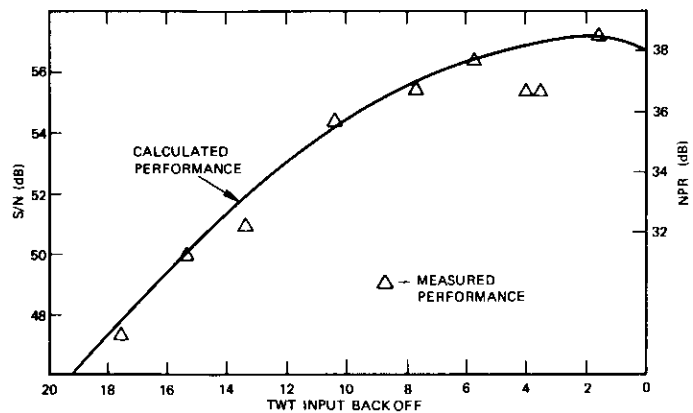


Figure 64. *S/N vs TWT Backoff for carrier no. 1 of case 1.*

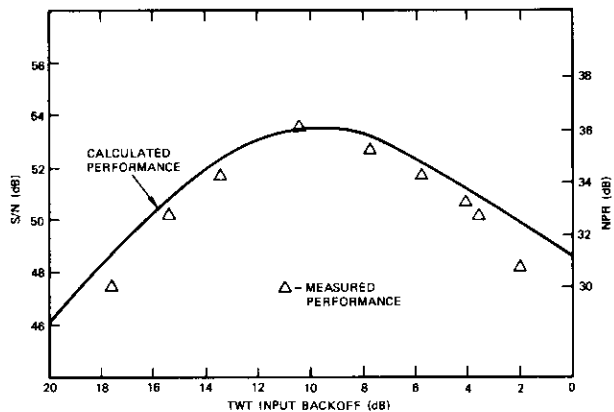


Figure 65. *S/N vs TWT Backoff for carrier no. 2 of case 1.*

multicarrier satellite system, there may be more than one element within the link which can generate crosstalk. (For instance, crosstalk can be generated in the HPA, up-converters, down-converters, IF amplifiers, and demodulators.) In general, however, the major contributor will be the TWTA of the satellite transponder.

Since crosstalk is dependent upon the composite amplitude variation which precedes the satellite TWTA, the amplitude characteristics of the

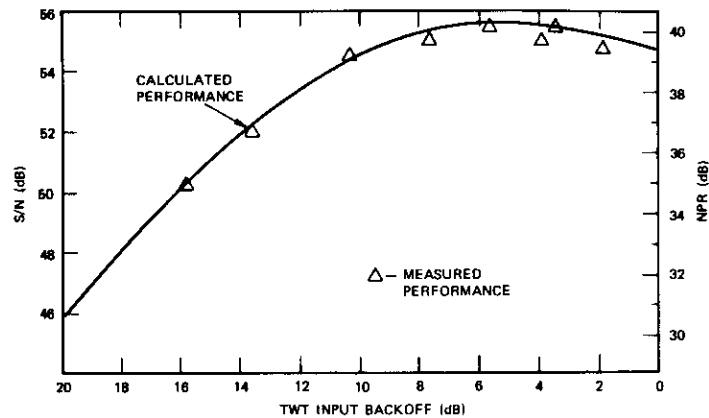


Figure 66. *S/N vs TWT Backoff for carrier no. 3 of case 1.*

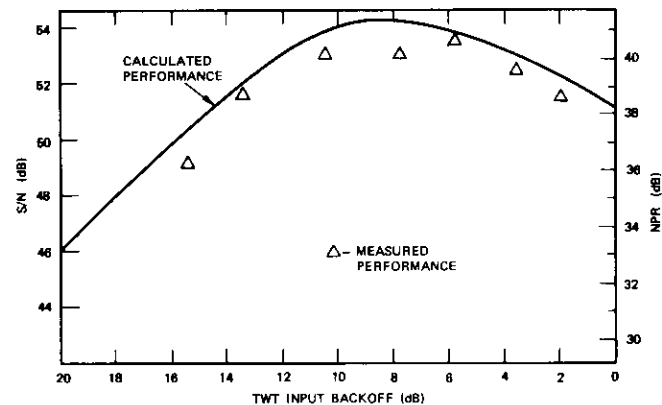


Figure 67. *S/N vs TWT Backoff for carrier no. 4 of case 1.*

transmitting earth station equipment may have a significant effect on the resulting crosstalk. Therefore, the crosstalk measurements made at one earth station can provide only an estimate of the crosstalk performance for similar carriers generated at other earth stations.

Because the number of carrier combinations which could be investigated for crosstalk was quite high, two worst-case configurations were considered:

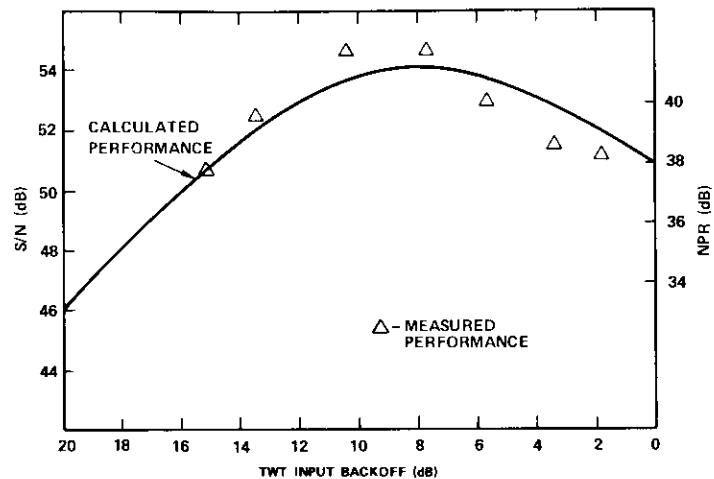


Figure 68. *S/N vs TWT Backoff for carrier no. 5 of case 1.*

- a. two identical 432-channel carriers in a spot-beam configuration, and
- b. two identical 432-channel carriers in a global-beam contingency configuration (case 4).

The crosstalking carrier was noise modulated in the conventional manner, but the top baseband channel was replaced by a 0-dBm0 test tone. The test tone which transfers from the crosstalking carrier to the wanted carrier is a measure of the crosstalk.

The measured results for the worst-case configurations are presented in Figures 69 and 70. The data plotted in Figure 69 are a function of input backoff for the 432-channel spot-beam configuration. In Figure 70, crosstalk is plotted as a function of the crosstalking carrier location at an input backoff of 10 dB. Crosstalk as a function of location for other backoffs may be estimated by combining Figures 69 and 70. The nominal backoff for this worst case configuration is approximately 15 dB; thus it can be seen that the crosstalk ratio will not exceed the C.C.I.T.T. recommendation of 58 dB.

**Dual-path effect**

The dual-path effect occurs in a communications system when the isolation between adjacent transmission channels is less than perfect. In the

case of the INTELSAT IV repeater, this effect occurs because of the overlap in the filter skirts of both the input and output multiplexers. If a dual path exists, a carrier which is located near the band edge may also be partly transmitted through the adjacent channel and recombined at the receiving earth station, thus causing distortion in the transmitted signal.

Field measurement of the dual-path effect was performed on a carrier using expanded parameters. In such a case, the dual-path effect would be more pronounced because of the higher bandwidth utilization of the carrier. The results of measurements made on a 132-channel/5-MHz carrier

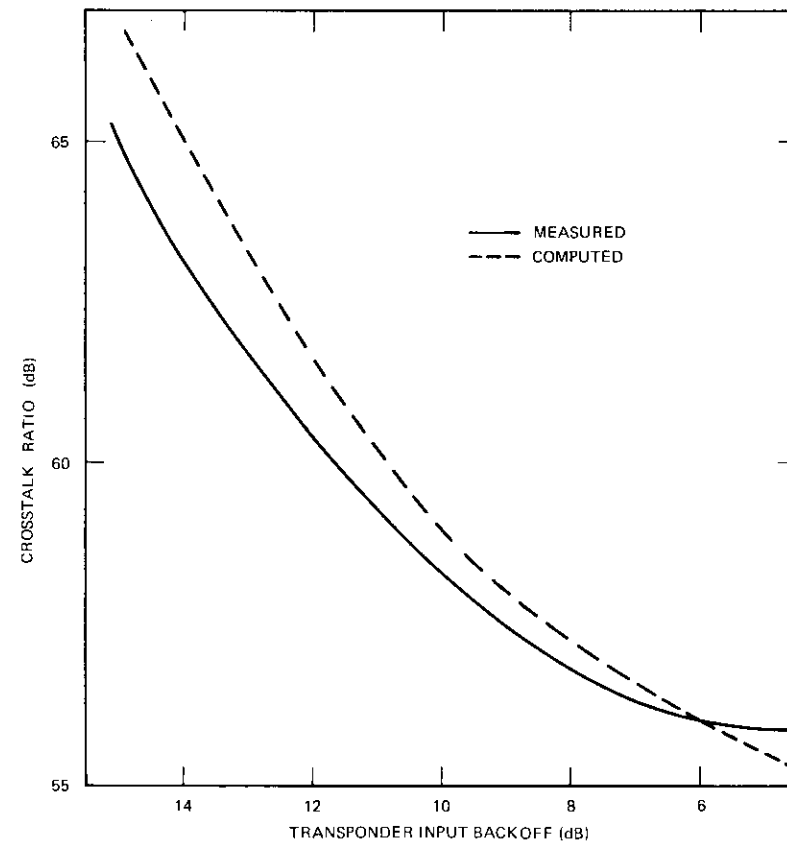


Figure 69. *Equal Carrier Test (432-channel spot-beam carrier, gain setting 1, crosstalking carrier frequency = 6102 MHz)*

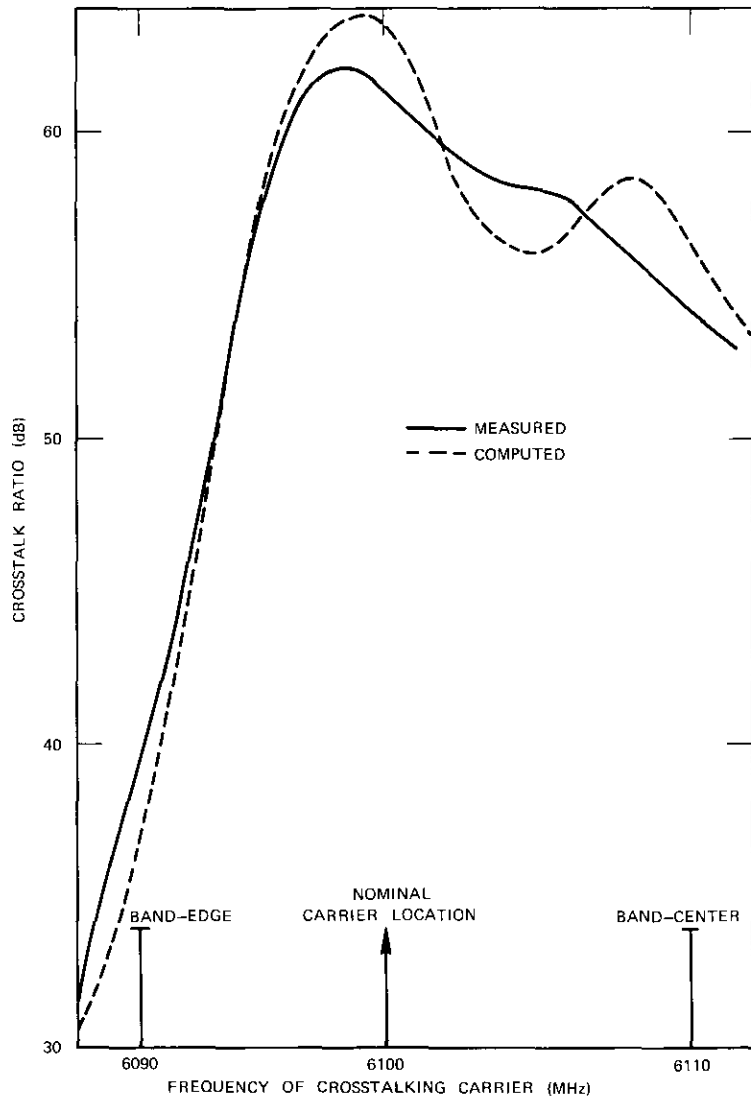


Figure 70. Equal Carrier Test, (432-channel spot-beam carrier, gain setting 1, input backoff = 10 dB)

are shown in Figure 71. Since the thermal noise contribution has been minimized, the results which are presented indicate primarily the distortion noise contribution. The dual-path effect does become quite noticeable when the test carrier is displaced by more than 2 MHz from the nominal location toward the band edge. For example, as the gain setting in transponder no. 5 was increased from 1 to 3 to 5 (corresponding to a gain reduction in the direct path), the relative effective gain of the adjacent path increased. Thus, the increase in dual-path distortion at higher gain settings can be understood.

Extrapolation of measurements of the dual-path effect to the nominal carrier location indicate that the noise level is on the order of several hundred picowatts for this carrier configuration. Since the geographical location of the station affects the relative phasing between channels, these results cannot be generalized for other earth stations.

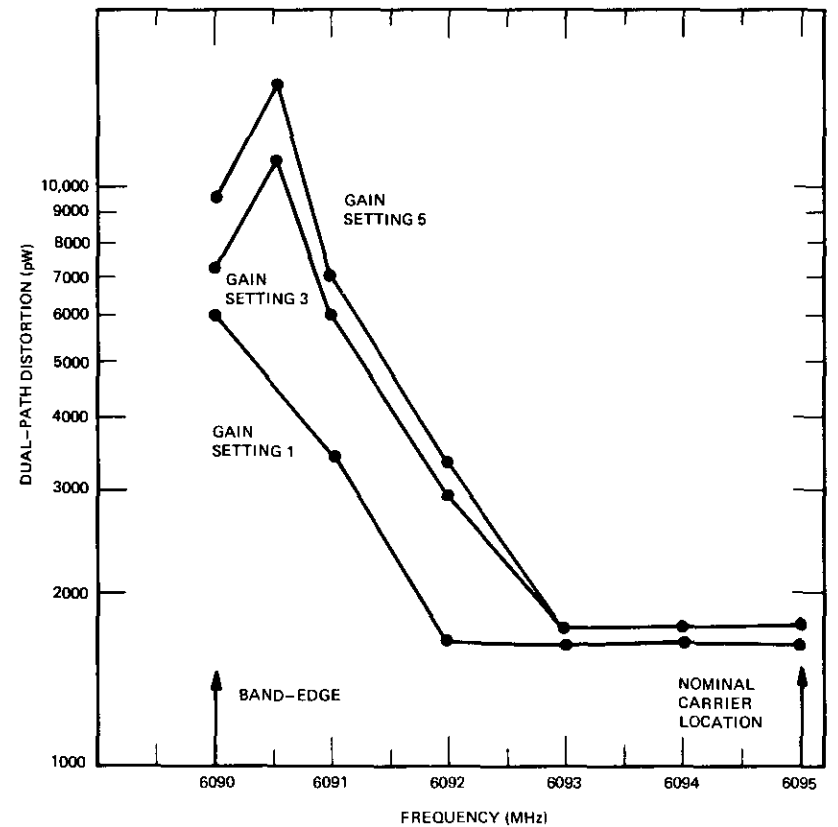


Figure 71. Field Measurement of the Dual-Path Effect on a 132-Channel/5-MHz Carrier

## **Operational planning**

F. J. BURKITT AND R. J. RODGERS

The first INTELSAT IV was brought into service in the Atlantic Ocean region in early 1971. In the same 500-MHz allocated bandwidth, this satellite achieved a capacity about five times greater than that of the previous satellite by using a higher e.i.r.p. per unit of bandwidth. To utilize this additional e.i.r.p., the transmission parameters (power and bandwidth) assigned to all earth stations had to be changed when the INTELSAT IV was placed in service without interrupting the commercial service being provided by the system. Therefore, operational plans had to be developed and approved in time to permit all earth stations to procure the necessary equipment, and detailed transition plans were needed to implement the INTELSAT IV operational system without loss of commercial service. This section will discuss some of the factors involved to bringing the INTELSAT IV satellite into commercial service.

### **System operating philosophy**

The global INTELSAT system has been divided into three regions of operation: the Atlantic, Pacific, and Indian Ocean areas. Within these regions it is desirable for each earth station to have direct contact with any other earth station. To achieve this direct contact by using a single antenna per region for each country, a satellite must have sufficient capacity to handle all the requirements of the region.

One INTELSAT III over the Pacific and one over the Indian Ocean provided sufficient capacity to meet requirements in those regions. However, two INTELSAT IIIs were needed in the Atlantic region.

During the INTELSAT III operations period, it was necessary to divide the Atlantic region into two "communities of interest" (i.e., groups of countries having similar communications requirements) so that two satellites could be employed. Hence, most of the circuits required by a country could be provided directly and the remaining circuits could be provided by routing via an adjacent earth station. For example, circuits from Germany

---

*F. J. Burkitt is Manager, INTELSAT Plans, Communications System Management, COMSAT.*

*R. J. Rodgers is a Senior Staff Engineer, INTELSAT Plans, Communications System Management, COMSAT.*

to destinations in Africa might be routed via France, while circuits from France to destinations in South America might be routed via Germany. While this met the service requirements of all administrations, it did not provide direct contact among all earth stations in the region.

For direct access among all earth stations in a region while operating more than one satellite per region, COMSAT has developed a technique employing a primary satellite and a major path satellite. Basically this technique permits all countries to access a single primary satellite; the larger users can then construct second antennas to access the major path satellite for their large traffic requirements. This technique also permits the larger users to diversify their requirements between two satellite paths, thereby reducing the probability of total loss of service on these routes. This concept can be extended so that very large users can operate with a third or fourth satellite for the very heavy traffic routes, thereby extending the useful operating period of smaller capacity satellites. One of the advantages of this concept is that only the large users need to construct second antennas; these users generally wish to construct additional antennas to provide protection for their service. This concept is applicable to all three regions, although for the foreseeable future it is unlikely that the Indian Ocean region will require more than one satellite.

### **Development and coordination of operational and contingency plans**

The foundation of all operational plans is the INTELSAT traffic data base. To produce this data base, traffic experts from all administrations meet once a year and agree to the number of circuits required between each country. This country-to-country traffic is then converted to earth-station-to-earth-station requirements, since some of the countries requiring service do not yet have earth stations and must route their circuits via another country.

From this approved traffic data base, COMSAT develops operational plans showing the carrier size, frequency, and baseband configuration needed to meet all stated requirements. For the INTELSAT IV, the main transmission scheme utilizes frequency modulation/frequency-division multiplex/frequency-division multiple access FM/FDM/FDMA). A single global-beam transmit carrier handling all of a country's requirements can be received by all other earth stations in the region. However, to take advantage of the increased capacity available through the spot-beam antennas, requirements for earth stations within the coverage pattern of

those antennas are separated and assigned to another transmit carrier. This means that an earth station may have to transmit three separate carriers to satisfy its requirements, e.g., one to the east spot beam, a second to the west spot beam, and a third to the global beam. After the requirements have been sorted according to spot-or global-beam transmissions, carriers are arranged in standard INTELSAT sizes. Table 24 shows the baseband arrangements for the INTELSAT IV carrier sizes. A transmit carrier may be received by 10 earth stations, each demodulating the specific supergroups, groups, or channels assigned to this service.

Included on each transmit carrier are two engineering service circuits (ESCs) assigned to the 4- to 8-kHz and 8- to 12-kHz portions of the base-

band and used by maintenance personnel to report problems and to test and maintain service on the carrier. Each ESC contains one voice channel and up to five telegraph channels so that a total of 10 telegraph channels per transmit carrier are available. INTELSAT operational plans include assignment of these "order-wire" services between earth stations and from earth stations to the INTELSAT technical and operational control centers of each region for coordination and control of system operation.

### System planning

Operational planning for the INTELSAT IV system requires two steps:

- a. development and coordination of operational and contingency plans, and
- b. development of transition and implementation plans.

First, COMSAT, as Manager for INTELSAT, reviews the operational requirements for a particular year and develops frequency plans showing the carrier sizes and baseband arrangements needed to satisfy all operational requirements. These plans are coordinated with representatives of all concerned administrations and, when an agreement has been reached, they constitute an INTELSAT operating plan. Similarly, COMSAT prepares contingency plans for maintenance or restoration of service in the event of a satellite failure or partial failure. After these plans have been approved, plans for implementation and transition to the new INTELSAT operational plan are developed. These include arrangements for continuation of existing service, either by using temporary support carriers or by using another country's earth station while new carriers are being established, lined up, and tested.

### Earth station constraints

In addition to the service requirements, INTELSAT plans must consider various system constraints which limit to some extent the frequency plans which may be developed. These primarily fall into the category of frequency restrictions and earth station equipment or design limitations. The frequency constraints are generally due to potential interference between terrestrial microwave systems and earth stations operating on selected frequencies. Therefore, some earth stations cannot be assigned to transmit or receive selected frequencies. In a large system of 40 or more earth stations, each transmitting to five or more other stations, this can cause considerable difficulty. The constraints caused by earth station

TABLE 24. BASEBAND COMPOSITION FOR INTELSAT IV CARRIERS

No. of Channels	Baseband Composition	Frequency Band (kHz)
24	Group A (erect) [26] plus Group 5 of SG1 (inverted)	12-108
36	Group A (erect) [26] plus Groups 5 and 4 of SG1 (inverted)	12-156
60	Group A (erect) [26] plus Groups 5-2 of SG1 (inverted)	12-252
72	Group A (erect) [26] plus SG1 (inverted)	12-300
96	Group A (erect) [26] plus SG1 (inverted) plus Groups 1 & 2 of SG2	12-408
132	Group A (erect) [26] plus SG1 (inverted) plus SG2 (erect) [27]	12-552
192	Group A (erect) [26] plus SG1 (inverted), SG2 (erect), and SG3 (inverted) [27]	12-804
252	Group A (erect) [26] plus SG1 (inverted), SG2 (erect), and SG3 and SG4 (inverted) [27]	12-1052
312	Group A (erect) [26] plus SG1 (inverted), SG2 (erect), and SG3-5 (inverted) [27]	12-1300
432	Group A (erect) [26] plus SG1 (inverted), SG2 (erect) and SG3-7 (inverted) [27]	12-1796
612	Group A (erect) [26] plus SG1 (inverted), SG2 (erect) and SG3 10 (inverted) [27]	12-2540
792	Group A (erect) [26] plus SG1 (inverted), SG2 (erect), and SG3-13 (inverted) [27]	12-3284
972	Group A (erect) [26] plus SG1 (inverted), SG2 (erect), and SG3 16 (inverted) [27]	12-4208
1092	Group A (erect) [26] plus SG1 (inverted), SG2 (erect), and SG3-16 (inverted) [27] plus SG16 and 15 (erect, modulated) [27]	12 4892
1872	Group A (erect) [26] plus SG1 (inverted), SG2 (erect), and SG3-16 (inverted) [27], plus SG16 3 (erect) and SG2 (inverted, modulated) [27]	12-8120

equipment or design generally delay implementation of operational plans until the earth station owner can procure the necessary equipment or make necessary modifications in the station.

#### **Coordination of operating plans**

After COMSAT has prepared the operating plans, considering service requirements and system constraints, the plans are sent to each earth station owner in the region for coordination and approval. These plans, which usually cover a period of one to three years, are prepared two years in advance. Because changes requested by any earth station owner can affect many other earth stations, it is generally impractical to coordinate these plans through correspondence. Therefore, INTELSAT has established an operational organization, consisting of representatives of all present and planned earth stations. This body meets as required (generally annually) to agree on future operating plans and resolve mutual operating problems. Agreement by all operational representatives of a region constitutes a mutual agreement among all countries to procure the necessary equipment to implement the plan.

In a similar manner, contingency plans are developed and coordinated to deal with emergency situations that can arise in the event of satellite failure. As an example, the Atlantic region, presently operating with two INTELSAT IV satellites, has no spare in-orbit satellite. It has been agreed that, until a spare in-orbit satellite is available, all service will be restored through the surviving satellite if one satellite fails. When a spare satellite becomes available, a restoration will be achieved by transferring all affected earth stations to this satellite. For the Pacific and Indian Ocean regions, plans have been developed to revert to the predecessor satellite (INTELSAT III) until a spare in-orbit INTELSAT IV is available.

Other contingency plans include provisions for a failure of one of the 12 transponders of an INTELSAT IV. These plans are also coordinated with the operational representatives to ensure that all earth stations will have the necessary equipment to implement the plan.

#### **Transition and implementation plans**

After a plan has been approved, the next step is to develop detailed plans for implementing it. These can be relatively simple plans involving modification of existing carriers or quite complex plans requiring changes in transmission parameters, frequency assignment, and baseband arrange-

ments, but all such plans are intended to prevent interruption of existing services. Therefore, arrangements must be made to provide continuity of service while changes are being made in the existing system. For example, temporary carriers can be established on the television frequency to carry the service, or service can be transferred to another earth station until changes are completed.

Transition and implementation plans must be detailed, day-by-day, step-by-step plans. At each significant step, performance must be measured and documented so that records of the lineup performance are available for future reference during maintenance. Before a transition is started, all earth stations must be prepared to follow the plan, since failure of any earth station to meet its commitment can have a snowballing effect on previously approved support arrangements. In many cases steps taken are interim arrangements that cannot be sustained for extended periods without jeopardizing the integrity of service. Therefore, it is important for operating plans to be approved in time to permit all earth stations to be properly equipped. In some cases the required lead time to purchase equipment is on the order of 18 months.

The transition from INTELSAT III to INTELSAT IV in the Atlantic area was a rather complex operation involving 27 major steps, each requiring up to 50 coordinated actions at the earth stations. The first action required was to rearrange the carriers on INTELSAT III so that a direct pointover to INTELSAT IV could be made. This was necessary because INTELSAT IV has 12 transponders, each 36 MHz wide, with 4-MHz gaps between transponders, whereas INTELSAT III has two transponders, each having a 225-MHz bandwidth. Some of the carriers assigned to INTELSAT III would have fallen into the gaps between the INTELSAT IV transponders unless the frequency plan had been rearranged prior to pointover.

To rearrange the frequency plan without interrupting service, it was necessary to establish temporary support carriers in the band reserved for occasional use (e.g., for television and restoration of services on in-operative submarine cables), line up these carriers with all receive stations, and transfer the traffic to them while changes in the original carrier were being made. In some cases it was impossible to move directly to the INTELSAT IV frequency because another earth station was transmitting in that spot. It was then necessary to assign services to an interim carrier until the ultimate frequency band could be cleared. All of these actions had to be planned around scheduled television programs and provisions for reverting to previous operation in the event of a break in a submarine cable.

After the necessary carrier rearrangements were completed, a pointover to the INTELSAT IV was made. Because this step would cause an interruption of service, it was accomplished in the early morning hours (about 2 AM), when traffic was at a minimum. At the time of pointover, all INTELSAT IV transponders were switched to the global transmit antennas so that the carrier operating through INTELSAT III (which did not have spot beams) could be accepted. After a rapid readjustment of earth station power to account for the difference in satellite receive gain, service was again restored to the customers.

The next step was to bring the spot beams of the INTELSAT IV into service. To do this, it was necessary to transfer all service from the transponder to the temporary support carrier in the occasional use band. After the transponder was cleared and switched, the new carriers using spot-beam transmission parameters were brought into service one at a time. When each new carrier had been lined up, the traffic was transferred from the support carrier and the support carrier was discontinued. This process was repeated until the three transponders required for INTELSAT IV service were switched to the spot-beam mode. (Transfer of traffic from one carrier to another is done at the baseband level and can be accomplished in less than one second. Therefore, the transfer of service from one carrier to another does not affect the telephone user.)

Because it was necessary to maintain normal service during the transition, it was essential to confirm that all earth stations were ready before any step could begin. It was also necessary to document results of each step so that a benchmark would be available for future maintenance. If this documentation were not done, it would be difficult to locate faults in the system, since the normal system measurements would not be known. Therefore, the transition to the INTELSAT IV required over six months from start to finish. It is noteworthy that this transition was carried out virtually without noticeable interruption of service to the communications users.

To help establish and maintain service, INTELSAT has provided a monitoring system which can measure the characteristics of signals being received from the satellite. This system has been fully described previously [28].

#### **System planning guidelines**

Naturally the most important goal of INTELSAT planning is to meet all service requirements. The next most important objective is to make the most efficient use of the available satellite capacity so that the maximum

number of circuits can be derived and the cost of providing service can eventually be reduced. A further consideration is that of providing for expansion without requiring extensive changes at earth stations so that costs to earth station owners can be reduced. This is particularly important in a system using multdestination carriers, since changes in one transmit carrier can affect 10 receive earth stations, some of which will not derive additional service to offset the added expenses. If possible, operational plans should cover a period of several years so that a degree of stability can be introduced into the system. Ideally a plan should cover the period from the initiation of service via a particular satellite to the time when that satellite is operating at its maximum capacity. In practice, because of changes in requirements and the introduction of new services made possible by satellites, this ideal situation is not achieved. Generally plans can be formulated for a period of only two or three years.

For the INTELSAT IV, the planning cycle for the Atlantic region has required three plans over the lifetime of the satellite. The first plan implemented was intended to bring the new satellite into the system and to convert from INTELSAT III transmission parameters. At that time it was impossible to assign carriers which would be useful throughout the satellite lifetime, since it was necessary to maintain spare satellite capacity to accomplish the required carrier changes.

The second plan was designed to provide for all of the services that had been forecast for the useful life of the satellite. This plan used all of the design capacity of INTELSAT IV and in effect defined the time when additional satellite capacity would be required.

Since these plans were approved, additional requirements have been introduced which cannot be satisfied by using the second generation plan. Therefore, it has become necessary to implement a third generation plan to satisfy these new requirements until a satellite with a larger capacity becomes available. The third generation plan must deviate somewhat from the basic concept of operation to provide the additional capacity required. Specifically, it will be necessary to transfer some earth stations having a limited community of interest from the primary satellite to the major path satellite. When the larger capacity satellites become available, the transition plan for these satellites will include a return to the basic system concept. Therefore, the third generation plan can be considered to be a stopgap plan to be used until larger capacity satellites are available.

#### **New transmission systems**

INTELSAT is presently introducing a new system for providing com-

munications via satellite known as SPADE, an acronym derived from Single-channel-Per-carrier PCM multiple-Access Demand-assignment Equipment [29].

To serve SPADE, an initial pool of 400 circuits has been made available in the INTELSAT IV satellite. These circuits will permit 400 simultaneous telephone conversations. Depending on factors such as required minutes per day per link and peak busy hour spread, they may provide service equivalent to 1500 preassigned voice circuit links. In addition to providing for small traffic routes, SPADE will permit service between large users during periods when all preassigned circuits are busy. Therefore, it is unnecessary for countries to provide additional preassigned circuits which are idle most of the time to meet the requirements of peak busy periods.

## References

- [1] International Radio Consultative Committee (C.C.I.R.), "Allowable Noise Power in the Hypothetical Reference Circuit," Recommendation 353-2, *XIIth Plenary Assembly, New Delhi, 1970*, Vol. IV, Pt. II, p. 87, Geneva: International Telecommunication Union, 1970.
- [2] "Performance Characteristics of Earth Stations in the INTELSAT IV System," ICSC-45-13E W/1/70 (Rev 1), June 23, 1972.
- [3] International Radio Consultative Committee (C.C.I.R.), "Requirements for the Transmission of Television Signals Over Long Distances (System I excepted)," Recommendation 421-1, *XIth Plenary Assembly, Oslo, 1966*, Vol. V, p. 66, Geneva: International Telecommunication Union, 1967.
- [4] International Radio Consultative Committee (C.C.I.R.), "Requirements for the Transmission of Television Signals Over Long Distances (System I only)," Recommendation 451, *XIth Plenary Assembly, Oslo, 1966*, Vol. V, p. 86, Geneva: International Telecommunication Union, 1967.
- [5] A. C. Dickieson, "The Telstar Experiment," *Bell System Technical Journal*, Vol. XLI, No. 4, July 1963, pp. 739-747.
- [6] U.S. Seminar on Communications Satellite Earth Station Technology, *Edited Lectures*, Washington D.C., 1966.
- [7] R. W. Kreutel and A. O. Pacholder, "The Measurement of Gain and Noise Temperatures of a Satellite Communications Earth Station," *Microwave Journal*, Vol. 12, No. 10, October 1969, p. 61.
- [8] J. G. Puente and A. M. Werth, "Demand-Assigned Service for the INTELSAT Global Network," *IEEE Spectrum*, Vol. 8, No. 1, January 1971, pp. 59-69.
- [9] *INTELSAT Earth Station Performance Seminar*, Washington, D.C., October 1971.
- [10] J. Fagot and P. Magne, *Frequency Modulation Theory*, New York: Pergamon Press, 1961.
- [11] Bell Telephone Laboratories, *Transmission Systems for Communications*, Chapter 21.
- [12] C. L. Ruthroff, "Computation of FM Distortion in Linear Networks for Band Limited Periodic Signals," *Bell System Technical Journal*, Vol. 47, No. 6, July-August 1968, pp. 1043-1063.
- [13] D. Ongaro and F. Rocca, "Microwave and Nearly-Optimum Phase-Lock Demodulator," *Alta Frequenza*, Vol. XXXV, No. 8, August 1966, pp. 145-155.
- [14] F. Carassa and F. Rocca, "Advances in Phase-Lock Demodulation," *IEEE International Conference on Communications*, Boulder, Colorado, June 1969, *Conference Record*, pp. 12-9 to 12-14.
- [15] M. R. Wachs, "Analysis of Adjacent Channel Interference in a Multi-carrier FM Communications System," *COMSAT Technical Review*, Vol. 1, No. 1, Fall 1971, pp. 139-171.
- [16] F. Assal, "Amplitude and Group-Delay Equalized Bandpass Elliptic Function Filter," *Proceedings of the National Electronics Conference*, Vol. 26, 1970.
- [17] A. Berman and E. Podraczky, "Experimental Determination of Intermodulation Distortion Produced in a Wideband Communications Repeater," *1967 IEEE International Convention Record*, Vol. 15, Pt. 2.
- [18] A. Berman and C. Mahle, "Nonlinear Phase Shift in Traveling Wave Tubes as Applied to Multiple Access Communication Satellites," *IEEE Transactions on Communications Technology*, COM-18, No. 1, February 1970, pp. 37-47.
- [19] O. Shimbo, "Effects of Intermodulation, AM-PM Conversion and Additive Noise in Multicarrier TWT Systems," *Proceedings of IEEE*, Vol. 59, No. 2, February 1971, pp. 230-238.
- [20] N. Chitre and J. Fuenzalida, "Baseband Distortion Caused by Intermodulation in Multicarrier FM Systems," *COMSAT Technical Review*, Vol. 2, No. 1, Spring 1972, pp. 147-173.
- [21] R. C. Chapman, Jr. and J. B. Millard, "Intelligible Crosstalk Between Frequency Modulated Carriers Through AM-PM Conversion," *IEEE Transactions on Communications Technology*, COM-12, No. 2, June 1964, pp. 160-166.
- [22] International Radio Consultative Committee (C.C.I.R.), "Radio-Relay Systems for Telephony Using Frequency-Division Multiplex," Recommendation 275-1, *XIth Plenary Assembly, Oslo, 1966*, Vol. IV, Pt. 1, p. 83, Geneva: International Telecommunication Union, 1967.

- [23] International Radio Consultative Committee (C.C.I.R.), "Radio-Relay Systems for Television," Recommendation 405, *XIth Plenary Assembly, Oslo, 1966*, Vol. IV, Pt. 1, p. 92, Geneva: International Telecommunication Union, 1967.
- [24] "Technical Evaluation of Draft Atlantic Region INTELSAT IV Frequency Plan," ICSC/T-33-10E, W/11/69, October 16, 1969.
- [25] "Summary of Specification changes to the INTELSAT IV Contract, ICSC/T-45-13E, R/5/72, May 11, 1972.
- [26] International Telegraph and Telephone Consultative Committee (C.C.I. T.T.), "General Characteristics Recommended for Transistor-Type Systems on Symmetric Pair Cables," Recommendation G.322, *IVth Plenary Assembly, Mar del Plata, 1968*, Vol. III, Pt. 1, p. 4, Geneva: International Telecommunication Union, 1969.
- [27] International Telegraph and Telephone Consultative Committee (C.C.I. T.T.), "Interconnection at the Baseband Frequencies of Frequency-Division Multiplex Radio-Relay Systems," Recommendation G.423, *IVth Plenary Assembly, Mar del Plata, 1968*, Vol. III, Pt. 2, pp. 5-6, Geneva: International Telecommunication Union, 1969.
- [28] E. E. Steinbrecher and L. F. Gray, "A Computer-Controlled Satellite Signal Monitoring System," *COMSAT Technical Review*, Vol. 1, No. 1, Fall 1971, pp. 79-116.
- [29] B. I. Edelson and A. M. Werth, "SPADE System Progress and Application," *COMSAT Technical Review*, Vol. 2, No. 1, Spring 1962, pp. 221-242.

## ***Le satellite Intelsat IV***

ÉDITÉ PAR E. T. JILG

### ***Sommaire***

On décrit le satellite de télécommunication INTELSAT IV en traitant séparément de chaque sous-système. Le satellite, conçu pour une durée de vie de 7 ans, pèse 1410 kg au lancement, et 730 kg après fonctionnement du moteur d'apogée. Tout le sous-système de télécommunication est placé dans la partie du satellite qui est en contre-rotation. Chacune des deux antennes à 6 GHz, à couverture globale, alimente une paire de récepteurs redondants ayant 500 MHz de bande. Pour chacun des douze canaux de 36 MHz de bande l'amplification est fournie par une paire de TOP redondants. A l'émission il y a deux antennes à faisceau global, et deux autres antennes à faisceau étroit, d'ouverture angulaire de 4, 5 degrés.

La majeure partie du satellite (450 kg) tourne sur elle-même à une vitesse nominale de 51 tours par minute; elle comprend les sous-systèmes d'alimentation électrique, de commande de contre-rotation, de maintien en position et d'orientation. Deux panneaux solaires cylindriques fournissent une puissance utile de 365 watts; deux batteries de 25 éléments au nickel-cadmium assurent l'alimentation lors des éclipses. Le satellite est en rotation autour d'un axe correspondant à un moment d'inertie minimum, sa stabilité est maintenue par deux amortisseurs pendulaires à courants de Foucault.

## ***Lancement et mise en orbite des satellites Intelsat IV***

A. M. McCASKILL, D. V. NEILL, A. A. SATTERLEE

### ***Sommaire***

On décrit Atlas-Centaur, le véhicule de lancement d'INTELSAT IV, et la séquence d'événements lors de son envol. On établit une liste des contraintes auxquelles est soumise la fenêtre de lancement, et on indique